**Doctoral thesis**
**International cotutelle**
**University of Málaga**
**and**
**University of Mascara**

# THE PREPARATION OF CARBON-BASED MATERIALS FROM BIOMASS BY-PRODUCT FOR APPLICATION IN ADSORPTION AND HETEROGENEOUS CATALYTIC PROCESSES

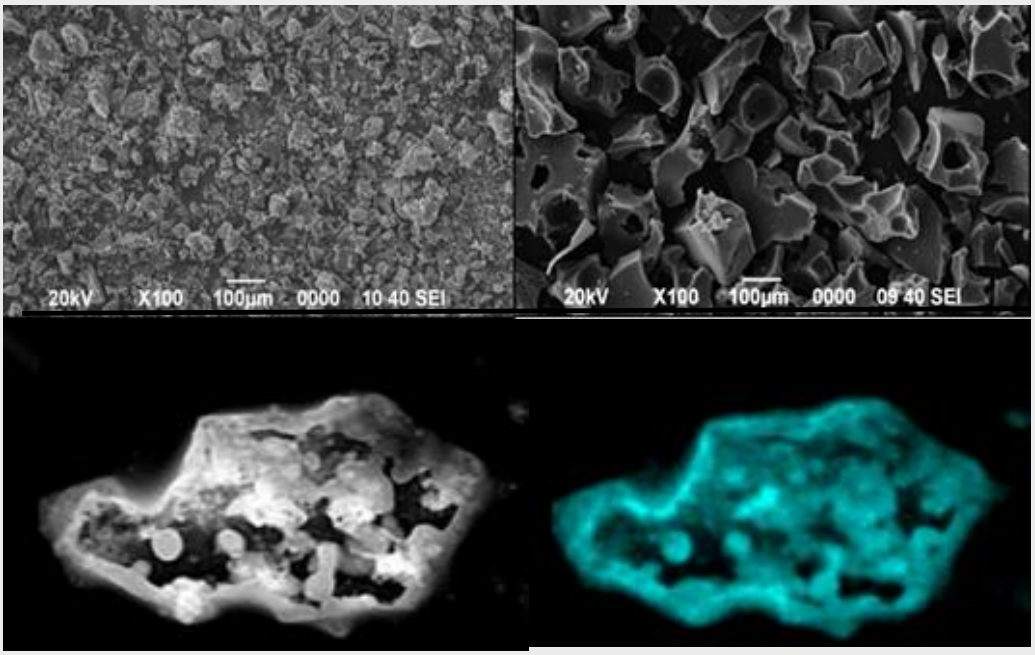


Supervisors:
Prof. Dr. D. José Rodríguez Mirasol
Dr. Dña. Juana M.ª Rosas Martínez
Prof. Dr. Abdelghani Benyoucef

**Imane Moulefera**

**Málaga, 2020**

UNIVERSIDAD DE MÁLAGA

UNIVERSIDAD
DE MÁLAGA

AUTOR: Imane Moulefera

http://orcid.org/0000-0003-3395-4786

EDITA: Publicaciones y Divulgación Científica. Universidad de Málaga

Esta obra está bajo una licencia de Creative Commons Reconocimiento-NoComercial-SinObraDerivada 4.0 Internacional:
http://creativecommons.org/licenses/by-nc-nd/4.0/legalcode
Cualquier parte de esta obra se puede reproducir sin autorización
pero con el reconocimiento y atribución de los autores.
No se puede hacer uso comercial de la obra y no se puede alterar, transformar o hacer obras derivadas.

Esta Tesis Doctoral está depositada en el Repositorio Institucional de la Universidad de Málaga (RIUMA): riuma.uma.es

UNIVERSIDAD
DE MÁLAGA

UNIVERSIDAD DE MÁLAGA

جامعة مصطفى اسطمبولي
بمعسكر

**FACULTAD DE CIENCIAS**
**DEPARTAMENTO DE INGENIERÍA QUÍMICA**

**DOCTORAL PROGRAM**

**Química y Tecnologías Químicas, Materiales y Nanotecnología**

# Doctoral thesis

## (International cotutelle)

# *The preparation of carbon-based materials from biomass by-product for application in adsorption and heterogeneous catalytic processes*


Author: Imane Moulefera

Supervisors: Prof. Dr. D. José Rodríguez Mirasol

Dr. Dña. Juana M.ª Rosas Martínez

Prof. Dr. Abdelghani Benyoucef


**Málaga, April 2020**


UNIVERSIDAD DE MÁLAGA

# DECLARACIÓN DE AUTORÍA Y ORIGINALIDAD DE LA TESIS PRESENTADA PARA OBTENER EL TÍTULO DE DOCTOR

D./Dña IMANE MOULEFERA
Estudiante del programa de doctorado QUÍMICA Y TECNOLOGÍAS QUÍMICAS, MATERIALES Y NANOTECNOLOGÍA de la Universidad de Málaga, autor/a de la tesis, presentada para la obtención del título de doctor por la Universidad de Málaga, titulada: THE PREPARATION OF CARBON-BASED MATERIALS FROM BIOMASS BY PRODUCTS FOR APPLICATION IN ADSORPTION AND HETEROGENEOUS CATALYTIC PROCESSES

Realizada bajo la tutorización de JOSÉ RODRÍGUEZ MIRASOL y dirección de JOSÉ RODRÍGUEZ MIRASOL, JUANA M.ª ROSAS MARTÍNEZ Y ABDELGHANI BENYOUCEF (si tuviera varios directores deberá hacer constar el nombre de todos)

DECLARO QUE:

La tesis presentada es una obra original que no infringe los derechos de propiedad intelectual ni los derechos de propiedad industrial u otros, conforme al ordenamiento jurídico vigente (Real Decreto Legislativo 1/1996, de 12 de abril, por el que se aprueba el texto refundido de la Ley de Propiedad Intelectual, regularizando, aclarando y armonizando las disposiciones legales vigentes sobre la materia), modificado por la Ley 2/2019, de 1 de marzo.

Igualmente asumo, ante a la Universidad de Málaga y ante cualquier otra instancia, la responsabilidad que pudiera derivarse en caso de plagio de contenidos en la tesis presentada, conforme al ordenamiento jurídico vigente.

En Málaga, a 20 de 05 de 2020

Fdo.:



UNIVERSIDAD DE MÁLAGA

**INFORME ANTIPLAGIO**

Doña Imane Moulefera

Estudiante del programa de doctorado QUÍMICA Y TECNOLOGÍAS QUÍMICAS, MATERIALES Y NANOTECNOLOGÍA de la Universidad de Málaga, autora de la tesis, presentada para la obtención del título de doctor por la Universidad de Málaga, titulada: THE PREPARATION OF CARBON-BASED MATERIALS FROM BIOMASS BY PRODUCTS FOR APPLICATION IN ADSORPTION AND HETEROGENEOUS CATALYTIC PROCESSES

Realizada bajo la tutorización de JOSÉ RODRÍGUEZ MIRASOL y dirección de JOSÉ RODRÍGUEZ MIRASOL, JUANA M.ª ROSAS MARTÍNEZ Y ABDELGHANI BENYOUCEF.

DECLARO QUE:

Tras aplicar el programa antiplagio "UNICHECK" recomendado por la Escuela de Doctorado y disponible en el campus virtual, a la tesis presentada. El programa ha proporcionado los siguientes resultados:

| ITEM A VALORAR | % DE PLAGIO |
|---|---|
| **Coincidencias** | 1,08 |
| **Citas** | 5,43 |
| **Exclusiones** | 8,30 |

Resultados que avalan la originalidad de esta obra.

En Málaga, a 20 de Mayo de 2020

Fdo:

UNIVERSIDAD DE MÁLAGA

D. José Rodríguez Mirasol, Catedrático de Ingeniería Química de la Universidad de Málaga,

Dña. Juana M ª Rosas Martínez, Profesora Titular de Ingeniería Química de la Universidad de Málaga,

D. Abdelghani Benyoucef, Profesor de Química de la Universidad de Mascara (Argelia)

CERTIFICAN: Que el trabajo de investigación recogido en la presente Memoria ha sido realizado bajo su dirección en el Departamento de ingeniería Quimica de la Universidad de Málaga por Doña. Imane Moulefera, reúne, a su juicio contenido científico suficiente y las condiciones necesarias para ser presentado y defendido ante el Tribunal correspondiente para optar el Grado de Doctor el régimen de cotutela internacional.

Málaga, April 2020

Fdo.: José Rodríguez Mirasol

Fdo.: Juana M.ª Rosas Martínez

Fdo.: Abdelghani Benyoucef

UNIVERSIDAD DE MÁLAGA

# Contents

Objectives and Overviews ..... 9

NOMENCLATURE ..... 11

List of Tables ..... 14

List of Figures ..... 16

1 Chapter I: Introduction ..... 20

1.1 Biomass ..... 20

1.2 Lignin ..... 22

1.3 Pulping process ..... 25

1.3.1 Kraft pulping ..... 25

1.3.2 Sulfite pulping ..... 26

1.3.3 Soda process ..... 27

1.3.4 Hydrothermal process ..... 28

1.3.5 Organosolv pulping ..... 29

1.4 Activated carbon ..... 31

1.5 Activated carbons preparation methods ..... 32

1.5.1 Physical activation ..... 33

1.5.2 Chemical activation ..... 36

1.5.2.1 Chemical activation with phosphoric acid ($H_3PO_4$) ..... 37

1.5.2.2 Chemical activation with other activating agents ..... 39

1.6 Activated carbons from lignin ..... 41

1.7 Application of activated carbons ..... 44

1.7.1 Activated carbon as adsorbent ..... 44

1.7.1.1 Emerging contaminants (ECs) ..... 46

1.7.2 Activated carbon in heterogeneous catalysis ..... 47

1.7.2.1 Activated Carbons as catalyst support ..... 47

UNIVERSIDAD DE MÁLAGA

1.7.2.2 Activated carbons as catalyst ..... 48
1.7.2.3 Alcohols decomposition ..... 49
1.7.2.3.1 Catalytic decomposition of propanol ..... 50
1.7.2.3.2 Catalytic decomposition of ethanol ..... 52
1.7.2.3.3 Catalytic decomposition of methanol ..... 54
References ..... 56
2 Chapter II: Experimental methods ..... 78
2.1 Preparation of activated carbons ..... 78
2.1.1 Chemical activation ..... 78
2.1.1.1 Preparation of activated carbon by co-solution of lignin with the activating agent…… ..... 78
2.1.1.2 Preparation of activated carbons from powder lignin ..... 78
2.1.1.3 Washing and drying ..... 79
2.1.2 Physical activation ..... 79
2.2 Characterization of activated carbons ..... 80
2.2.1 Ultimate Analysis and ash content ..... 80
2.2.2 Textural properties ..... 81
2.2.3 Surface Chemistry ..... 81
2.2.3.1 Temperature-Programmed Desorption (TPD) ..... 81
2.2.3.2 X-ray Photoelectron Spectroscopy (XPS) ..... 82
2.2.3.3 Fourier Transform Infrared Spectroscopy (FTIR) ..... 82
2.2.3.4 Nuclear Magnetic Resonance Spectroscopy (NMR) ..... 82
2.2.4 Thermogravimetric Analysis (TGA) ..... 82
2.2.5 Differential Scanning Calorimetry (DSC) ..... 83
2.2.6 Surface Morphology ..... 83
2.3 Experimental set-up for adsorption experiments ..... 84
2.4 Experimental set-up for alcohols decomposition ..... 85
References ..... 86

UNIVERSIDAD DE MÁLAGA

3 Chapter III: Effect of co-solution of carbon precursor and activating agent on the textural properties of highly porous activated carbon obtained by chemical activation of lignin with $H_3PO_4$ ..... 89

Abstract ..... 89

3.1 Introduction ..... 90

3.2 Experimental section ..... 91

3.2.1 Activated carbons preparation ..... 91

3.2.2 Activated carbons characterization ..... 92

3.3 Results and discussion ..... 94

3.3.1 Surface chemistry characterization of as-received and ethanol-dissolved lignin ..... 94

3.3.2 Effect of $H_3PO_4$ and low temperature oxidative treatment on lignin surface chemistry ..... 96

3.3.3 Characterization of activated carbons ..... 102

3.3.4 Effect of temperature of the oxidative treatment ..... 107

3.4 Conclusions ..... 112

References ..... 113

4 Antipyrine Adsorption on Nanoporous Lignin-Derived Activated Carbons ..... 121

Abstract ..... 121

4.1 Introduction ..... 122

4.2 Experimental section ..... 123

4.2.1 Activated carbons preparation ..... 123

4.2.2 Activated carbons characterization ..... 124

4.2.3 Adsorption experiments ..... 124

4.3 Results and Discussion ..... 125

4.3.1 Activated carbons characterization ..... 125

4.3.1.1 Effect of the $H_3PO_4$ to lignin mass ratio ..... 125

4.3.1.2 Effect of the activation temperature ..... 131

4.3.2 Antipyrine adsorption ..... 133

4.3.2.1 Surface chemistry ..... 133

UNIVERSIDAD DE MÁLAGA

4.3.2.2 Antipyrine adsorption results ..... 135
4.4 Conclusions ..... 141
References ..... 142
5 Chapter V: Alcohol Dehydrogenation on Kraft Lignin-Derived Chars with Surface Basicity ..... 147
Abstract ..... 147
5.1 Introduction ..... 148
5.2 Materials and Methods ..... 149
5.2.1 Catalyst Preparation ..... 149
5.2.2 Catalyst Characterization ..... 149
5.2.3 Alcohol Dehydration ..... 150
5.3 Results and Discussion ..... 151
5.3.1 Characterization of the Catalysts ..... 151
5.3.1.1 Textural Properties ..... 152
5.3.1.2 Surface Morphology ..... 154
5.3.1.3 Surface Chemistry ..... 155
5.3.1.4 Catalytic Activity ..... 161
5.4 Conclusions ..... 164
References ..... 165
6 Chapter VI: General Conclusions and Future Perspectives ..... 169
Abstract ..... 172
Resumen ..... 185
ملخص ..... 199
Dédicace ..... 209
Acknowledgments ..... 210

UNIVERSIDAD DE MÁLAGA

# Objectives and Overviews

The aim of this PhD thesis is the development of a methodology for the valorization of different types of lignins, Organosolv (Alcell) and Kraft, by the preparation of porous activated carbons with different textural and surface chemistry properties that allow a large adsorption capacity of emerging pollutants in aqueous phase and a high catalytic activity for alcohols decomposition reactions in gas phase.

Specifically, the effect of co-solution of carbon precursor and activating agent on the textural and surface chemistry properties of activated carbons prepared by chemical activation of Alcell lignin with phosphoric acid was analyzed, highlighting the possibility of using directly the liquors produced in organosolv process (Alcell) to prepare activated carbons by chemical activation with phosphoric acid. The influence of different parameters, such as $H_3PO_4$ to lignin mass ratio, activation temperature, gas atmosphere (oxidant or inert) and a further low temperature oxidative treatment on the porosity and surface chemistry of the resulting activated carbons was studied. The properties of these activated carbons were compared to those of activated carbons prepared by the conventional method of Alcell lignin impregnation with the activation agent ($H_3PO_4$) at similar preparation conditions. The activated carbons thus prepared were tested for the adsorption of an emerging contaminant (antipyrine) from water at low concentrations and at room temperature.

On the other hand, the preparation of basic activated carbons by carbonization of kraft lignin (sodium-lignosulphonate powder) at various temperatures followed by partial gasification with $CO_2$ was analyzed. The influence of the inorganic matter of the kraft lignin on the textural, surface chemistry and catalytic properties of the final activated carbons was also investigated. In this sense, the catalytic activity of the activated carbons obtained for the 2-propanol, ethanol and methanol decomposition reaction was also studied.

This Ph.D. thesis report is divided into 6 Chapters. Chapter I is a bibliographic review which provides information about (i) the different types of lignin and their valorization possibilities, (ii) the definition and properties of activated carbons and their preparation methods: physical activation vs chemical activation, and (iii) the main applications of

UNIVERSIDAD DE MÁLAGA

activated carbons, with special attention to adsorption (emerging pollutant from water) and heterogeneous catalysis (alcohol decomposition reactions) processes.

Chapter II describes the general methodology and experimental set-ups used in this thesis. This Chapter analyzes the preparation of the different carbon materials, their characterization and the equipment and installations used for adsorption and catalytic experiments.

Chapter III is devoted to study the effect of co-solution of carbon precursor and activating agent on the porosity and surface chemistry of activated carbons prepared by chemical activation of Alcell lignin with phosphoric acid.

Chapter IV explores in depth the influence of the $H_3PO_4$ to lignin mass ratio and the activation temperature on the textural and surface chemistry properties of the activated carbons prepared by co-solution of the carbon precursor and the activating agent. Different activated carbons were tested for the adsorption of antipyrine in aqueous solution in batch and column experiments. The adsorption equilibrium and kinetics of antipyrine on different activated carbons were analyzed.

Chapter V studied the preparation of basic carbons by direct carbonization of kraft lignin at different temperatures, followed by partial gasification of the chars with $CO_2$. The activated carbons thus prepared were tested as catalysts for the decomposition of different alcohols: 2-propanol, ethanol and methanol.

Chapter VI presents the general conclusions about the results obtained in this PhD thesis and future perspectives.

UNIVERSIDAD DE MÁLAGA

# NOMENCLATURE

| | |
|---|---|
| a | Empirical parameter ($s^{-1}$) |
| $A_{BET}$ | Surface area calculated by the BET method ($m^2/g$) |
| $A_{DR}$ | Narrow microporous surface area obtained by DR method ($m^2/g$) |
| $A_t$ | External surface area obtained by t method ($m^2/g$) |
| $a_s$ | Surface area calculated by the $\alpha_s$ method ($m^2/g$) |
| $A_s$ | External surface area obtained by $\alpha_s$ method ($m^2/g$) |
| BET | Brunauer, Emmett and Teller |
| B.O | Burn off |
| Ce | Equilibrium concentration (mg/L) |
| $C_t/C_0$ | Relative concentration |
| $C_i$ | Intel concentration (mg/L) |
| $C_t$ | Concentration at time t (mg/L) |
| d.a.f. | Dry ash free basis |
| $D_v$ | Effective internal diffusion coefficient ($m^2/min$) |
| DME | Dimethyl ether |
| DR | Dubinin-Radushkevich |
| DSC | Differential scanning calorimetry |
| FTIR | Fourier transform infrared spectroscopy |
| $K_f$ | Equilibrium constant by Freundlich equation (L/g) |
| $K_L$ | Equilibrium constant by Langmuir equation $(mg/g)(L/mg)^{1/n}$ |
| $K_{Th}$ | Thomas kinetic coefficient (mL/min mg) |
| $K_s$ | Adsorption rate constant (g/mg min) |
| NMR | Nuclear magnetic resonance spectroscopy |

UNIVERSIDAD DE MÁLAGA

| | |
|---|---|
| n | Empirical parameter depicting the energetic heterogeneity of the adsorption sites |
| $q_e$ | Adsorption accumulation capacity of carbon (mg/g) |
| $q_L$ | Maximum adsorption capacity at equilibrium of Langmuir equation (mg/g) |
| $q_m$ | Empirical parameter (mg/g) |
| $q_t$ | Adsorption capacity of carbon as a function of the contact time (mg/g) |
| Po $_{ALC}$ | Partial alcohol pressure on atm |
| $P/P_0$ | Relative pressure |
| PSD | Pore size distribution |
| R | Impregnation ratio (weight of $H_3PO_4$/weight of precursor) |
| SEM | Scanning electron microscopy |
| SEM-EDX | scanning electron microscopy with energy-dispersive X-ray |
| t | Time (min) |
| T | Temperature (°C, K) |
| TGA | Thermogravimetric analysis |
| TPD | Temperature-programmed desorption |
| V | Volume of solution (L) |
| $V_{ads}$ | Adsorbed volume ($cm^3/g$) |
| $V_{DR}$ | Narrow micropore volume obtained by DR method ($cm^3/g$) |
| $V_t$ | Micropore volume obtained by t method ($cm^3/g$) |
| $V_s$ | Micropore volume obtained by $\alpha_s$ method ($cm^3/g$) |
| $V_{meso}$ | Mesopore volume ($cm^3/g$) |
| W | Mass of the carbon (mg) |
| W | Adsorbent dose (g/L) |
| W/ $Fo_{ALC}$ | Space time (g s /µmol) |

UNIVERSIDAD DE MÁLAGA

| | |
|---|---|
| XPS | X-ray photoelectron spectroscopy |

UNIVERSIDAD DE MÁLAGA

# List of Tables

**Table 1.1.** Polymeric components of raw biomass and plant-based materials.

**Table 1.2.** Yield of Organosolv lignin under various extraction conditions.

**Table 1.3.** Kind of lignin and type of activation used to prepare activated carbons.

**Table 1.4.** Adsorption processes in water treatment.

**Table 2.1.** Nomenclature used for activated carbons prepared by chemical activation.

**Table 2.2.** Nomenclature used for activated carbons prepared by physical activation.

**Table 3.1.** Mass surface concentration of the different $H_3PO_4$-lignin derived samples and the corresponding contribution of different phosphorus surface group obtained by XPS analyses.

**Table 3.2.** Yield values of the lignin activated carbons.

**Table 3.3.** Textural properties of the different lignin derived activated carbons obtained from the $N_2$ and $CO_2$ isotherms.

**Table 3.4.** Yield values of the lignin-derived activated carbons obtained at 400 ºC and $H_3PO_4$/lignin mass ratio of 2, treated at different temperatures and stabilization times.

**Table 3.5.** Textural properties of the different lignin activated carbons obtained at 400 ºC and $H_3PO_4$/lignin mass ratio of 2, treated at different temperatures and activation times under air atmosphere, obtained from the $N_2$ and $CO_2$ isotherms.

**Table 4.1.** Textural properties of the different activated carbons prepared at 400 ºC and different $H_3PO_4$ to lignin mass ratios.

**Table 4.2.** Textural properties of the different activated carbons prepared by co-solution of lignin and $H_3PO_4$ at different activation temperatures and a $H_3PO_4$/lignin mass ratio of 2.

**Table 4.3.** Chemical characterization of the activated carbons prepared at different $H_3PO_4$/ lignin mass ratios and activation temperatures.

**Table 4.4.** Langmuir and Freundlich adsorption parameters obtained from equilibrium isotherms of antipyrine for the activated carbons.

**Table 4.5.** Parameters obtained from kinetics curves for the antipyrine ($C_0$ = 1 mg/L; adsorbent concentration = 50 mg/L).

**Table 4.6**. Parameters obtained from experimental data of breakthrough curves of the column adsorption process of antipyrine.

**Table 5.1.** Ash content, preparation yields, and ultimate analyses of the different samples.

**Table 5.2.** Textural parameters obtained from $N_2$ and $CO_2$ isotherms at −196 °C and 0 °C, respectively, of all the carbon catalysts.

UNIVERSIDAD DE MÁLAGA

**Table 5.3.** Mass surface concentration determined by X-ray photoelectron spectroscopy (XPS) analyses and amounts of CO and $CO_2$ evolved with temperature during the temperature-programmed desorption (TPD) experiment for the different carbon catalysts.

UNIVERSIDAD DE MÁLAGA

# List of Figures

**Figure 1.1.** Chemical structures of cellulose and hemicellulose.

**Figure 1.2.** Chemical representation of the three monolignols, the building blocks of lignin.

**Figure 1.3.** Structure model of lignin proposed by Adler.

**Figure 1.4.** Photographs of typical technical lignins.

**Figure 1.5**. Preparation steps of activated carbons by physical and chemical activation.

**Figure 1.6.** Mechanism of phosphate ester formation by phosphorylation of cellulose.

**Figure 1.7.** Basic terms of adsorption.

**Figure 2.1.** Experimental set-up for the preparation of activated carbons by chemical and physical activation.

**Figure 2.2.** Experimental set-up used for thermogravimetric analysis.

**Figure 2.3.** The adsorption installation of equilibrium and kinetic study.

**Figure 2.4.** The adsorption installation of column experiments.

**Figure 2.5.** Installation used for decomposition of alcohols.

**Figure 3.1.** Normalized CPMAS 13C NMR spectra (A) and FTIR spectra (B) of as-received Alcell lignin and dissolved in ethanol.

**Figure 3.2.** FTIR spectra of the different $H_3PO_4$-lignin derived samples.

**Figure 3.3.** XPS P2p spectra of the different H3PO4-lignin derived samples and deconvolution of LE2PS sample (C-O-P groups: continuous line, $P_2O_5$, dashed line).

**Figure 3.4.** A) Thermogravimetric analysis in inert atmosphere for different lignin-derived samples; B) Weight loss differences during TG analyses between the non-treated and low temperature oxidized (air) treated samples.

**Figure 3.5.** (A) DSC curves during pyrolysis of different lignin-derived samples and (B) DSC curves during treatment of L2P and LE2P with air at 200 ºC.

**Figure 3.6.** $N_2$ adsorption-desorption isotherms obtained at – 196 ºC of the different activated carbons obtained at 400 ºC and with H3PO4 to lignin mass ratio of 2.

**Figure 3.7.** Micropore size distribution of the different activated carbons obtained at 400 ºC and with $H_3PO_4$ to lignin mass ratio of 2.

**Figure 3.8.** CO and $CO_2$ evolution of the different activated carbons.

**Figure 3.9.** $N_2$ adsorption-desorption isotherms obtained at – 196 ºC of the different activated carbons obtained at 400 ºC and $H_3PO_4$/lignin mass ratio of 2, treated at different temperatures.

UNIVERSIDAD DE MÁLAGA

**Figure 4.1.** Total yields (in mass percentage) of the activated carbons prepared by conventional impregnation followed by chemical activation (LXP400) and by co-solution of lignin and phosphoric acid followed by low-temperature oxidation and chemical activation (LEXPS400) at 400 ºC as a function of $H_3PO_4$ to lignin mass ratios.

**Figure 4.2.** $N_2$ adsorption-desorption isotherms obtained at –196 ºC of activated carbons prepared at an activation temperature of 400 ºC and different $H_3PO_4$ to lignin mass ratios (a) by conventional impregnation followed by chemical activation (LXP400) and (b) by co-solution of lignin and phosphoric acid followed by low-temperature oxidation and chemical activation (LEXPS400).

**Figure 4.3.** $\alpha_s$ curves for different activated carbons prepared at an activation temperature of 400 ºC and different $H_3PO_4$ to lignin mass ratios by conventional impregnation.

**Figure 4.4.** Micropores size distribution of the different activated carbons at different $H_3PO_4$ to lignin mass ratios and at 400 ºC.

**Figure 4.5.** $N_2$ adsorption-desorption isotherms obtained at – 196 ºC (a) and pore size distribution (b) of different activated carbons prepared by co-solution of lignin and $H_3PO_4$ at different activation temperatures and with a $H_3PO_4$ to lignin mass ratio value of 2

**Figure 4.6.** CO and $CO_2$ profiles of the activated carbons obtained during TPD experiments

**Figure 4.7.** Adsorption isotherms of antipyrine on different activated carbons at 20 °C (symbols: experimental values; continuous lines: fitting to the Langmuir equation).

**Figure 4.8.** Micropores size distribution of the different activated carbons;

**Figure 4.9.** Adsorption kinetics of antipyrine on different activated carbons at 20 °C, $C_0$ = 1 mg/L; adsorbent concentration = 50 mg/L (Experimental data: dots; hyperbolic equation fittings: full line, second order adsorption kinetic equation: dashed line).

**Figure 4.10.** Effective diffusion coefficients as a function of the adsorbed amount for the activated carbons.

**Figure 4.11.** Breakthrough curves of antipyrine adsorption at 20 ºC; $C_0$ = 1 mg/L; adsorbent mass = 200 mg; flow rate = 7 mL/min. (Experimental data: dots; Thomas model: continuous line.

**Figure 5.1.** $N_2$ adsorption-desorption isotherms at −196 ºC of (a) the carbon catalysts obtained at different carbonization temperatures and (b) the series of carbons prepared at 900 ºC. Micropore size distributions of (c) the carbon catalysts obtained at different carbonization temperatures and (d) the series of carbons prepared at 900 ºC.

**Figure 5.2.** SEM micrographs of the different carbon catalysts. (a) L500; (b) L700; (c) L900; (d) L900W; (e) L900G; (f) L900WG.

**Figure 5.3.** (a) and (e) C1s, (b) and (f) O1s, (c) and (g) S2p, and (d) and (h) Na1s spectra of the different carbon catalysts at different temperatures and carbon catalysts prepared at 900 ◦C, respectively.

UNIVERSIDAD DE MÁLAGA

**Figure 5.4.** Sodium dispersion mapping from SEM equipped with energy-dispersive X-ray analyses (SEM-EDX) of the different carbon catalysts.

**Figure 5.5.** TPD profiles of the different carbon catalysts. (a, b) CO evolution; (c, d) $CO_2$ evolution of different carbon catalysts.

**Figure 5.6.** Evolution of the steady-state conversions of 2-propanol (a,b) and selectivity to acetone (filled marks) and propylene (hollow marks) with the temperature (c,d) for all the carbon catalysts in a helium flow (PoALC = 0.0185 atm; W/FoALC = 0.073 g s $\mu mol^{-1}$.

**Figure 5.7.** Evolution of the steady-state conversions of ethanol (a) and methanol (b) and selectivity to aldehydes and ketones (filled marks) and olefins and ethers (hollow marks) with the temperature for all the carbon catalysts in a helium flow (PoALC = 0.0185 atm; W/FoALC = 0.073 g s $\mu mol^{-1}$); ethanol(c) and methanol (d) conversions as a function of time on stream at different temperatures with PoALC = 0.0185 atm and W/FoALC = 0.073 g s $\mu mol^{-1}$.

UNIVERSIDAD DE MÁLAGA

# Chapter I

UNIVERSIDAD
DE MÁLAGA

# 1 Chapter I: Introduction

## 1.1 Biomass

The extended concern over fossil fuel scarcity, green house effects, climate warming issues and environmental pollution have promoted the use of renewable materials and processes [1]. The use of biomass as renewable raw materials can be an interesting approach. According to the definition of the Unites States International Trade Commission, biomass is any organic matter that is available on a renewable or recurring basis, including agricultural crops and trees, wood and wood wastes and residues, plants (including aquatics plants), grasses, residues, fibers, and animal wastes, municipal wastes and other waste materials [2]. In other words, biomass can come from a variety of sources including:

- ✓Wood from natural forests and woodlands
- ✓Forestry plantations
- ✓Forestry residues
- ✓Agricultural residues such as straw, cane trash and green agricultural wastes
- ✓Agro-industrial wastes, such as sugarcane bagasse and rice husk
- ✓Animal wastes
- ✓Industrial wastes, such as black liquor from paper manufacturing
- ✓Sewage
- ✓Municipal solid wastes (MSW)
- ✓Food processing wastes

The annual global production of biomass is predestined to exceed 100 trillion kilograms [3]. Historically, biomass has been considered as a primary source of energy for humans. Nowadays, biomass and waste accounted for about two-thirds of all renewable energy consumption in the European Union (EU) [4]. The percentage of bioenergy, defined as agricultural biomass, forest biomass and renewable waste, in EU's gross final energy consumption, increased from 5.9% in 2005 to 10.3% in 2017 [5]. However, this percentage could be exceeded, due to the great potential of biomass, which can be also considered as an important renewable source for the production of bioproducts (fine chemicals and other materials). In this sense, industrial biomass is a valuable renewable and underestimated

UNIVERSIDAD DE MÁLAGA

source of carbon for the chemical industry. For instance, it can be very useful for the production of simple building blocks (directly or indirectly), which are essential platform molecules for the chemical industry. Furthermore, some interesting biomassic components can be extracted by different techniques, such as chemical, physical, microbial or enzymatic treatments, to be applied in industrial sectors like chemistry, energy, materials, etc. Regarding the applications, the conversion technologies applied for producing materials with high added value will depend on the chemical composition of biomass (percentage ratio of its main constituents: cellulose, hemicellulose and lignin) [6]. The microfibrils of biomass are divided in the cell walls from cellulose chains that are adjusted and held together by hydrogen bonding between the hydroxyl groups on the repeating glucose units. Microlibrils groups are linked by amorphous cellulose (about 10-20% of the total cellulose) and hemicellulose, such as the array which is enclosed by lignin and some hemicellulose. The space between the microfibrils in an array is of the order of a few nanometers and in the same size range as larger micropores and mesopores [7]. Typical ranges for these biopolymer contents of hardwoods are: 42-50% cellulose, 19-25% hemicellulose and 16-25% lignin [8]. Figure 1.1 shows a representation of the molecular structures of hemicellulose and cellulose [7].

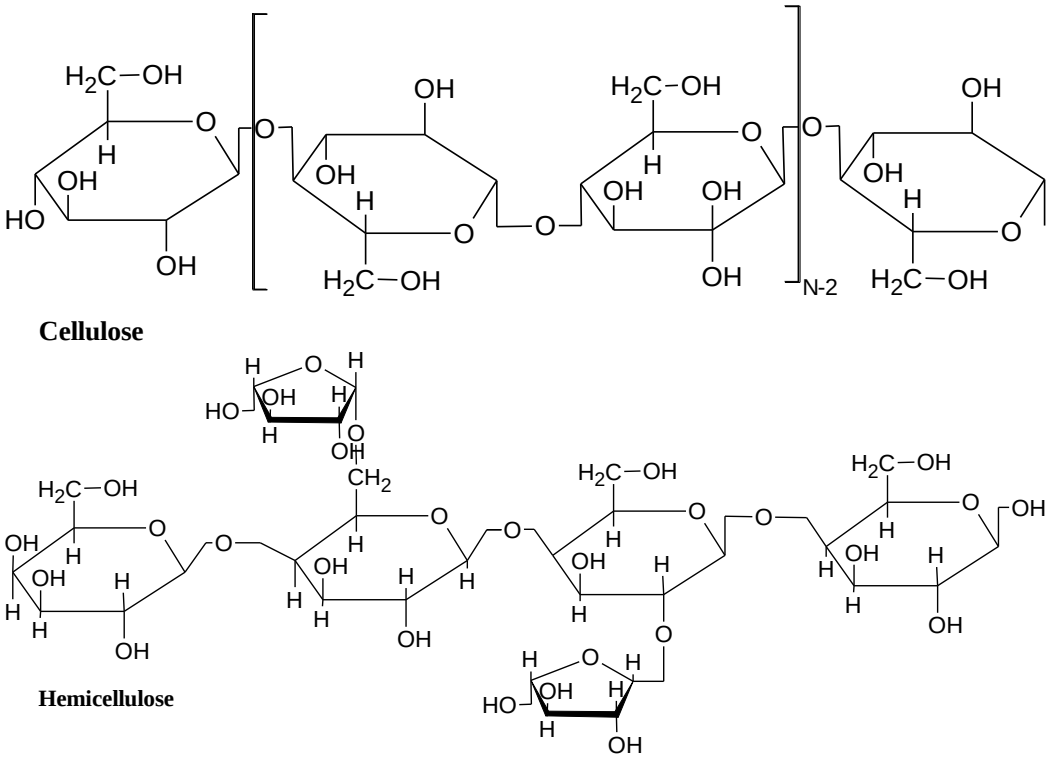


**Figure 1.1.** Chemical structures of cellulose and hemicellulose [7].

UNIVERSIDAD DE MÁLAGA

## 1.2 Lignin

Lignin is the second largest renewable source after cellulose and the most important source of aromatic compounds on Earth [9]. Specifically, lignin is present in the cell walls of wood or agricultural crops and plants, in order to provide structural strength. Lignin can have a variety of particular structures and compositions, depending on the specific plant or tree species [10], the season, the climate and the plant age, varying its composition in lignocellulosic biomass, both in terms of p-coumaryl (H), coniferyl (G), and sinapyl (S) alcohols (Figure.1.2), as well as in the relative abundance of the chemical linkages in the polymer [11]. In addition, the total content of lignin in a lignocellulosic material can also vary from 3% to 30%wt.

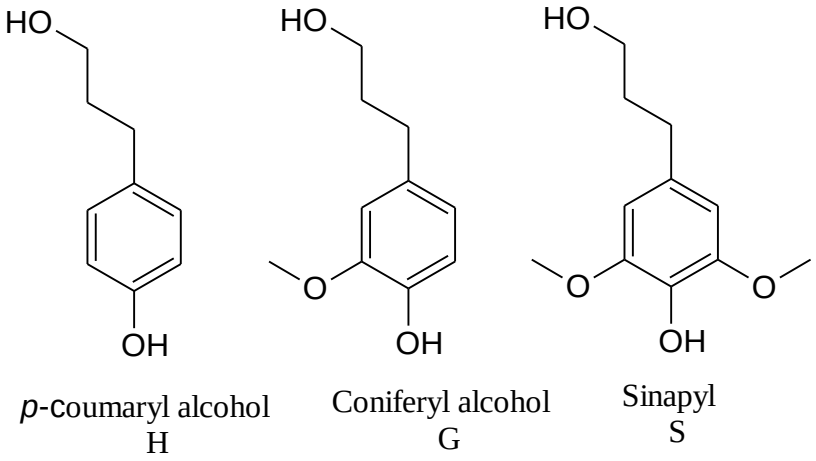


**Figure 1.2.** Chemical representation of the three monolignols, the building blocks of lignin.

Lignin is a polyphenolic polymer with a three-dimensional network. However, the final structure of the isolated lignin may present great differences due to the variety of separation methods and conditions used in the diverse delignification process, which include covalent bond rupture of natural lignin. Furthermore, different plant sources, or even lignin isolated from the same plant but in different ways, would have different categories of linkages and composition of functional groups, resulting in the complicated structure of lignin. Therefore, a structural model was usually used to represent the structure of lignin. Through nearly two decades of research on lignin structure, a dozen structural models have been proposed. This kind of structural models only describes a hypothetical structure inferred from the average results [12–14]. Figure 1.3 collects the most common structural model of lignin. As can be seen, lignin is composed of up to three different phenyl propane monomers [15]. Conferral alcohol occurs in all species and is the dominant monomer in



UNIVERSIDAD DE MÁLAGA

conifers (softwoods). Deciduous (hardwood) species contain up to 40% syringyl alcohol units while grasses and agricultural crops may also contain coumaryl alcohol units [15]. Table.1.1 shows diverse sources of lignin from different raw biomass and plant-based materials such as cotton and bagasse. Raw wood species, hardwood and softwood contain a high percentage of lignin, between 25% and 40% [16]. An additional complexity of lignin comes from the many possible bonding patterns between individual units. Thus, our knowledge about lignin chemical structure is less precise than our knowledge about other natural and synthetic polymers [14,17,18]**.**

Traditionally, the extraction of lignin from wood is carried out by different technical processes such as kraft and sulfite pulping, where it is precipitated in the formation of cellulosic fibers that are further used in commodity products like packaging, printing papers, and tissues, whereas the lignin, in most cases, is utilized as internal fuel in the process [19].

UNIVERSIDAD DE MÁLAGA

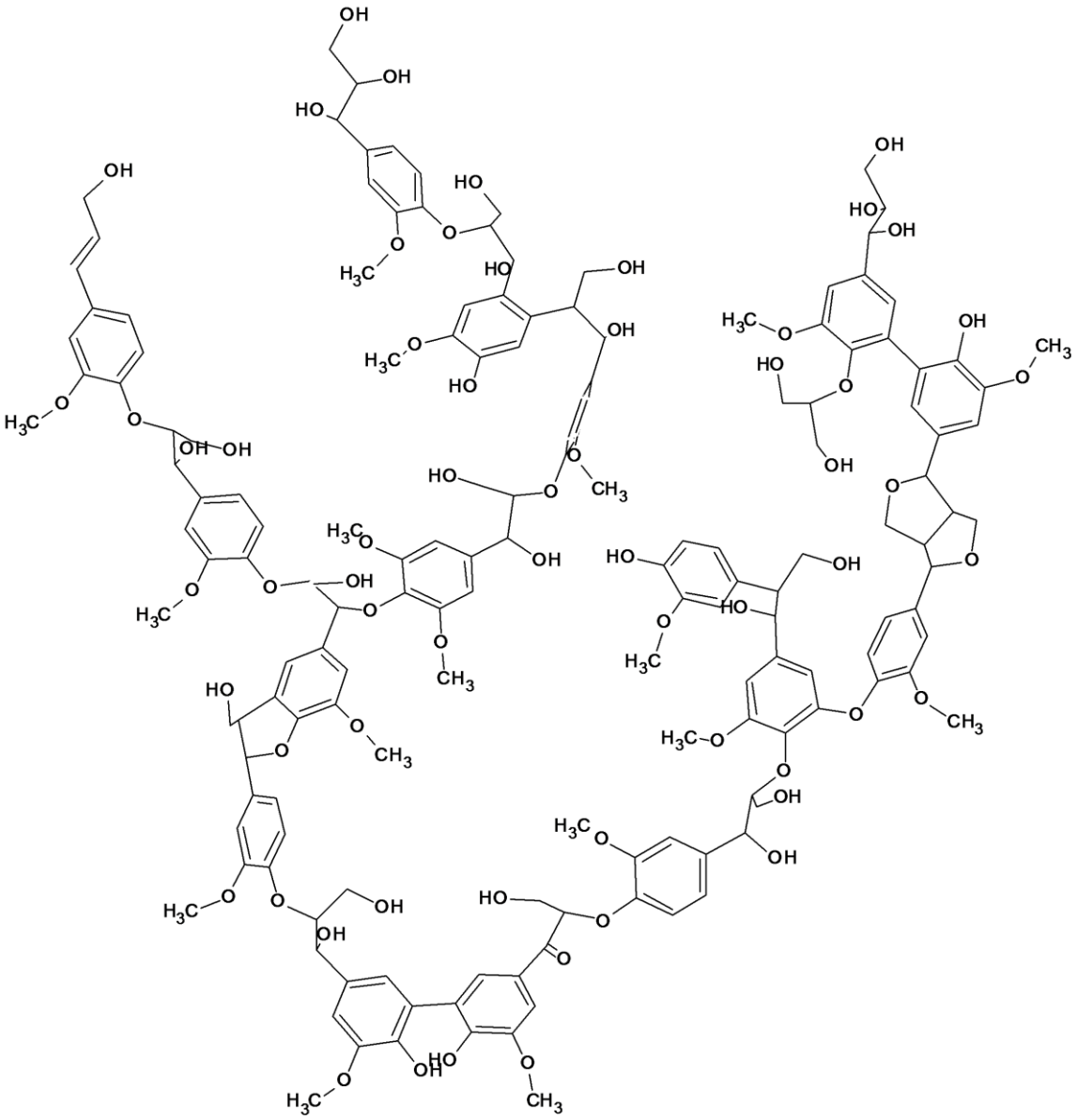

**Figure 1.3.** Structure model of lignin proposed by Adler [20].

UNIVERSIDAD DE MÁLAGA

**Table.1.1.** Polymeric components composition (%w) of raw biomass and plant-based materials [16]**.**

| Source | (%) Lignin | (%) Hemicellulose | (%) Cellulose | (%) Extract |
|---|---|---|---|---|
| Hardwood | 16-24 | 25-35 | 43-47 | 2-8 |
| Softwood | 25-31 | 25-29 | 40-44 | 1-5 |
| Bagasse | 20 | 30 | 40 | 10 |
| Coir | 43-49 | 10-20 | 32-43 | 4 |
| Corn cobs | 15 | 35 | 45 | 5 |
| Corn stalks | 35 | 25 | 35 | 5 |
| Flax (retted) | 2 | 21 | 71 | 6 |
| Hemp | 6 | 22 | 70 | 2 |
| Jute | 13 | 14 | 71 | 2 |
| Sisal | 11 | 14 | 73 | 2 |
| Wheat straw | 15 | 50 | 30 | 5 |

## 1.3 Pulping process

One of the most important possibilities of a biorefinery is to produce value-added products. In this context, many processes for producing lignin-based chemicals could be integrated into the pulping industry [9]. For historical reasons, the development of methods for lignin isolation were devoted to wood materials in the paper industry, although these methods have also been applied to grass plants, but with limited success [21,22]. Recently, some other processes for lignin isolation by industrial pulping such as soda, alkali-hydrogen peroxide and organosolv have also been studied [23–26].

### 1.3.1 Kraft pulping

The kraft pulping process is the chemical pulping method most commonly used to produce pure cellulose fibers from wood and plant sources, the main component of paper [27]. The global production of cellulose fibers using kraft pulping is the largest among all production methods, about 630,000 tons per year in 2015 [28], making kraft lignin the most common form of lignin [19,29]. Kraft pulping is one of the chemical pulping method that uses chemical agents to degrade and dissolve lignin in order to isolate pure cellulose from wood [27]. The most important step of the kraft pulping is the treatment of biomass with

UNIVERSIDAD DE MÁLAGA

sodium hydroxide and sodium sulfide (white liquors), which breaks the ether linkage by sulfide and bisulfide ions [30], at temperatures between 150 and 180°C for 2 h [31,32]. The aim of this process is the conversion of phenolic groups to quiononemethide groups by sodium hydroxide and then, the formation of a benzylthiolate anion by the attack of α-carbon atoms with hydrogen sulfide ions [16]. After that, the β-phenolate anion is liberated from the benzylthiolate anion to generate free phenolic groups. The free phenolic groups produce quiononemethide again and the same process is repeated to cleave ether bonds continuously and produce lower molecular weight soluble fragments [16]. The formation of lignin bonds C-C takes place in the last stage of the process; this generally implies a condensation reaction and yields a very strong lignin complex [27,33], as those schematized in Schemes 1.1 and 1.2. The lignin produced from this pulping process is a hydrophobic material at neutral pH and it contains approximately 1% sulfur (in atomic %), as aliphatic thiol groups [34] and with high ash content, approximately 35% [35]. Kraft lignin can be also composed of important functional groups as methoxy group (14%), aliphatic hydroxyl group (10%), phenolic hydroxyl group (2-5%), and carboxylic acid groups, whose presence can vary depending on the plant source and processing conditions [34,36]. On the other hand, most of kraft lignin obtained as by-product is used as fuel for the production of energy in the paper production and to recover inorganic components [33,34,36,37].

### 1.3.2 Sulfite pulping

The process of sulfite pulping is a method that consists of the reaction of wood or biomass with sulfur dioxide ($SO_2$) as reactive agent. This sulfur dioxide reacts with water to give sulfonic acid, under temperatures between 125-150°C and activation times of 3-7 h [16]. This process is acid-catalyzed to cleave α-ether linkage and ß-ether linkages during the pulping process [38]. Lignin can be recuperated after dissolving and separating in aqueous solution by the sulfonic acids introduced to α-carbon of ether linkages [33]. The main functional groups found in lignin from sulfate process are lignosulfonic acid, lignosulfonate, carboxylic groups together with phenolic/aliphatic hydroxyl groups [39]. Due to the high content of sulfonate, the produced lignin is water soluble. Sulfite lignin has broad molecular weights distribution and relatively high ash content. The contents of carboxylic acid and sulfonate are approximately 4% and 13%, respectively [34]. Thus, there are not wide areas of applications of these materials, being essentially used as animal feeds, particle boards, surfactants, adhesives, cement additives and stabilizer/dispersing agents

UNIVERSIDAD DE MÁLAGA

[39,40]. The lignin obtained from this process is also used as a fuel to produce energy for the pulp mill and to allow the recovery of inorganic components [33,36].

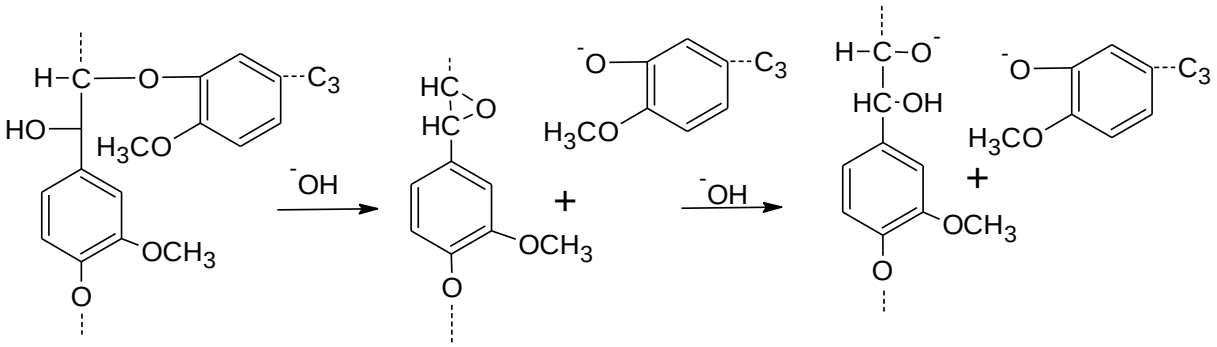

**Scheme 1.1.** Reaction of β-aryl ether linkages in nonphenolic phenylpropane units [16].

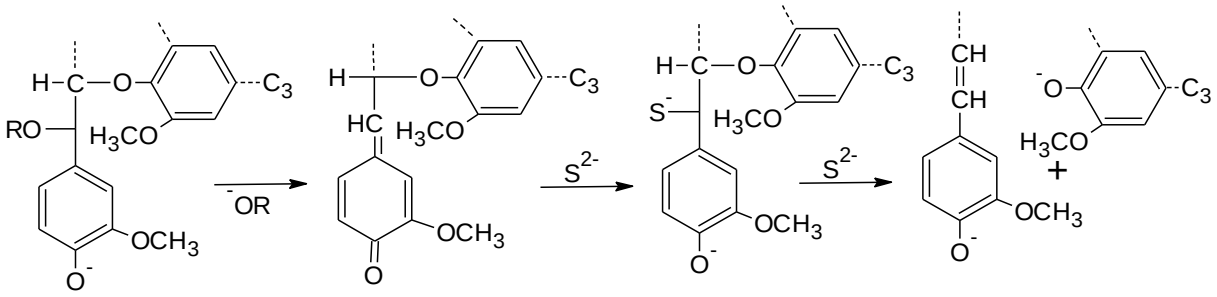

**Scheme 1.2.** Reaction of sulfide with phenolic phenylpropane units. Styrenic products are capable of further reactions to form a complex polymer mixture [16].

### 1.3.3 Soda process

The soda process is the oldest method that uses sodium hydroxide as the chemical agent of the pulping process in industry [16], and is now being used to process nonwood materials, which includes mainly annual plants and agricultural waste, such as wheat straw, sisal, kenaf, hemp and bagasse [16]. This process involves the reaction between the biomass (raw material) and sodium hydroxide, with concentrations of ca. 1 M, at temperature of about 170°C and high pressure (ca. 10 psi) [41]. During the soda process, the bond α-ether can be easily hydrolytically cleaved (Scheme 1.3), resulting in fragments of molecules of lignin with high solubility, making it an effective process for delignification [16]. Frequently, the anthraquinone (AQ) is also added to the reaction, which can oxidize the carbohydrates and forms anthrahydroquinine (AHQ). The β-O-4 ether linkage can be easily cleaved by the AHQ dianion during this process, via nucleophilic attack by reacting with quinine methides resulted from the soda reactions, thus regenerating the AQ (Scheme 1.4).

UNIVERSIDAD DE MÁLAGA

Addition of AQ can significantly increase the delignification rates; Lunquist et al reported a reduction in cooking time from 250 min for soda to 90 min for soda-anthraquinone in studies on spruce wood [42]. Moreover, the lignin obtained from the soda process is considered as being closer to natural one. These lignins have been used as precursor for raw materials in a wide range of applications due to the absence of sulfur functionalities [33,41].

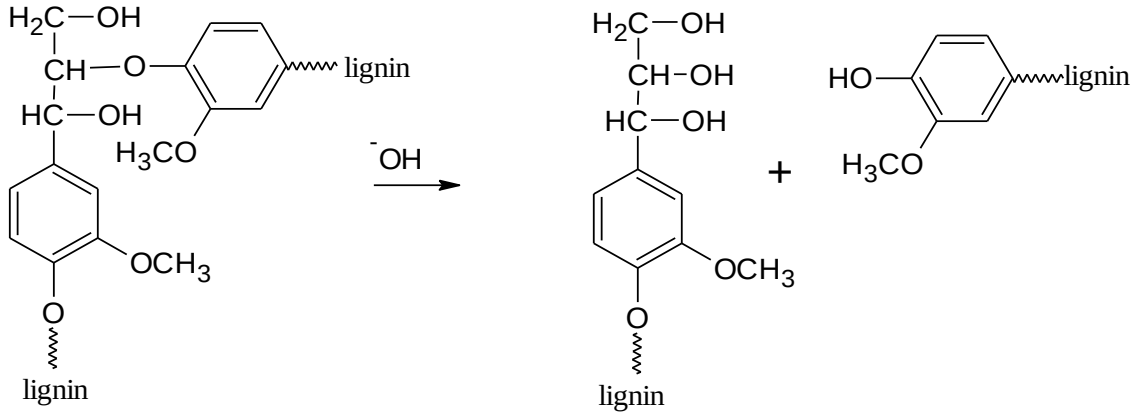


**Scheme 1.3.** Cleavage of the α -ether bond in lignin during the soda process [16].

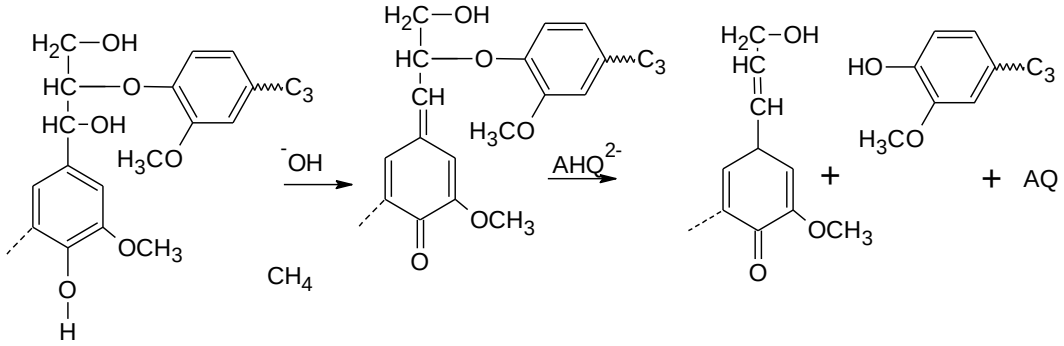


**Scheme 1.4.** Cleavage of the β-O-4 ether linkage in the presence of anthrahydroquinine in the soda process [16].

### 1.3.4 Hydrothermal process

The hydrothermal process also known as “steam explosion process” needs highly compressed water, high pressure (200-2000 psi) and high temperature (180-230°C) during a short processing time of 1-20 min in the presence of a catalyst [43–46]. Hydrolysis, aryl ether cleavage and homolytic cleavage of carbon-carbon (C-C) bond, demethoxylation, alkylation, and condensation reactions occur during the steam process [47,48], whereas the aromatic groups in the lignin obtained are not demeaned by the steam. However, β-O-4 ether linkages and Cα-Cβ bonds are being cleaved during the process. The resulting lignin presents

UNIVERSIDAD DE MÁLAGA

a similar character as that of organosolv lignin, such as a low molecular weight and good solubility in organic solvents [38,49]. Steam explosion has a great potential as the first step to produce biofuel prior to fermentation of polysaccharide [50].

### 1.3.5 Organosolv pulping

A wide range of organic solvents has been proposed for the delignification of lignocellulosic raw materials. Organosolv processes represent a large family of methods used to delignify biomass and there are several reviews on these methods [39,51–54].

Organosolv pulping process consists of delignification of wood using organic solvents and has been the subject of significant research activity since the idea was proposed in the last century [51]. Organosolv lignins are usually recovered from spent organosolv pulping liquors by precipitation in water after evaporating organic solvents [49]. The most organic solvents used in organosolv pulping process are alcohols with low boiling point, such as ethanol and methanol, as specific alcohols, although other solvents have also been proposed, such as acetic and formic acids [49].

The Alcell method is a type of organosolv pulping process based on ethanol as solvent that uses sulfuric acid as catalyst, which has been commonly studied for the pretreatment of lignocellulosic materials for ethanol production [31]. Ethanol is the most efficient solvent to solubilize lignin cleavage products formed as a result of catalyst action [16]. While it was originally developed for hardwoods, some studies have focused on adapting this method for softwoods, such as pine [55], as well as agricultural residues [56]. Table 1.2 compiles the yields of organosolv lignin under diverse extraction conditions, such as solvent, volume ratio of ethanol/water, temperature, time and concentration of $H_2SO_4$. As can be seen, the optimized conditions for 79% of lignin recovery from the softwood are 170°C, 60 min, 1.1% $H_2SO_4$, and 65% ethanol/35% water [57]. Characteristic molecular weights for these lignins are $M_w$ ~ 2000 g/mol with a polydispersity of ~ 2.0. Interestingly, Alcell lignin products tend to be richer in phenolic hydroxyl groups, making them highly effective at radical scavenging [58].

UNIVERSIDAD DE MÁLAGA

**Table 1.2.** Yields of Organosolv lignins under various extraction conditions [49].

| **Organics solvents/water[1]** | | **Ethanol/water[2]** | | **Ethanol/water[3]** | | **Ethanol/water[4]** | |
|---|---|---|---|---|---|---|---|
| **Organic solvent** | **Yield (%)** | **Volume ratio** | **Yield (%)** | **$H_2SO_4$ concentration** | **Yield (%)** | **Time (h)** | **Yield (%)** |
| Ethanol | 27.7 | 40/60 | 24.8 | 0 | 20.0 | 1.0 | 24.1 |
| Methanol | 24.2 | 50/50 | 24.9 | 0.01 N | 19.9 | 1.5 | 26.9 |
| 1-Propanol | 27.1 | 60/40 | 27.7 | 0.02 N | 27.7 | 2.0 | 27.7 |
| n-Butanol | 23.9 | 70/30 | 31.2 | 0.03 N | 27.6 | 2.5 | 27.8 |
| Dioxane | 24.2 | 80/20 | 29.8 | 0.1 N | 27.9 | 3.0 | 28.0 |
| Acetone | 26.4 | 90/10 | 24.1 | 0.5 N | 32.5 | 5.0 | 28.3 |
| | | | | 1.0 N | 43.4 | 12.0 | 28.7 |

[1] Organics solvents volume ratio of 60/40, 0.02 N $H_2SO_4$ at 75 ºC for 2 h

[2] 75 ºC for 2 h

[3] Ethanol/water volume ratio of 60/40 at 75 ºC for 2 h

[4] Ethanol/water volume ratio of 60/40 at 75 ºC and 0.02 N $H_2SO_4$

Figure 1.4 collects some photographs of the different types of technical lignins. The images clearly evidence differences in their physical appearance, such as colour and morphology.

**Figure 1.4.** Photographs of typical technical lignins.

The global production of lignin was about 1300 thousand Mt in 2017 [59]. The main current use of lignin is as fuel and power generation and only a small percentage of the produced lignin is being marketed. However, lignin has also a high potential for its



UNIVERSIDAD DE MÁLAGA

conversion into value-added products (advanced chemicals and carbon materials) that could considerably enhance the economics of a biorefinery [60]. Specifically, lignin can be considered as a green alternative to many petroleum-derived substances, such as fuels, resins, rubber additives, thermoplastic blends, binders, dispersants, dust suppressants, food additives, pharmaceuticals and also being a source for industrial aromatic productions, such as phenolics compounds, guaiacol, bio-plastics, vanillin, etc. [61–69]. Due to its high carbon content (varying between 51 and 65%) [70–72], lignin can be deemed as an ideal precursor for carbon materials such as carbon black, glassy carbon, amorphous carbon, fullerenes, carbon nanotubes, intercalation compounds, pyrolytic carbon, polymer-derived carbon, carbon fibers, activated carbon etc.

Currently, the use of lignin in the preparation of multi-component (low price and high performances) materials have been increased due to the resulting properties derived from the use of lignin, such as non-toxic materials, low density, high hardness, good thermal properties and chemical, friction and humidity resistance [60,61]. Among them, the preparation of activated carbons from different technical lignins was evaluated in this thesis. The textural and surface chemical properties of activated carbons will depend on the method of isolation and type of surface functional groups of lignin [73], in addition to the preparation method.

## 1.4 Activated carbon

Activated carbon is a generic term for a family of highly porous carbonaceous materials, with high internal surface area [74], usually prepared by carbonizing and activating organic substances. Activated carbons usually have a well-developed porous texture with a large internal surface area, ranging from 500 to 2000 $m^2/g$ [75], high thermal and chemical stability and, in addition, with a surface chemistry that can be easily modified. Various raw materials are commonly used to manufacture activated carbons, like sawdust, peat, lignin, lignite, coal, wood, residues, coconut shells, petroleum coke, among others [74].

Activated carbon is considered as a complex material and a better understanding of its structural characterization, activation kinetics and surface chemistry is pivotal for interests toward industrial application of this product [76]. Porosity in activated carbons can be considered as molecular space. Porosity is created during the carbonization process of an organic macromolecular precursor (such as cellulose and lignin). During this process,

UNIVERSIDAD DE MÁLAGA

hydrogen and oxygen atoms are released and the removal of small volatile molecules produces some "distortions" within the structure of the precursor. Meanwhile, the resultant "skeletal" structures become extremely unstable and carbon atoms within these structures combine with other near-neighbor-carbon atoms to create positions of maximum stability (minimum energy), as far as the available stereochemistry allows it [77]. Based on pore sizes, the International Union of Pure and Applied Chemistry, has classified porous into three types:

- ✓ micropores < 2.0 nm
- ✓ mesopores 2.0-50 nm
- ✓ macropores >50 nm

Activated carbons contain, in addition to carbon atoms, other elements, such as hydrogen and oxygen, as well as, nitrogen and sulphur and inorganic mineral matter depending on the precursors used to their manufacture. The presence of these atoms in the structure modifies the properties of the carbons, but the significant influence comes from the oxygen, especially edge-bonded-oxygen. An efficient industrial application of activated carbons necessitates a comprehension of these surface oxygen complexes [77]. Some of these surface oxygen-containing groups of activated carbons present acid character such as carboxylic, lactonic and anhydride groups, some others show basic character such as carbonyl, ether, quinone and phenol groups [78]. Actually, the final commercial activated carbons are the results of many intensive researches to optimize their physico-chemical properties to their proper corresponding applications [79,80].

## 1.5 Activated carbons preparation methods

The available methods for activating the carbon precursors can be classified in two types, namely, physical activation and chemical activation, depending on the activating agent used.

UNIVERSIDAD DE MÁLAGA

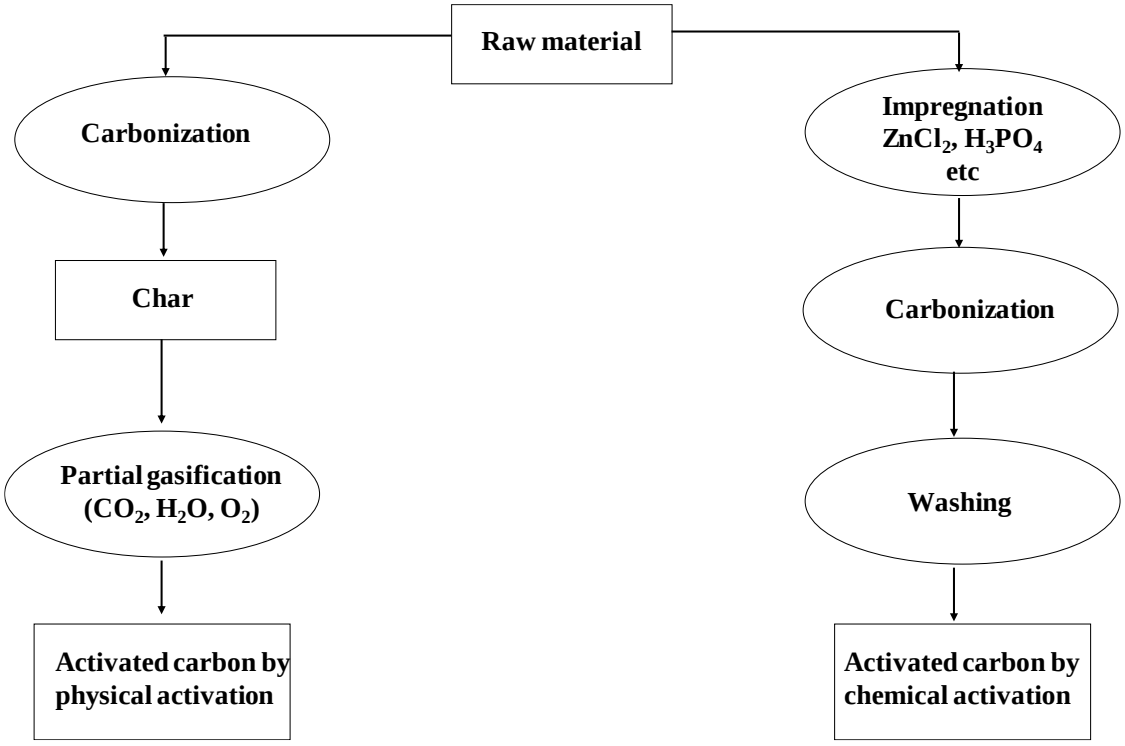


**Figure 1.5**. Preparation steps of activated carbons by physical and chemical activation.

### 1.5.1 Physical activation

Physical activation is a process in which the raw material is transformed into a porous carbon using a gas as activating agent in a two-step process [75]. The first stage is known as carbonization (or pyrolysis) and it involves the formation of a char, which is normally nonporous, by heat treatment of the precursor at temperatures in the range between 500–900°C under an inert atmosphere, usually nitrogen or the pyrolysis gases themselves [81–84]. Pyrolysis can be considered as the thermal decomposition of biomass in the absence of oxygen. During pyrolysis, the release of volatile takes place, along with the formation of a non-porous (or a very narrow microporous) carbonaceous solid, known as char. This process also involves the release of water, $CO_2$, CO, $CH_4$ and traces of $H_2$ and $C_2$ hydrocarbons. The composition of the chars in primary reactions depends on the raw materials used and the conditions of the pyrolysis process (as temperature and heating rate) [85]. In the secondary reactions, where the decomposition of volatile matter is achieved, volatile condensable organic products are converted into low-molecular weight gases and char at high temperature. Moreover, the commonly chemical composition in the second pyrolysis step usually is carbon dioxide, acetylene, ethylene, ethane and hydrogen [85]. The resulting char

UNIVERSIDAD DE MÁLAGA

may be affected by the pyrolysis conditions such as temperature, heating rate and residence time that can further affect to the properties of the final products (activated carbon).

Activation is the second step of the process, which consists of the partial gasification of the char obtained in the first step (pyrolysis or carbonization) with an oxidizing gas, such as $CO_2$, $O_2$ or steam, at a temperature range between 600–1200°C. This treatment results in the removal of less ordered carbon structure, with the formation of a well-developed micropore structure [81,82,86,87]. During the gasification of the chars with $CO_2$ as the reacting gas, the following reactions occur [85]:

$$C_f + CO_2 \longrightarrow C(O) + CO \quad (1)$$

$$C(O) + CO \longrightarrow C_f + CO_2 \quad (2)$$

$$C(O) \longrightarrow CO + C_f \quad (3)$$

In the presence of steam ($H_2O_v$) as oxidising gas, the reactions follow the steps:

$$C_f + H_2O \longrightarrow C(O) + H_2 \quad (4)$$

$$C(O) + H_2 \longrightarrow C_f + H_2O \quad (5)$$

$$C(O) \longrightarrow CO + C_f \quad (6)$$

$$C_f + H_2 \longrightarrow C(H)_2 \quad (7)$$

$$C(H)_2 \longrightarrow C_f + H_2 \quad (8)$$

$$C_f\ 1/2\ H_2 \longrightarrow C(H) \quad (9)$$

$$C(H) \longrightarrow C_f + \tfrac{1}{2}\ H_2 \quad (10)$$

During the partial gasification in the presence of $O_2$, the following reactions take place [85]:

$$2C_f + O_2 \longrightarrow 2\,C(O) \quad (11)$$

$$C(O) \longrightarrow CO \quad (12)$$

$$2C(O) \longrightarrow CO_2 + C_f \quad (13)$$

$$C(O) + O_2 \longrightarrow CO_2 / C(O) + C(O) \quad (14)$$

$$C_f + CO_2 \longrightarrow CO + C(O) \quad (15)$$

Where $C_f$ represents an active site of the carbon, C(O) a surface carbon-oxygen complex and $C(H)_2$ a surface hydrogen inhibition complexe [85,88–92].

Physical activation is considered to be an environmentally benign technology, because it does not produce wastewater during the washing steps, due to the use of gaseous agents, which supposes an advantage over other methods (chemical activation). However, it takes long time and much energy for producing microporous activated carbon through these two steps. In addition, another inherent drawback of this method is the large amount of

UNIVERSIDAD DE MÁLAGA

carbonaceous mass eliminated to obtain a well-developed porous structure, which reduces the preparation yields, having an inversely proportional relationship with the development of the porous texture.

The preparation of activated carbon from lignocellulose materials by physical activation has been studied by several authors. Among them, Lussier et al. analyzed the production of activated carbon from fruit stones under steam and $CO_2$ gas at two different temperatures 800 and 900 °C, with activation times between 2 and 3 h [83]. They obtained an activated carbon from cherry stone with apparent surface area close to 1300 $m^2/g$ under steam activation at 800 °C and 2 h. The results demonstrated that the use of steam as reacting agents was more effective than $CO_2$ to produce an activated carbon with a well-developed structure. On the other hand, Chang et al. reported the effect of burn-off on the porous structure of activated carbons prepared by steam and $CO_2$ activation of corn cob at 800 and 900 °C [93]. The highest surface (1705 $m^2/g$) area was obtained by $CO_2$ activation at 900 °C, for a burn-off of about 71 %wt. Ahmadpour and Do also evaluated the preparation of activated carbon from coal with $CO_2$ as activating agent. They obtained the highest porosity development at 800°C, for carbons with surface area and pore volume values of 754 $m^2/g$ and 0.316 $cm^3/g$, respectively [84]. The physical activation of palm shell under $CO_2$ and steam at 850 ºC and at different activation times was reported by Arami-Niya al. [94]. They observed that the surface area and micropore volume increased continuously with the increase of both the burn-off and activation time, obtaining a maximum surface area of 1213 $m^2/g$, with a micropore volume of 0.58 $cm^3/g$. Williams and Reed analyzed the preparation of activated carbon from biomass waste under steam/nitrogen as activating agent at 800 ºC [95]. The authors investigated the effect of carbonization temperature (450, 550 and 650 ºC) of the chars on the textural properties of the final activated carbons. They revealed that physical activation increased the microporous structure at low degrees of carbon burn-off but developed the mesoporous structure at higher degrees of burn-off. The highest area obtained was about 840 $m^2/g$. Namasivayam and kadirvelu used coir pith as precursor for producing activated carbons by physical activation under steam for 1 h and evaluated the effect of activation temperature (400-800 ºC) and the mixing of water with coir pith [96]. The activated carbons obtained display apparent surface areas between 300 and 500 $m^2/g$. Rodriguez-Reinoso and Molina-Sabio reported the physical activation of olive stones, peach stones and almond shell in $CO_2$ or in steam-nitrogen mixtures [97]. They proved that the physical activation with $CO_2$ opened the microporosity, also increasing the mesoporosity

UNIVERSIDAD DE MÁLAGA

and/or macroporosity. The final activated carbons had a well-developed micro- and macroporosity, with a relatively small contribution of mesoporosity; whereas the gasification with water-nitrogen mixtures produced an activated carbon with well-developed macroporosity. The preparation of activated carbon by carbonization of orange skin and partial gasification with $CO_2$ was reported by Rosas et al. [98]. $CO_2$ gasification was catalyzed by potassium and calcium present in the inorganic matter of the char. After a thermal treatment up to 900 ºC followed by the removal of the inorganic matter, an activated carbon with a highly developed porous structure (surface area close to 1200 $m^2/g$) and a significant contribution of mesopores was obtained. Alcañiz-Monge et al. prepared activated carbon fibres by $CO_2$ and steam activation of a pitch-based carbon fibre at 887 ºC [99]. They reported that the surface area and microporous volume increase with the increase of burn-off. The highest surface area obtained was 1930 $m^2/g$ and 1700 $m^2/g$ with $CO_2$ and steam activation, respectively. They concluded also that the $CO_2$ activation generated the narrow microporosity while the steam produced wider pore size distribution. Cazorla-Amorós et al analyzed the effect of the calcium in the porosity development during the activation of almond shell in steam and $CO_2$ [100]. They stated that calcium is more active to CO, than to steam. They reported that the use of calcium in the activation process can be a good procedure to create wider pores compared to uncatalyzed carbon during gasification steps.

### 1.5.2 Chemical activation

Chemical activation proceeds upon carbonization of biomass with the introduction of certain activating agents that facilitate the thermal decomposition of the carbon precursor with a reduced formation of tarry matter. From this preparation method, activated carbons present high porosity without requiring a further gasification steps, as that needs in physical activation [75]. Chemical activation involves impregnation with the activating agent, mainly phosphoric acid [7,101], although zinc chloride [102] and sulphuric acid have also been used as activating agents. Other chemical agents also suggested for its use are potassium, sodium and calcium carbonates, hydroxides, and also chloride salts of magnesium, calcium, ferric iron, and aluminium [62,75,102–105]. These chemicals have in common their strength as dehydrating agents and act under heating in a nitrogen flow at temperatures in the range between 300–900°C, depending on the activating agent used. Carbonization and activation proceed simultaneously, and the method often leads to activated carbon materials with higher weight yields, surface areas and micropore volumes and wider micropore size

UNIVERSIDAD DE MÁLAGA

distribution. In general, these materials are more suitable, for instance, for liquid phase adsorption applications [86].

#### 1.5.2.1 Chemical activation with phosphoric acid ($H_3PO_4$)

The activating process of biomass materials with phosphoric acid has been studied in detail by Jagtoyen and Derbyshire [7], who analyzed the evolution of the reaction with temperature. The phosphoric acid reacts with the biomass raw material straight away, once the components are mixed [7]. After increasing the temperature to 50°C, there are evidences of chemical and physical changes in the structure of the raw material. For the case of wood, as Jagtoyen and Derbyshire confirmed, phosphoric acid firstly attacks hemicellulose and lignin, maybe due to the easier access to these amorphous biopolymers than to the crystalline cellulose [7]. Even at high temperature, the general integrity of the cellulose structure is retained after reaction with phosphoric acid [106], moreover the structure of the cellulose has been reported to be more resistant to acid hydrolysis than other polysaccharides [107].

The principal effects of phosphoric acid attack are to hydrolyze glycosidic linkages in polysaccharides (hemicellulose and cellulose) and to cleave aryl ether bonds in lignin. These reactions are also accompanied by dehydration, degradation and condensation [107]. Principally, the initial reaction of hemicellulose and lignin with phosphoric acid can lead to a reduction of molecular weight in the structure of biomass [7]. When increasing activation temperature ($150<T<450$ °C), cross-linking reactions predominate over the reactions of depolymerization and link-breaking [7]. The greater yield of carbon obtained by acid treatment above about 300°C is attributed to a high incidence of structural crosslinking that serves to retain relatively low molecular weight species in the solid phase [7]. Figure 1.6 represents the formation of phosphate esters by reaction of cellulose with phosphoric acid. As Jagtoyen and Derbyshire detailed in their work [7], the addition or insertion of phosphate group separates the organic species and generates a dilation of the structure.

UNIVERSIDAD DE MÁLAGA

T<450°C: Formation of phosphate on cellulose side chains and crosslinking

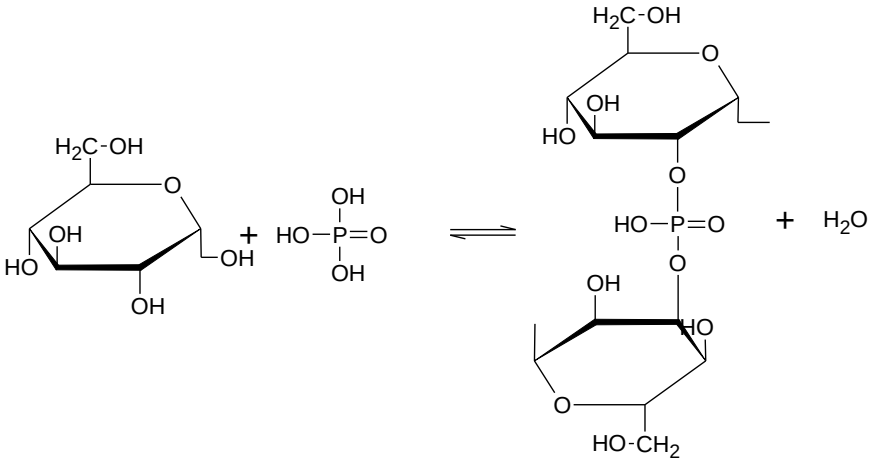

Esters can be derivatives of ortho-pyro-and meta-phosphoric acids

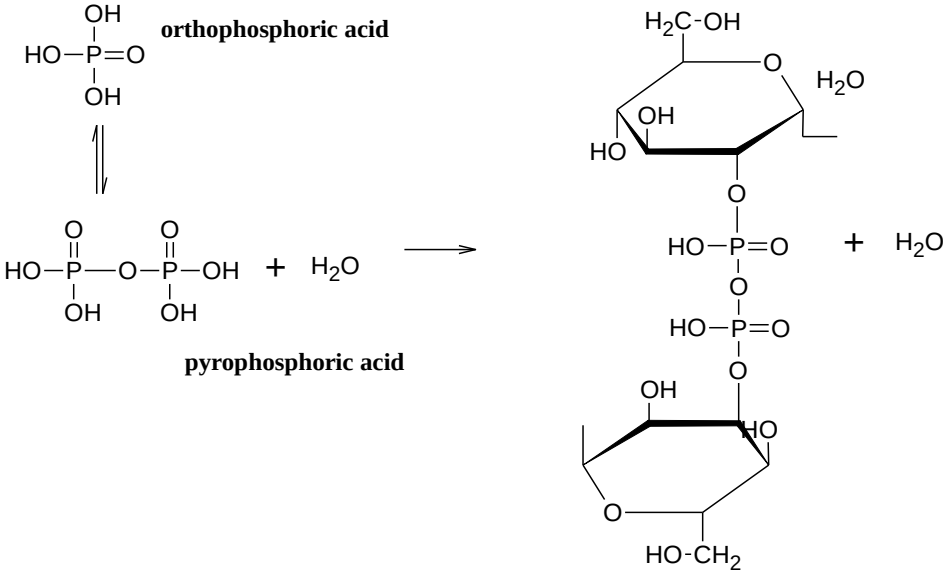


T>450 °C: Elimination of $H_3PO_4$

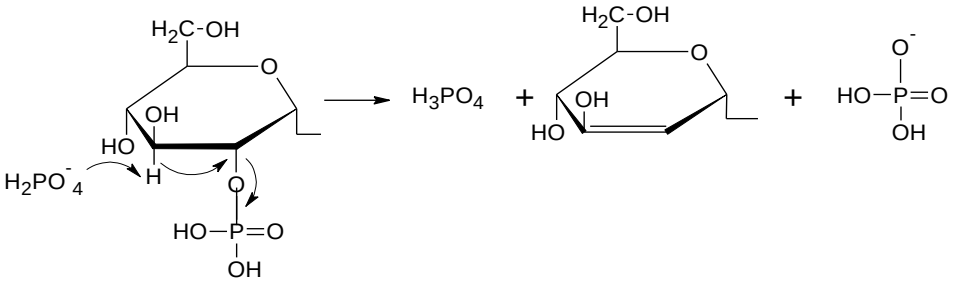

**Figure 1.6.** Mechanism of phosphate ester formation by phosphorylation of cellulose [7].

At 280°C, the structure is considered to be composed of quietly small polyaromatic units that are linked mainly by phosphate and polyphosphate bridges that can combine polyethylene linkages [$(CH_2)_n$]. As the temperature increases, cycling and condensation

UNIVERSIDAD DE MÁLAGA

reactions occur, which increase the aromaticity and size of the polyaromatic units, as a result of the splitting of the C-O-P type bonds [7].

Therefore, phosphoric acid seems to function in two ways: (i) as an acid catalyst favorizing bond cleavage reactions and the formation of crosslinks trough the cyclization, and condensation processes; (ii) and by combining with organic species to form phosphate linkages, as phosphate and polyphosphate esters that can obey to link and crosslink biopolymer fragments [108].

On other hand, it has been reported that the activation with phosphoric acid generates some P-complexes, which remain on the carbon surface even after the hot washing step of the preparation procedure [102-105]. These phosphorus surface complexes are mainly in form of C–O–$PO_3$, C–$PO_3$ and C–P groups [109,110] and present a high thermal stability (up to 800 ºC under inert atmosphere) [111]. In addition, the presence of these C−O−P type surface groups are responsible for an interesting redox functionality of high chemical and thermal stability, as well as of the high oxidation resistance, surface acidity and high oxygen content of these activated carbons [111,112].

#### 1.5.2.2 Chemical activation with other activating agents

Chemical activation of lignocellulosic materials presents great interest and advantages not only from environment, but also from an economical point of view. Lillo-Ródenas et al. prepared activated carbon form Spanish anthracite by chemical activation, they analyzed the effect of different preparation variables such as the activating agents (KOH and NaOH), heating rate, activation temperature, activation time and, finally, the activation atmosphere, on the pore structure of activated carbons [113–115]. They succeeded to produce an activated carbon with very high surface area and micropore volume values, up to 3290 $m^2/g$ and 1.45 $cm^3/g$, respectively, using KOH as activating agent, at 700 °C and an impregnation ratio of 4. Carvalho et al. also evaluated the effect of KOH as reacting agent for the chemical activation of cork waste for the preparation of activated carbons [116]. They produced activated carbons with apparent surface area of 1415 $m^2/g$ and micropore volume of 0.60 $cm^3/g$. They demonstrated that the supermicroporosity of the carbon increased proportionally to the activation temperature. The production of activated carbon by chemical activation of fruit stones and shells with $ZnCl_2$ was reported by Aygün et al. [117]. The activated carbon obtained had a relative high surface area (793 $m^2/g$) and a developed micropore structure. They mentioned that the natural materials used appeared to be very suitable starting materials for the preparation of activated carbons because of their low ash



UNIVERSIDAD DE MÁLAGA

content. Moreover, Nayak et al. compared the activation of lignocellulosic waste by $ZnCl_2$ and KOH [118]. They proved that under similar conditions of temperature and impregnation ratio (600 ºC and 1.05, respectively), the carbons presented significant differences in the porosity and, hence, in the surface area, which were much higher for the carbon prepared by $ZnCl_2$ (2430 $m^2/g$) than for the carbon from KOH (1506 $m^2/g$). More recently, Bedia et al. prepared activated carbon from Tara gam by chemical activation with $FeCl_3$, varying the activation temperature in the range between 400-1000 ºC and the impregnation ratio between 0.5-3 [119]. They obtained an activated carbon with a well-developed microporous structure, a BET surface area of 1680 $m^2/g$ and a pore volume about 1 $cm^3/g$, at a temperature of 800 ºC and an impregnation ratio of 2.

On the other hand, Sych et al. prepared an activated carbons with very high surface areas by activation of corncob with $H_3PO_4$ at 400 ºC and at impregnation ratios ranging between 0.5 and 1.25 [120]. The highest surface area, 2081 $m^2/g$ with pore volume of 1.1 $cm^3/g$, was obtained at an impregnation ratio value of 1. The authors stated that the contained carbons showed a wide amount of acidic surface groups. Molina-Sabio et al. also reported the preparation of activated carbons by heat treatment of peach stones impregnated with $H_3PO_4$ [121]. They obtained activated carbons with high apparent surface areas, up to 1634 $m^2/g$. On the other hand, Benaddi et al. evaluated separately the role of the different gases ($N_2$, $O_2$, $CO_2$, $H_2O$) on activation of wood by phosphoric acid at 480 ºC and impregnation ratio of 2.4 [122]. The results obtained showed a highly development of porosity, with surface areas ranging from 1500 to 2200 $m^2/g$. Moreover, they concluded that the lowest surface areas resulted under carbon dioxide and steam. Bedia et al. prepared activated carbons by chemical activation of olive stone, plywood waste and hemp canes with phosphoric acid [110]. The surface area obtained depended on the impregnation ratio and also on the nature of the precursors. Rosas et al. also prepared activated carbon by chemical activation of hemp fibres and canes with phosphoric acid. They studied the effect of impregnation ratio and activation temperature on the porous structure [109,123]. A surface area of 1300 $m^2/g$ and a significant mesopores contribution with a volume up to 1.25 $cm^3/g$ were obtained from hemp fibres, at the optimal preparation conditions (550ºC and impregnation ration of 3). Activated carbon monoliths with a maximum BET surface area of 1500 $m^2/g$ and mesopore volume of 0.6 $cm^3/g$ were also obtained from hemp canes. In this case, the porosity development was strongly influenced by both impregnation ratio and activation temperature, with the increase in the amount of phosphoric acid leading mainly

UNIVERSIDAD DE MÁLAGA

the mesopores development. García-Mateos et al. synthesized activated carbon from olive stones with phosphoric acid at 500 ºC and at impregnation of 3 for an activation time of 2 h [124]. After a thermal treatment at 900 ºC, the activated carbon still showed a well-developed structure with a surface area of 1000 $m^2/g$ and pore volume of 0.91$cm^3/g$. Moreover, Valero-Romero et al. studied the effect of increasing the activation temperature on the textural properties of the final porous solid. They also used olive stone as precursor to prepared activated carbons by chemical activation with $H_3PO_4$ at 800 ºC and impregnation ratio of 2, for 2h and relative high surface area values (1380 $m^2/g$) were also obtained [111].

The preparation of activated carbons by chemical activation with other less conventional reacting agents such as $Ba(OH)_2$, $Ca(OH)_2$ and $H_2SO_4$ has been also studied [102,125]. In general, the activated carbons obtained showed a microporous structure with apparent surface areas between 68 and 754 $m^2/g$.

## 1.6 Activated carbons from lignin

The high carbon content and the similarity in terms of molecular structure to bituminous coal make the lignin an ideal precursor for the preparation of activated carbons. Table 1.3 summarizes some works in which the preparation of activated carbons from lignin by physical and chemical activation were analyzed. This table includes the oxidizing/gasification gas, chemical activation agents used, and the surface area of the activated carbon obtained. Among these works, the studies of Rodriguez-Mirasol et al. using eucalyptus kraft lignin as precursor for the preparation of activated carbons can be highlighted, in which they reported $CO_2$ partial gasification at temperature of 850 °C for 20 h to obtain activated carbon with surface area value of 1850 $m^2/g$ and micropore volume of 0.57 $cm^3/g$ with [81,82]. They concluded that the microporosity and the widening of micropore size distribution increased proportional to the activation time. On the other hand, Baklanova et al. analyzed the effect of carbonization temperature using hydrolytic lignin as raw material. It was suggested that carbonization temperatures of 600–700 °C could be used for producing microporous char materials with narrow micropores using argon [126]. These porous carbons presented apparent surface area of 865 $m^2/g$ and micropores volume of 0.37 $cm^3/g$, with an average width of 0.60–0.66 nm. Carrott et al. evaluated the use of kraft and hydrolytic lignins for the preparation of activated carbons with $CO_2$ or steam. They obtained activated carbons with different textural properties due to the differences in raw materials and in the oxidising gas used. The produced carbons had surface areas between 1400 and 1600 $m^2/g$, with micropore volumes between 0.5 and 0.6 $cm^3/g$ [127].

UNIVERSIDAD DE MÁLAGA

With regard to the chemical activation of lignin, Gonzalez-Serrano et al. evaluated the effect of the amount of phosphoric acid on textural properties of activated carbons prepared from kraft black liquors [128]. They concluded that the activation with $H_3PO_4$ allows obtaining high surface area activated carbons (up to 1459 $m^2/g$), with microporous structure (micropore volume of 0.89 $cm^3/g$). On the other hand, Gonzalez-Serrano et al. also synthesized highly microporous carbon materials with high apparent surface areas, up to 1800 $m^2/g$, by activation of kraft lignin with $ZnCl_2$. The optimal preparation conditions were a temperature of 500 ºC and an impregnation ratio of 2.3 [102]. They reported that an increase in the activation temperature and in the amount of $ZnCl_2$ provided microporous activated carbons with a significant contribution of mesoporosity.

UNIVERSIDAD DE MÁLAGA

**Table 1.3.** Kind of lignin and type of activation used to prepare activated carbons [60].

| Type of lignin | Activation agent | $A_{BET}$ ($m^2/g$) | Reference |
|---|---|---|---|
| | **Physical activation** | | |
| Eucalyptus kraft lignin | $CO_2$ | 1853 | [81] |
| Eucalyptus kraft lignin | $CO_2$ | 700-1900 | [129–138] |
| Hydrolytic lignin | $H_2O_V$ | 865 | [126] |
| Hydrolytic lignin | Air | 769 | [139] |
| Kraft and Hydrolytic lignin | $CO_2$ and $H_2O_V$ | 1400-1600 | [127] |
| Black liquor lignin | $H_2O_V$ | 310 | [140] |
| Cron Straw lignin | Steam ($CO_2$ /$N_2$) | 1010 | [141] |
| | **Chemical activation** | | |
| Kraft black liquours | $ZnCl_2$ | 1800 | [102] |
| Kraft lignin | $ZnCl_2$ | 1164 | [142] |
| Kraft lignin | $ZnCl_2$<br>alkali metals<br>$H_3PO_4$ | 700-2000 | [103] |
| Kraft lignin | KOH | 514 | [143] |
| Kraft lignin | KOH | 1946 | [62] |
| Kraft lignin | KOH | 2763 | [144] |
| Black liquor | KOH | 2943 | [145] |
| Kraft lignin | KOH<br>NaOH | 3000<br>2400 | [104,105] |
| Kraft lignin | NaOH | 2400 | [146] |

UNIVERSIDAD DE MÁLAGA

**Table 1.3.** continuation

| Type of lignin | Activation agent | $A_{BET}$ ($m^2/g$) | Reference |
|---|---|---|---|
| Cronstalk lignin | $K_2CO_3$ | 1410 | [147] |
| Kraft lignin | $K_2CO_3$ | 41 | [148] |
| Lignin+urea | $K_2CO_3$ | 3400 | [149] |
| Kraft lignin | $H_3PO_4$ | 1459 | [128] |
| Kraft lignin | $H_3PO_4$ | 1305 | [150,151] |
| Kraft lignin | $H_3PO_4$ | 820 | [152] |
| Kraft lignin | $H_3PO_4$ | ~ 1500 | [153] |
| Kraft lignin | $H_3PO_4$ | ~ 1500 | [154] |
| Kraft lignin | $H_3PO_4$ | ~ 1500 | [155] |
| Alcell lignin | $H_3PO_4$ | 1099 | [110] |
| Alcell lignin | $H_3PO_4$ | 1015 | [112] |
| Hydrolytic lignin | KOH | 2753 | [156] |

## 1.7 Application of activated carbons

The enormous diversity of structural, textural and surface chemistry properties of activated carbons allow their use in a wide variety of applications in the fields and areas of heterogeneous catalysis, adsorption, electrochemistry, environmental engineering, chemical engineering, energy and biomedicine, among others. The following sections will deal with the applications of activated carbons in adsorption and heterogeneous catalysis, given that they are one of the fields of application of greatest interest to these porous solids in the industrial sector.

### 1.7.1 Activated carbon as adsorbent

Adsorption is a phase transfer process that is widely used in purification and separation process and especially in the removal of the pollutant substances from fluid phases (gas or liquid). In the solid surface, the adsorption segregates molecules or ions from the aqueous solution [157]. Figure 1.7 collects the basic terms of adsorption theory. The solid material

UNIVERSIDAD DE MÁLAGA

that contributes to the surface for adsorption is indicated as adsorbent; the species that will be adsorbed are denominated as adsorbate. By changing the adsorption conditions, such as concentration, temperature and pressure, the adsorbate is released from the surface and carried out back into the liquid phase. This reverse process is named as desorption [157]. Since adsorption is a surface process, the surface area and the surface chemistry are key quality parameters of adsorbents. Technical adsorbents are generally highly porous materials with surface areas in the range between 100 and 1000 $m^2/g$ [157].

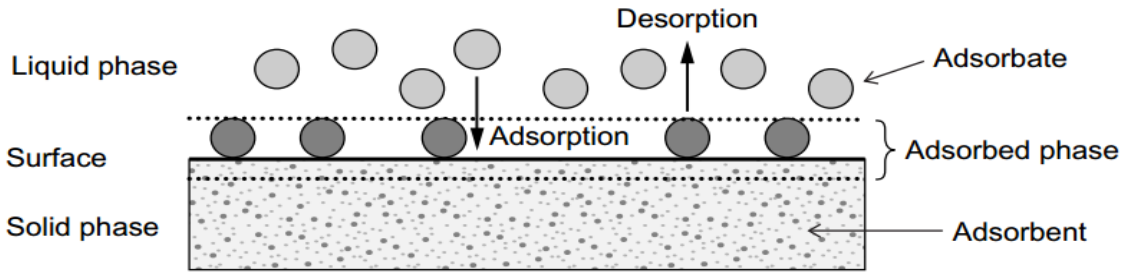


**Figure 1.7.** Basic terms of adsorption [157].

In water treatment, adsorption has been revealed as an efficient removal process for a multiplicity of contaminants and activated carbon is widely used as adsorbent to remove organic substances from different types of waters, such as drinking water, wastewater, groundwater, landfill leachate, swimming-pool water and aquarium water. There are also other adsorbents used for these treatments, but these are less often applied [157]. Their application is restricted to special adsorbates or types of water. Table 1.4 presents an overview of typical application fields and treatment objectives.

UNIVERSIDAD DE MÁLAGA

**Table 1.4.** Adsorption processes in water treatment [157].

| Application field | Objective | Adsorbent |
|---|---|---|
| Drinking water treatment | Removal of dissolved organic matter | Activated carbon |
| | Removal of organic micropollutants | Activated carbon |
| | Removal of arsenic | Aluminum oxide, iron hydroxide |
| Urban wastewater treatment | Removal phosphate | Aluminum oxide iron hydroxide |
| Industrial wastewater treatment | Removal of micropollutants | Activated carbon |
| | Removal or recycling of specific chemicals | Activated carbon<br>Polymeric adsorbents |
| Swimming-pool water treatment | Removal of organic substances | Activated carbon |
| Treatment of landfill leachate | Removal of organic substances | Activated carbon |
| Aquarium water treatment | Removal of organic substances | Activated carbon |

Due to the importance of treatment of drinking and waste waters for health, the application of activated carbon as adsorbent was evinced to be efficient for removal of a wide range of organic pollutants, like phenols, chlorinated hydrocarbons, pesticides, pharmaceuticals, personal care products, corrosion inhibitors and emerging pollutants.

#### 1.7.1.1 Emerging contaminants (ECs)

Emerging contaminants (ECs) are a group of natural and synthetic chemicals and their transformation products that can be found in water bodies throughout the globe. ECs are actually not controlled in the environment, but have a high potential of causing environmental damage, with detrimental effects on a wide variety of ecosystems and human health [158]. The steady release of ECs has been supposed to be taking place for a long time and through diverse sources [158,159], with varied concentrations between μg/L and a few ng/L and sometimes even below [159,160]. Owing to the development of new



UNIVERSIDAD DE MÁLAGA

sophisticated detection methods and analytical technologies, the detection, discovery and controlling of such low concentrations of these contaminants have been viable only recently, in the last decades [158,161,162]. The list of emerging compounds is extremely large and is ever expanding with the introduction of new commercial chemicals, changes in use and disposal of chemicals currently in widespread use and further identification of new molecules that form part of this classification [158,163]. However, the emerging contaminants cannot be totally eliminated in treatments plants, whose rate of removal depends on the concentrations of ECs. In this sense, diverse methods can be used to remove ECs from wastewater. Among these methods, adsorption on activated carbons can be applied due to their relatively high efficiency [119,164,165].

### 1.7.2 Activated carbon in heterogeneous catalysis

Catalysts accelerate reactions by orders of magnitude without them changing significantly during the chemical process, allowing reactions to be achieved faster at much lower temperatures and pressures. Hence an efficient catalyst, in combination with optimized reactor and total plant design are the key factors in reducing both the investment and operation costs (such as energy and time) of a chemical process [166].

Heterogeneous catalysis is an interesting field in constant development and mutation. In particular, catalysts have been regarded as an important characteristic of the green chemistry approach for sustainable progress. In catalytic applications, activated carbons have proved to be materials with high potential due to their high porous structure and their versatility and easily tunable surface properties [167]. Porous carbons have been developed and applied as heterogenous catalyst in various chemical synthesis as a sustainable and economical alternative to other catalyst solids [167–170]. Specifically, activated carbons have been used in heterogeneous catalysis, mainly as support of different active phases for multiple reactions like noble metals for hydrogenation reactions and in fuel cells, but also as catalyst in the synthesis of vinyl acetate and vinyl chloride [170–172].

#### 1.7.2.1 Activated Carbons as catalyst support

The preparation of carbon-supported catalysts is performed mainly by wet impregnation of the carbonaceous support with a solution containing the precursor of the active phase. In this process, different types of interactions occur between the surface of the carbon and the active phase of the precursor, from weak dispersive forces to electrostatic interactions, ion exchange or chemical reactions. The main important properties of a support



UNIVERSIDAD DE MÁLAGA

in catalytic reactions are mechanical strength, adequate pore distribution and chemical and thermal stability. Catalyst supports can be inert or active in some reactions and, in some cases, they might act as a stabilizer to preclude the agglomeration of lower melting-point materials or be as a reservoir for semi molten salts [173]. In order to achieve a high dispersion of the metal, which is generally essential to obtain high catalytic activities, a well-developed porous structure with a high surface area is necessary. Activated carbons generally have greater surface area and porosity than those presented by other substrates such as alumina and silica, with a significant part of this porosity being in the form of micropores. Activated carbons can be applied as support for metals, organocatalysts or organometallic catalysts in many reactions [174,175]. Some examples are those activated carbons used in the preparation of noble metal catalysts and electrocatalysts for energy applications [169,176]. Generally, the distribution of metals on the carbon support surface is related to the solvent applied for impregnation and to the presence of surface oxygenated groups. In this sense, Derbyshire et al. [177] and Prado-Burguete et al. [178,179] analyzed the dispersion of Pt on a black carbon with high surface area as catalyst support. They treated it at high temperature in hydrogen to remove most surface oxygenated groups. Subsequently, it was oxidized with $H_2O_2$ under different conditions to obtain different supports with the same porosity but different amount of surface oxygenated groups. The authors concluded that the acid groups introduced with the $H_2O_2$ decreased the hydrophobicity of carbon favoring the dispersion of the metal during the impregnation with aqueous solution and the presence of the oxygenated groups not only favored the dispersion of the Pt, but also increased the interactions between the metal precursor and the support, minimizing the sintering tendency of the metal [171]. The role of carbon as support is not merely that of a carrier; indeed, it can sometimes contribute to catalytic activity (hydrogen spillover) and reacts to some extent with other catalysts during the catalytic process [180].

#### 1.7.2.2 Activated carbons as catalyst

Activated carbons are most frequently used in catalysis applications as a support for an active phase, as previously mentioned, although, for certain reactions, activated carbons can be used as catalysts themselves. Among the reactions that use activated carbons as a catalyst, the most important is the production of phosgene or carbonyl chloride, $COCl_2$, which is used in the synthesis of different chemicals and polymers. On an industrial level, phosgene ($COCl_2$) is produced by passing carbon monoxide purified together with chlorine

UNIVERSIDAD DE MÁLAGA

in the gas phase through a carbon bed with a high development of porosity [171]. In this way, the activated carbon acts as a catalyst and the phosgene is produced according to the chemical reaction:

$$CO+Cl_2 \longrightarrow COCl_2$$

In some cases, a good correlation has been found between the activity of the activated carbons and the apparent surface area of the carbons. However, in most cases, this relationship does not occur due to the strong influence of surface chemistry of carbon on the different catalytic reactions. Thus, as an example, Szymanski and Rychlick observed that an activated carbon with a high apparent surface area and treated in hydrogen at 950 ºC showed low activity for dehydration and decomposition of alcohols, due to the hydrogen treatment produces a carbon with basic character [181]. However, the same carbon oxidized with nitric acid considerably increased its activity, due to the treatment with nitric acid produces carboxyl-type groups, of acid character, on the surface of the activated carbon.

#### 1.7.2.3 Alcohols decomposition

Decomposition of alcohols by dehydrogenation or dehydration is a very interesting process, commonly used for studying the acid/basic character of the catalyst surfaces. The activity and selectivity of this reaction are governed by textural effects, the acid/basic character and electronic properties of the catalyst [182]. Alcohol dehydrogenation products like aldehydes and ketones are preferentially formed on basic catalysts, while the dehydration products, like olefins and ethers, are favored when acid sites are present [183]. The decomposition of several alcohols over different inorganic supports has been extensively studied [184,185]. However, less effort has been focused on the decomposition of alcohols over organic supports [186,187]. Szymanski et al. studied the decomposition reactions of different alcohols and suggested that the dehydrogenation reaction takes place simultaneously on Lewis basic and acid sites located at the external surface of the particles [186,188,189]. The dehydration reaction takes place, according to the same authors, on acid sites essentially located at the external surface of the particles.

Among the possible different alcohols, 2-propanol, ethanol and methanol were selected as model compounds for the catalytic decomposition reactions in this thesis. The main characteristics for the catalytic decomposition of these alcohols are analyzed below.

UNIVERSIDAD DE MÁLAGA

*1.7.2.3.1 Catalytic decomposition of propanol*

The decomposition of 2-propanol has been studied primarily to characterize the acid-base properties of different types of catalysts. Most authors accept that the conversion of 2-propanol to propylene or di-isopropyl ether (dehydration) is indicative of acidic sites, while the presence of acetone (dehydrogenation) is indicative of basic sites [190]. In addition, other authors have found interesting correlations between the initial reaction rates of dehydration and dehydrogenation and the total basicity of the catalysts used [191].

Campelo et al. studied the conversion of different types of alcohols, including 2-propanol, on aluminum phosphates and found that increasing the temperature of the reaction increased the conversion of 2-propanol and the selectivity to propylene and decreased the selectivity to di-isopropyl ether and acetone [192]. They observed a correlation between the dehydration reaction and the acidity of the catalysts measured by irreversible adsorption of pyridine and 2,6-dimethylpyridine vapours. Bautista et al. stated that adding aluminum to vanadium phosphates produced catalysts that had a higher activity in the decomposition of 2-propanol [172,183]. This increase in activity occurred for both the dehydration reaction and the dehydrogenation reaction. The presence of aluminum not only generated a greater number of acid sites, but also produced stronger acid sites and increased the activity in the dehydration of 2-propanol. On the other hand, the activity of dehydrogenation seemed to be more related to the amount of vanadium in the solid. The authors calculated the values of the apparent energies of activity for the formation of propylene and acetone assuming first order reaction, finding that the activation energy for dehydration (62.7-108.7 KJ / mol) was greater than that for dehydrogenation (25.1-71.1 KJ/mol). The decomposition of 2-propanol was also studied by Bautista et al. on vanadium oxide systems supported on sepoilites and $TiO_2$-sepoilite mixtures [183]. Vanadium systems showed activity values for both dehydration and dehydrogenation, whereas sepoilites only generated dehydration products. Aremendai et al. used the decomposition of 2-propanol, among other reactions, to characterize the acid-base properties of different magnesium oxide catalysts, assuring that due to the basic character of the magnesium oxides, the dehydrogenation reaction predominated on dehydration and assumed an E1cB (Elimination, Unimolecular, Conjugate Base) type mechanism as dominant for solids with a lot of basic sites [193,194].

Regarding the decomposition of 2-propanol on carbonaceous catalysts, the works carried out by Rioux and Vannice studied the decomposition of 2-propanol on catalysts of

UNIVERSIDAD DE MÁLAGA

Pt, Cu and Cu-Pt supported on an activated carbon and on the activated carbons without metal phase supported [187,195]. In their first work, they used carbons subjected to different types of treatments as catalyst, which were also tested after depositing different amounts of Cu on them. Only the active carbons treated with nitric acid generated dehydration products (propylene) at steady state, as a consequence of the introduction of oxygenated surface groups of acidic nature during the treatment with acid [195]. For the rest of the activated carbons, with or without metallic phase, the selectivity towards acetone in the steady state was 100%. In the second work, they compared the activities of Cu, Pt and Pt-Cu catalysts supported on activated carbons [187]. They noted that Pt monometallic catalysts had the highest specific activities, about 5 times higher than that of Cu monometallic catalysts. Pt-Cu bimetallic catalysts showed intermediate specific activities. In all cases, the decomposition of 2-propanol generated only acetone, that is, it only produced the dehydrogenization reaction, concluding that the reaction proceeded according to a mechanism of Langmuir-Hinshelwood type, in which it is assumed that the controlling stage of the reaction is the loss of a first hydrogen atom by the breakdown of the O-H bond of the alcohol group of adsorbed 2-propanol molecules.

On the other hand, Szymanski and Rychlichki used activated carbons obtained by physical activation of furfuryl alcohol with $CO_2$ and the ones obtained by this treatment followed by oxidation with nitric acid for the catalytic decomposition of 2-propanol and found that both catalysts generated dehydration products (propylene and di-isopropyl ether) and dehydrogenation (acetone) [186]. The oxidation of carbons produced greater yields for the dehydration product as a consequence of the presence of carboxyl groups, formed during the oxidation stage. According to the authors, dehydration reaction could take place on the external surface of the carbon particles, while dehydrogenation reaction was produced inside the pores of the catalyst.

The decomposition of 2-propanol was also reported by Bedia et al. over carbon catalysts prepared by chemical activation of different lignocellulosic materials with phosphoric acid. The catalytic decomposition of 2-propanol yielded only propylene and low amount of di-isopropyl ether, as dehydration products [110]. The authors associated these results to the acidic character of the carbon catalysts derived from the activation with the phosphoric acid. In this line, some other carbon catalysts were prepared from hemp residues by chemical activation with $H_3PO_4$ [196], also showing a high activity and selectivity. In

UNIVERSIDAD DE MÁLAGA

other work reported by the same authors, the decomposition of 2-propanol was tested over carbon catalysts prepared by chemical activation of biomass waste with different activating agents. The resulting activated carbons presented acidic and basic character. The acid activated carbons prepared by chemical activation with phosphoric acid showed selectivity to propylene of 100%. However, in case of the basic carbon catalysts prepared by chemical activation with $Ba(OH)_2$, isopropanol was mainly dehydrogenated to acetone, with a low production of propylene. The carbon catalysts prepared by chemical activation with $Ca(OH)_2$ displayed acid and basic surface sites yielding both propylene and acetone [125].

1.7.2.3.2 Catalytic decomposition of ethanol

In the case of ethanol, unlike with 2-propanol, most of the researches are focused on obtaining high added value products for the industry. In particular, some works analysed the production of ethylene from the dehydration of ethanol obtained by fermentation of biomass (bioethanol) [197,198]. Ethylene is a compound of great importance for the petrochemical industry, which is currently obtained mainly from the cracking of petroleum or natural gas. The production of ethylene by dehydration of bioethanol, currently, is only used on a commercial scale in a few countries such as India and Brazil, due to its high cost of production and high energy consumption. However, the growing scarcity of natural resources and energy as well as the increase in the price of petroleum make the catalytic dehydration of ethanol (specifically bioethanol) an increasingly competitive alternative.

The decomposition of ethanol has been studied in different types of catalysts such as pure or doped aluminium [199,200], zeolites [197,198,201], magnesium oxide [202,203], cobalt [204], chromium [205], mixed oxide [206] , tungstophosphoric acid [207], etc. In this sense, El katatny et al. analyzed the dehydration of ethanol on catalysts with 1-10% $FeO_x$ on $Al_2O_3$ [208]. The activity tests, at temperatures between 140 and 250°C, showed that increasing in the $FeO_x$ content changed the product selectivity from diethyl ether to ethylene, although in all cases the majority product was the ethers. Zaki et al. studied the catalytic dehydration of ethanol using different types of metal oxide catalysts, including $Fe_2O_3$, $Mn_2O_3$ and mixtures of both unsupported and supported on alumina and/or silica [203]. The dehydration of ethanol was analyzed between 200 and 500 °C, obtaining a maximum conversion of 70%. The main products obtained were ethylene and diethyl ether, with lower amounts of acetaldehyde and ethane. As the reaction temperature increased, the selectivity to ethylene increased and, therefore, decreased to diethyl ether. These authors concluded

UNIVERSIDAD DE MÁLAGA

that the activity in the dehydration reaction was strongly related to Brønsted acidity measured by adsorption of pyridine [208,209].

Di Cosimo et al. employed the decomposition of ethanol to characterize the density and reactivity of the basic sites of mixed Mg-Al oxides at molar Mg/Al ratios between 0.5-9.0. The majority products of the reaction were ethylene, diethyl ether, acetaldehyde, n-butanol and n-butylaldehyde [210]. They also observed traces of acetate ethyl, 2-propano, l acetone and 2-pentanone. The dehydrogenation of ethanol generated acetaldehyde as the main product and a subsequent aldol condensation formed n-butanol. The dehydration produced diethyl ether and ethylene. The pure magnesium oxide had shown low reaction rates in the decomposition of ethanol. The samples with low Al content dehydrogenated ethanol to acetaldehyde, whereas with high Al contents, it was dehydrated, producing mainly ethylene and diethyl ether. The pure aluminum showed the highest acidity of all the samples, with the high reactivity and selectivity towards ethylene [210].

Most of the studies had focused on the decomposition of ethanol on quite complex catalysts, studying even mixtures of different metal oxides. However, there were few works in which decomposition of ethanol on carbonaceous materials were analyzed [189,211,212]. Grunewald and Drago analyzed the conversion of different alcohols on a carbonaceous molecular sieve [211]. When the ethanol was dulled in $N_2$ and reacted on the molecular sieve at 230 °C, the catalyst showed a low activity with a high selectivity towards ethylene. However, when the gas was changed from $N_2$ to air, the activity of the catalyst increased, reaching conversions close to 70%. In this case, the main products were acetaldehyde and ethyl acetate. Szymanski et al. investigated the decomposition of ethanol on activated carbons prepared from polyfurfuryl alcohol by physical activation with $CO_2$, without oxidizing and oxidizing with nitric acid and also after the deposition of Ni [189]. The initial activated carbon showed a very low activity in the decomposition of ethanol. The dehydrogenation and dehydration products were produced, with acetaldehyde (majority), ethylene and diethyl ether, together with small amounts of diethylacetal, as main products. Oxidation with nitric acid produced a carbon with a more acidic surface, which resulted in a very significant increase in carbon activity towards dehydration. The introduction of Ni produced an increase in the dehydrogenation reaction, as a consequence of the presence of $Ni^{+2}$ cations on the carbon surface. Carrasco-Marin et al. used two activated carbons obtained by physical activation of olive stone with water vapor and they oxidized them with

UNIVERSIDAD DE MÁLAGA

ammonium persulfate [212]. All the carbons showed a moderate activity and dehydration products were obtained, mainly, diethyl ether (majority) and a small amount of dehydrogenation products, when the reaction gas was He. The authors confirmed that the activity is a consequence of the introduction of carboxyl groups during the oxidation treatment. The dehydrogenation reaction increased when the reaction gas was air instead of He. This phenomenon was previously observed by Szymanski et al., who attributed this effect to the reduction of superficial active sites by ethanol and the following regeneration by air [189].

Ethanol decomposition was also studied on carbon catalysts prepared by chemical activation of olive stones with phosphoric acid. These carbon catalysts yielded mainly dehydration products, with very high selectivity to ethylene [168]. The authors demonstrated the importance of the presence of oxygen in the gas phase, which inhibits the coke deposition on the acid active sites.

1.7.2.3.3 Catalytic decomposition of methanol

The dehydration of methanol to obtain dimethyl ether and/or hydrocarbons have been widely studied [213–215]. Dimethyl ether is a base compound for the production of multiple chemicals, such as methyl acetate, dimethyl sulfate and light olefins/gasolines. Its use is also increasing as a propellant in the formation of aerosols, replacing chlorofluorocarbons (CFC), which have been shown to destroy the ozone layer [171,216]. The greatest increase in demand is due to its use as a clean alternative fuel, since its efficiency is very similar to that of traditional diesel fuels, they reduce the formation of NOx and decrease the noise generated by combustion engines. Dimethyl ether is produced by dehydration of methanol using porous acidic materials, such as silico-alumina or $\gamma$-$Al_2O_3$ zeolites, as catalysts [171].

As already mentioned above, the synthesis of ether from alcohols is a reaction catalyzed by acids. However, the majority of solid acid catalysts generate unwanted products such as hydrocarbons due to the presence of strong acid sites [217,218]. In addition, the dehydration of methanol produces a rapid and generally irreversible deactivation of the catalysts, due to the deposition of coke. To prevent the deposition of coke and increase the selectivity to dimethyl ether, the strength of the acid sites of the catalyst must be lowered.

UNIVERSIDAD DE MÁLAGA

On the other hand, the technology to convert methanol to hydrocarbons (MTH) had initially been studied as a method to convert carbon into gasoline of high octane, via gasification. Later, this technology was extended to the formation of other fuels and chemical compounds in general, allowing the generation of practically any product obtained from crude petroleum, but from coal or natural gas [217]. Methanol can be obtained from synthesis gas (a mixture of carbon monoxide and hydrogen), which can be produced by steam reforming of natural gas or carbon gasification.

Jasińska et al. tested carbon catalysts prepared with different chemical agent for the catalytic decomposition of ethanol and methanol [219]. They reported that the conversion of methanol to dimethyl ether was only observed over the carbon oxidized with nitric acid, sulphuric acid and air, and they stated that no dehydrogenation process took place. Zeolites promoted with alkali metals were used for methanol dehydration reaction, showing an enhanced stability under wider operating temperature ranges, with methanol conversions higher than 50% and selectivity to dimethyl-ether as high as 99% [220–222]. Moreno-Castilla et al. analyzed the conversion of methanol to dimethyl-ether over oxidized activated carbons [223]. They suggested that the activated carbon oxidized with $(NH_4)_2S_2O_8$ exhibited the strongest acid groups and presented the highest activity in the methanol dehydration reaction due to the existence of acidic groups, such as carboxylic groups. However, the presence of these stronger acid groups showed no chemical and thermal stability, lasting a very small fraction of time under reaction conditions, due to decomposition of carboxylic group took place at low temperatures, with formation of $CO_2$.

Conversion of methanol to DME over carbon catalysts prepared by chemical activation of lignocellulosic biomass waste with phosphoric acid has also been reported [224–226]. Valero-Romero et al. prepared carbon catalysts from olive stones, which presented a methanol conversion of 20% at 300 ºC and selectivity to dimethyl-ether of 95%, showing a high catalytic stability under air atmosphere [224]. On the other hand, Ibeh et al. analyzed the conversion of methanol to DME on carbon catalyst monoliths prepared from different lignocellulosic biomass waste [225]. The carbon monoliths prepared from olive stones presented the highest catalytic activity, with conversion of 70%, selectivity to DME higher than 90% and high stability under the operating condition evaluated. In addition, methanol to DME conversion over Zr-loaded activated carbons prepared by chemical activation of olive stones with phosphoric acid was also analyzed by Palomo et al. [226]. They suggested that the conversion increased with the increase in the metal loadings up to

UNIVERSIDAD DE MÁLAGA

a fixed loading amount (of around 5% (w/w)), from which no further increasing in the steady-state methanol conversion was observed. They obtained conversions close to the thermodynamic equilibrium, keeping selectivity towards DME higher than 95%. They concluded that the zirconium phosphate species presented on catalysts surface were responsible for this high and stable catalytic activity.

## References


[1] M. Höök, X. Tang, Depletion of fossil fuels and anthropogenic climate change-A review, Energy Policy. 52 (2013) 797–809. https://doi.org/10.1016/j.enpol.2012.10.046.

[2] D.T. Okun, C.R. Lane, I.A. Williamson, D.A. Pinkert, Development & adoption of industrial biotechnology by the US chemical & biofuel industries, Ind. Biotechnol. 4 (2008) 262–287. https://doi.org/10.1089/ind.2008.4.262.

[3] A. V. Bridgwater, Review of fast pyrolysis of biomass and product upgrading, Biomass and Bioenergy. 38 (2012) 68–94. https://doi.org/10.1016/j.biombioe.2011.01.048.

[4] Directive of the european parliament and of the council on the promotion of the use of energy from renewable sources (recast), European Commission, Brussels, 2017.

[5] M. Banja, R. Sikkema, M. Jégard, V. Motola, J.F. Dallemand, Biomass for energy in the EU – The support framework, Energy Policy. 131 (2019) 215–228. https://doi.org/10.1016/j.enpol.2019.04.038.

[6] S. Irmak, Biomass as Raw Material for Production of High-Value Biomass as Raw Material for Production of High-Value Products, in: J.S. Tumuluru (Ed.), Biomass Vol. Estim. Valorization Energy, Order a hardcopy of the Edited Volume, 2017: pp. 200–217. https://doi.org/http://dx.doi.org/10.5772/57353.

[7] M. Jagtoyen, F. Derbyshire, Activated carbons from yellow poplar and white oak by $H_3PO_4$ activation, Carbon. 36 (1998) 1085–1097. https://doi.org/10.1016/S0008-6223(98)00082-7.

[8] R. H. Marchessault, The Chemistry of Wood, Interscience (Wiley), New York, 1963. https://doi.org/10.1002/pol.1964.100020442.

[9] J. Zheng Fang , Richard L. Smith, ed., Biofuels and Biorefineries : Production of Biofuels and Chemicals from Lignin, Springer, 2016. https://doi.org/10.1007/978-981-10-1965-4.

[10] W.Qui. H Chen, Structure, function and higher value application of lignin, J. Cellul. Sci. Technol. 14 (2006) 56–65.


UNIVERSIDAD DE MÁLAGA

[11] J. Zakzeski, P.C.A. Bruijnincx, A.L. Jongerius, B.M. Weckhuysen, The catalytic valorization of lignin for the production of renewable chemicals, Chem. Rev. 110 (2010) 3552–3599. https://doi.org/10.1021/cr900354u.

[12] A. Prakash, R. Singh, B. Balagurumurthy, T. Bhaskar, A.K. Arora, S.K. Puri, Thermochemical Valorization of Lignin, in: P.Ashok, M. Stöcker, T. Bhaskar, R.K.Sukumaran (Ed.), Recent Adv. InThermochemical Convers. Biomass, 2015: pp. 455–478. https://doi.org/10.1016/B978-0-444-63289-0.00016-8.

[13] H. Chen, ed., Biotechnology of Lignocellulose, Springer, 2014. https://doi.org/10.1007/978-94-007-6898-7.

[14] J. H. Shiyu, F. L. Gan, ed., Structure and Characteristics of Lignin, in: Lignin Chem. Appl., Elsevier, 2019: pp. 25–50. https://doi.org/10.1016/b978-0-12-813941-7.00002-3.

[15] B.W. Pieter Bruijnincx, Lignin Valorisation : The Importance of a Full value chain approach, Utr. Univ. APC. (2016) 2–22.

[16] H. Chung, N.R. Washburn, Extraction and Types of Lignin, in:. M.Sain, O.Faruk (Ed.), Lignin Polym. Compos., Elsevier Inc., 2016: pp. 13–25. https://doi.org/10.1016/B978-0-323-35565-0.00002-3.

[17] M. Suchy, D.S. Argyropoulos, Catalysis and activation of oxygen and peroxide delignification of chemical pulps: A review, Tappi J. 1 (2002) 9–26. https://doi.org/10.1021/bk-2001-0785.ch001.

[18] E.I. Akpan, Chemistry and Structure of Lignin, in: E.I. Akpan, S.O. Adeosun (Eds.), Sustain. Lignin Carbon Fibers Princ. Tech. Appl., Springer International Publishing, Cham, 2019: pp. 1–50. https://doi.org/10.1007/978-3-030-18792-7_1.

[19] G. Gellerstedt, Softwood kraft lignin: Raw material for the future, Ind. Crops Prod. 77 (2015) 845–854. https://doi.org/10.1016/j.indcrop.2015.09.040.

[20] E. Alder, Lignin Chemistry-Past, Present and Future, Wood Sci. Technol. 11 (1977) 169–218. https://doi.org/10.1038/237054a0.

[21] E. Adler, G. Miksche, W. Brown, Comparative studies on cellulolytic enzyme lignin and milled wood lignin of sweetgum and spruce, Holzforschung. 29 (1975) 153–159. https://doi.org/10.1515/hfsg.1975.29.5.153.

[22] A. Bjorkman, Extraction of lignin with neutral solvents, Stud. Finely Divid. Wood. Part 1. 59 (1956) 477–485.

[23] J. Hu, Q. Zhang, D.J. Lee, Kraft lignin biorefinery: A perspective, Bioresour. Technol. 247 (2018) 1181–1183. https://doi.org/10.1016/j.biortech.2017.08.169.



UNIVERSIDAD DE MÁLAGA

[24] L. Lagerquist, A. Pranovich, A. Smeds, S. von Schoultz, L. Vähäsalo, J. Rahkila, I. Kilpeläinen, T. Tamminen, S. Willför, P. Eklund, Structural characterization of birch lignin isolated from a pressurized hot water extraction and mild alkali pulped biorefinery process, Ind. Crops Prod. 111 (2018) 306–316. https://doi.org/10.1016/j.indcrop.2017.10.040.

[25] S. Al Arni, Extraction and isolation methods for lignin separation from sugarcane bagasse: A review, Ind. Crops Prod. 115 (2018) 330–339. https://doi.org/10.1016/j.indcrop.2018.02.012.

[26] X. Tan, Q. Zhang, W. Wang, X. Zhuang, Y. Deng, Z. Yuan, Comparison study of organosolv pretreatment on hybrid pennisetum for enzymatic saccharification and lignin isolation, Fuel. 249 (2019) 334–340. https://doi.org/10.1016/j.fuel.2019.03.117.

[27] H. Sixta, Handbook of Pulp, WILEY-VCH Verlag GmbH &Co. KGaA, Weinheim, 2006. https://doi.org/10.1002/9783527619887.

[28] H. Chen, Lignocellulose Biorefinery Engineering : Principles and Applications, Woodhead Publishing, 2015. https://doi.org/10.1016/C2014-0-02702-5

[29] K. T. Vijay. K. T. Manju, R. K. Michael, Handbook of Composites from Renewable Materails, Structure and Chemistry, NJ, USA, 2017.

[30] E. Sjostrom., Wood chemistry: Fundamentals and Applications. Academic, Academic Press, San Diego, 1993.

[31] J.E. Holladay, J.F. White, J.J. Bozell, D. Johnson, Top Value-Added Chemicals from Biomass: Volume II — Results of Screening for Potential Candidates from Biorefinery Lignin., Pacific Northwest Natl. Lab. , U.S. Dep. Energy. (2007). http://www.ntis.gov/ordering.htm.

[32] N. H. H. Ullmann, Encyclopedia of Industrial Chemistry, Wiley-VCH Verlag GmbH & Co. KGaA, 2000. https://doi.org/10.1002/14356007.

[33] . B. Saake, R.. Lehnen, Lignin, in: Ulmann's Encycl. Industial Chem., Wiley-VCH Verlag GmbH & Co. KGaA, Weinheim, 2012: pp. 21–36. https://doi.org/10.1002/14356007.a15.

[34] N.E. El Mansouri, J. Salvadó, Analytical methods for determining functional groups in various technical lignins, Ind. Crops Prod. 26 (2007) 116–124. https://doi.org/10.1016/j.indcrop.2007.02.006.

[35] J. Sameni, S. Krigstin, D. dos S. Rosa, A. Leao, M. Sain, Thermal characteristics of lignin residue from industrial processes, BioResources. 9 (2014) 725–737. https://doi.org/10.15376/biores.9.1.725-737.

[36] W.O.S. Doherty, P. Mousavioun, C.M. Fellows, Value-adding to cellulosic ethanol: Lignin



UNIVERSIDAD DE MÁLAGA

polymers, Ind. Crops Prod. 33 (2011) 259–276. https://doi.org/10.1016/j.indcrop.2010.10.022.

[37] M.N.S. Kumar, A.K. Mohanty, L. Erickson, M. Misra, Lignin and its applications with polymers, J. Biobased Mater. Bioenergy. 3 (2009) 1–24. https://doi.org/10.1166/jbmb.2009.1001.

[38] K. Shimizu, K. Sudo, H. Ono, M. Ishihara, T. Fujii, S. Hishiyama, Integrated process for total utilization of wood components by steam-explosion pretreatment, Biomass and Bienergy. 14 (1998) 195–203. https://doi.org/10.1016/S0961-9534(97)10044-7.

[39] A. Vishtal, A. Kraslawski, Challenges in industrial applications of technical lignins, BioResources. 6 (2011) 3547–3568. https://doi.org/10.15376/biores.6.3.3547-3568.

[40] S. Laurichesse, L. Avérous, Chemical modification of lignins: Towards biobased polymers, Prog. Polym. Sci. 39 (2014) 1266–1290. https://doi.org/10.1016/j.progpolymsci.2013.11.004.

[41] J. Gierer, Chemical aspects of kraft pulping, Wood Sci. Technol. 14 (1980) 241–266. https://doi.org/10.1007/BF00383453.

[42] K. Lundquist, R. Simonson, K. Tingsvik, Investigation of Lignins from Soda and Soda-Anthraquinone Cooking of Spruce Wood, Pap. Ja Puu-Paper Timber. 63 (1981) 709-.

[43] E. Ahmad, K.K. Pant, Lignin Conversion: A Key to the Concept of Lignocellulosic Biomass-Based Integrated Biorefinery, in: S.K. Thallada Bhaskar, Ashok Pandey, Mohan, S. Venkata, Lee, Duu-Jong, Khanal (Ed.), Waste Biorefinery, Elsevier, 2018: pp. 409–444. https://doi.org/10.1016/b978-0-444-63992-9.00014-8.

[44] J.H. Lora, M. Wayman, Autohydrolysis of aspen milled wood lignin, Can. J. Chem. 58 (1980) 669–676. https://doi.org/10.1139/v80-102.

[45] K.L. Meiyun Zhang, Yongjian Xu, Removal of Residual Lignin of Ethanol-Based Organosolv Pulp by an Alkali Extraction Process, J. Appl. Polym. Sci. 106 (2007) 630–636. https://doi.org/10.1002/app.26622.

[46] E. Ruiz, C. Cara, P. Manzanares, M. Ballesteros, E. Castro, Evaluation of steam explosion pre-treatment for enzymatic hydrolysis of sunflower stalks, Enzyme Microb. Technol. (2008). https://doi.org/10.1016/j.enzmictec.2007.09.002.

[47] J. Wang, R.S.J. Manley, D. Feldman, Synthetic polymer-lignin copolymers and blends, Prog. Polym. Sci. 17 (1992) 611–646. https://doi.org/10.1016/0079-6700(92)90003-H.

[48] S. Kang, X. Li, J. Fan, J. Chang, Classified separation of lignin hydrothermal liquefied products, Ind. Eng. Chem. Res. 50 (2011) 11288–11296. https://doi.org/10.1021/ie2011356.



UNIVERSIDAD DE MÁLAGA

[49] F. Lu, J. Ralph, Lignin, in: R.. C. Sun (Ed.), Cereal Straw as a Resour. Sustain. Biomater. Biofuels, 1 st, Elsevier, 2010: pp. 169–207. https://doi.org/10.1016/B978-0-444-53234-3.00006-7.

[50] W.G. Glasser, R.S. Wright, Steam-assisted biomass fractionation. II. Fractionation behavior of various biomass resources, Biomass and Bioenergy. 14 (1998) 219–235. https://doi.org/10.1016/S0961-9534(97)10037-X.

[51] T.J. Mcdonough, The chemistry of organosolv delignification, Tappi J. 76 (1993) 186–193.

[52] S. Kubo, J.F. Kadla, Poly(ethylene oxide)/organosolv lignin blends: Relationship between thermal properties, chemical structure, and blend behavior, Macromolecules. 37 (2004) 6904–6911. https://doi.org/10.1021/ma0490552.

[53] A. Berlin, M. Balakshin, Industrial Lignins: Analysis, Properties, and Applications, in: F.X. Vijai Gupta, Maria Tuohy , Christian Kubicek, Jack Saddler (Ed.), Bioenergy Res. Adv. Appl., Elsevier, 2014: pp. 315–336. https://doi.org/10.1016/B978-0-444-59561-4.00018-8.

[54] A. Shrotri, H. Kobayashi, A. Fukuoka, Catalytic Conversion of Structural Carbohydrates and Lignin to Chemicals, in: C. Song (Ed.), Adv. Catal., 1 st, Elsevier Inc., 2017: pp. 59–123. https://doi.org/10.1016/bs.acat.2017.09.002.

[55] X. Pan, C. Arato, N. Gilkes, D. Gregg, W. Mabee, K. Pye, Z. Xiao, X. Zhang, J. Saddler, Biorefining of softwoods using ethanol organosolv pulping: Preliminary evaluation of process streams for manufacture of fuel-grade ethanol and co-products, Biotechnol. Bioeng. 90 (2005) 473–481. https://doi.org/10.1002/bit.20453.

[56] I. Cybulska, G. Brudecki, K. Rosentrater, J.L. Julson, H. Lei, Comparative study of organosolv lignin extracted from prairie cordgrass, switchgrass and corn stover, Bioresour. Technol. 118 (2012) 30–36. https://doi.org/10.1016/j.biortech.2012.05.073.

[57] X. Pan, D. Xie, R.W. Yu, D. Lam, J.N. Saddler, Pretreatment of lodgepole pine killed by mountain pine beetle using the ethanol organosolv process: Fractionation and process optimization, Ind. Eng. Chem. Res. 46 (2007) 2609–2617. https://doi.org/10.1021/ie061576l.

[58] X. Pan, J.F. Kadla, K. Ehara, N. Gilkes, J.N. Saddler, Organosolv ethanol lignin from hybrid poplar as a radical scavenger: Relationship between lignin structure, extraction conditions, and antioxidant activity, J. Agric. Food Chem. 54 (2006) 5806–5813. https://doi.org/10.1021/jf0605392.

[59] Global Lignin Products Market 2019 With Top Countries Data : Market Size, Concentration Rate, Production Volume, Price, Gross Margin and Revenue, (2019). https://doi.org/.1037//0033-2909.I26.1.78.

UNIVERSIDAD DE MÁLAGA

[60] J.M. Rosas, R. Berenguer, M.J. Valero-Romero, J. Rodrí-guez-Mirasol, T. Cordero, Preparation of Different Carbon Materials by Thermochemical Conversion of Lignin, Front. Mater. 1 (2014) 1–17. https://doi.org/10.3389/fmats.2014.00029.

[61] A. Agrawal, N. Kaushik, S. Biswas, Derivatives and Applications of Lignin–An Insight, SciTech J. 1 (2014) 30–36.

[62] K. Babeł, K. Jurewicz, KOH activated lignin based nanostructured carbon exhibiting high hydrogen electrosorption, Carbon. 46 (2008) 1948–1956. https://doi.org/10.1016/j.carbon.2008.08.005.

[63] J. Rodríguez-Mirasol, T. Cordero, J.J. Rodríguez, High-temperature carbons from kraft lignin, Carbon. (1996). https://doi.org/10.1016/0008-6223(95)00133-6.

[64] X. Zhang, Q. Zhang, T. Wang, L. Ma, Y. Yu, L. Chen, Hydrodeoxygenation of lignin-derived phenolic compounds to hydrocarbons over Ni/$SiO_2$-$ZrO_2$ catalysts, Bioresour. Technol. 134 (2013) 73–80. https://doi.org/10.1016/j.biortech.2013.02.039.

[65] L.R.C. Barclay, F. Xi, J.Q. Norris, Antioxidant properties of phenolic lignin model compounds, J. Wood Chem. Technol. 17 (1997) 73–90. https://doi.org/10.1080/02773819708003119.

[66] R.L. Crawford, L.E. Robinson, R.D. Foster, Polyguaiacol: a Useful Model Polymer for Lignin Biodegradation Research, Appl. Environ. Microbiol. 41 (1981) 1112–1116. https://doi.org/10.1128/aem.41.5.1112-1116.1981.

[67] M. Brodin, M. Vallejos, M.T. Opedal, M.C. Area, G. Chinga-Carrasco, Lignocellulosics as sustainable resources for production of bioplastics – A review, J. Clean. Prod. 162 (2017) 646–664. https://doi.org/10.1016/j.jclepro.2017.05.209.

[68] J.D.P. Araújo, C.A. Grande, A.E. Rodrigues, Vanillin production from lignin oxidation in a batch reactor, Chem. Eng. Res. Des. 88 (2010) 1024–1032. https://doi.org/10.1016/j.cherd.2010.01.021.

[69] J.M.Cruz, A.B Moldes, G.Bustos, A.Torrado, J.M.Domínguez, Integral utilisation of barley husk for the production of food additives, J. Sci. Food Agric. 87 (2007) 1000–1008. https://doi.org/10.1002/jsfa.

[70] M. Witczak, M. Walkowiak, W. Cichy, M. Komorowicz, The application of elemental analysis for the determination of the elemental composition of lignocellulosic materials, Ann. Warsaw Univ. Life Sci. - SGGW. For. Wood Technol. 92 (2015) 200–205.

[71] G. Lv, S. Wu, Analytical pyrolysis studies of corn stalk and its three main components by TG-MS and Py-GC/MS, J. Anal. Appl. Pyrolysis. 97 (2012) 11–18.



UNIVERSIDAD DE MÁLAGA

https://doi.org/10.1016/j.jaap.2012.04.010.

[72] A. Ház, M. Jablonský, I. Šurina, F. Kačík, T. Bubeníková, J. Ďurkovič, Chemical composition and thermal behavior of kraft lignins, Forests. 10 (2019) 1–12. https://doi.org/10.3390/f10060483.

[73] T.S. Sabornie Chatterjee, Lignin-Derived Carbon Materials, ChemSusChem. 9 (2016) 1–14. https://doi.org/10.1002/cssc.201.

[74] H. Marsh, F. Rodríguez-Reinoso, Activated Carbon (Origins), in: Act. Carbon, Harry Mars, Elsivier, 2006: pp. 1–16. https://doi.org/10.1016/B978-0-08-044463-5.50016-9.

[75] J.J. Rodríguez, T. Cordero, J. Rodríguez-Mirasol, Carbon Materials from Lignin and Their Applications, in: Z. Fang, R.L. Smith Jr. (Eds.), Prod. Biofuels Chem. from Lignin, Springer Singapore, Singapore, 2016: pp. 217–262. https://doi.org/10.1007/978-981-10-1965-4_8.

[76] H. Marsh, F. Rodríguez-Reinoso, Introduction to the Scope of the Text, in: F.R.-R. Marsh .Harry (Ed.), Act. Carbon, Elsivier, 2006: pp. 1–12. https://doi.org/10.1016/b978-008044463-5/50015-7.

[77] A.W.P. Fung, A.M. Rao, K. Kuriyama, M.S. Dresselhaus, G. Dresseliiaus, M. Endot, Characterization of Activated Carbon, in: F.R.R. H. Marsh (Ed.), Act. Carbon, Elsevier, 2006: pp. 143–241. https://doi.org/10.1557/proc-209-335.

[78] J.L. Figueiredo, M.F.R. Pereira, M.M.A. Freitas, J.J.M. Órfão, Modification of the surface chemistry of activated carbons, Carbon N. 37 (1999) 1379–1389. https://doi.org/10.1016/S0008-6223(98)00333-9.

[79] H. Marsh, F. Rodríguez-Reinoso, Applicability of Activated Carbon, in: Act. Carbon, Elsevier, 2006: pp. 383–453. https://doi.org/10.1016/b978-008044463-5/50022-4.

[80] A.L. Cukierman, Development and Environmental Applications of Activated Carbon Cloths, ISRN Chem. Eng. 2013 (2013) 261523. https://doi.org/10.1155/2013/261523.

[81] J. Rodríguez-Mirasol, T. Cordero, J.J. Rodríguez, Preparation and characterization of activated carbons from eucalyptus kraft lignin, Carbon. 31 (1993) 87–95. https://doi.org/10.1016/0008-6223(93)90160-C.

[82] J. Rodríguez-Mirasol, T. Cordero, J.J. Rodríguez, Activated Carbons from $CO_2$ Partial Gasification of Eucalyptus Kraft Lignin, Energy and Fuels. 7 (1993) 133–138. https://doi.org/10.1021/ef00037a021.

[83] M.G. Lussier, J.C. Shull, D.J. Miller, Activated carbon from cherry stones, Carbon. 32 (1994) 1493–1498. https://doi.org/10.1016/0008-6223(94)90144-9.

UNIVERSIDAD DE MÁLAGA

[84] A. Ahmadpour, D.D. Do, The preparation of active carbons from coal by chemical and physical activation, Carbon N. Y. 34 (1996) 471–479. https://doi.org/10.1016/0008-6223(95)00204-9.

[85] C. Di Blasi, Combustion and gasification rates of lignocellulosic chars, Prog. Energy Combust. Sci. 35 (2009) 121–140.

[86] Suhas, P.J.M. Carrott, M.M.L. Ribeiro Carrott, Lignin--from natural adsorbent to activated carbon: a review., Bioresour. Technol. 98 (2007) 2301–2312. https://doi.org/10.1016/j.biortech.2006.08.008.

[87] J. Rodríguez-Mirasol, T. Cordero, J.J. Rodriguez, $CO_2$-reactivity of eucalyptus kraft lignin chars, Carbon. 31 (1993) 53–61. https://doi.org/10.1016/0008-6223(93)90155-4.

[88] A. Linares-Solano, O.P. Mahajan, P.L. Walker, Reactivity of heat-treated coals in steam, Fuel. 58 (1979) 327–332. https://doi.org/10.1016/0016-2361(79)90148-0.

[89] P. González-Vilchez, A. Linares-Solano, J. de, F. Rodríguez-Reinoso, The controlled reaction of active carbons with air at 350°C-I. Reactivity and changes in surface area, Carbon. 17 (1979) 441–446. https://doi.org/10.1016/0008-6223(79)90031-9.

[90] M.J. Muñoz-Guillena, M.J. Illán-Gómez, J.M. Martín-Martínez, A. Linares-Solano, C. Salinas-Martínez de Lecea, Activated Carbons from Spanish Coals. 1. Two-Stage $CO_2$ Activation, Energy and Fuels. 6 (1992) 9–15. https://doi.org/10.1021/ef00031a002.

[91] D. Cazorla-Amorós, A. Linares-Solano, C.S.M. de Lecea, F. Kapteijn, Assessment of the $CO_2$-carbon gasification catalyzed by calcium. A transient isotopic study, Carbon. 32 (1994) 423–430. https://doi.org/10.1016/0008-6223(94)90162-7.

[92] J. Alcañiz-Monge, D. Cazorla-Amorós, A. Linares-Solano, Production of activated carbons: Use of CO2 versus H2O as activating agent, Carbon. 35 (1997) 1665–1668. https://doi.org/10.1016/S0008-6223(97)82798-4.

[93] C.F. Chang, C.Y. Chang, W.T. Tsai, Effects of burn-off and activation temperature on preparation of activated carbon from corn cob agrowaste by $CO_2$ and steam, J. Colloid Interface Sci. 232 (2000) 45–49. https://doi.org/10.1006/jcis.2000.7171.

[94] A. Arami-Niya, W.M.A.W. Daud, F.S. Mjalli, Comparative study of the textural characteristics of oil palm shell activated carbon produced by chemical and physical activation for methane adsorption, Chem. Eng. Res. Des. 89 (2011) 657–664. https://doi.org/10.1016/j.cherd.2010.10.003.

[95] P.T. Williams, A.R. Reed, Development of activated carbon pore structure via physical and chemical activation of biomass fibre waste, Biomass and Bioenergy. 30 (2006) 144–152.

UNIVERSIDAD DE MÁLAGA

https://doi.org/10.1016/j.biombioe.2005.11.006.

[96] C. Namasivayam, K. Kadirvelu, Activated carbons prepared from coir pith by physical and chemical activation methods, Bioresour. Technol. 62 (1997) 123–127. https://doi.org/10.1016/S0960-8524(97)00074-6.

[97] F. Rodríguez-Reinoso, M. Molina-Sabio, Activated carbons from lignocellulosic materials by chemical and/or physical activation: an overview, Carbon. 30 (1992) 1111–1118. https://doi.org/10.1016/0008-6223(92)90143-K.

[98] J.M. Rosas, J. Bedia, J. Rodríguez-Mirasol, T. Cordero, On the preparation and characterization of chars and activated carbons from orange skin, Fuel Process. Technol. 91 (2010) 1345–1354. https://doi.org/10.1016/j.fuproc.2010.05.006.

[99] J. Alcañiz-Monge, D. Cazorla-Amorós, A. Linares-Solano, S. Yoshida, A. Oya, Effect of the activating gas on tensile strength and pore structure of pitch-based carbon fibres, Carbon. 32 (1994) 1277–1283. https://doi.org/10.1016/0008-6223(94)90113-9.

[100] D. Cazorla-Amorós, D. Ribes-Pérez, M.C. Román-Martínez, A. Linares-Solano, Selective porosity development by calcium-catalyzed carbon gasification, Carbon. 34 (1996) 869–878. https://doi.org/10.1016/0008-6223(96)00026-7.

[101] D. Montané, V. Torné-Fernández, V. Fierro, Activated carbons from lignin: Kinetic modeling of the pyrolysis of Kraft lignin activated with phosphoric acid, Chem. Eng. J. 106 (2005) 1–12. https://doi.org/10.1016/j.cej.2004.11.001.

[102] E. Gonzalez-Serrano, T. Cordero, J. Rodríguez-Mirasol, J.J. Rodríguez, Development of Porosity upon Chemical Activation of Kraft Lignin with $ZnCl_2$, Ind. Eng. Chem. Res. 36 (1997) 4832–4838. https://doi.org/10.1021/ie970261q.

[103] J. Hayashi, A. Kazehaya, K. Muroyama, A.P. Watkinson, Preparation of activated carbon from lignin by chemical activation, Carbon. 38 (2000) 1873–1878. https://doi.org/10.1016/S0008-6223(00)00027-0.

[104] V. Fierro, V. Torné-Fernández, A. Celzard, Methodical study of the chemical activation of Kraft lignin with KOH and NaOH, Microporous Mesoporous Mater. 101 (2007) 419–413. https://doi.org/10.1016/j.micromeso.2006.12.004.

[105] V. Fierro, V. Torné-Fernández, A. Celzard, Highly microporous carbons prepared by activation of kraft lignin with KOH, Stud. Surf. Sci. Catal. 160 (2007) 607–614. https://doi.org/10.1016/s0167-2991(07)80078-4.

[106] M. Jagtoyen, F. Derbyshire, Some considerations of the origins of porosity in carbons from chemically activated wood, Carbon N. Y. 31 (1993) 1185–1192.



UNIVERSIDAD DE MÁLAGA

https://doi.org/10.1016/0008-6223(93)90071-H.

[107] David. N. S. .Hong, N. Shiraishi. Wood and Cellulosic Chemistry, 1 st, Marcel Dekker, NewYork., 1991.

[108] R. Delobel, M. Le Bras, N. Ouassou, R. Descressain, Fire retardance of polypropylene by diammonium pyrophosphate-pentaerythritol: Spectroscopic characterization of the protective coatings, Polym. Degrad. Stab. 30 (1990) 41–56. https://doi.org/10.1016/0141-3910(90)90116-O.

[109] J.M. Rosas, J. Bedia, J. Rodríguez-Mirasol, T. Cordero, Preparation of hemp-derived activated carbon monoliths. Adsorption of water vapor, Ind. Eng. Chem. Res. 47 (2008) 1288–1296. https://doi.org/10.1021/ie070924w.

[110] J. Bedia, J.M. Rosas, J. Márquez, J. Rodríguez-Mirasol, T. Cordero, Preparation and characterization of carbon based acid catalysts for the dehydration of 2-propanol, Carbon. 47 (2009) 286–294. https://doi.org/10.1016/j.carbon.2008.10.008.

[111] M.J. Valero-Romero, F.J. García-Mateos, J. Rodríguez-Mirasol, T. Cordero, Role of surface phosphorus complexes on the oxidation of porous carbons, Fuel Process. Technol. 157 (2017) 116–126. https://doi.org/10.1016/j.fuproc.2016.11.014.

[112] J.M. Rosas, R. Ruiz-Rosas, J. Rodríguez-Mirasol, T. Cordero, Kinetic study of the oxidation resistance of phosphorus-containing activated carbons, Carbon. 50 (2012) 1523–1537. https://doi.org/10.1016/j.carbon.2011.11.030.

[113] D. Lozano-Castelló, M.A. Lillo-Ródenas, D. Cazorla-Amorós, A. Linares-Solano, Preparation of activated carbons from Spanish anthracite - I. Activation by KOH, Carbon. 39 (2001) 741–749. https://doi.org/10.1016/S0008-6223(00)00185-8.

[114] M.A. Lillo-Ródenas, D. Lozano-Castelló, D. Cazorla-Amorós, A. Linares-Solano, Preparation of activated carbons from Spanish anthracite - II. Activation by NaOH, Carbon. 39 (2001) 751–759. https://doi.org/10.1016/S0008-6223(00)00186-X.

[115] M.. Lillo-Ródenas, D. Cazorla-Amorós, A. Linares-Solano, Understanding chemical reactions between carbons and NaOH and KOH, Carbon. 41 (2002) 267–275. https://doi.org/10.1016/s0008-6223(02)00279-8.

[116] A.P. Carvalho, B. Cardoso, J. Pires, M. Brotas de Carvalho, Preparation of activated carbons from cork waste by chemical activation with KOH, Carbon. 41 (2003) 2873–2876. https://doi.org/10.1016/S0008-6223(03)00323-3.

[117] A. Aygün, S. Yenisoy-Karakaş, I. Duman, Production of granular activated carbon from fruit stones and nutshells and evaluation of their physical, chemical and adsorption properties,

UNIVERSIDAD DE MÁLAGA

Microporous Mesoporous Mater. 66 (2003) 189–195. https://doi.org/10.1016/j.micromeso.2003.08.028.

[118] A. Nayak, B. Bhushan, V. Gupta, P. Sharma, Chemically activated carbon from lignocellulosic wastes for heavy metal wastewater remediation: Effect of activation conditions, J. Colloid Interface Sci. 493 (2017) 228–240. https://doi.org/10.1016/j.jcis.2017.01.031.

[119] J. Bedia, C. Belver, S. Ponce, J. Rodriguez, J.J. Rodriguez, Adsorption of antipyrine by activated carbons from $FeCl_3$-activation of Tara gum, Chem. Eng. J. 333 (2018) 58–65. https://doi.org/10.1016/j.cej.2017.09.161.

[120] N. V. Sych, S.I. Trofymenko, O.I. Poddubnaya, M.M. Tsyba, V.I. Sapsay, D.O. Klymchuk, A.M. Puziy, Porous structure and surface chemistry of phosphoric acid activated carbon from corncob, Appl. Surf. Sci. 261 (2012) 75–82. https://doi.org/10.1016/j.apsusc.2012.07.084.

[121] M. Molina-Sabio, F. RodRíguez-Reinoso, F. Caturla, M.J. Sellés, Porosity in granular carbons activated with phosphoric acid, Carbon. 33 (1995) 1105–1113. https://doi.org/10.1016/0008-6223(95)00059-M.

[122] H. Benaddi, D. Legras, J.N. Rouzaud, F. Beguin, Influence of the atmosphere in the chemical activation of wood by phosphoric acid, Carbon. (1998) 306–309. https://doi.org/10.1016/S0008-6223(98)80123-1.

[123] J.M. Rosas, J. Bedia, J. Rodríguez-Mirasol, T. Cordero, Hemp-derived activated carbon fibers by chemical activation with phosphoric acid, Fuel. 88 (2009) 19–26. https://doi.org/10.1016/j.fuel.2008.08.004.

[124] F.J. García-Mateos, R. Ruiz-Rosas, M.D. Marqués, L.M. Cotoruelo, J. Rodríguez-Mirasol, T. Cordero, Removal of paracetamol on biomass-derived activated carbon: Modeling the fixed bed breakthrough curves using batch adsorption experiments, Chem. Eng. J. 279 (2015) 18–30. https://doi.org/10.1016/j.cej.2015.04.144.

[125] J. Bedia, J.M. Rosas, D. Vera, J. Rodríguez-Mirasol, T. Cordero, Isopropanol decomposition on carbon based acid and basic catalysts, Catal. Today. 158 (2010) 89–96. https://doi.org/10.1016/j.cattod.2010.04.043.

[126] O.N. Baklanova, G. V. Plaksin, V.A. Drozdov, V.K. Duplyakin, N. V. Chesnokov, B.N. Kuznetsov, Preparation of microporous sorbents from cedar nutshells and hydrolytic lignin, Carbon. 41 (2003) 1793–1800. https://doi.org/10.1016/S0008-6223(03)00149-0.

[127] P.J.M. Carrott, Suhas, M.M.L. Ribeiro Carrott, C.I. Guerrero, L.A. Delgado, Reactivity and porosity development during pyrolysis and physical activation in $CO_2$ or steam of kraft and

UNIVERSIDAD DE MÁLAGA

hydrolytic lignins, J. Anal. Appl. Pyrolysis. 82 (2008) 264–271. https://doi.org/10.1016/j.jaap.2008.04.004.

[128] E. Gonzalez-Serrano, T. Cordero, J. Rodriguez-Mirasol, L. Cotoruelo, J.J. Rodriguez, Removal of water pollutants with activated carbons prepared from $H_3PO_4$ activation of lignin from kraft black liquors, Water Res. 38 (2004) 3043–3050. https://doi.org/10.1016/j.watres.2004.04.048.

[129] J.Bedia . J.Rodríguez-Mirasol, T.Cordero, Water vapor adsorption on lignin-based activated carbon, J. Chem. Technol. Biotechnol. 82 (2007) 548–557. https://doi.org/10.1002/jctb.

[130] L.M. Cotoruelo, M.D. Marqués, J. Rodríguez-Mirasol, T. Cordero, J.J. Rodríguez, Adsorption of aromatic compounds on activated carbons from lignin: Equilibrium and thermodynamic study, Ind. Eng. Chem. Res. 46 (2007) 4982–4990. https://doi.org/10.1021/ie061415h.

[131] L.M. Cotoruelo, M.D. Marqués, F.J. Díaz, J. Rodríguez-Mirasol, T. Cordero, J.J. Rodríguez, Activated carbons from lignin: Their application in liquid phase adsorption, Sep. Sci. Technol. 42 (2007) 3363–3389. https://doi.org/10.1080/01496390701626800.

[132] L.M. Cotoruelo, M.D. Marqués, J. Rodríguez-Mirasol, J.J. Rodríguez, T. Cordero, Lignin-based activated carbons for adsorption of sodium dodecylbenzene sulfonate: Equilibrium and kinetic studies, J. Colloid Interface Sci. 332 (2009) 39–45. https://doi.org/10.1016/J.JCIS.2008.12.031.

[133] L.M. Cotoruelo, M.D. Marqués, F.J. Díaz, J. Rodríguez-Mirasol, J.J. Rodríguez, T. Cordero, Equilibrium and kinetic study of congo red adsorption onto lignin-based activated carbons, Transp. Porous Media. 83 (2010) 573–590. https://doi.org/10.1007/s11242-009-9460-8.

[134] L.M. Cotoruelo, M.D. Marqués, J. Rodríguez-Mirasol, J.J. Rodríguez, T. Cordero, Cationic dyes removal by multilayer adsorption on activated carbons from lignin, J. Porous Mater. 18 (2011) 693–702. https://doi.org/10.1007/s10934-010-9428-7.

[135] L.M. Cotoruelo, M.D. Marqués, A. Leiva, J. Rodríguez-Mirasol, T. Cordero, Adsorption of oxygen-containing aromatics used in petrochemical, pharmaceutical and food industries by means of lignin based active carbons, Adsorption. 17 (2011) 539–550. https://doi.org/10.1007/s10450-010-9319-x.

[136] L.M. Cotoruelo, M.D. Marqués, F.J. Díaz, J. Rodríguez-Mirasol, J.J. Rodríguez, T. Cordero, Adsorbent ability of lignin-based activated carbons for the removal of p-nitrophenol from aqueous solutions, Chem. Eng. J. 184 (2012) 176–183. https://doi.org/10.1016/J.CEJ.2012.01.026.

UNIVERSIDAD DE MÁLAGA

[137] L.M. Cotoruelo, M.D. Marqués, F.J. Díaz, J. Rodríguez-Mirasol, T. Cordero, J.J. Rodríguez, Lignin-Based Activated Carbons as Adsorbents for Crystal Violet Removal from Aqueous Solutions, Environ. Prog. Sustain. Energy. 31 (2011) 386–396. https://doi.org/10.1002/ep.10560.

[138] J. Rodríguez-Mirasol, J. Bedia, T. Cordero, J. Rodríguez, Influence of water vapor on the adsorption of VOCs on lignin-based activated carbons, Sep. Sci. Technol. 40 (2005) 3113–3135. https://doi.org/10.1080/01496390500385277.

[139] B.N. Kuznetsov, M.L. Shchipko, The conversion of wood lignin to char materials in a fluidized bed of AlCuCr oxide catalysts, Bioresour. Technol. 52 (1995) 13–19. https://doi.org/10.1016/0960-8524(94)00140-V.

[140] K. Fu, Q. Yue, B. Gao, Y. Sun, L. Zhu, Preparation, characterization and application of lignin-based activated carbon from black liquor lignin by steam activation, Chem. Eng. J. 228 (2013) 1074–1082. https://doi.org/10.1016/j.cej.2013.05.028.

[141] J.P.Zhang, Y. Sun, M.W. Woo, L. Zhang, K.Z. Xu, Preparation of steam activated carbon from black liquor by flue gas precipitation and its performance in hydrogen sulfide removal: Experimental and simulation works, Rev. Mex. Urol. 76 (2016) 395–404. https://doi.org/10.1016/j.jtice.2015.09.005.

[142] A. V. Maldhure, J.D. Ekhe, Preparation and characterizations of microwave assisted activated carbons from industrial waste lignin for Cu(II) sorption, Chem. Eng. J. 168 (2011) 1103–1111. https://doi.org/10.1016/j.cej.2011.01.091.

[143] L. Khezami, A. Chetouani, B. Taouk, R. Capart, Production and characterisation of activated carbon from wood components in powder: Cellulose, lignin, xylan, Powder Technol. 157 (2005) 48–56. https://doi.org/10.1016/j.powtec.2005.05.009.

[144] Q.-X.G. Xian-Fa Li, Qing Xu, Yao Fu, Preparation and Characterization of Activated Carbon from Kraft Lignin via KOH Activation, Environ. Prog. Sustain. Energy. 33 (2014) 519–526. https://doi.org/10.1002/ep.

[145] Y. Gao, Q. Yue, B. Gao, Y. Sun, W. Wang, Q. Li, Y. Wang, Preparation of high surface area-activated carbon from lignin of papermaking black liquor by KOH activation for Ni(II) adsorption, Chem. Eng. J. 217 (2013) 345–353. https://doi.org/10.1016/j.cej.2012.09.038.

[146] V. Torné-Fernández, J.M. Mateo-Sanz, D. Montané, V. Fierro, Statistical optimization of the synthesis of highly microporous carbons by chemical activation of kraft lignin with NaOH, J. Chem. Eng. Data. 54 (2009) 2216–2221. https://doi.org/10.1021/je800827n.

[147] Y. Sun, J. Wei, Y.S. Wang, G. Yang, J.P. Zhang, Production of activated carbon by

UNIVERSIDAD DE MÁLAGA

$K_2CO_3$activation treatment of cornstalk lignin and its performance in removing phenol and subsequent bioregeneration, Environ. Technol. 31 (2010) 53–61. https://doi.org/10.1080/09593330903338411.

[148] X.F. Li, Y. Zuo, Y. Zhang, Y. Fu, Q.X. Guo, In situ preparation of $K_2CO_3$ supported Kraft lignin activated carbon as solid base catalyst for biodiesel production, Fuel. 113 (2013) 435–442. https://doi.org/10.1016/j.fuel.2013.06.008.

[149] N. Tsubouchi, M. Nishio, Y. Mochizuki, Role of nitrogen in pore development in activated carbon prepared by potassium carbonate activation of lignin, Appl. Surf. Sci. 371 (2016) 301–306. https://doi.org/10.1016/j.apsusc.2016.02.200.

[150] V. Fierro, V. Torné-Fernández, A. Celzard, Kraft lignin as a precursor for microporous activated carbons prepared by impregnation with ortho-phosphoric acid: Synthesis and textural characterisation, Microporous Mesoporous Mater. 92 (2006) 243–250. https://doi.org/10.1016/j.micromeso.2006.01.013.

[151] V. Fierro, V. Torné-Fernández, A. Celzard, D. Montané, Influence of the demineralisation on the chemical activation of Kraft lignin with orthophosphoric acid, J. Hazard. Mater. 149 (2007) 126–133. https://doi.org/10.1016/j.jhazmat.2007.03.056.

[152] Y. Sun, G. Yang, J. Zhang, Y. Wang, M. Yao, Activated carbon preparation from lignin by $H_3PO_4$ activation and its application to gas separation, Chem. Eng. Technol. 35 (2012) 309–316. https://doi.org/10.1002/ceat.201100309.

[153] Y. Guo, D.A. Rockstraw, Physical and chemical properties of carbons synthesized from xylan, cellulose, and Kraft lignin by $H_3PO_4$ activation, Carbon. 44 (2006) 1464–1475. https://doi.org/10.1016/j.carbon.2005.12.002.

[154] E. Guillén, R. Rico, J.M. López-Romero, J. Bedia, J.M. Rosas, J. Rodríguez-Mirasol, T. Cordero, Pd-activated carbon catalysts for hydrogenation and Suzuki reactions, Appl. Catal. A Gen. 368 (2009) 113–120. https://doi.org/10.1016/j.apcata.2009.08.016.

[155] J. Bedia, J.M. Rosas, J. Rodríguez-Mirasol, T. Cordero, Pd supported on mesoporous activated carbons with high oxidation resistance as catalysts for toluene oxidation, Appl. Catal. B Environ. 94 (2010) 8–18. https://doi.org/10.1016/j.apcatb.2009.10.015.

[156] Y. Zou, B.X. Han, Preparation of activated carbons from Chinese coal and hydrolysis lignin, Adsorpt. Sci. Technol. 19 (2001) 59–72. https://doi.org/10.1260/0263617011493971.

[157] E. Worch, Adsorption Technology in Water Treatment, Walter de Gruyter GmbH & Co. KG, Berlin/Boston, Berlin, Boston, 2012. https://doi.org/10.1515/9783110240238.

[158] V. Geissen, H. Mol, E. Klumpp, G. Umlauf, M. Nadal, M. van der Ploeg, S.E.A.T.M. van de



UNIVERSIDAD DE MÁLAGA

Zee, C.J. Ritsema, Emerging pollutants in the environment: A challenge for water resource management, Int. Soil Water Conserv. Res. 3 (2015) 57–65. https://doi.org/10.1016/j.iswcr.2015.03.002.

[159] A. Pal, Y. He, M. Jekel, M. Reinhard, K.Y.H. Gin, Emerging contaminants of public health significance as water quality indicator compounds in the urban water cycle, Environ. Int. 71 (2014) 46–62. https://doi.org/10.1016/j.envint.2014.05.025.

[160] J. Wilkinson, P.S. Hooda, J. Barker, S. Barton, J. Swinden, Occurrence, fate and transformation of emerging contaminants in water: An overarching review of the field, Environ. Pollut. 231 (2017) 954–970. https://doi.org/10.1016/j.envpol.2017.08.032.

[161] Y. Xu, F. Luo, A. Pal, K.Y.H. Gin, M. Reinhard, Occurrence of emerging organic contaminants in a tropical urban catchment in Singapore, Chemosphere. 83 (2011) 963–969. https://doi.org/10.1016/j.chemosphere.2011.02.029.

[162] J. Gasperi, C. Sebastian, V. Ruban, M. Delamain, S. Percot, L. Wiest, C. Mirande, E. Caupos, D. Demare, M.D.K. Kessoo, M. Saad, J.J. Schwartz, P. Dubois, C. Fratta, H. Wolff, R. Moilleron, G. Chebbo, C. Cren, M. Millet, S. Barraud, M.C. Gromaire, Micropollutants in urban stormwater: Occurrence, concentrations, and atmospheric contributions for a wide range of contaminants in three French catchments, Environ. Sci. Pollut. Res. 21 (2014) 5267–5281. https://doi.org/10.1007/s11356-013-2396-0.

[163] O.M. Rodriguez-Narvaez, J.M. Peralta-Hernandez, A. Goonetilleke, E.R. Bandala, Treatment technologies for emerging contaminants in water: A review, Chem. Eng. J. 323 (2017) 361–380. https://doi.org/10.1016/j.cej.2017.04.106.

[164] T. Deblonde, C. Cossu-Leguille, P. Hartemann, Emerging pollutants in wastewater: A review of the literature, Int. J. Hyg. Environ. Health. 214 (2011) 442–448. https://doi.org/10.1016/j.ijheh.2011.08.002.

[165] S. Dey, F. Bano, A. Malik, Pharmaceuticals and personal care product (PPCP) contamination—a global discharge inventory, in: Butterworth-Heinemann (Ed.), Pharm. Pers. Care Prod. Waste Manag. Treat. Technol., Elsevier Inc., 2019: pp. 1–26. https://doi.org/10.1016/b978-0-12-816189-0.00001-9.

[166] I. Chorkendorff, J.W. Niemantsverdriet, Concepts of Modern Catalysis and Kinetics, 2 nd, WILEY-VCH Verlag GmbH &Co. KGaA, 2007. https://pdfs.semanticscholar.org/f327/2e1d98b5c8deea4eda9428bbf2f220a08931.pdf.

[167] I. Matos, M. Bernardo, I. Fonseca, Porous carbon: A versatile material for catalysis, Catal. Today. 285 (2017) 194–203. https://doi.org/10.1016/j.cattod.2017.01.039.

UNIVERSIDAD DE MÁLAGA

[168] J. Bedia, R. Barrionuevo, J. Rodríguez-Mirasol, T. Cordero, Ethanol dehydration to ethylene on acid carbon catalysts, Appl. Catal. B Environ. 103 (2011) 302–310. https://doi.org/10.1016/j.apcatb.2011.01.032.

[169] S. Sharma, B.G. Pollet, Support materials for PEMFC and DMFC electrocatalysts - A review, J. Power Sources. 208 (2012) 96–119. https://doi.org/10.1016/j.jpowsour.2012.02.011.

[170] F.J. García-Mateos, T. Cordero-Lanzac, R. Berenguer, E. Morallón, D. Cazorla-Amorós, J. Rodríguez-Mirasol, T. Cordero, Lignin-derived Pt supported carbon (submicron)fiber electrocatalysts for alcohol electro-oxidation, Appl. Catal. B Environ. 211 (2017) 18–30. https://doi.org/10.1016/j.apcatb.2017.04.008.

[171] J.B. García-Matamoros. (2008). Catalizadores Carbonosos obtenidos mediante Activación Química de Residuos Lignocelulósicos. (Doctoral thesis ). Universidad de Málaga, Málaga, Spain.

[172] F.M. Bautista, J.M. Campelo, A. García, D. Luna, J.M. Marinas, A.A. Romero, M.T. Siles, Vanadyl-aluminum binary phosphate: Al/V ratio influence on their structure and catalytic behavior in the 2-propanol conversion, Catal. Today. 78 (2003) 269–280. https://doi.org/10.1016/S0920-5861(02)00352-8.

[173] E. Lam, J.H.T. Luong, Carbon materials as catalyst supports and catalysts in the transformation of biomass to fuels and chemicals, ACS Catal. 4 (2014) 3393–3410. https://doi.org/10.1021/cs5008393.

[174] E. Pérez-Mayoral, V. Calvino-Casilda, E. Soriano, Metal-supported carbon-based materials: Opportunities and challenges in the synthesis of valuable products, Catal. Sci. Technol. 6 (2016) 1265–1291. https://doi.org/10.1039/c5cy01437a.

[175] B.I. Kharisov, O. V. Kharissova, Coordination and organometallic compounds in the functionalization of carbon nanotubes, J. Coord. Chem. 67 (2014) 3769–3808. https://doi.org/10.1080/00958972.2014.888063.

[176] D.C. Elliott, T.R. Hart, Catalytic hydroprocessing of chemical models for bio-oil, Energy and Fuels. 23 (2009) 631–637. https://doi.org/10.1021/ef8007773.

[177] F.J. Derbyshire, V.H.J. de Beer, G.M.K. Abotsi, A.W. Scaroni, J.M. Solar, D.J. Skrovanek, The influence of surface functionality on the activity of carbon-supported catalysts, Appl. Catal. 27 (1986) 117–131. https://doi.org/10.1016/S0166-9834(00)81051-9.

[178] C. Prado-Burguete, A. Linares-Solano, F. Rodríguez-Reinoso, C.S.M. de Lecea, The effect of oxygen surface groups of the support on platinum dispersion in Pt/carbon catalysts, J. Catal. 115 (1989) 98–106. https://doi.org/10.1016/0021-9517(89)90010-9.

UNIVERSIDAD DE MÁLAGA

[179] C. Prado-Burguete, A. Linares-Solano, F. Rodriguez-Reinoso, C.S.M. De Lecea, Effect of carbon support and mean Pt particle size on hydrogen chemisorption by carbon-supported Pt ctalysts, J. Catal. 128 (1991) 397–404. https://doi.org/10.1016/0021-9517(91)90298-I.

[180] V. Machek, J. Hanika, K. Sporka, V. Růžička, J. Kunz, Relation between the distribution of platinum, its dispersion, and activity of catalysts prepared by impregnation of activated carbon with chloroplatinic acid solutions, Collect. Czechoslov. Chem. Commun. 46 (1981) 3270–3277. https://doi.org/10.1135/cccc19813270.

[181] G.R. GS Szymanski, Influence of oxygen surface groups in catalytic dehydration and dehydrogentation of 2-butanol promoted by carbon catalysts, Carbon. 29 (1991) 489–498.

[182] T. Yashima, H. Suzuki, N. Hara, Decomposition of 2-propanol over alkali cation exchanged zeolites, J. Catal. 33 (1974) 486–492. https://doi.org/10.1016/0021-9517(74)90295-4.

[183] M.A. Aramendía, V. Borau, C. Jiménez, J.M. Marinas, A. Porras, F.J. Urbano, Magnesium oxides as basic catalysts for organic processes: Study of the dehydrogenation-dehydration of 2-propanol, J. Catal. 161 (1996) 829–838. https://doi.org/10.1006/jcat.1996.0246.

[184] M.J.L. Gines, E. Iglesia, Bifunctional condensation reactions of alcohols on basic oxides modified by copper and potassium, J. Catal. 176 (1998) 155–172. https://doi.org/10.1006/jcat.1998.2009.

[185] J. Macht, C.D. Baertsch, M. May-Lozano, S.L. Soled, Y. Wang, E. Iglesia, Support effects on Brønsted acid site densities and alcohol dehydration turnover rates on tungsten oxide domains, J. Catal. 277 (2004) 479–491. https://doi.org/10.1016/j.jcat.2004.08.014.

[186] G.S. Szymański, G. Rychlicki, Catalytic conversion of propan-2-ol on carbon catalysts, Carbon N. Y. 31 (1993) 247–257. https://doi.org/10.1016/0008-6223(93)90028-9.

[187] R.M. Rioux, M.A. Vannice, Hydrogenation/dehydrogenation reactions: Isopropanol dehydrogenation over copper catalysts, J. Catal. 216 (2003) 362–376. https://doi.org/10.1016/S0021-9517(02)00035-0.

[188] G.S. Szymański, G. Rychlicki, Importance of oxygen surface groups in catalytic dehydration and dehydrogenation of butan-2-ol promoted by carbon catalysts, Carbon. 29 (1991) 489–498. https://doi.org/10.1016/0008-6223(91)90112-V.

[189] G.S. Szymański, G. Rychlicki, A.P. Terzyk, Catalytic conversion of ethanol on carbon catalysts, Carbon N. Y. 32 (1994) 265–271. https://doi.org/10.1016/0008-6223(94)90189-9.

[190] D.C. Tomczak, J.L. Allen, K.R. Poeppelmeier, Characterization of the acidic and basic properties of αLiAlO2, γLiAlO2, and calcined "$HAlO_2$" using isopropyl alcohol, J. Catal. 146 (1994) 155–165. https://doi.org/10.1016/0021-9517(94)90018-3.

UNIVERSIDAD DE MÁLAGA

[191] A. Gervasini, A. Auroux, Acidity and basicity of metal oxide surfaces II. Determination by catalytic decomposition of isopropanol, J. Catal. 131 (1991) 190–198. https://doi.org/10.1016/0021-9517(91)90335-2.

[192] J.M. Campelo, A. Garcia, J.F. Herencia, D. Luna, J.M. Marinas, A.A. Romero, Conversion of alcohols (α-Methylated series) on ALPO4 catalysts, J. Catal. 151 (1995) 307–314. https://doi.org/10.1006/jcat.1995.1032.

[193] M.A. Aramendía, V. Boráu, I.M. García, C. Jiménez, A. Marinas, J.M. Marinas, A. Porras, F.J. Urbano, Comparison of different organic test reactions over acid-base catalysts, Appl. Catal. A Gen. 184 (1999) 115–125. https://doi.org/10.1016/S0926-860X(99)00096-4.

[194] M.A. Aramendía, V. Borau, C. Jiménez, A. Marinas, J.M. Marinas, J.R. Ruiz, F.J. Urbano, Magnesium-containing mixed oxides as basic catalysts: Base characterization by carbon dioxide TPD-MS and test reactions, J. Mol. Catal. A Chem. 218 (2004) 81–90. https://doi.org/10.1016/j.molcata.2004.04.006.

[195] R.M. Rioux, M.A. Vannice, Dehydrogenation of isopropyl alcohol on carbon-supported Pt and Cu-Pt catalysts, J. Catal. 233 (2005) 147–165. https://doi.org/10.1016/j.jcat.2005.04.020.

[196] J. Bedia, R. Ruiz-Rosas, J. Rodríguez-Mirasol, T. Cordero, A kinetic study of 2-propanol dehydration on carbon acid catalysts, J. Catal. 271 (2010) 33–42. https://doi.org/10.1016/j.jcat.2010.01.023.

[197] A.G. Gayubo, A.M. Tarrío, A.T. Aguayo, M. Olazar, J. Bilbao, Kinetic modelling of the transformation of aqueous ethanol into hydrocarbons on a HZSM-5 zeolite, Ind. Eng. Chem. Res. 40 (2001) 3467–3474. https://doi.org/10.1021/ie001115e.

[198] A.T. Aguayo, A.G. Gayubo, A.M. Tarrío, A. Atutxa, J. Bilbao, Study of operating variables in the transformation of aqueous ethanol into hydrocarbons on an HZSM-5 zeolite, J. Chem. Technol. Biotechnol. 77 (2002) 211–216. https://doi.org/10.1002/jctb.540.

[199] S. Golay, R. Doepper, A. Renken, Reactor performance enhancement under periodic operation for the ethanol dehydration over γ-alumina, a reaction with a stop-effect, Chem. Eng. Sci. 54 (1999) 4469–4474. https://doi.org/10.1016/S0009-2509(99)00105-0.

[200] G. Chen, S. Li, F. Jiao, Q. Yuan, Catalytic dehydration of bioethanol to ethylene over $TiO_2$/γ-$Al_2O_3$ catalysts in microchannel reactors, Catal. Today. 125 (2007) 111–119. https://doi.org/10.1016/j.cattod.2007.01.071.

[201] R. Le Van Mao, T.M. Nguyen, G.P. McLaughlin, The bioethanol-to-ethylene (B.E.T.E.) process, Appl. Catal. 48 (1989) 265–277. https://doi.org/10.1016/S0166-9834(00)82798-0.

[202] P. Berteau, B. Delmon, Modified Aluminas : Relationship between activity in 1-butanol



UNIVERSIDAD DE MÁLAGA

dehydration and acidity measured by $NH_3$ TPD, Catal. Today. 5 (1989) 121–137. https://doi.org/10.1016/0920-5861(89)80020-3.

[203] T. Zaki, Catalytic dehydration of ethanol using transition metal oxide catalysts, J. Colloid Interface Sci. 284 (2005) 606–613. https://doi.org/10.1016/j.jcis.2004.10.048.

[204] G.A. El-Shobaky, M.M. Doheim, A.M. Ghozza, H.A. El-Boohy, Catalytic conversion of ethanol over Co3O4/MgO system treated with γ-irradiation, Mater. Lett. 57 (2002) 525–531. https://doi.org/10.1016/S0167-577X(02)00823-6.

[205] B.M. Abu-Zied, A.M. El-Awad, The synergism of cadmium on the catalytic activity of Cd-Cr-O system II. Ethanol decomposition, catalysts reducibility, and in situ electrical conductivity measurements, J. Mol. Catal. A Chem. 176 (2001) 227–246. https://doi.org/10.1016/S1381-1169(01)00263-1.

[206] X. Gao, I.E. Wachs, Titania-silica as catalysts: Molecular structural characteristics and physico-chemical properties, Catal. Today. 51 (1999) 233–254. https://doi.org/10.1016/S0920-5861(99)00048-6.

[207] J. Haber, K. Pamin, L. Matachowski, B. Napruszewska, J. Połtowicz, Potassium and silver salts of tungstophosphoric acid as catalysts in dehydration of ethanol and hydration of ethylene, J. Catal. 207 (2002) 296–306. https://doi.org/10.1006/jcat.2002.3514.

[208] E.A. El-Katatny, S.A. Halawy, M.A. Mohamed, M.I. Zaki, Recovery of ethene-selective FeOx/Al2O3 ethanol dehydration catalyst from industrial chemical wastes, Appl. Catal. A Gen. 199 (2000) 83–92. https://doi.org/10.1016/S0926-860X(99)00539-6.

[209] D. Varisli, T. Dogu, G. Dogu, Ethylene and diethyl-ether production by dehydration reaction of ethanol over different heteropolyacid catalysts, Chem. Eng. Sci. 62 (2007) 5349–5352. https://doi.org/10.1016/j.ces.2007.01.017.

[210] J.I.Di-Cosimo, V.K.Diez, M.Xu, E.Iglesia, C.R. Apesteguia, Structure and Surface and Catalytic Properties of Mg-Al Basic Oxides, J. Catal. 178 (1998) 499–510.

[211] G.C. Grunewald, R.S. Drago, Carbon Molecular Sieves as Catalysts and Catalyst Supports, J. Am. Chem. Soc. 113 (1991) 1636–1639. https://doi.org/10.1021/ja00005a029.

[212] F. Carrasco-Marín, A. Mueden, C. Moreno-Castilla, Surface-treated activated carbons as catalysts for the dehydration and dehydrogenation reactions of ethanol, J. Phys. Chem. B. 102 (1998) 9239–9244. https://doi.org/10.1021/jp981861l.

[213] D.M. Brown, B.L. Bhatt, T.H. Hsiung, J.J. Lewnard, F.J. Waller, Novel technology for the synthesis of dimethyl ether from syngas, Catal. Today. 8 (1991) 279–304. https://doi.org/10.1016/0920-5861(91)80055-E.

UNIVERSIDAD DE MÁLAGA

[214] W.W. Kaeding, S.A. Butter, Production of chemicals from methanol. I. Low molecular weight olefins, J. Catal. 61 (1980) 155–164. https://doi.org/10.1016/0021-9517(80)90351-6.

[215] G. Cai, Z. Liu, R. Shi, H. Changqing, L. Yang, C. Sun, Y. Chang, Light alkenes from syngas via dimethyl ether, Appl. Catal. A, Gen. 125 (1995) 29–38. https://doi.org/10.1016/0926-860X(94)00291-6.

[216] H.T. Tsutomu Shikada, Kaoru Fujimoto, Michiharu Miyauchi, Vapor phase carbonylation of dimethyl ether and methyl acetate with nickel-active carbon catalysts, Appl. Catal. 7 (1983) 361–368. https://doi.org/0166-9834/83.

[217] M. Xu, J.H. Lunsford, D.W. Goodman, A. Bhattacharyya, Synthesis of dimethyl ether (DME) from methanol over solid-acid catalysts, Appl. Catal. A Gen. 149 (1997) 289–301. https://doi.org/10.1016/S0926-860X(96)00275-X.

[218] T. Takeguchi, K.I. Yanagisawa, T. Inui, M. Inoue, Effect of the property of solid acid upon syngas-to-dimethyl ether conversion on the hybrid catalysts composed of Cu-Zn-Ga and solid acids, Appl. Catal. A Gen. 192 (2000) 201–209. https://doi.org/10.1016/S0926-860X(99)00343-9.

[219] J. Jasińska, B. Krzyżyńska, M. Kozłowski, Influence of activated carbon modifications on their catalytic activity in methanol and ethanol conversion reactions, Cent. Eur. J. Chem. 9 (2011) 925–931. https://doi.org/10.2478/s11532-011-0078-7.

[220] V. Vishwanathan, K.W. Jun, J.W. Kim, H.S. Roh, Vapour phase dehydration of crude methanol to dimethyl ether over Na-modified H-ZSM-5 catalysts, Appl. Catal. A Gen. 276 (2004) 251–255. https://doi.org/10.1016/j.apcata.2004.08.011.

[221] S.D. Kim, S.C. Baek, Y.J. Lee, K.W. Jun, M.J. Kim, I.S. Yoo, Effect of γ-alumina content on catalytic performance of modified ZSM-5 for dehydration of crude methanol to dimethyl ether, Appl. Catal. A Gen. 309 (2006) 139–143. https://doi.org/10.1016/j.apcata.2006.05.008.

[222] G. Laugel, X. Nitsch, F. Ocampo, B. Louis, Methanol dehydration into dimethylether over ZSM-5 type zeolites: Raise in the operational temperature range, Appl. Catal. A Gen. 402 (2011) 139–145. https://doi.org/10.1016/j.apcata.2011.05.039.

[223] C. Moreno-Castilla, F. Carrasco-Marín, C. Parejo-Pérez, M. V. López Ramón, Dehydration of methanol to dimethyl ether catalyzed by oxidized activated carbons with varying surface acidic character, Carbon N. Y. 39 (2001) 869–875. https://doi.org/10.1016/S0008-6223(00)00192-5.

[224] M.J. Valero-Romero, E.M. Calvo-Muñoz, R. Ruiz-Rosas, J. Rodríguez-Mirasol, T. Cordero,

UNIVERSIDAD DE MÁLAGA

Phosphorus-Containing Mesoporous Carbon Acid Catalyst for Methanol Dehydration to Dimethyl Ether, Ind. Eng. Chem. Res. 58 (2019) 4042–4053. https://doi.org/10.1021/acs.iecr.8b05897.

[225] P.O. Ibeh, F.J. García-Mateos, R. Ruiz-Rosas, J.M. Rosas, J. Rodríguez-Mirasol, T. Cordero, Acid mesoporous carbon monoliths from lignocellulosic biomass waste for methanol dehydration, Materials (Basel). 12 (2019) 2394–2407. https://doi.org/10.3390/ma12152394.

[226] J. Palomo, J. Rodríguez-Mirasol, T. Cordero, Methanol dehydration to dimethyl ether on Zr-loaded P-containing mesoporous activated carbon catalysts, Materials (Basel). 12 (2019) 1–17. https://doi.org/10.3390/ma12132204.

UNIVERSIDAD DE MÁLAGA

# Chapter II

UNIVERSIDAD
DE MÁLAGA

# 2 Chapter II: Experimental methods

## 2.1 Preparation of activated carbons

Two different types of lignins were selected as precursors for the preparation of different activated carbons in this thesis: one organosolv lignin, concretely, derived from Alcell method (supplied by Repap Technologies Inc Co.) and one kind of kraft lignin, specifically, a sodium-lignosulphonate powder with high purity derived from wood (supplied by Sappi Biotech GmbH, Stockstadt, Germany).

### 2.1.1 Chemical activation

2.1.1.1 Preparation of activated carbon by co-solution of lignin with the activating agent

Activated carbons have been prepared by dissolving the raw material (Alcell lignin) with ethanol to simulate the composition of dissolved lignin in the Organosolv liquors [1,2]. Then, co-solution of lignin and the activating agent, $H_3PO_4$ 85% (w/w), was carried out at room temperature. The mixture has been stirred until evaporation of the ethanol and dried for 24 hours at 60 °C in a vacuum dryer. The $H_3PO_4$ to lignin mass ratio (weight of $H_3PO_4$/weight of lignin) was varied from 0.3 to 5. The samples were subsequently treated in air or nitrogen atmosphere (150 $cm^3$/min) and at different temperatures between 100 and 300 ºC, with a heating rate of 3 °C/min, followed by activation treatment in inert atmosphere of nitrogen or air at different temperatures between 400 and 900 °C, reached at heating rate of 10 °C/min. The activation and cooling step were carried out in a conventional laboratory tubular furnace. The experimental set-up for the oxidative treatment and activation of lignin is displayed in Figure.2.1.

2.1.1.2 Preparation of activated carbons from powder lignin

For comparison purposes, activated carbons have been also prepared from solid Alcell lignin, where no dissolved lignin in ethanol was mixed directly with the activation agent ($H_3PO_4$), but at the same preparation conditions as those used when lignin is dissolved in ethanol. The mixture was dried for 24 hours at 60 °C in a vacuum dryer. The impregnation ratio (weight of $H_3PO_4$/weight of lignin) value was varied from 0 to 4 . The precursor was activated under continuous $N_2$ flow (150 $cm^3$/min) in the conventional tubular furnace at different activation temperatures, reached at a heating rate of 10 °C/ min, the samples were

UNIVERSIDAD DE MÁLAGA

activated and cooled inside a furnace, as that schematized in Figure.2.1. Table 2.1 presents the nomenclature used in the thesis for activated carbons prepared by chemical activation with phosphoric acid.

**Table 2.1.** Nomenclature used for the activated carbons prepared by chemical activation.

| **Nomenclature** | **L** | **E** | **X** | **P** | **S** | **T** |
|---|---|---|---|---|---|---|
| **LEXPST** | Precursor (Alcell lignin ) | Ethanol | $H_3PO_4$ to lignin mass ratio | Activating agent ($H_3PO_4$) | Oxidative treatment | Activation temperature |

2.1.1.3 Washing and drying

It is necessary to carry out a washing process to extract the activating agent that is occluding the pores and, in this way, release the porous structure of the carbons. The washing is carried out with distilled water at 60 °C in a vacuum filtration system up to constant pH. Once the sample was filtered, the resulting solid was dried in an oven for 24 hours at 60 ºC, obtaining the dried carbon.

### 2.1.2 Physical activation

Activated carbons were also obtained by physical activation of a sodium-lignosulphonate powder derived from wood with high purity. The precursor was submitted to a carbonization treatment at different temperatures between 500 and 900 °C under a continuous $N_2$ flow (150 $cm^3$/min). The carbon materials obtained at 900°C were also partially gasified under a continuous $CO_2$ atmosphere (150 $cm^3$/min) at 750 °C for 30 min. Figure 2.1 collects the experimental set-up for the carbonization of lignin and $CO_2$ partial gasification of carbon. Table 2.2 collects the nomenclature proposed for activated carbons prepared by physical activation.

UNIVERSIDAD DE MÁLAGA

**Table 2.2.** Nomenclature used for the activated carbons prepared by physical activation.

| Nomenclature | L | T | W | G |
|---|---|---|---|---|
| **L900WG** | Precursor (Kraft lignin) | Carbonization temperature | Washing Step | Gasification step |

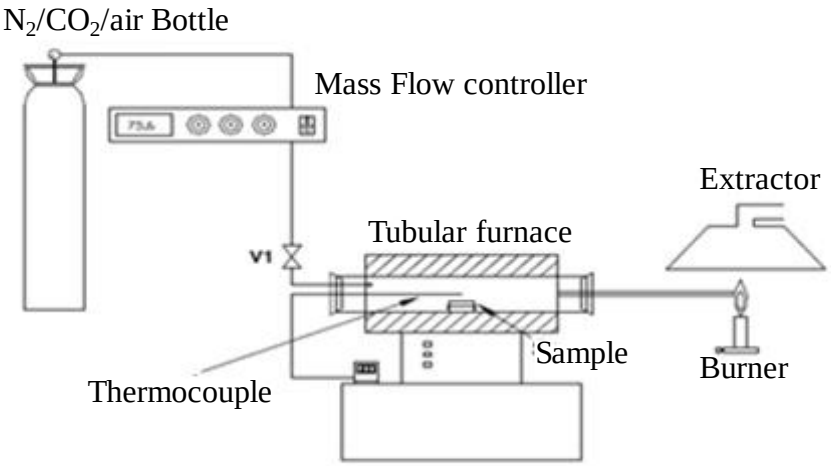


**Figure 2.1. .** Experimental set-up for the preparation of activated carbons by chemical and physical activation

## 2.2 Characterization of activated carbons

Different techniques have been applied to characterize the different activated carbons prepared in this thesis to ascertain the qualities and properties of the materials produced:

### 2.2.1 Ultimate Analysis and ash content

The ultimate analysis provides the total content of carbon, hydrogen, nitrogen and sulfur of the sample. Oxygen is obtained by difference of the total dry sample, discounted the ashes (dry ash free basis (d.a.f.)).

The ultimate analyses are carried out in a LECO® CHNS-932 analyser, in which the dried sample pre-weighed and pre-packaged is placed in a tin/aluminium container at a temperature of approximately 1000°C in a pure oxygen atmosphere and the quantities of $CO_2$, $SO_2$ and $H_2O$ are quantified by means of infrared sensors and $N_2$ by means of a catarometer.

The ash on a dry basis (d.b.), has been calculated by using a muffle furnace. The sample (approximately 1 g) is deposited in a crucible, which is then placed in the muffle, increasing

UNIVERSIDAD DE MÁLAGA

the temperature to 650 ºC. This temperature is kept until weight remains constant, as established by ASTM 2866-83.

### 2.2.2 **Textural properties**

The porosity of the samples was characterized by $N_2$ adsorption–desorption and $CO_2$ adsorption at -196 and 0 ºC, respectively, using a micromeritics instrument (ASAP 2020 model). The samples were previously outgassed for at least 8 hours at 150 ºC. From the $N_2$ isotherm, the apparent surface area ($A_{BET}$) was determined by applying the BET equation [3]; micropore volume ($V_t$) and external surface area ($A_t$) were calculated using the t-method ;mesopore volume ($V_{mes}$) was determined as the difference between the maximum adsorbed volume of $N_2$ ($V_p$), at a relative pressure of 0.99 and the micropore volume ($V_t$) [4]; the $\alpha_s$ method was also used to determine the values of the external surface area (As), the micropore volume (Vs), and the specific surface area (as), obtained by the high resolution method proposed by Kaneko et al. [5–7], using a non-porous carbon black (Elftex-120) as standard. From the $CO_2$ adsorption data, the narrow micropore volumen ($V_{DR}$) and surface area ($A_{DR}$) were calculated using the Dubinin–Radushkevich equation [8]. Pore size distributions were obtaining by applying the 2D-NLDFT heterogeneous surface model from $N_2$ adsorption isotherm [9].

### 2.2.3 Surface Chemistry

The surface chemistry has been analyzed by temperature-programmed desorption (TPD), X-ray photoelectron spectroscopy (XPS), FTIR and NMR.

#### 2.2.3.1 Temperature-Programmed Desorption (TPD)

TPD technique is employed to characterize the carbon–oxygen surface groups, the groups of acidic character (carboxylic, lactonic) evolve as $CO_2$, whereas the non-acidic (carbonyl, ether, quinone) and phenol groups give rise to CO. Anhydride surface groups evolve as both CO and $CO_2$ [10].

TPD profiles were performed in a quartz tubular reactor placed inside an electrical furnace. The samples were heated from room temperature up to 900 °C at a heating rate of 10 °C/min in a helium flow (200 $cm^3$/min). The amounts of CO and $CO_2$ desorbed from the samples were monitored with non-dispersive infrared (NDIR) gas analyzers (Siemens ULTRAMAT 22).

UNIVERSIDAD DE MÁLAGA

#### 2.2.3.2 X-ray Photoelectron Spectroscopy (XPS)

X-ray photoelectron spectroscopy (XPS) is a surface technique that provides an estimation of the chemical composition of materials surface up to few nm depth and also about the oxidation state of each element. [11]. XPS analyses of the samples were obtained using a 5700C model Physical Electronics apparatus, with MgKα radiation (1253.6 eV). For the analysis of the XPS peaks, the C1s peak position was set at 284.5 eV and used as reference to position the other peaks [12,13]. The fitting of the XPS peaks was done by least squares using Gaussian–Lorentzian peak shapes.

#### 2.2.3.3 Fourier Transform Infrared Spectroscopy (FTIR)

Fourier-Transform Infrared Spectroscopy (FTIR) is a technique used to obtain an infrared spectrum of absorption or emission of a solid, liquid or gas. An FTIR spectrometer simultaneously collects high-spectral-resolution data over a wide spectral range. The FTIR spectra in this thesis were recorded in a Bruker Optics Vertex 70 FTIR spectrometer, in the 500-4000 $cm^{-1}$ range, in KBr disks (ca. 1% (w/w)). A KBr beam splitter and a Golden gate single reflection diamond ATR system detector were used. The spectra were collected for 2 minutes, with 4 $cm^{-1}$ resolution.

#### 2.2.3.4 Nuclear Magnetic Resonance Spectroscopy (NMR)

Nuclear Magnetic Resonance (NMR) spectroscopy is an analytical chemistry technique used for determining the content and purity of a sample as well as its molecular structure. Solid-state $^{13}C$ and $^{31}P$-NMR spectra were recorded with an NMR spectrometer (400 WB Plus model from Bruker) using the Cross-Polarization Magic Angle Spinning (CPMAS) and high-power decoupling (HPDEC) techniques, using a 3.2 mm MAS triple-channel probe at a spinning frequency of 15 kH, with SPINAL-64 $^{1}H$ decoupling conditions.

### 2.2.4 Thermogravimetric Analysis (TGA)

Pyrolysis of different samples was carried out in a gravimetric thermobalance system, CI electronics. The thermobalance automatically measures the weight of the sample and the temperature as a function of time. Experiments were carried out in inert atmosphere ($N_2$), and in air atmosphere, for a total flow rate of 150 $cm^3$/min, using sample mass of approximately 10 mg. The sample temperature was increased at a heating rate of 10 ºC/min.

UNIVERSIDAD DE MÁLAGA

Thermogravimetric experiments were performed in a thermobalance unit as that represented in Figure 2.2.

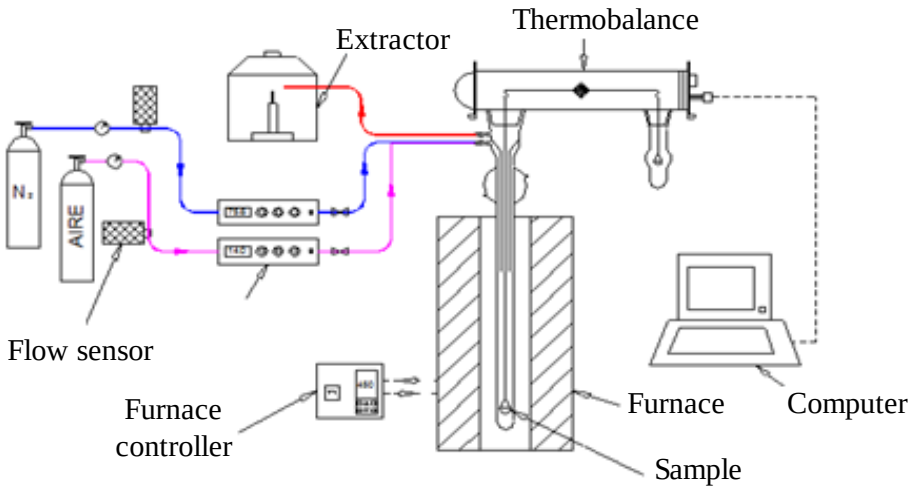


**Figure. 2.2.** Experimental set-up used for thermogravimetric analyses.

### 2.2.5 Differential Scanning Calorimetry (DSC)

Differential Scanning Calorimetry (DSC) is a thermal analysis technique that looks at how the heat capacity of a material is changed by temperature. A sample of known mass is heated or cooled and the changes in its heat capacity are tracked as changes in the heat flow [14]. DSC experiments were obtained by a thermal analyzer (Mettler Toledo equipment) coupled to a Mass Spectrometer (Pfeiffer Vacuum model ThermoStar TM GSD 320). The measuring cell consists of a 400W model silver furnace operating between RT-700 °C, with a maximum heating speed of 100 °C/min, and a HSS8 ceramic sensor consisting of 120 Au-Au / thermocouples P.S. The equipment also incorporates a cooling system using liquid $N_2$ that allows to lower the minimum operating temperature to -150 ºC. A continuous flow of $N_2$ of 20 $cm^3$/min is used as a protective gas. The tests were carried out in $Al_2O_3$ crucibles of 70 µl in the temperature range 30-250 °C, with an air or nitrogen flow of 50 $cm^3$/.min and a heating rate of 2 °C/min. Sample masses between 5 and 10 mg have been used.

### 2.2.6 Surface Morphology

Surface morphology was examined by scanning electron microscopy (SEM) (JEOL USA, Inc., Pleasanton, CA, USA), using a JSM 6490LV JEOL microscope working at 25

UNIVERSIDAD DE MÁLAGA

kV. The atomic distribution of the particle surfaces was analyzed in a FEI Quanta 250 FEG Scanning Electron. Microscope equipped with energy-dispersive X-ray analyses (SEM-EDX) (Thermo Fisher Scientific, Hillsboro, OR, USA).

## 2.3 Experimental set-up for adsorption experiments

The adsorption experiments using activated carbons as adsorbents were carried out at 20 °C. For the equilibrium tests, 10 mg of dried activated carbons (200-400 µm) were put inside glass flasks and contacted with 150 mL of the contaminated solution at different initial concentrations in an orbital incubator (Gallenkamp, model INR-250) at 200 rpm equivalent stirring rate for 7 days. A scheme of the installation used for the kinetic tests is shown in Figure 2.3. In a typical kinetic experiment, a solution of 1 mg/L was put in contact with 10 mg of the activated carbon and agitated for different times with adsorbent doses of 50 mg/L. Column adsorption experiments (installation shown in Figure 2.3) were carried out in a thermostatized glass column (± 0.5 °C), with internal diameter of 4 mm. 100 mg of activated carbon was packed between two slices of inert quartz wool inside the column. The solution (1 mg/L) was pumped downflow through the column at controlled flow rate (7 $cm^3$/min) using a peristaltic pump. Before the column test was started, water was feed to the column for 20 min in order to remove the trapped air and to wet the activated carbon porosity. The adsorbate concentrations were determined at λmax: 240 nm, with an UV–Vis (Varian, Model Cary 1E) spectrophotometer.

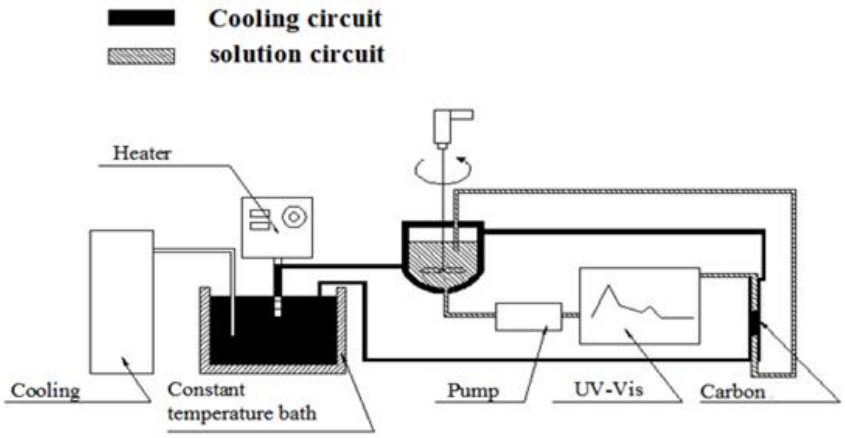


**Figure 2.3.** Installation used for the adsorption kinetics experiments.

UNIVERSIDAD DE MÁLAGA

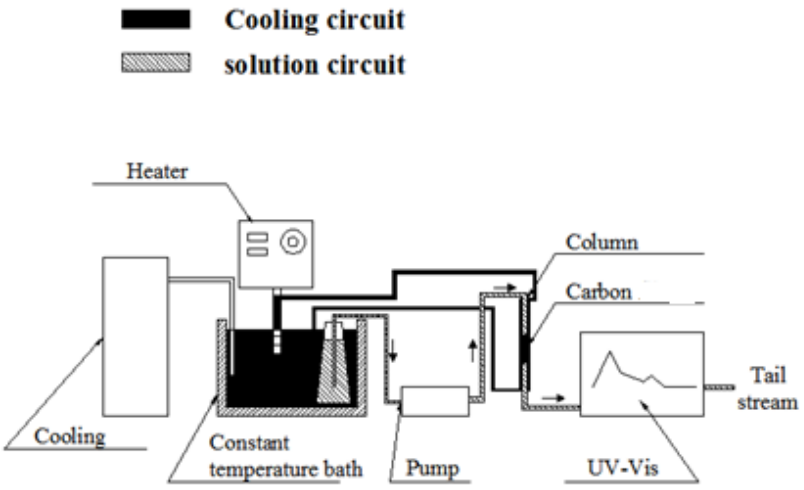


**Figure 2.4.** The adsorption installation of column experiments.

## 2.4 Experimental set-up for alcohols decomposition

The activities of the catalysts were measured by the decomposition of alcohols performed at atmospheric pressures, in a quartz fixed bed microreactor (4 mm i.d.) (Alba Nueva Científica S.A., Alhaurín de la Torre, Málaga, Spain) placed inside a vertical furnace with temperature control, using 100 mg of catalyst (200–400 µm particle size). Alcohols were fed into the system in a controlled way by using a syringe pump (Cole-Parmer® 74900-00-05 model (Cole-Parmer Instrument Company, LLC., Vernon Hills, IL, USA)) and the helium flow adjusted to obtain, in each case, a total inlet stream of 100 $cm^3$/min. To avoid condensation of alcohol or any reaction product, all lines were heated up to 130 °C. The space time used was W/Fo Alcohol = 0.073 g s/µmol. Reactant and product concentrations were measured by gas chromatography (490 micro-GC equipped with PPQ, 5A molsieve, and Wax columns, Agilent Technologies, Santa Clara, CA, USA). Figure 2.5 shows a scheme of the installation used for these types of experiments.

UNIVERSIDAD DE MÁLAGA

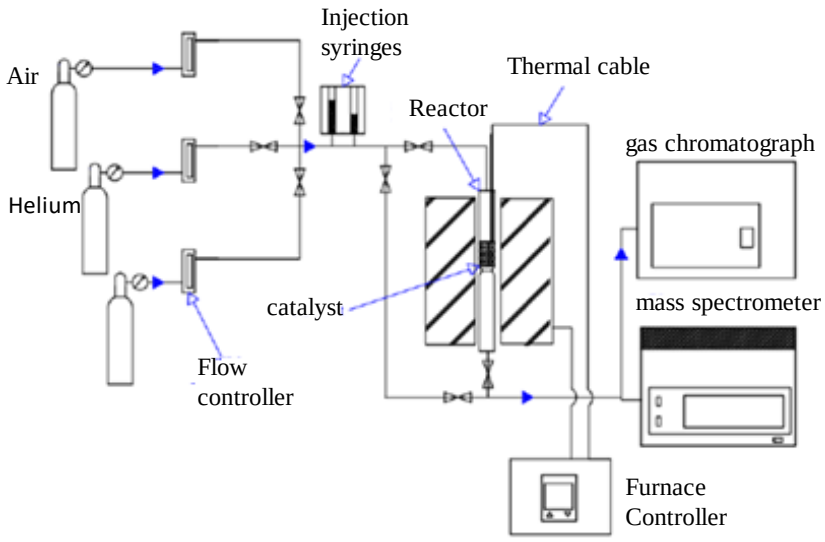


**Figure 2.5.** Installation used for alcohol decomposition.

## References

[1] M. Lallave, J. Bedia, R. Ruiz-Rosas, J. Rodríguez-Mirasol, T. Cordero, J.C. Otero, M. Marquez, A. Barrero, I.G. Loscertales, Filled and hollow carbon nanofibers by coaxial electrospinning of Alcell lignin without binder polymers, Adv. Mater. 19 (2007) 4292–4296. https://doi.org/10.1002/adma.200700963.

[2] R. Ruiz-Rosas, J. Bedia, M. Lallave, I.G. Loscertales, A. Barrero, J. Rodríguez-Mirasol, T. Cordero, The production of submicron diameter carbon fibers by the electrospinning of lignin, Carbon. 48 (2010) 696–705. https://doi.org/10.1016/j.carbon.2009.10.014.

[3] S. Brunauer, P.H. Emmett, E. Teller, Adsorption of Gases in Multimolecular Layers, J. Am. Chem. Soc. 60 (1938) 309–319.

[4] F. Rodríguez-Reinoso, M. Molina-Sabio, M.T. González, The use of steam and $CO_2$ as activating agents in the preparation of activated carbons, Carbon. 33 (1995) 15–23. https://doi.org/10.1016/0008-6223(94)00100-E.

[5] K. Kaneko, C. Ishii, Superhigh surface area determination of microporous solids, Colloids and Surfaces. 67 (1992) 203–212. https://doi.org/10.1016/0166-6622(92)80299-H.

[6] K. Kaneko, C. Ishii, M. Ruike, H. kuwabara, Origin of superhigh surface area and microcrystalline graphitic structures of activated carbons, Carbon. 30 (1992) 1075–1088. https://doi.org/10.1016/0008-6223(92)90139-N.

[7] K. Kaneko, Determination of Pore Size and Pore Size Distribution: 1. Adsorbents and Catalysts, J. Membr. Sci. 96 (1994) 59–89. https://doi.org/10.1016/0376-7388(94)00126-X.

[8] M.M. Dubinin, The potential theory of adsorption of gases and vapors for adsorbents with energetically nonuniform surfaces, Chem. Rev. 60 (1960) 235–241. https://doi.org/10.1021/cr60204a006.

UNIVERSIDAD DE MÁLAGA

[9] J. Jagiello, J.P. Olivier, 2D-NLDFT adsorption models for carbon slit-shaped pores with surface energetical heterogeneity and geometrical corrugation, Carbon. 55 (2013) 70–80. https://doi.org/10.1016/j.carbon.2012.12.011.

[10] J.L. Figueiredo, M.F.R. Pereira, M.M.A. Freitas, J.J.M. Órfão, Modification of the surface chemistry of activated carbons, Carbon. 37 (1999) 1379–1389. https://doi.org/10.1016/S0008-6223(98)00333-9.

[11] J. F. Moulder, W. F. Stickle, P. E. Sobol, K.D. Bomben, Handbook of X-ray Photoelectron Spectroscopy, in J. Chastain (ed) ,Perkin-Elmer Corporation ,Physical Electronics Division 6509 Flying Cloud Drive, 1992

[12] E. Desimoni, G.I. Casella, A. Morone, A.M. Salvi, XPS determination of oxygen-containing functional groups on carbon-fibre surfaces and the cleaning of these surfaces, Surf. Interface Anal. 15 (1990) 627–634. https://doi.org/10.1002/sia.740151011.

[13] S. Biniak, G. Szymański, J. Siedlewski, A. Światkoski, The characterization of activated carbons with oxygen and nitrogen surface groups, Carbon. 35 (1997) 1799–1810. https://doi.org/10.1016/S0008-6223(97)00096-1.

[14] J.D. Menczel, L. Judovits, R.B. Prime, H.E. Bair, M. Reading, S. Swier, Differential Scanning Calorimetry (DSC), 2008. https://doi.org/10.1002/9780470423837.ch2.

UNIVERSIDAD DE MÁLAGA

# Chapter III

UNIVERSIDAD DE MÁLAGA

# 3 Chapter III: Effect of co-solution of carbon precursor and activating agent on the textural properties of highly porous activated carbon obtained by chemical activation of lignin with $H_3PO_4$


## Abstract

In this chapter, it is analyzed the effect of co-solution of carbon precursor and activating agent on the textural and surface chemistry properties of highly nanoporous activated carbons obtained by chemical activation of Alcell lignin with phosphoric acid. The success of this methodology highlights the possibility of directly using the liquors produced in organosolv process (Alcell) to prepare activated carbons by chemical activation with phosphoric acid. Co-solutions of lignin and phosphoric acid were submitted to a two steps thermal treatment, which consisted of a first oxidative treatment in air at 200 ºC, followed by a thermal treatment in $N_2$ at 400 ºC, where activation of the oxidized lignin with phosphoric acid took place. A lignin-derived activated carbon with very high apparent surface area (2550 $m^2/g$) and pore volume (1.30 $cm^3/g$) was obtained with an initial phosphoric acid to lignin mass ratio of 2. Up to now, this is one of the highest values of apparent surface area reported not only for activated carbons prepared from lignin, but even for porous carbons prepared by chemical activation of other lignocellulosic materials with phosphoric acid. The use of lignin and phosphoric acid co-solution provided larger and more homogeneous effective interactions between the carbon precursor and the activating agent, by the formation of phosphate esters in the lignin matrix, which seems to be a key factor in the subsequent treatments: promoting crosslinking reactions in the carbonaceous matrix during the oxidative treatment in air at 200 ºC and enhancing the development of a wide porosity during the following activation thermal treatment.


UNIVERSIDAD DE MÁLAGA

## 3.1 Introduction

Within a biorefinery scheme, the conversion of the major components of lignocellulosic biomass (cellulose, hemicellulose and lignin) into energy and chemicals is essential. However, lignin has been used, up to date, mainly, as a fuel to recover energy and chemical reactants in the pulp and paper industry and only a 2% of the produced lignin is currently commercialized [1–4]. There are different pretreatments to fractionate lignocellulosic biomass into their main components, but Organosolv process becomes an ideal candidate in the biorefinery context, given the need of using environmentally friendly treatments. During Organosolv process, lignin is fractionated into smaller parts, dissolved from the lignocellulosic biomass with organic compounds and separated in the form of a liquor rich in phenolic compounds [5–7]. The next step consists of lignin precipitation from the liquors by partially evaporating the organic solvent, lowering the temperature or a combination of those, followed by a separation step through centrifugation, filtration, etc. The lignin derived from this method presents lower molecular weight and higher purity than others obtained by other processes, such as Kraft one. All these properties make this type of lignin an ideal precursor for the preparation of activated carbon, an added-value material, whose production process would imply both economic and environmental advantages.

Chemical activation with phosphoric acid is a well-known method to prepare activated carbons from different biomass precursors [8–11]. Many papers have been reported dealing with the optimization of the preparation conditions in order to obtain activated carbons with a high development of the porous texture. The influence of the impregnation ratio and the activation temperature on the textural properties of activated carbons prepared from different biomassic waste has been deeply analyzed [12–16]. However, the effect of the gas atmosphere during the activation step on these properties is not so clear and some contradictions have appeared in this respect in the literature. Generally, activation takes place under inert atmosphere, although some authors have proposed the preparation of activated carbons by chemical activation with phosphoric acid under air atmosphere in order to enhance the textural properties (increase apparent surface area, $A_{BET}$) [17]. However, Benaddi et al. reported no significant influence of the atmosphere on the textural characteristics of activated carbons prepared by chemical activation of wood with phosphoric acid [18]. They obtained values of apparent surface area of approximately 2100 $m^2/g$, independently of the use of air or nitrogen as activation atmosphere. In contrast, Moreno Castilla et al. reported the preparation of activated

UNIVERSIDAD DE MÁLAGA

carbons from olive-mill waste with similar $A_{BET}$ (~ 400 $m^2/g$), using either nitrogen, $CO_2$ or $H_2O$ atmospheres [19], but the $A_{BET}$ value decreased (~ 180 $m^2/g$) when they used air as gas atmosphere.

With regard to lignin, activated carbons with very high $A_{BET}$ values (around 3000 $m^2/g$) by chemical activation of Kraft lignin with KOH has been reported [20], but these carbon materials presented a very narrow microporosity. Chemical activation of Kraft lignin with zinc chloride and phosphoric acid gave rise to activated carbons with a much wider porosity, depending on the activation temperature and impregnation ratio, but with $A_{BET}$ values lower than 1800 $m^2/g$ [21–23]. However, no much information can be found in the literature regarding the preparation of activated carbons from Alcell lignin [24,25], a co-product that appears dissolved in the liquors produced in one of the most important Organosolv process.

Thus, the objective of this work was to analyze the effect of co-solution of carbon precursor and activating agent on the textural and surface chemistry properties of activated carbons obtained by chemical activation of Alcell lignin with phosphoric acid, in order to assess the possibility of directly using the liquors produced in the Organosolv process (Alcell), which would avoid the lignin precipitation and separation steps in this process. The influence of the use of a low temperature oxidative thermal treatment, previous to the activation process, on the surface chemistry and textural properties of the final lignin-derived carbons obtained was also studied.

## 3.2 Experimental section

### 3.2.1 Activated carbons preparation

Alcell lignin (supplied by Repap Technologies Inc. Co.) was used as raw material for the activated carbons preparation. Different procedures were used for the preparation of activated carbons from lignin. Alcell lignin was dissolved in ethanol to simulate the composition of dissolved lignin in the Organosolv liquors. Solid Alcell lignin was directly impregnated with aqueous $H_3PO_4$ 85% (w/w) at room temperature. Co-solution of lignin and the activating agent, $H_3PO_4$ 85% (w/w), was also prepared at room temperature and the ethanol/lignin/$H_3PO_4$ solution was stirred until evaporation of the ethanol (which could be recovered). Both the impregnated lignin and there solid derived from the co-solution of lignin and $H_3PO_4$ were dried for 24 hours at 60°C in a vacuum dryer. The amounts of lignin and $H_3PO_4$ used in both cases were those to obtain a final $H_3PO_4$/lignin mass ratio of 2. The as-received lignin and that



UNIVERSIDAD DE MÁLAGA

dissolved in ethanol were denoted by L and LE, respectively. $H_3PO_4$ impregnated lignin and the solid derived from the lignin/ethanol/$H_3PO_4$ solution once dried were denoted as L2P and LE2P, respectively. These two samples were subsequently submitted to a low temperature oxidative treatment at 200 ºC in air atmosphere for 1.5 hours, followed by an activation treatment under inert atmosphere at 400 °C, both inside a laboratory horizontal tubular furnace. The heating rate to reach the oxidative and the activation temperature was 3 and 10 ºC/min, respectively. Once the activation temperature was reached the samples were cooled inside the furnace under inert atmosphere and then washed with distilled water at 60°C until neutral pH. The resulting activated carbons were dried at 60°C.

L2P and LE2P submitted to the oxidative treatment in air at 200 ºC for 1.5 h were denoted by adding the letter S to the corresponding names (L2PS and LE2PS, respectively). The final activated carbons obtained at 400 ºC in inert atmosphere were denoted by adding 400 to the respective notations (L2PS400 and LE2PS400, respectively). In case of oxidative treatments at different temperatures, the activated carbons notation will include at the end of the name the temperature of the treatment. For the sake of comparison, some samples were directly activated at 400 ºC under air atmosphere without being subjected to the previous oxidative low temperature treatment. In these cases, the letter S was not included in their corresponding notations (L2P400 and LE2P400) and the letter A was added at the end of its corresponding name. In order to also evaluate the influence of the gas atmosphere during the low temperature treatment, a sample was treated under inert atmosphere at 200 ºC for 1.5h and was denoted by adding the letter N to its corresponding notation.

### 3.2.2 Activated carbons characterization

The porosity of the samples was characterized by $N_2$ adsorption–desorption and $CO_2$ adsorption at -196 and 0 ºC, respectively, using a micromeritics instrument (ASAP 2020 model). The samples were previously outgassed for at least 8 h at 150 ºC. From the $N_2$ isotherm, the apparent surface area ($A_{BET}$) was determined by applying the BET equation [26]; micropore volume ($V_t$) and external surface area ($A_t$) were calculated using the t-method [27]; mesopore volume ($V_{mes}$) was determined as the difference between the maximum adsorbed volume of $N_2$ ($V_p$) at a relative pressure of 0.99 and the micropore volume ($V_t$) [28]. From the $CO_2$ adsorption data, the narrow micropore volume ($V_{DR}$) and surface area ($A_{DR}$) were calculated using the

UNIVERSIDAD DE MÁLAGA

Dubinin–Radushkevich equation (Dubinin et al., 1947). Pore size distributions were obtaining by applying the 2D-NLDFT heterogeneous surface model from $N_2$ adsorption isotherm [30] .

Thermal treatments of different samples were carried out in a gravimetric thermobalance system, CI electronics. The thermobalance automatically measures the weight of the sample and the temperature as a function of time. Experiments were carried out in inert atmosphere ($N_2$) and in air atmosphere, for a total flow rate of 150 $cm^3$ (STP)/min, employing sample mass of approximately 10 mg. The sample temperature was increased at a heating rate of 10 ºC/min. Differential scanning calorimetry (DSC) experiments were also obtained by a thermal analyzer (Mettler Toledo equipment) coupled to a Mass Spectrometer (Pfeiffer Vacuum model ThermoStar TM GSD 320).

The FTIR spectra of lignin and lignin-derived samples were recorded in a Bruker Optics Vertex 70 FTIR spectrometer, in the 500-4000 $cm^{-1}$ range, in KBr disks (ca. 1% (w/w)). A KBr beam splitter and a Golden gate single reflection diamond ATR system detector were used. The spectra were collected for 2 minutes, with 4 $cm^{-1}$ resolution.

Solid-state $^{13}C$ and $^{31}P$-NMR spectra of lignin and lignin-derived samples were recorded, as well, with a NMR spectrometer (400 WB Plus model from Bruker) using the Cross Polarization Magic Angle Spinning (CPMAS) and high power decoupling (HPDEC) techniques and a 3.2 mm MAS triple-channel probe at a spinning frequency of 15 kH, with SPINAL-64 $^1H$ decoupling conditions.

X-ray photoelectron spectroscopy (XPS) analyses of the samples were carried out in a PHI 5700C model Physical Electronics apparatus, with MgKα radiation (1253.6 eV). For the analysis of the XPS peaks, the C1s peak position was set at 284.5 eV and used as reference to position the other peaks. For the deconvolution of the peaks, Gaussian–Lorentzian curves were used. The deconvolution of the phosphorus spectrum was carried out by using two doublet peaks with an area ratio of 0.5 and a separation between peaks of 0.84 eV for each phosphorus groups. TPD experiments were carried out in a customized quartz fixed-bed reactor placed inside an electrical furnace. CO and $CO_2$, as output gases, were measured by a non-dispersive infrared (NDIR) gas analyzer, Siemens ULTRAMAT 22 (Siemens AG, Munich, Germany). Eighty mg of dried carbon sample was heated from room temperature to 930 °C at a heating rate of 10 °C/min under $N_2$ flow (200 $cm^3$/min).

UNIVERSIDAD DE MÁLAGA

## 3.3 Results and discussion

### 3.3.1 Surface chemistry characterization of as-received and ethanol-dissolved lignin

Alcell lignin is a type of lignin derived from Organosolv process, a pulping technique that uses an organic solvent to solubilize lignin and hemicellulose. This type of lignin contains very small amounts of inorganic compounds [31]. Delignification is mostly the result of high-temperature uncatalyzed hydrolysis of lignin ether linkages by water. The solvent in the system mainly serves to dissolve the lignin fragments (Girard and Van Heiningen, 2000). One of the most used solvents in the Organosolv process is ethanol, which has been the solvent selected in this work to dissolve lignin.

Figure 3.1.A shows the normalized CPMAS $^{13}C$ NMR spectra of the as-received Alcell lignin and that dissolved in ethanol. Some differences can be observed, which suggest modifications of the lignin structure by its solution in ethanol. The main difference of both spectra is observed in the range of 15-27 ppm, which can be associated to terminal $CH_3$ groups. The increase of this signal suggests the accumulation of saturated alkyl structures after dissolving the lignin with ethanol. The predominant signal around 62-68 ppm, which remains practically the same after dissolving the lignin in ethanol, can be assigned to $C_5$ in xylose internal unit and $C_\gamma$, in β-0-4-linked unit; C4 in xylose nonreducing end and $C_\gamma$, in β-O-4-linked unit with C=O. However, the signal around 144-148 ppm slightly increases after solution with ethanol, which can be associated to an increase of $C_3$ and $C_4$ in etherified guaiacyl; $C_4$ and $C_{4'}$ in etherified 5-5' units and $C_\alpha$, in cinnamic acid and ester [33], and maybe related to the interaction of -OH groups of ethanol with those of lignin, which would also explain the increase of the signal between 15-27 ppm.

UNIVERSIDAD DE MÁLAGA

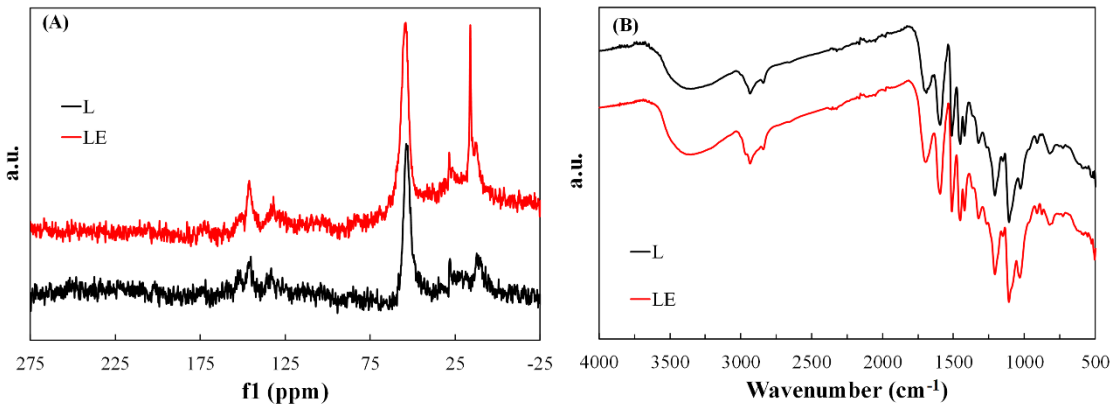


**Figure 3.1.** Normalized CPMAS $^{13}C$ NMR spectra (A) and FTIR spectra (B) of as-received Alcell lignin and that dissolved in ethanol.

Figure 3.1.B represents the corresponding FTIR spectra of both samples. The spectrum of lignin is complicated and most of the bands observed are produced by contribution of various types of vibrations of different functional groups. Therefore, assignment of the bands is possible only in the approximation of the predominant contribution of certain atomic groups [34]. Alcell lignin shows a broad band at 3410–3460 $cm^{-1}$, attributed to the hydroxyl groups in phenolic and aliphatic structures, which remains the same after dissolving with ethanol. The bands centered around 2935 and 2840 $cm^{-1}$ can be predominantly associated to CH stretching in aromatic methoxyl groups and in methyl and methylene groups of side chains. In the LE sample also appears a band around 2965 $cm^{-1}$ related to stretching vibration of aliphatic C-H. This appearance is in concordance to the accumulation of saturated alkyl structures, suggested by CPMAS $^{13}C$ NMR spectra, after dissolving lignin with ethanol. In the carbonyl/carboxyl region, a band around 1700 $cm^{-1}$is found, originating from unconjugated carbonyl/carboxyl stretching, which is more intense in the case of the sample LE. Typical bands of lignin are those at 1600, 1515 and 1425 $cm^{-1}$ related to aromatic skeleton vibrations and at 1460 $cm^{-1}$ associated to the C–H deformation combined with aromatic ring vibration [34,35], which are practically the same in both samples.

The samples show the characteristic vibrations for the guaiacyl unit (G ring and C=O stretch at around 1260 $cm^{-1}$; CH in-plane deformation at 1150 $cm^{-1}$; and C–H out-of plane vibrations in position 2, 5 and 6 of guaiacyl units at 830 and 915 $cm^{-1}$). Syringyl (S) and guaiacyl (G) units are detected by aromatic skeleton vibrations at 1600 and 1325 $cm^{-1}$ (S), 1515 and 1260 $cm^{-1}$ (G), and aromatic in plane C−H vibrations at 1110 (S) and 1030 $cm^{-1}$ (G). This

UNIVERSIDAD DE MÁLAGA

last band is more intense in case of the LE sample [34,35]. Another band at 880 $cm^{-1}$, related to C-C asymmetrical stretching mode, is more accused in sample LE, which also evidences the modification of the chemical structure of lignin after dissolving it with ethanol.

Finally, both samples also contain a weak band at 1370–1375 $cm^{-1}$ originating from phenolic OH and aliphatic C–H in methyl groups and a strong vibration at 1215–1220 $cm^{-1}$ that can be associated with C–C, C–O, and/or C=O stretching. The aromatic C–H deformation at 1030 $cm^{-1}$ appears as a complex vibration associated with the C–O, C–C stretching and C–OH bending in polysaccharides [34,35].

### 3.3.2 Effect of $H_3PO_4$ and low temperature oxidative treatment on lignin surface chemistry

Figure 3.2 shows the corresponding FTIR spectra of the $H_3PO_4$ impregnated lignin and the solid derived from the lignin/ethanol/$H_3PO_4$ solution, L2P and LE2P, respectively. Most of the absorption peaks corresponding to functional groups for these two samples were diminished compared to those corresponding to the samples L and LE. Spectra of samples L2P and LE2P are very similar, showing an important decrease of the intensity in the bands associated to the presence of O-H stretching of hydroxyl functional groups (3500 to 3300 $cm^{-1}$). This reduction is due to the presence of phosphoric acid, which acts as dehydrating agent immediately after impregnation, even at room temperature. The band around 2965 $cm^{-1}$ related to stretching vibration of aliphatic C-H is also substantially reduced due to the increase of aromaticity (conversion of aliphatic to aromatic compounds). This loss of aliphatic character takes place at low temperatures and is caused by the cleavage of aliphatic side chains. Jagtoyen and Derbyshire also reported that the primary effects of acid attack are to cleave aryl ether bonds in lignin, accompanied by dehydration, degradation and condensation reactions [8], which are the responsible of the decrease observed at 1600, 1515 and 1425 $cm^{-1}$,related to aromatic skeleton vibrations of phenyl skeletons and, at 1460 $cm^{-1}$, associated to the C–H deformation, combined with aromatic ring vibration. Furthermore, the acid-catalyzed hydrolysis of ether linkages in lignin can lead to the formation of ketones, as can be observed in the characteristic band that appears at 1685 $cm^{-1}$.

The typical bands for guaiacyl unit are also significantly reduced, those at 1215–1220 $cm^{-1}$ and at 1030 $cm^{-1}$, associated to C–C, C–O, and/or C=O stretching and C–O, C–C stretching and C–OH bending in polysaccharides, respectively. However, the appearance of

UNIVERSIDAD DE MÁLAGA

other bands probably related to phosphorus compounds is also observed. In this sense, the broad band at 965 $cm^{-1}$ and the intense peak at 635 $cm^{-1}$ could be initially associated to P-O-P and P-C bending of aromatic compounds, respectively, although the peak at 635 $cm^{-1}$ can be also related to $C \equiv CH$ bonds [36]. In addition, disappearance of this band, at 635 $cm^{-1}$, is observed for samples submitted to the oxidative treatment in air at 200 ºC (L2PS and LE2PS), which can be related to the formation of more oxidized species of phosphorus or to decomposition of non-stable species. Furthermore, a decrease of the intensity of the bands at 1600, 1515, 1460 and 1425 $cm^{-1}$ were also detected after this low temperature treatment in air.

In order to analyze if phosphoric acid can act as an oxygen donor to the lignin matrix at this low temperature, sample L2P was treated at 200 ºC for 1.5 h, but under inert ($N_2$) atmosphere (L2PS-N). The FTIR results for L2PS-N are also shown in Figure 3.2. As it can be seen, all the bands already mentioned were also reduced for L2PS-N, which suggests that the presence of oxygen coming from the $H_3PO_4$ is more than enough to produce crosslinking reactions [37]. In this sense, phosphoric species could be combined with organic species to form phosphate linkages that can serve to connect and crosslink lignin fragments [8]. These reactions are probably responsible for the reduction of these typical bands of lignin.

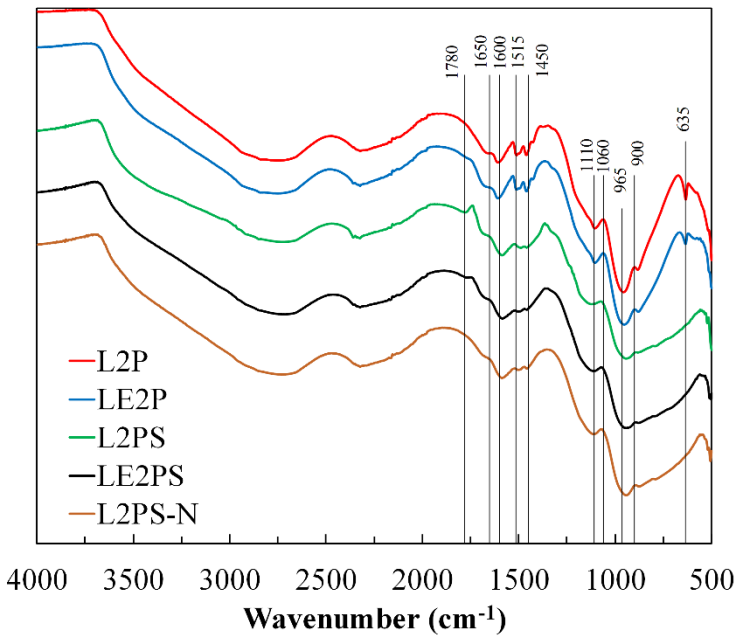


**Figure 3.2**. FTIR spectra of the different $H_3PO_4$-lignin derived samples.

UNIVERSIDAD DE MÁLAGA

The results obtained from XPS analysis confirmed the presence of phosphorus groups on the surface of L2P, LE2P, L2PS and LE2PS samples (see Fig. 3.3). The XPS P2p spectrum for L2P showed a broad band with a main peak at a binding energy around 134.3 eV, characteristic of pentavalent tetracoordinated phosphorus, as in phosphates and/or polyphosphates [38]. The obtained P2p broad band indicated the presence of different surface phosphorus species. Lower binding energies (around 133 eV) are characteristic of C-P bonding, as in C-$PO_3$ surface groups, which seem to be practically negligible in these samples (see Table 3.1); whereas higher values (134.2 eV) are ascribed to more oxidized phosphorus species, with C-O-P type bonds, as those in C-O-$PO_3$ surface groups [38,39]. The contribution of these species was higher than 85%, suggesting that all phosphorus was mainly present in form of C-O-$PO_3$ surface groups. However, due to these samples were not yet activated, the presence of even more oxidized phosphorus species as $P_2O_5$ (135.7 eV) cannot be disregarded. It seems clear that co-solution of lignin with phosphoric acid generated a higher contribution of oxidized P surface groups to the total P surface groups than the traditional impregnation process (LE2P vs L2P). On the other hand, the lower P content value observed for LE2P, when compared with that for L2P (see Table 3.1), suggests that this sample presents more P in the inner part of the lignin matrix, due probably to a better dispersion and to a more homogeneous distribution of P through the entire lignin matrix obtained by co-solution of the activating agent, phosphoric acid, and the carbon precursor, lignin. After the low temperature oxidative treatment both samples, L2PS and LE2PS, presented a similar surface P content value. However, the amount of surface O was significantly higher for the sample prepared by co-solution of lignin and $H_3PO_4$, LE2PS, which suggests that this preparation procedure enhances the lignin oxidation process at low temperature.

UNIVERSIDAD DE MÁLAGA

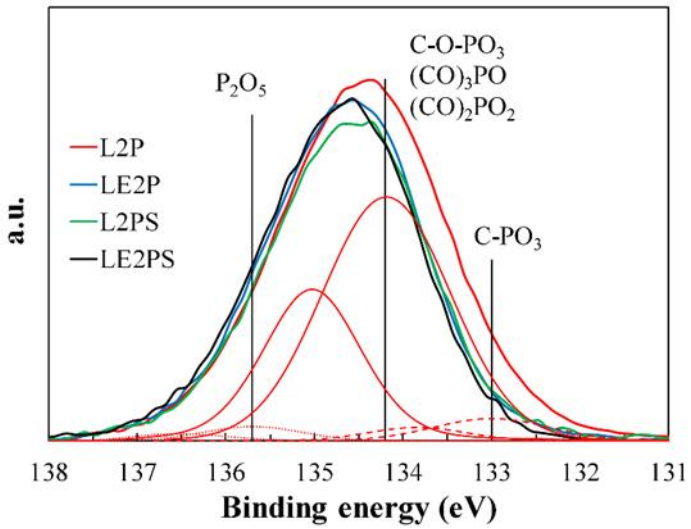


**Figure 3.3**. XPS P2p spectra of the different $H_3PO_4$-lignin derived sample and deconvolution of P2p spectrum for LE2PS sample ($C\text{-}PO_3$ groups: dashed lines; C-O-P groups: continuous lines, $P_2O_5$, dotted lines).

**Table 3.1**. Mass surface concentration of the different $H_3PO_4$-lignin derived samples and the corresponding contribution of different phosphorus surface group obtained by XPS analyses.

| Sample | Surface concentration by XPS | | | Phosphorus surface groups | | |
|---|---|---|---|---|---|---|
| | C (%) | O (%) | P (%) | $P_2O_5$ (%) | C-O-P (%) | $C\text{-}PO_3$ (%) |
| **L2P** | 30.7 | 45.3 | 24 | 3.9 | 89.05 | 7.05 |
| **LE2P** | 40.1 | 39 | 20.9 | 9.9 | 89.6 | 0.5 |
| **L2PS** | 48.8 | 31.3 | 19.9 | 5.85 | 93.7 | 0.45 |
| **LE2PS** | 42.9 | 36.5 | 20.6 | 9.24 | 89.59 | 1.17 |

Thermal decomposition of the different lignin-derived samples was studied by TG analyses. Figure 3.4.A represents the weight loss of the different lignin-derived samples as a function of temperature, under inert atmosphere and at a heating rate of 10 ºC/min. In general, three different ranges can be observed in all the samples. First, there is a small weight loss at temperatures lower than 200 ºC that can be partially attributed to release of water. Water can come from the phosphoric acid solution and produced by the reaction between phosphoric acid and lignin. As abovementioned, phosphoric acid cleaves aryl ether bonds in lignin, producing many transformations that include dehydration, degradation and condensation [8]. At temperatures lower than 150 ºC, the acid catalyzes the hydrolysis of ether linkages, leading to

UNIVERSIDAD DE MÁLAGA

the formation of ketones. These and other bond cleavage reactions that proceed through ionic mechanism promotes the release of $H_2O$, CO, $CO_2$ and $CH_4$ at these low temperatures, and can contribute to the corresponding weight loss observed in Figure 3.4.A.

Between 200 and 500 ºC a further decrease of mass is observed associated to the release of light compounds from lignin degradation. In this temperature range, crosslinking reactions dominate over bond cleavage and de-polimerization reactions. At 250 ºC the structures are considered to be small polyaromatic units connected mainly by phosphate and polyphosphate bridges, including polyethylene linkages. As the temperature increases, cyclization and condensation reactions lead to increases in aromaticity and size of the poliaromatic units, enabled by the scission of P-O-C bonds [8].

A change in the slope of the weight-loss curve can be also observed at temperatures higher than 500 ºC, probably associated to volatilization of carbon–oxygen complexes generated by the activation process, and to a lesser extent, to decomposition of phosphorous-compounds (as $P_2O_5$), produced by the reaction of phosphoric acid with the carbon matrix [10].

The profiles of L2P and LE2P are very similar, suggesting the low impact of using dissolved lignin in ethanol in the thermal decomposition reactions. However, the weight loss curves of the samples treated with air (L2PS and LE2PS) are above those of L2P and LE2P samples. If the difference between the weight loss for a specific temperature of the non-treated and treated samples is represented as a function of temperature (Figure 3.4.B), an important weight loss deviation around 700 ºC can be noticed for both curves, suggesting that the treatment with air generates significant differences to the samples treated with phosphoric acid. Montane et al. proposed that the peak observed at 650 ºC in the DTG curves was attributed to the volatilization of $P_2O_5$ [10]. On the other hand, Martinez de Yuso et al. found a band around 800 ºC, which they associated to the more important crosslinking reactions to produce aromatic units [40]. Therefore, the treatment with air seems to stabilize or increase the number of phosphate and polyphosphate bridges, and/or to increase other crosslinking reactions. With this regard, although the weight loss percentage from 800 ºC is the same for the samples L2PS and LE2PS (around 10%), the remaining weight is not equal, due to a higher weight loss between 750 to 800 ºC. The weight loss observed in this range temperature coincides with the higher CO evolution observed in the TPD analysis (see **Figure 3.7**) for the LE2PS400 sample, and it is associated to the higher presence of C-O-$PO_3$ surface groups [24].

UNIVERSIDAD DE MÁLAGA

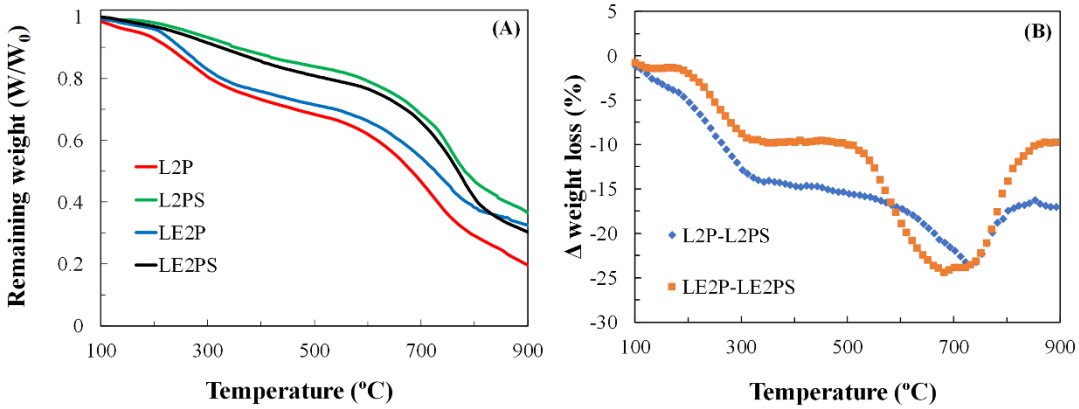


**Figure 3.4**. (A) Thermogravimetric analysis in inert atmosphere for different lignin-derived samples; (B) Weight loss differences during TG analyses between the non-treated and low temperature oxidized (air) treated samples.

Differential scanning calorimetry (DSC) scans of all the lignin-derived samples are shown in Figure 3.5. Figure 3.5.A shows a broad endothermic peak near 80 ºC from absorbed moisture for all the impregnated samples. The impregnated lignin L2P also presents a broad endotherm peak around 235 ºC, which can be associated to the decomposition and depolymerization reactions of lignin. Similarly, Karacan and Soy related an endothermic peak around 214 ºC to decomposition and depolymerization reactions of cellulose [41]. Another exothermic peak was observed around 300 ºC. This peak coincides with a maximum in the CO and $CO_2$ evolution and is due mainly to the crosslinking reactions taking place during the decomposition process [8], which could be softened by the endothermic polymerization and condensation reactions that take also place at this temperature range [42]. The scan of LE2P is very similar to that of L2P, but a shift of the endothermic peak is observed to 225 ºC, which suggests an earlier beginning of the decomposition and depolymerization reactions of lignin. In the case of the L2PS and LE2PS samples, the treatment with air results in the reduction of the endothermic peak, probably because the endothermic reaction has already taken place during the treatment with air (at 200 ºC for 1.5 hour). From this temperature, a broad but much less intense exothermic peak can be observed centered on 300 ºC.

UNIVERSIDAD DE MÁLAGA

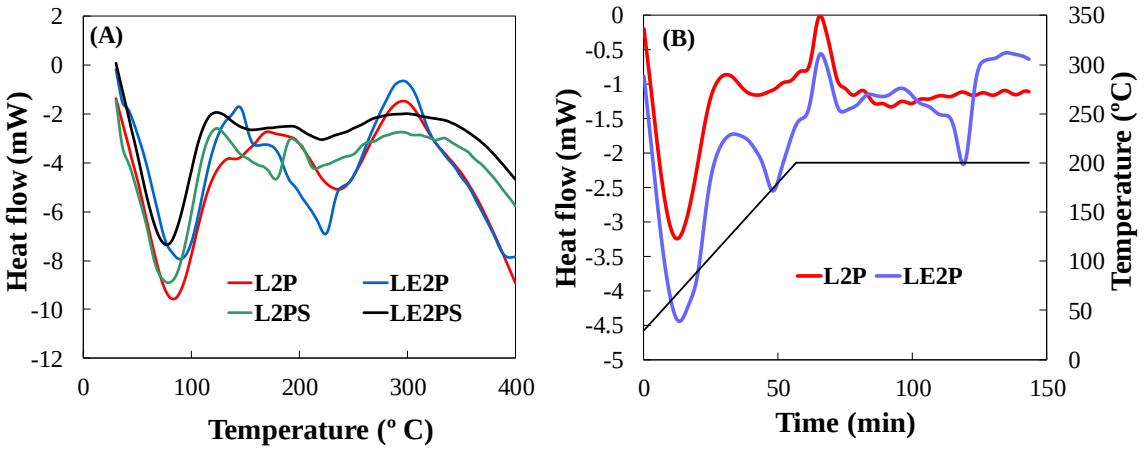


**Figure 3.5.** (A) DSC curves during pyrolysis of different lignin-derived samples and (B) DSC curves during treatment of L2P and LE2P with air at 200 ºC.

A further experiment was carried out trying to simulate the oxidative treatment at 200 ºC. The corresponding DSC curves are shown in Figure 3.5.B. As can be seen, a sharp exothermic peak appears once the temperature is reached. This exothermic peak could be related to that shown in Figure 3.5.A at 300 ºC in samples L2P and LE2P, due to different exothermic crosslinking reactions. In this sense, Jagtoyen and Derbyshire proposed that crosslinking reactions begin to dominate over depolymerization reactions from 200 ºC [8] .Therefore, if enough time is provided, the reactions could take place at lower temperatures. Another important aspect is the presence of two endothermic peaks only in the sample LE2P. These two peaks could be related to the splitting of the endothermic peak that appears in **Figure 3.5.A** around 220 ºC, caused by the superposition of several depolymerization and condensation reactions with different kinetic rates. In this sense, Montane et al. already observed with isothermal experiments the existence of several reactions which appears overlapped during DTG analyses [10] of impregnated samples.

### 3.3.3 Characterization of activated carbons

Table 3.2 shows the yield values of each treatment step and the total yield values for the different prepared activated carbons. As it is well known, phosphoric acid limits the formation of tars during the carbonization treatment, increasing the yield of the remaining solid product [8]. In this case, the yield of the treatment with air at 200 ºC is, approximately, 90% for both samples derived from co-solution of lignin and phosphoric acid and impregnated with phosphoric acid. The yield of the activation step (mass of activated sample/mass of impregnated

UNIVERSIDAD DE MÁLAGA

or treated with air sample) was around 75% for samples non-treated with air, and about 85% for samples treated with air. There was approximately a difference of 10%, which practically corresponded to the loss of light hydrocarbons from the lignin degradation that was previously observed during the treatment with air at 200 ºC. The washing yield (mass of washed sample/mass of activated sample) was around 25%, very similar in all cases, and a total yield of around 60% was obtained for all the activated carbons, with no significant differences observed when lignin was co-dissolved or not with the activated agent and/or when the oxidative stabilization step was or was not performed. The total yield values (mass of activated carbon/mass of lignin) are considerably higher than others reported in the literature for lignin and other lignocellulosic materials [10,43,44].

**Table 3.2.** Yield values of the lignin activated carbons.

| Activated carbon | Oxidative treatment yield (%) | Activation yield (%) | Washing yield (%) | Total yield (%) |
|---|---|---|---|---|
| **L2P400** | — | 75.9 | 28.0 | 63.8 |
| **LE2P400** | — | 75.9 | 25.9 | 59.2 |
| **L2PS400** | 87.3 | 87.8 | 27.3 | 62.9 |
| **LE2PS400** | 90.7 | 81.6 | 25.2 | 63.3 |

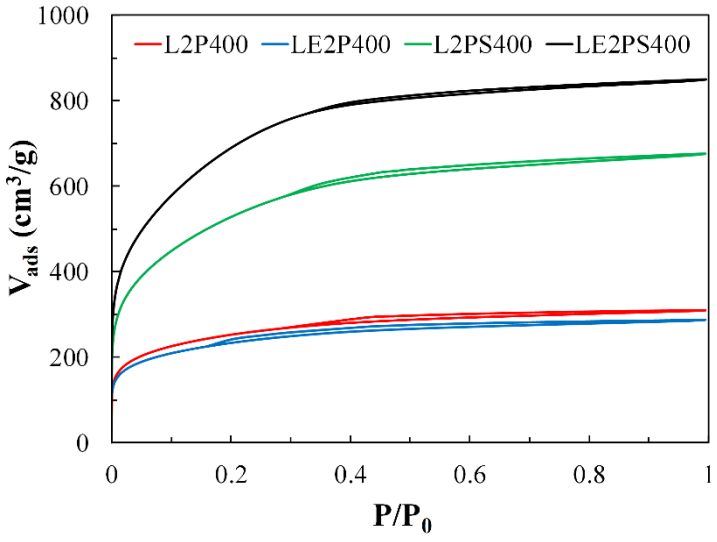


**Figure 3.6.** $N_2$ adsorption-desorption isotherms obtained at – 196 ºC of the different activated carbons obtained at 400 ºC and with $H_3PO_4$ to lignin mass ratio of 2.



UNIVERSIDAD DE MÁLAGA

Figure 3.6 shows the $N_2$ adsorption-desorption isotherms at -196 ºC of the different activated carbons, prepared at 400 ºC and with an $H_3PO_4$ to lignin mass ratio of 2. The isotherm of the activated carbon L2P400 is a type I isotherm, characteristic of a typical microporous solid, which adsorbs almost all $N_2$ at low relative pressures. No significant changes in the $N_2$ isotherm were observed when lignin was co-dissolved with the activating agent. However, the treatment with air at 200 ºC produced solids with a remarkable increased $N_2$ adsorbed volume up to 0.4 of relative pressure, which indicated a larger presence of wider microporosity in these carbonaceous solids. This $N_2$ adsorption volume increase was significantly more pronounced when co-solution of lignin and phosphoric acid was carried out previously to the oxidative stabilization step (air at 200 ºC). The small hysteresis cycle at medium relative pressures shown by the $N_2$ adsorption isotherms indicates the presence (to a lesser extent) of narrow mesopores.

**Table 3.3.** Textural properties of the different lignin derived activated carbons obtained from the $N_2$ and $CO_2$ isotherms.

| | **$N_2$ Isotherm** | | | | | **$CO_2$ Isotherm** | |
|---|---|---|---|---|---|---|---|
| | **$A_{BET}$ ($m^2/g$)** | **$A_t$ ($m^2/g$)** | **$V_t$ ($cm^3/g$)** | **$V_p$ ($cm^3/g$)** | **$V_{meso}$ ($cm^3/g$)** | **$A_{DR}$ ($m^2/g$)** | **$V_{DR}$ ($cm^3/g$)** |
| **L2P400** | 912 | 55 | 0.41 | 0.48 | 0.06 | 438 | 0.18 |
| **LE2P400** | 845 | 36 | 0.40 | 0.44 | 0.05 | 407 | 0.16 |
| **L2PS400** | 1937 | 131 | 0.89 | 1.04 | 0.15 | 673 | 0.27 |
| **LE2PS400** | 2551 | 143 | 1.16 | 1.31 | 0.15 | 859 | 0.34 |

The textural properties obtained from the $N_2$ and $CO_2$ isotherms of the different activated carbons are summarized in Table 3.3. The differences between the micropore volumes obtained from $N_2$ ($V_t$) and $CO_2$ ($V_{DR}$) isotherms, with higher values for those from $N_2$ ones, confirmed the presence of a wide microporosity for the lignin-derived activated carbons. However, the mesopore volumes are quite low in all the samples. The apparent surface area ($A_{BET}$) values increased considerably from 912 $m^2/g$ for L2P400 to 1937 $m^2/g$ for L2PS400, and to 2551 $m^2/g$ for LE2PS400. This last value is much higher than others reported in the literature for lignin-derived activated carbons using other activation methods [13,22,53,54,45–52], including the same activating agent ($H_3PO_4$), at similar temperatures and impregnation ratios [21,25,55–57]. Only a few works reported the preparation of activated carbons from lignin with higher apparent

UNIVERSIDAD DE MÁLAGA

surface areas (~3000 $m^2/g$ ) by using KOH activation, but at much higher activation temperatures than those used in this work [20,58–61]. In the method here proposed, the use of lower activation temperatures would substantially decrease the cost of the obtained activated carbons, without compromising the high development of porosity.

Figure 3.7 collects the micropore size distribution of the different activated carbons obtained at 400 ºC and $H_3PO_4$ to lignin mass ratio of 2. The activated carbon prepared by direct impregnation of lignin shows a bimodal micropore size distribution, with a main band with a maximum at around 6.7 Å and a second one (shoulder), less intense, with a maximum at around 16 Å, ending at a pore size value of about 40 Å, indicating the presence of narrow mesopores. The micropore size distribution of the activated carbon when lignin was co-dissolved with the activating agent is practically the same as that of the activated carbon prepared by direct impregnation of lignin. However, the treatment with air at 200 ºC produces a clear change in the bimodal micropore size distribution. This treatment produced an increase of both bands, with the maximum of the first one slightly shifting to higher micropore sizes (from 6.7 to approximately 8.5 Å). However, the increase of the band corresponding to micropores of about 16 Å was proportionally higher than that corresponding to the lower micropore sizes (6.7 to 8.5 Å ), even surpassing it in the case of LE2PS400. These results suggest that the treatment with air at 200 ºC increased the volume of micropores, especially that of the largest pore size (16 Å), and this effect was clearly enhanced by the co-solution of lignin and phosphoric acid. However, this treatment does not appear to greatly affect the micropore (or mesopore) size of the obtained activated carbons.

UNIVERSIDAD DE MÁLAGA

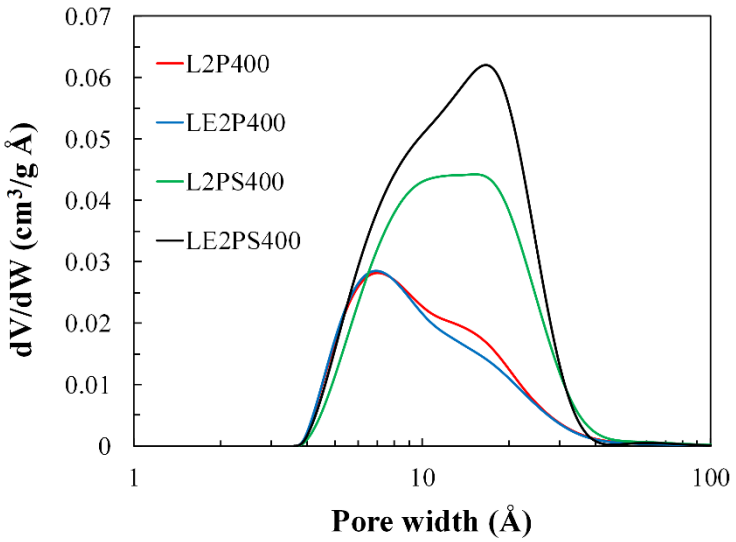


**Figure 3.7.** Micropore size distribution of the different activated carbons obtained at 400 ºC and with $H_3PO_4$ to lignin mass ratio of 2.

The present results indicate that the use of co-solution of lignin with phosphoric acid in combination with an oxidative treatment at 200 ºC provides activated carbons with extremely high specific surface area and a large and wide microporosity. These significant differences in the porous texture seem to be the result of larger and more homogeneous interactions between lignin and the activating agent when they are co-dissolved that may increase the formation of effective phosphate esters, which are the responsible of the cross-linking reactions in the carbonaceous matrix during the oxidative stabilization process [44]. To support this hypothesis, TPD (Figure 3.8**)** and XPS (not shown) analyses were carried out for the different activated carbons. As it was observed in previous works, activated carbons prepared by chemical activation with phosphoric acid presented most of CO evolution at temperatures higher than 700 ºC, due to the presence of oxygen-containing P surface groups, which include metaphosphates, mainly as C-O-$PO_3$ groups and C-$PO_3$ groups, which decompose as gaseous CO, producing C-P type surface groups [12,24]. In addition, XPS P2p spectra of the different activated carbons, which were very similar to those of the corresponding lignin-derived samples (Figure 3), also evidence the presence of, mainly, C-O-P ones (CO-$PO(OH)_2$ and $(C\text{-}O)_3PO$) at 134.2 eV and C-P-O groups (such as C-$PO(OH)_2$ or $C_2$-PO(OH)) at 133 eV. The similarity among the spectra indicated that the contribution of this kind of groups is very similar in the different obtained activated carbons, independently of the preparation method used. In this sense, a similar P surface concentration value of 1.6 %w was obtained for L2P400, L2PS400

UNIVERSIDAD DE MÁLAGA

and LE2P400. However, the combined effect of the co-solution of lignin and phosphoric acid and the oxidative treatment at low temperature increased this value to 2.4 %wt.

TPD CO profiles for the activated carbon prepared from dissolved and not-dissolved lignin are very similar, showing most of their CO release between 700 and 900 ºC (Fig. 3.8). However, the treatment with air at 200 ºC and the combined use of this treatment with co-solution of lignin and the activating agent provided a higher release of CO, even at temperatures lower than 700 ºC. This CO evolution at lower temperatures can be associated to decomposition of mainly phenol and ether surface groups and, to a lesser extent, to anhydride surface groups. As decomposition of this last group also should produce $CO_2$ evolution, the low $CO_2$ evolution for these activated carbons at this temperature range provided evidences of the low presence of anhydride surface groups on those samples. On the other hand, the sample LE2PS400 presented the highest CO evolution between 700 and 800 ºC, which suggests a higher presence of metaphosphates (C-O-$PO_3$ and/or C-$PO_3$ type) surface groups on this sample [24]. These P surface groups, with C-O-P bonds, decompose to gas CO and P surface groups of C-P bond type at these temperatures [38]. The larger evolution of CO observed in the TPD for LE2PS400 can be associated to a higher generation of phosphate esters during the preparation process, as it was evidenced by FTIR analyses (**Figure 3.2**) and by the higher surface P content (2.4%wt) of this activated carbon, revealed by XPS results.

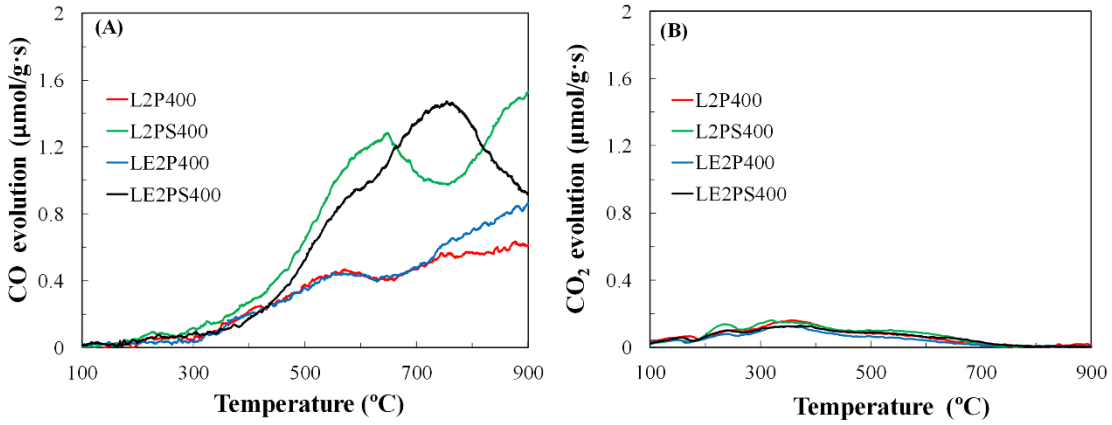


**Figure 3.8.** (A) CO and (B) $CO_2$ evolution of the different activated carbons.

### 3.3.4 Effect of temperature of the oxidative treatment

Although to our best knowledge the co-solution of the carbon precursor and the activating agent has not been previously reported, some authors have already proposed the activation in two different steps. Toles et al. analyzed different approaches of acid-activation/oxidation to



UNIVERSIDAD DE MÁLAGA

produce activated carbons with high metals and organics compounds adsorption uptakes [62]. They observed no significant differences on the porosity of samples directly activated in air at 450 ºC and compared with samples prepared with a further intermediate step at 170 ºC, obtaining a maximum apparent surface area of $A_{BET}$=1662 $m^2/g$. They suggested that the intermediate step was not necessary because the time spent during the ramping stage (averaging approximately 0.8 h) to 450 ºC was sufficient to allow penetration of the activating agent (phosphoric acid) and any preliminary reactions to take place. Dastgheib and Rockstraw proposed also a two steps activation process, both of them in air, with the first one up to 215 ºC, temperature from which ortho-phosphoric acid dehydrates, losing half a molecule of water and forming pyrophosphoric acid, but they do not compare the porosity of activated carbons prepared in other gas atmospheres [63].

In order to deep in the role of this oxidative treatment, further oxidative treatments were carried out at different temperatures. Table 3.4 shows the yield values of the lignin derived activated carbons obtained at 400 ºC and $H_3PO_4$/lignin mass ratio of 2, but previously treated at different temperatures under air atmosphere. As can be seen, the yield of the treatment in air decreases as the temperatures increases, due to a higher release of light hydrocarbons and water. The activation and washing yields remain approximately the same regardless of the treatment previously carried out, since the impregnation ratio and the activation temperature is the same in all the samples. Therefore, the total yield values follow the same sequence found for the treatments with air.

**Table 3.4.** Yield values of the lignin-derived activated carbons obtained at 400 ºC and $H_3PO_4$/lignin mass ratio of 2, treated at different temperatures and stabilization times.

| Sample | Oxidative treatment yield (%) | Activation yield (%) | Washing yield (%) | Total yield (%) |
|---|---|---|---|---|
| **LE2PS400-100ºC** | 98.1 | 85.8 | 25.7 | 65.0 |
| **LE2PS400-200ºC** | 90.7 | 81.6 | 22.2 | 63.3 |
| **LE2PS400-300ºC** | 87.7 | 88.7 | 24.0 | 56.0 |
| **LE2P400-A** | - | 80.1 | 27.2 | 64.9 |
| **LE2PS(N)400** | 88.8 | 87.3 | 26.2 | 60.9 |

UNIVERSIDAD DE MÁLAGA

Figure 3.9 shows the $N_2$ adsorption-desorption isotherms at – 196 ºC of the different activated carbons prepared at 400 ºC and $H_3PO_4$/lignin mass ratio of 2, treated at different oxidative temperatures. The isotherms of the series are all of them type I isotherms. The results indicate that the oxidative treatment at 100  C did not generate large porosity development compared to that of the sample without any oxidative treatment. The highest amount of $N_2$ adsorbed volume was observed for the sample treated at 200 ºC. An increase of this temperature to 300 ºC slightly reduced the $N_2$ adsorbed volumes. Table 3.5 collects the textural properties derived from the $N_2$ and $CO_2$ isotherms of the different lignin derived activated carbons obtained at 400 ºC, a $H_3PO_4$/lignin mass ratio of 2 and treated at different oxidative temperatures. As can be seen, the textural properties of the sample treated at 100 ºC are very similar to those reported in Table 3.3 for the sample L2P400, which was not submitted to any oxidative treatment. It can also be observed that maximum pore volume (1.31 $cm^3/g$) and apparent surface area (2551 $m^2/g$) were obtained with an oxidative treatment at 200 ºC, while a relative decrease in the apparent surface area to 2128 $m^2/g$ was noticed when the oxidative treatment was performed at 300 ºC.

The treatment in air at low temperature seems to enhance the formation of phosphate and polyphosphate bridges, which are responsible for connecting and crosslinking the lignin fragments. These phosphorus groups are inserted in the carbon matrix, separating the organic species. These groups generate an expansional process that, after removal of the acid, leaves the matrix in an expanded state, with a high pore development structure. In this case, the highest porosity development is observed when the oxidative treatment is performed at intermediate temperatures (200 ºC). The treatment at 100 ºC does not produce any enhancement in the porosity, and at 300 ºC some reduction begins to be noticed. These differences can be explained, according to the findings of Jagtoyen et al., by the fact that bond cleavage reactions that proceed through ionic mechanisms are taking place at low temperature and cross-linking reaction dominates over bond cleavage and de-polymerization reactions from 150 ºC [8]. Therefore, the results seem to indicate that the presence of oxygen promotes preferentially the cross-linking reactions around 200 ºC and from this temperature some over-oxidation could take place.

UNIVERSIDAD DE MÁLAGA

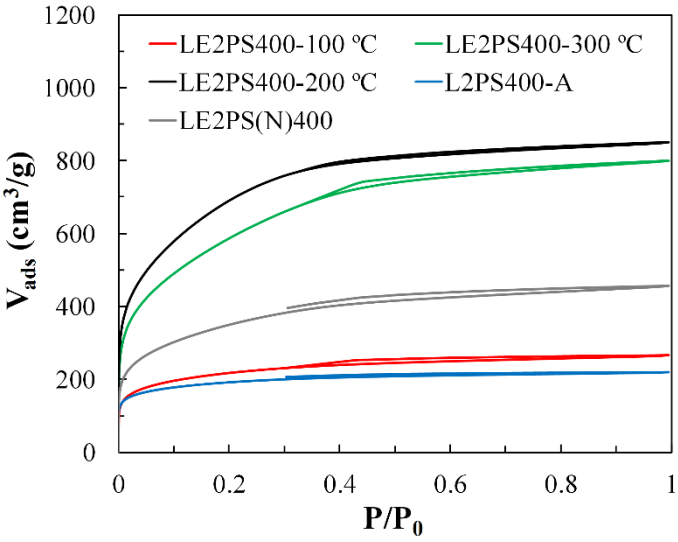


**Figure 3.9.** $N_2$ adsorption-desorption isotherms obtained at – 196 ºC of the different activated carbons obtained at 400 ºC and $H_3PO_4$/lignin mass ratio of 2, treated at different temperatures.

In addition, other experiment was carried out but treating the lignin/$H_3PO_4$ samples at 200 ºC under inert ($N_2$) atmosphere (instead of air), followed by activation also in $N_2$ at 400 ºC (LE2PS(N)400). The amount of $N_2$ adsorbed volume over the entire range of relative pressure for the sample thus obtained was significantly higher than that observed for the LE2P400 sample, evidencing the presence of larger and wider microporosity. These results suggest that some reactions are being promoted at 200 ºC even under inert atmosphere, when sufficient time is provided. According to DSC results, it must be related to crosslinking reactions taking place during the decomposition process [41] and/or to the polymerization and condensation reaction with $H_3PO_4$ [42]. Based on these results, it seems that, in agreement with the hypothesis of Toles et al., there are some kinetic limitations, as can be deduced from the increase of the microporosity with the treatment at 200 ºC under inert atmosphere, mainly associated to some crosslinking reactions [62].However, the use of an oxidative atmosphere becomes necessary to boost the porosity development, as pointed out by Dastgheib and Rockstraw [63], but at adequate experimental conditions, as those previously observed.

UNIVERSIDAD DE MÁLAGA

**Table 3.6.** Textural properties of the different lignin activated carbons obtained at 400 ºC and $H_3PO_4$/lignin mass ratio of 2, treated at different temperatures and activation times under air atmosphere, obtained from the $N_2$ and $CO_2$ isotherms.

| | **$N_2$ Isotherm** | | | | | **$CO_2$ Isotherm** | |
|---|---|---|---|---|---|---|---|
| | **$A_{BET}$ ($m^2/g$)** | **$A_t$ ($m^2/g$)** | **$V_t$ ($cm^3/g$)** | **$V_p$ ($cm^3/g$)** | **$V_{mes}$ ($cm^3/g$)** | **$A_{DR}$ ($m^2/g$)** | **$V_{DR}$ ($cm^3/g$)** |
| **LE2PS400-100 ºC** | 877 | 61 | 0.39 | 0.46 | 0.07 | 420 | 0.17 |
| **LE2PS400-200 ºC** | 2551 | 143 | 1.16 | 1.31 | 0.15 | 859 | 0.34 |
| **LE2PS400-300 ºC** | 2128 | 181 | 1.04 | 1.24 | 0.18 | 570 | 0.23 |
| **LE2P400-A** | 707 | 26 | 0.31 | 0.34 | 0.03 | 501 | 0.20 |
| **LE2PS(N)400** | 1263 | 111 | 0.58 | 0.71 | 0.13 | 483 | 0.19 |

In order to provide evidences of a possible over-oxidation of the activated carbon, which avoids the porosity development, a further activation of the LE2P sample at 400ºC but directly in air was carried out. The isotherm of the corresponding activated carbon, LE2P400-A, (shown in **Figure 3.9**) presented lower $N_2$ adsorption volumes than the ones for the corresponding carbon materials obtained by activation under inert atmosphere. The same tendency was found for the sample L2P also activated in air at 400 ºC (not shown). In particular, a reduction in the apparent surface area of almost 200 $m^2/g$ (Table 3.5) was observed, suggesting that some over-oxidation has occurred, causing some pores to collapse [64]. In this line, several authors prepared activated carbons under different gas atmospheres in order to analyze their influence on the porous texture development. However, some discrepancies can be found in these works. Laine et al. observed an increase of the surface area of activated carbons from coconut shell at 400 ºC, when forced air was used, varying from 180 (in $N_2$) to 860 (in air) $m^2/g$ [17]. Molina-Sabio et al. suggested that the presence of oxygen at 450 ºC, at low impregnation ratios (R<0.32), inhibits the aromatization process, thus reducing the influence of the phosphoric acid in both promoting the development of porosity and reducing the extent of contraction produced during the heat treatment of peach stones. At higher impregnation ratios (R>0.32), they proposed that the access of air will be more restricted and will have smaller effect on the process [65]. Benaddi et al reported very similar micropores volumes and surface areas independently of the gas atmosphere ($O_2$ or $N_2$) used to prepare activated carbons from wood at 480 ºC [18].

UNIVERSIDAD DE MÁLAGA

Puziy et al. associated a maximum of porosity in activated carbons prepared from a styrene–divinylbenzene copolymer in air, at 900 ºC, to a further air gasification [66]. Wang et al. mixed ammonium persulfate with phosphoric acid [64]. They proposed that the oxygen generated from decomposition of ammonium persulfate enhanced both the formation of phosphate esters and the formation of CO and $CO_2$ by gasification. At low oxygen dosages, the formation of phosphate esters predominated, hence promoting the crosslinking between phosphoric acid and lignin. They also pointed out that lignin presents higher carbon content than wood and can thus produce more phosphate esters. However, the excessive amount of persulfate leads to over-oxidation and carbon deletion. Furthermore, the over-oxidation also can cause some pores to collapse [64].

Based on our results and taking into account the statements of all these authors, it seems that in our experimental conditions, the presence of oxygen at intermediate temperatures, where cross-linking reactions dominate, promote the porosity development due to the creation of more phosphate esters, but at higher temperatures, where the aromatization process preferentially takes place, an excess of oxygen was counter-productive, generating an over-oxidation that would inhibit the increase of the porosity.

This new methodology can be an interesting alternative for the valorization of Alcell lignin into highly porous activated carbons. The high apparent surface area obtained and the presence of surface phosphorus functional groups, which provides to the activated carbons with surface acid character [67] and oxidation resistance [25], open the possibilities for different applications[16] . Specifically, these activated carbons can be used in adsorption processes (gas and liquid phases), like adsorbent for basic compounds [68–70], in heterogeneous catalytic processes, like catalyst or catalytic support [24,57] and even in electrochemistry applications [71].

## 3.4 Conclusions

This work analyzes the effect of co-solution of carbon precursor and activating agent on the textural and surface chemistry properties of highly nanoporous activated carbons obtained by chemical activation of Alcell lignin with phosphoric acid. The success of this methodology highlights the possibility of directly using the liquors produced in organosolv process (Alcell) to prepare activated carbons by chemical activation with phosphoric acid. Co-solutions of lignin and phosphoric acid were submitted to a two steps thermal treatment, which consisted of a first

UNIVERSIDAD DE MÁLAGA

oxidative stabilization in air at 200 ºC, followed by a thermal treatment in $N_2$ at 400 ºC, where activation of the oxidized lignin with phosphoric acid took place. A lignin-derived activated carbon with very high apparent surface area (2550 $m^2/g$) and pore volume (1.30 $cm^3/g$) was obtained with an initial phosphoric acid to lignin mass ratio of 2. Up to now, this is one of the highest values of apparent surface area reported not only for activated carbons prepared from lignin, but even for porous carbons prepared by chemical activation of other lignocellulosic materials with phosphoric acid. The use of lignin and phosphoric acid solutions provided more homogeneous and effective interactions between the carbon precursor and the activating agent, by the formation of phosphate esters in the lignin matrix, which seems to be a key factor in the subsequent treatments: promoting crosslinking reactions in the carbonaceous matrix during the oxidative treatment in air at 200 ºC and enhancing the development of a wide porosity during the followed activation thermal treatment.

## References

[1] J.M. Rosas, R. Berenguer, M.J. Valero-Romero, J. Rodrí-guez-Mirasol, T. Cordero, Preparation of Different Carbon Materials by Thermochemical Conversion of Lignin, Front. Mater. 1 (2014) 1–17. https://doi.org/10.3389/fmats.2014.00029.

[2] S. Laurichesse, L. Avérous, Chemical modification of lignins: Towards biobased polymers, Prog. Polym. Sci. 39 (2014) 1266–1290. https://doi.org/10.1016/j.progpolymsci.2013.11.004.

[3] N. Smolarski, High-Value Opportunities for Lignin: Unlocking its Potential Lignin potential, Frost & Sullivan. (2012) 1–15.

[4] H.A. Smith.C, Lignin. NNFCC Renewable Chemicals Factsheet The National Non-Food Crops Centre, York, UK. 8 (2011).

[5] J.L. Espinoza-Acosta, P.I. Torres-Chávez, E. Carvajal-Millán, B. Ramírez-Wong, L.A. Bello-Pérez, B. Montaño-Leyva, Ionic liquids and organic solvents for recovering lignin from lignocellulosic biomass, BioResources. 9 (2014) 3660–3687. https://doi.org/10.15376/biores.9.2.3660-3687.

[6] H.A. Ruiz, D.S. Ruzene, D.P. Silva, F.F.M.I. Da Silva, A.A. Vicente, J.A. Teixeira, Development and characterization of an environmentally friendly process sequence (autohydrolysis and organosolv) for wheat straw delignification, Appl. Biochem. Biotechnol. 164 (2011) 629–641. https://doi.org/10.1007/s12010-011-9163-9.

[7] F. Xu, J.X. Sun, R. Sun, P. Fowler, M.S. Baird, Comparative study of organosolv lignins from wheat straw, Ind. Crops Prod. 23 (2006) 180–193. https://doi.org/10.1016/j.indcrop.2005.05.008.

[8] M. Jagtoyen, F. Derbyshire, Activated carbons from yellow poplar and white oak by

UNIVERSIDAD DE MÁLAGA

$H_3PO_4$ activation, Carbon. 36 (1998) 1085–1097. https://doi.org/10.1016/S0008-6223(98)00082-7.

[9] L.J. Kennedy, J.J. Vijaya, G. Sekaran, Effect of Two-Stage Process on the Preparation and Characterization of Porous Carbon Composite from Rice Husk by Phosphoric Acid Activation, Ind. Eng. Chem. Res. 43 (2004) 1832–1838. https://doi.org/10.1021/ie034093f.

[10] D. Montané, V. Torné-Fernández, V. Fierro, Activated carbons from lignin: Kinetic modeling of the pyrolysis of Kraft lignin activated with phosphoric acid, Chem. Eng. J. 106 (2005) 1–12. https://doi.org/10.1016/j.cej.2004.11.001.

[11] N. V. Sych, S.I. Trofymenko, O.I. Poddubnaya, M.M. Tsyba, V.I. Sapsay, D.O. Klymchuk, A.M. Puziy, Porous structure and surface chemistry of phosphoric acid activated carbon from corncob, Appl. Surf. Sci. 261 (2012) 75–82. https://doi.org/10.1016/j.apsusc.2012.07.084.

[12] J.M. Rosas, J. Bedia, J. Rodríguez-Mirasol, T. Cordero, Hemp-derived activated carbon fibers by chemical activation with phosphoric acid, Fuel. 88 (2009) 19–26. https://doi.org/10.1016/j.fuel.2008.08.004.

[13] J. Hayashi, A. Kazehaya, K. Muroyama, A.P. Watkinson, Preparation of activated carbon from lignin by chemical activation, Carbon. 38 (2000) 1873–1878. https://doi.org/10.1016/S0008-6223(00)00027-0.

[14] M. Molina-Sabio, F. Rodríguez-Reinoso, Role of chemical activation in the development of carbon porosity, Colloids Surfaces A Physicochem. Eng. Asp. 241 (2004) 15–25. https://doi.org/10.1016/j.colsurfa.2004.04.007.

[15] M. Jagtoyen, J. Groppo, F. Derbyshire, Activated carbons from bituminous coals by reaction with H3PO4: The influence of coal cleaning, Fuel Process. Technol. 34 (1993) 85–96. https://doi.org/10.1016/0378-3820(93)90093-J.

[16] A.M. Puziy, O.I. Poddubnaya, B. Gawdzik, J.M.D. Tascón, Phosphorus-containing carbons: Preparation, properties and utilization, Carbon. 157 (2020) 796–846. https://doi.org/10.1016/j.carbon.2019.10.018.

[17] J. Laine, A. Calafat, M. Labady, Preparation and characterization of activated carbons from coconut shell impregnated with phosphoric acid, Carbon N. Y. 27 (1989) 191–195. https://doi.org/10.1016/0008-6223(89)90123-1.

[18] H. Benaddi, D. Legras, J.N. Rouzaud, F. Beguin, Influence of the atmosphere in the chemical activation of wood by phosphoric acid, Carbon. (1998) 306–309. https://doi.org/10.1016/S0008-6223(98)80123-1.

[19] C. Moreno-Castilla, F. Carrasco-Marín, M.V. López-Ramón, M.A. Alvarez-Merino, Chemical and physical activation of olive-mill waste water to produce activated carbons, Carbon N. Y. 39 (2001) 1415–1420. https://doi.org/10.1016/S0008-6223(00)00268-2.

[20] V. Fierro, V. Torné-Fernández, A. Celzard, Methodical study of the chemical activation

UNIVERSIDAD DE MÁLAGA

of Kraft lignin with KOH and NaOH, Microporous Mesoporous Mater. 101 (2007) 419–413. https://doi.org/10.1016/j.micromeso.2006.12.004.

[21] E. Gonzalez-Serrano, T. Cordero, J. Rodriguez-Mirasol, L. Cotoruelo, J.J. Rodriguez, Removal of water pollutants with activated carbons prepared from $H_3PO_4$ activation of lignin from kraft black liquors, Water Res. 38 (2004) 3043–3050. https://doi.org/10.1016/j.watres.2004.04.048.

[22] E. Gonzalez-Serrano, T. Cordero, J. Rodríguez-Mirasol, J.J. Rodríguez, Development of Porosity upon Chemical Activation of Kraft Lignin with $ZnCl_2$, Ind. Eng. Chem. Res. 36 (1997) 4832–4838. https://doi.org/10.1021/ie970261q.

[23] E. Guillén, R. Rico, J.M. López-Romero, J. Bedia, J.M. Rosas, J. Rodríguez-Mirasol, T. Cordero, Pd-activated carbon catalysts for hydrogenation and Suzuki reactions, Appl. Catal. A Gen. 368 (2009) 113–120. https://doi.org/10.1016/j.apcata.2009.08.016.

[24] J. Bedia, J.M. Rosas, J. Márquez, J. Rodríguez-Mirasol, T. Cordero, Preparation and characterization of carbon based acid catalysts for the dehydration of 2-propanol, Carbon. 47 (2009) 286–294. https://doi.org/10.1016/j.carbon.2008.10.008.

[25] J.M. Rosas, R. Ruiz-Rosas, J. Rodríguez-Mirasol, T. Cordero, Kinetic study of the oxidation resistance of phosphorus-containing activated carbons, Carbon. 50 (2012) 1523–1537. https://doi.org/10.1016/j.carbon.2011.11.030.

[26] S. Brunauer, P.H. Emmett, E. Teller, Adsorption of Gases in Multimolecular Layers, J. Am. Chem. Soc. 60 (1938) 309–319.

[27] B.C. Lippens, J.H. de Boer, Studies on pore systems in catalysts. V. The t method, J. Catal. 4 (1965) 319–323. https://doi.org/10.1016/0021-9517(65)90307-6.

[28] F. Rodríguez-Reinoso, M. Molina-Sabio, M.T. González, The use of steam and $CO_2$ as activating agents in the preparation of activated carbons, Carbon. 33 (1995) 15–23. https://doi.org/10.1016/0008-6223(94)00100-E.

[29] M. M. Dubinin, E. D. Zaverina, L. V. Radushkevich, Sorption and structure of active carbons. I. Adsorption of organic vapors, Zhurnal Fiz. Khimii. 21 (1947) 1352–1362.

[30] J. Jagiello, J.P. Olivier, 2D-NLDFT adsorption models for carbon slit-shaped pores with surface energetical heterogeneity and geometrical corrugation, Carbon. 55 (2013) 70–80. https://doi.org/10.1016/j.carbon.2012.12.011.

[31] S. Kubo, J.F. Kadla, Poly(ethylene oxide)/organosolv lignin blends: Relationship between thermal properties, chemical structure, and blend behavior, Macromolecules. 37 (2004) 6904–6911. https://doi.org/10.1021/ma0490552.

[32] R. D. Girard, A. R. P. Van Heiningen, Delignification rate of White birch chips during etanol-water cooking in a stirred batch reactor with rapid liquor displacement, J. Pulp Pap. Sci. 26 (2000) 1–7.

[33] G. Almendros, A.T. Martínez, A.E. González, F.J. González-Vila, R. Fründ, H.D. Lúdemann, CPMAS 13C NMR Study of Lignin Preparations from Wheat Straw

UNIVERSIDAD DE MÁLAGA

Transformed by Five Lignocellulose-Degrading Fungi, J. Agric. Food Chem. 40 (1992) 1297–1302. https://doi.org/10.1021/jf00019a043.

[34] I.F. Fiţigău, F. Peter, C.G. Boeriu, Structural Analysis of Lignins from Different Sources, World Acad. Sci. Eng. Technol. 7 (2013) 98–103.

[35] M.E. Vallejos, F.E. Felissia, A.A.S. Curvelo, M.D. Zambon, L. Ramos, M.C. Area, Chemical and physico-chemical characterization of lignins obtained from ethanol-water fractionation of bagasse, BioResources. 6 (2011) 1158–1171.

[36] S. Labruquère, R. Pailler, R. Naslain, B. Desbat, Oxidation inhibition of carbon fibre preforms and C/C composites by $H_3PO_4$, J. Eur. Ceram. Soc. 18 (1998) 1953–1960. https://doi.org/10.1016/S0955-2219(98)00135-6.

[37] F.J. García-Mateos, R. Berenguer, M.J. Valero-Romero, J. Rodríguez-Mirasol, T. Cordero, Phosphorus functionalization for the rapid preparation of highly nanoporous submicron-diameter carbon fibers by electrospinning of lignin solutions, J. Mater. Chem. A. 6 (2018) 1219–1233. https://doi.org/10.1039/c7ta08788h.

[38] X. Wu, L.R. Radovic, Inhibition of catalytic oxidation of carbon/carbon composites by phosphorus, Carbon. 44 (2006) 141–151. https://doi.org/10.1016/j.carbon.2005.06.038.

[39] A.M. Puziy, O.I. Poddubnaya, R.P. Socha, J. Gurgul, M. Wisniewski, XPS and NMR studies of phosphoric acid activated carbons, Carbon. 46 (2008) 2113–2123. https://doi.org/10.1016/j.carbon.2008.09.010.

[40] A. Martínez De Yuso, B. Rubio, M.T. Izquierdo, Influence of activation atmosphere used in the chemical activation of almond shell on the characteristics and adsorption performance of activated carbons, Fuel Process. Technol. 119 (2014) 74–80. https://doi.org/10.1016/j.fuproc.2013.10.024.

[41] I. Karacan, T. Soy, Structure and properties of oxidatively stabilized viscose rayon fibers impregnated with boric acid and phosphoric acid prior to carbonization and activation steps, J. Mater. Sci. 48 (2013) 2009–2021. https://doi.org/10.1007/s10853-012-6970-5.

[42] G.Z. Zhu, X.L. Deng, M. Hou, K. Sun, Y.P. Zhang, P. Li, F.M. Liang, Comparative study on characterization and adsorption properties of activated carbons by phosphoric acid activation from corncob and its acid and alkaline hydrolysis residues, Fuel Process. Technol. 144 (2016) 255–261. https://doi.org/10.1016/j.fuproc.2016.01.007.

[43] J.M. Rosas, J. Bedia, J. Rodríguez-Mirasol, T. Cordero, Preparation of hemp-derived activated carbon monoliths. Adsorption of water vapor, Ind. Eng. Chem. Res. 47 (2008) 1288–1296. https://doi.org/10.1021/ie070924w.

[44] A.M. Puziy, O.I. Poddubnaya, A. Martínez-Alonso, F. Suárez-García, J.M.D. Tascón, Surface chemistry of phosphorus-containing carbons of lignocellulosic origin, Carbon. 43 (2005) 2857–2868. https://doi.org/10.1016/j.carbon.2005.06.014.

[45] J. Rodríguez-Mirasol, T. Cordero, J.J. Rodríguez, Activated Carbons from $CO_2$ Partial Gasification of Eucalyptus Kraft Lignin, Energy and Fuels. 7 (1993) 133–138.

UNIVERSIDAD DE MÁLAGA

https://doi.org/10.1021/ef00037a021.

[46] L.M. Cotoruelo, M.D. Marqués, F.J. Díaz, J. Rodríguez-Mirasol, T. Cordero, J.J. Rodríguez, Activated carbons from lignin: Their application in liquid phase adsorption, Sep. Sci. Technol. 42 (2007) 3363–3389. https://doi.org/10.1080/01496390701626800.

[47] J. Rodríguez-Mirasol, T. Cordero, J.J. Rodríguez, Preparation and characterization of activated carbons from eucalyptus kraft lignin, Carbon. 31 (1993) 87–95. https://doi.org/10.1016/0008-6223(93)90160-C.

[48] P.J.M. Carrott, Suhas, M.M.L. Ribeiro Carrott, C.I. Guerrero, L.A. Delgado, Reactivity and porosity development during pyrolysis and physical activation in $CO_2$ or steam of kraft and hydrolytic lignins, J. Anal. Appl. Pyrolysis. 82 (2008) 264–271. https://doi.org/10.1016/j.jaap.2008.04.004.

[49] K. Babeł, K. Jurewicz, KOH activated lignin based nanostructured carbon exhibiting high hydrogen electrosorption, Carbon. 46 (2008) 1948–1956. https://doi.org/10.1016/j.carbon.2008.08.005.

[50] Y. Sun, J. Wei, Y.S. Wang, G. Yang, J.P. Zhang, Production of activated carbon by K2CO3activation treatment of cornstalk lignin and its performance in removing phenol and subsequent bioregeneration, Environ. Technol. 31 (2010) 53–61. https://doi.org/10.1080/09593330903338411.

[51] N.M.A. Al-Lagtah, A.H. Al-Muhtaseb, M.N.M. Ahmad, Y. Salameh, Chemical and physical characteristics of optimal synthesised activated carbons from grass-derived sulfonated lignin versus commercial activated carbons, Microporous Mesoporous Mater. 225 (2016) 504–514. https://doi.org/10.1016/j.micromeso.2016.01.043.

[52] J.L. Rowlandson, K.J. Edler, M. Tian, V.P. Ting, Toward Process-Resilient Lignin-Derived Activated Carbons for Hydrogen Storage Applications, ACS Sustain. Chem. Eng. 8 (2020) 2186–2195. https://doi.org/10.1021/acssuschemeng.9b05869.

[53] D. Kim, J. Cheon, J. Kim, D. Hwang, I. Hong, O.H. Kwon, W.H. Park, D. Cho, Extraction and characterization of lignin from black liquor and preparation of biomass-based activated carbon therefrom, Carbon Lett. 22 (2017) 81–88. https://doi.org/10.5714/CL.2017.22.081.

[54] J. Lin, F. Xue, G. Zhao, Soda lignin-based activated carbon and its adsorption properties, BioResources. 14 (2019) 376–386. https://doi.org/10.15376/biores.14.1.376-386.

[55] V. Fierro, V. Torné-Fernández, A. Celzard, D. Montané, Influence of the demineralisation on the chemical activation of Kraft lignin with orthophosphoric acid, J. Hazard. Mater. 149 (2007) 126–133. https://doi.org/10.1016/j.jhazmat.2007.03.056.

[56] Y. Guo, D.A. Rockstraw, Physical and chemical properties of carbons synthesized from xylan, cellulose, and Kraft lignin by $H_3PO_4$ activation, Carbon. 44 (2006) 1464–1475. https://doi.org/10.1016/j.carbon.2005.12.002.

[57] J. Bedia, J.M. Rosas, J. Rodríguez-Mirasol, T. Cordero, Pd supported on mesoporous

UNIVERSIDAD DE MÁLAGA

activated carbons with high oxidation resistance as catalysts for toluene oxidation, Appl. Catal. B Environ. 94 (2010) 8–18. https://doi.org/10.1016/j.apcatb.2009.10.015.

[58] Q.-X.G. Xian-Fa Li, Qing Xu, Yao Fu, Preparation and Characterization of Activated Carbon from Kraft Lignin via KOH Activation, Environ. Prog. Sustain. Energy. 33 (2014) 519–526. https://doi.org/10.1002/ep.

[59] Y. Zou, B.X. Han, Preparation of activated carbons from Chinese coal and hydrolysis lignin, Adsorpt. Sci. Technol. 19 (2001) 59–72. https://doi.org/10.1260/0263617011493971.

[60] C. Fernandez-Ruiz, J. Bedia, P. Bonal, J.J. Rodriguez, L.M. Gómez-Sainero, Chloroform conversion into ethane and propane by catalytic hydrodechlorination with Pd supported on activated carbons from lignin, Catal. Sci. Technol. 8 (2018) 3926–3935. https://doi.org/10.1039/c8cy00461g.

[61] J. Han, S.Y. Jeong, J.H. Lee, J.W. Choi, J.W. Lee, K.C. Roh, Structural and Electrochemical Characteristics of Activated Carbon Derived from Lignin-Rich Residue, ACS Sustain. Chem. Eng. 7 (2019) 2471–2482. https://doi.org/10.1021/acssuschemeng.8b05351.

[62] C.A. Toles, W.E. Marshall, M.M. Johns, Phosphoric acid activation of nutshells for metals and organic remediation: Process optimization, J. Chem. Technol. Biotechnol. 72 (1998) 255–263. https://doi.org/10.1002/(SICI)1097-4660(199807)72:3<255::AID-JCTB890>3.0.CO;2-P.

[63] S.A. Dastgheib, D.A. Rockstraw, Pecan shell activated carbon: Synthesis, characterization, and application for the removal of copper from aqueous solution, Carbon N. Y. 39 (2001) 1849–1855. https://doi.org/10.1016/S0008-6223(00)00315-8.

[64] Y. Wang, S. Zuo, Y. Zhu, Q. Shao, Y. Ni, Role of oxidant during phosphoric acid activation of lignocellulosic material, Carbon. 66 (2014) 734–737. https://doi.org/10.1016/j.carbon.2013.09.048.

[65] M. Molina-Sabio, F. Caturla, F. Rodriguez-Reinoso, Influence of the atmosphere used in the carbonization of phosphoric acid impregnated peach stones, Carbon. (1995) 1180–1182. https://doi.org/10.1016/0008-6223(95)91248-6.

[66] A.M. Puziy, O.I. Poddubnaya, A. Martínez-Alonso, F. Suárez-García, J.M.D. Tascón, Synthetic carbons activated with phosphoric acid III. Carbons prepared in air, Carbon. 41 (2003) 1181–1191. https://doi.org/10.1016/S0008-6223(03)00031-9.

[67] M.J. Valero-Romero, F.J. García-Mateos, J. Rodríguez-Mirasol, T. Cordero, Role of surface phosphorus complexes on the oxidation of porous carbons, Fuel Process. Technol. 157 (2017) 116–126. https://doi.org/10.1016/j.fuproc.2016.11.014.

[68] Suhas, P.J.M. Carrott, M.M.L. Ribeiro Carrott, Lignin--from natural adsorbent to activated carbon: a review., Bioresour. Technol. 98 (2007) 2301–2312. https://doi.org/10.1016/j.biortech.2006.08.008.

UNIVERSIDAD DE MÁLAGA

[69] J. Guo, W.S. Xu, Y.L. Chen, A.C. Lua, Adsorption of $NH_3$ onto activated carbon prepared from palm shells impregnated with $H_2SO_4$, J. Colloid Interface Sci. 281 (2005) 285–290. https://doi.org/10.1016/j.jcis.2004.08.101.

[70] K. László, Adsorption from aqueous phenol and aniline solutions on activated carbons with different surface chemistry, Colloids Surfaces A Physicochem. Eng. Asp. 265 (2005) 32–39. https://doi.org/10.1016/j.colsurfa.2004.11.051.

[71] D. Hulicova-Jurcakova, M. Seredych, G.Q. Lu, N.K.A.C. Kodiweera, P.E. Stallworth, S. Greenbaum, T.J. Bandosz, Effect of surface phosphorus functionalities of activated carbons containing oxygen and nitrogen on electrochemical capacitance, Carbon. 47 (2009) 1576–1584. https://doi.org/10.1016/j.carbon.2009.02.006.

UNIVERSIDAD DE MÁLAGA

# Chapter IV

UNIVERSIDAD DE MÁLAGA

# 4 Antipyrine Adsorption on Nanoporous Lignin-Derived Activated Carbons


## Abstract

This chapter analyzes the influence of the activating agent ($H_3PO_4$) to carbon precursor (lignin) mass ratio (values from 0.6 to 4) and the activation temperature (from 300 to 900 ºC) on the textural properties of the activated carbons, prepared by co-solution of lignin and $H_3PO_4$, followed by an oxidative (air) treatment at low temperature (200 ºC) before the activation step. For the sake of comparison, activated carbons prepared by traditional impregnation of (non-solved) lignin with $H_3PO_4$, followed by the activation step at similar operation conditions of $H_3PO_4$/lignin mass ratio and activation temperature were also studied. At low activation temperature (400 ºC), the maximum development of the porosity was reached for a value of $H_3PO_4$ to lignin mass ratio of 2, obtaining under these conditions the highest values of apparent surface area and of micropore volume (2550 $m^2/g$ and ~1.3 $cm^3/g$, respectively). At high activation temperature (900 ºC), a gradual development of the porous texture was observed with the $H_3PO_4$/lignin mass ratio up to a value of 4, from which a slight reduction in it was initiated. In general, the resulting activated carbons showed apparent surface areas higher than 2100 $m^2/g$ for a wide range of activating temperatures, between 350 ºC and 600 ºC, and at $H_3PO_4$/lignin mass ratio of 2.

Activated carbons with different pore size distributions were tested as adsorbent for antipyrine adsorption in aqueous solution, at low concentrations and at room temperature. The activated carbon with the narrowest pore size distribution showed the highest adsorption capacity of antipyrine (37 mg/g) for an equilibrium concentration as low as 1 mg/L. The antipyrine adsorption equilibrium and kinetic results were properly fitted by the Langmuir model and hyperbolic equation, respectively. The breakthrough times in column adsorption studies were successfully predicted by the Thomas model.


UNIVERSIDAD DE MÁLAGA

## 4.1 Introduction

Removal of pharmaceuticals and their metabolites from water has become an important challenge for recent society [1]. Even though they are usually present at very low concentrations of a few ppb [2], the problem of emerging pollutants is the lack of knowledge of their impact in the middle or long-term effect on human health, the environment and aquatic environments [3]. Analgesic and anti-inflammatory drugs are emerging pollutants frequently detected in wastewater treatment plants (WWTPs) effluents due to their extensively use without a medical prescription, with estimated annual consumption of several hundred tons in developed countries [4]. In this sense, antipyrine (phenazone) is an analgesic and anti-inflammatory drug, which has been considered as one of the emerging pollutants because of its endocrine-disrupting effects. However, the removal efficiencies of antipyrine in wastewater treatment plants (WWTPs) are around 35% [3,5,6]. Various treatment technologies have been proposed to remove these compounds from wastewater [7]. Among these methods, adsorption on powdered activated carbons is a well-known method for water purification [1], due to their effective and fast removal with low operating cost, simple design, easy to use and null production of harmful by-products [8].

Chemical activation with phosphoric acid has been widely used to prepare activated carbons from different precursors [9–12]. Among them, lignin can be considered as an ideal precursor for the preparation of chemicals and carbons materials [13,14]. In fact, isolation of different forms of lignin from pulping black liquors and the development of applications for them has gained a great interest in the biorefinery context. However, only 2% of lignin is actually commercialized, being most of lignin consumed as a fuel in the pulp–paper industry to recover energy and chemical reactant. Therefore, the development of value-added lignin-based products becomes necessary for the economic viability of biorefinery.

There are different papers dealing with the optimization of the preparation conditions in order to obtain activated carbons with high development of the textural properties from lignin [15–17]. In a previous paper, it was proposed a modification of the conventional chemical activation method to produce high surface area activated carbons from Alcell lignin [18]. This new methodology consisted of co-solution of the carbon precursor and the activating agent followed by two steps process: an oxidative treatment at low temperature followed by an activation step. The use of the co-solution of carbon precursor and activating agent produced a more homogeneous interaction between lignin and the activating agent (phosphoric acid). The

UNIVERSIDAD DE MÁLAGA

other variation was based on a treatment with air at 200 ºC, which was followed by activation in $N_2$ at 400 ºC. Both combined modifications generated a great development of porosity in the final activated carbons, with apparent surface area as high as 2550 $m^2/g$.

In this work, we deepen in the study of the influence of the $H_3PO_4$ to lignin mass ratio and the activation temperature on the textural properties of the activated carbons. For the sake of comparison, activated carbons were also prepared by direct impregnation of $H_3PO_4$ with powder lignin at similar operating conditions. These activated carbons were tested as adsorbents for antipyrine removal from aqueous phase by adsorption equilibrium and kinetic studies.

## 4.2 Experimental section

### 4.2.1 Activated carbons preparation

Alcell lignin was used as a biomass precursor for the preparation of activated carbons. Alcell lignin was dissolved in ethanol to simulate the composition of Alcell organosolv liquors. Aqueous $H_3PO_4$ 85% (w/w) was further contacted with the lignin-ethanol solution to obtain a co-solution of the carbon precursor and activating agent. This final solution was subsequently stirred at room temperature until evaporation of the ethanol and, finally, dried for 24 hours at 60°C in a vacuum dryer. The amount of $H_3PO_4$/lignin mass ratio was varied from 0 to 4.

The final lignin-$H_3PO_4$ dried mixture was further subjected to a low temperature oxidative treatment in air atmosphere at 200 ºC for 1.5 hour, using a heating ramp of 3 ºC/min, followed by a conventional chemical activation step (10 ºC/min) under inert atmosphere at different temperatures, between 300 and 900 °C. Once the activation temperature was reached, the samples were cooled inside the furnace and then washed with distilled water at 60 °C until neutral pH. The resulting activated carbons were dried at 60 °C. In these cases, the samples were named by the acronym LE of co-solution of lignin and phosphoric acid, followed by a number referring the $H_3PO_4$/lignin mass ratio, the letter P referring to $H_3PO_4$, the letter S to indicate the oxidative treatment and a number related to the activation temperature.

For the sake of comparison, solid Alcell lignin was also impregnated with $H_3PO_4$ in a conventional way, without dissolving the lignin in ethanol. In this case, the solid lignin (powder) was directly impregnated with aqueous phosphoric acid (85% (w/w)) at different $H_3PO_4$ to lignin mass ratios (from 0 to 4). The samples were dried at 60 ºC for 24 h before the activation step in inert atmosphere at different temperatures, at similar operation conditions as those used for the case of co-solution of lignin and $H_3PO_4$. Finally, the activated samples were washed with distilled

UNIVERSIDAD DE MÁLAGA

water. In this case, the activated carbons were denoted by the letter L followed by a number referring to the phosphoric acid to lignin mass ratio, a letter P related to $H_3PO_4$, and a number indicating the activation temperature.

### 4.2.2 Activated carbons characterization

The porosity of the samples was characterized by $N_2$ adsorption–desorption and $CO_2$ adsorption at -196 and 0 ºC, respectively, using a micromeritics instrument (ASAP 2020 model). The samples were previously outgassed for at least 8 hours at 150 ºC. From the $N_2$ isotherm, the apparent surface area ($A_{BET}$) was calculated by the BET equation [19]; the $\alpha_s$ method was used to determine the values of the external surface area (As), the micropore volume (Vs), and the specific surface area (as), obtained by the high resolution method proposed by Kaneko et al. [20–22], using a non-porous carbon black (Elftex-120) as standard. The mesopore volume (Vmes) was determined as the difference between the adsorbed volume of $N_2$ at a relative pressure of 0.995 and the micropore volume Vs[23]. From the $CO_2$ adsorption data, the narrow micropore volumen ($V_{DR}$) and surface area ($A_{DR}$) were calculated using the Dubinin–Radushkevich equation [24]. Pore size distributions were obtaining by applying the 2D-NLDFT heterogeneous surface model from $N_2$ adsorption isotherm [25].

The surface chemistry of the activated carbons was studied by X-ray photoelectron spectroscopy (XPS) and temperature-programmed desorption (TPD). XPS analyses of the samples were obtained in a 5700 C model Physical Electronics apparatus, with Mg Kα radiation (1253.6 eV, Physical Electronics, Feldkirchen, Germany). TPD was used for evaluating the carbon-oxygen surface groups. The surface groups of acidic character (carboxylic, lactonic) evolve as $CO_2$, whereas those of non-acid character (carbonyl, ether, quinone) and phenol groups give rise to CO. Anhydride surface groups evolve as both CO and $CO_2$. The evolution of CO and $CO_2$ as function of the temperature was obtained in a custom quartz fixed bed reactor placed inside an electrical furnace, by using non-dispersive infrared (NDIR) gas analyzers (Siemens ULTRAMAT 22, München, Germany). 100 mg of dried activated carbons were heated from room temperature to 930 °C, in $N_2$ flow (heating rate of 10 °C/min.).

### 4.2.3 Adsorption experiments

Antipyrine ($C_{11}H_{12}N_2O$ Sigma–Aldrich, molecular weight: 188.26 g/mol, melting point: 114 °C, solubility (25 °C): $5.19.10^4$ mg/L, pKa: 1.4, polar surface area 23.6 $Å^2$) solutions were prepared with distilled water at different initial concentrations. For the adsorption equilibrium

UNIVERSIDAD DE MÁLAGA

experiments, 10 mg of dried activated carbons (100-300 μm) were put inside glass flasks and contacted with 150 mL of the antipyrine solution at different initial concentrations in an orbital incubator (Gallenkamp, model INR-250) at 200 rpm equivalent stirring rate for 7 days and 20 °C. For the adsorption kinetic tests, an antypirine solution of 1 mg/L was put in contact with 10 mg of the activated carbon and agitated for different times with adsorbent doses of 50 mg/L. Column adsorption experiments were carried out in a thermostatized glass column (± 0.5 °C), with internal diameter of 4 mm. 100 mg of activated carbon was packed between two slices of inert quartz wool inside the column. Antipyrine solution (1 mg/L) was pumped downflow through the column bed at controlled flow rate (7 mL/min) using a peristaltic pump. Before the column test was started, water was feed to the column for 20 min in order to remove the trapped air and to wet the activated carbon porosity. The adsorbate concentrations were determined with an UV–Vis (Varian, Model Cary 1E) spectrophotometer, at λmax: 240 nm.

## 4.3 Results and Discussion

### 4.3.1 Activated carbons characterization

#### 4.3.1.1 Effect of the $H_3PO_4$ to lignin mass ratio

The effect of the $H_3PO_4$ to lignin mass ratio on the textural properties of activated carbons obtained by co-solution of lignin and phosphoric acid, followed by the low-temperature oxidation and chemical activation steps, has been analyzed. For the sake of comparison, this effect was also evaluated for the activated carbos obtained by the conventional chemical activation of lignin with phosphoric acid.

Figure 4.1 collects the total yields of the activated carbons prepared at 400 ºC for different $H_3PO_4$/lignin mass ratios, by both methodologies. Total yields values (mass of activated carbon to mass of initial lignin) from about 52%, for a low phosphoric acid to lignin mass ratio (0.6), to about 68%, for a high ratio value (4), were obtained for activated carbons prepared by co-solution of lignin/$H_3PO_4$. These values were slightly lower than those determined for activated carbons obtained by conventional impregnation of lignin (from about 62 to 71%). These values of total yields are considerably higher than others reported in the literature for activated carbons obtained from biomass natural waste [14-15], due to the highly aromatic and carbon-rich molecular structure of lignin, which devolatilizes to a lesser extent than cellulose and hemicellulose [28].

UNIVERSIDAD DE MÁLAGA

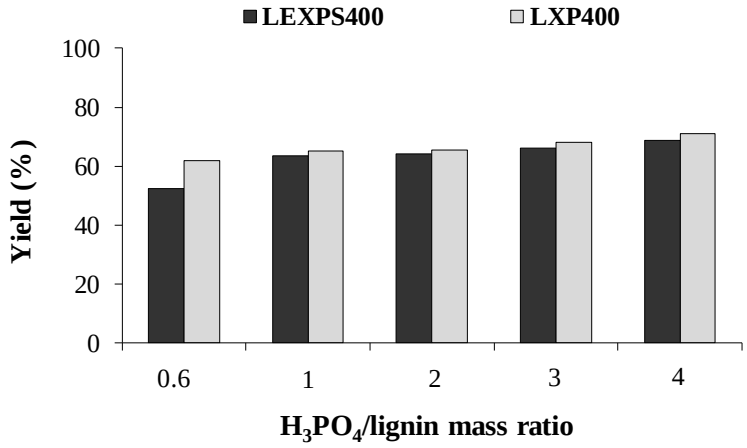


**Figure 4.1**. Total yields (in mass percentage) of the activated carbons prepared by conventional impregnation followed by chemical activation (LXP400) and by co-solution of lignin and phosphoric acid followed by low-temperature oxidation and chemical activation (LEXPS400) at 400 ºC as a function of $H_3PO_4$ to lignin mass ratios .

In general, phosphoric acid limits the formation of tars in biomass precursors during the carbonization treatment, increasing the yield of the remaining solid product. Some authors proposed that the yield values decrease slightly with the impregnation ratio, as a consequence of a deeper dehydration of the carbonaceous structure of the precursor and/or that the excess of phosphoric acid promote gasification of char and increase the total weight loss of carbon [9,29]. As can be seen, the influence of the $H_3PO_4$/lignin mass ratio on the total yield for both types of activated carbons is not very accused and it can be considered more or less constant. On the other hand, the differences in the yield values, with slightly lower values for activated carbons prepared from co-solution of lignin and phosphoric acid than for those of conventional impregnated lignin, can be associated to a more homogeneous and a better interaction of lignin oxygen groups and phosphoric acid in the case of co-solution of lignin with $H_3PO_4$, increasing the formation of phosphate and polyphosphate bridges, which are responsible for connecting and crosslinking the lignin fragments and for an enhancement of the oxidation process al low temperature, promoting a larger degree of activation (during the last step), with the consequent increase in the final loss of mass [29], which suggests a higher development of the porosity for the activated carbons obtained by co-solution of the carbon precursor and the activating agent. The phosphate and polyphosphate groups are inserted in the carbon matrix, separating the organic species, which produces an expansional process during the activation step that, after washing, leaves the carbon matrix in a dilated state, with a high porosity.

UNIVERSIDAD DE MÁLAGA

In this sense, the influence of the phosphoric acid to lignin mass ratio on the porous texture of the different activated carbons has also been analyzed. Figure 4.2 shows the $N_2$ adsorption-desorption isotherms obtained at – 196 ºC of the different activated carbons prepared at 400 ºC by both procedures, conventional chemical activation of lignin with $H_3PO_4$ and co-solution of lignin with $H_3PO_4$, for different values of lignin to $H_3PO_4$ mass ratios (between 0.6 and 4). For the case of conventional activation procedure, an increase in the relative amount of activation agent to lignin resulted in an increase of $N_2$ adsorption, indicating a higher development of porosity with the $H_3PO_4$ to lignin ratio. The isotherms for these activated carbons are mainly type I and exhibit an almost horizontal plateau starting at very low relative pressure, indicating that the porosity consists predominantly of narrow micropores. With the increase of the impregnation ratio up to 4, the amount of adsorbed $N_2$ increased in the whole relative pressure range and the presence of a hysteresis loop at high relative pressures revealed a widening of the porosity, in general, with a higher contribution of mesoporosity.

The activated carbons prepared by the co-solution of lignin and phosphoric acid showed isotherms type I at low $H_3PO_4$/lignin mass ratio (0.6), very similar to that observed for the activated carbon prepared by conventional impregnation at this low ratio. As this ratio increased up to a value of 2, the amount of adsorbed $N_2$ significantly increased in the whole range of relative pressure, well above the values observed for the isotherms of the activated carbons prepared by the conventional impregnation method at equal ratios, particularly at low relative pressure, which suggests a remarkable development of the wider microporosity. A further increase of the $H_3PO_4$/lignin mass ratio up to a value of 4 gradually reduced the amount of adsorbed $N_2$, changing the isotherm profile to type IV (due to a widening porosity), in which a hysteresis loop at medium values of relative pressure was clearly observed, indicating the presence of narrow mesopores.

An increase of the relative amount of phosphoric acid compared to that of lignin would increase the formation of phosphate and polyphosphate bridges and so the connections and crosslinking of lignin fragments, with the consequent enhancement of the oxidation process at low temperature and the larger degree of activation, responsible for the significant increase of porosity development up to a $H_3PO_4$ to lignin ratio of 2 for the activated carbons prepared by co-solution of $H_3PO_4$ and lignin. Actually, Valero et al. concluded that C-O-P bonds on activated carbons were responsible for an enhanced oxidation of the carbon surface when molecular oxygen was present at low temperatures (120-300 ºC) [45]. On the other hand, it is well-known

UNIVERSIDAD DE MÁLAGA

that phosphoric acid is a good oxidation retardant that can significantly increase the oxidation resistance of carbons, forming a barrier to prevent molecular oxygen from reaching the carbon surface [32]. In this sense, a value of $H_3PO_4$ to lignin ratio between 1 or 2 would promote the highest formation of C-O-P type groups between lignin and phosphoric acid, particularly in the case of co-solution of lignin with $H_3PO_4$, which would enhance the low temperature oxidation process. However, an excess of phosphoric acid on the surface of the carbonaceous matrix may act as a barrier for oxygen reaching the carbonaceous surface during the low temperature oxidative treatment. This could be the case for high values of $H_3PO_4$ to lignin ratio for activated carbons prepared by co-solution of lignin and $H_3PO_4$. For a $H_3PO_4$ to lignin ratio value of 4, the reactive groups of phosphoric acid would far exceed the oxygen groups of lignin, making in this case much less significant (almost negligible) the positive effect of the co-solution of lignin and $H_3PO_4$. The negative barrier impact of excess $H_3PO_4$ for the oxidation of the carbonaceous surface during the low temperature oxidative treatment explains the very similar porosity of LE4PS400 compared to that of L4P400, prepared by the conventional impregnation method. The low amount of phosphoric acid involved in the case of very low value of $H_3PO_4$ to lignin ratio (0.6) did not seem to play an important role to make a significant difference in the porous texture of the final activated carbons when they were prepared by any of the two procedures (see L06P400 and LE06PS400 in Figure 4.2, a and b, respectively).

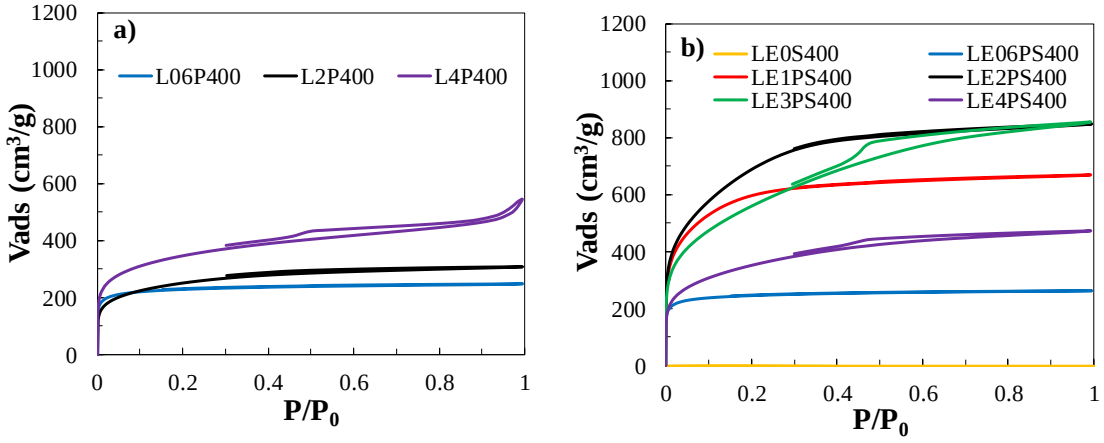


**Figure 4.2.** $N_2$ adsorption-desorption isotherms obtained at –196 ºC of activated carbons prepared at an activation temperature of 400 ºC and different $H_3PO_4$ to lignin mass ratios (a) by conventional impregnation followed by chemical activation (LXP400) and (b) by co-solution of lignin and phosphoric acid followed by low-temperature oxidation and chemical activation (LEXPS400) .

UNIVERSIDAD DE MÁLAGA

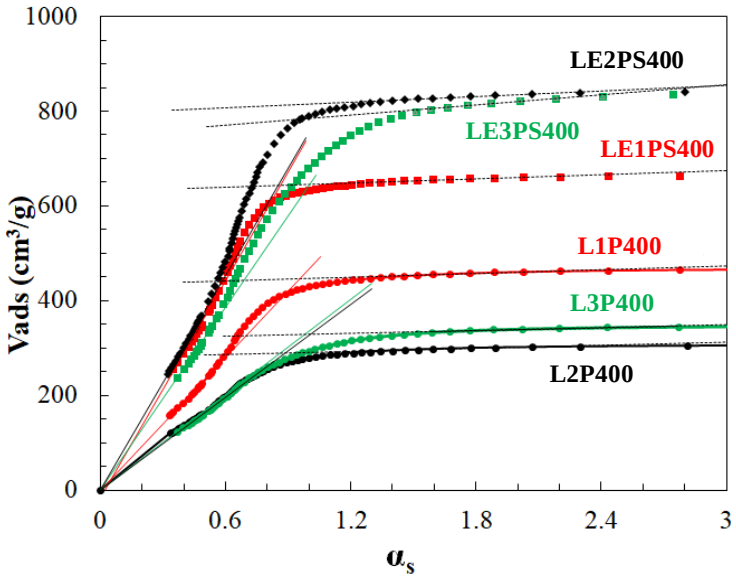


**Figure 4.3.** $\alpha_s$ curves for different activated carbons prepared at an activation temperature of 400 ºC and different $H_3PO_4$ to lignin mass ratios by conventional impregnation followed by chemical activation and by co-solution of lignin and phosphoric acid followed by low-temperature oxidation and chemical activation.

Figure 4.3 collects $\alpha_s$ curves for the different activated carbons at $H_3PO_4$/lignin mass ratios between 1 and 3 and at 400 ºC. The volume of $N_2$ adsorbed is represented versus $\alpha_s$, which is the ratio of the amount adsorbed by a non-porous standard (in this case, Elftex-120) at each relative pressure and at 0.4 relative pressure [30]. The linear multilayer region for $\alpha_s > 1.2$ (dashed line) is related to the adsorption on the non-microporous surface of the carbon. The extrapolation of this linear multilayer region at $\alpha_s=0$ and the corresponding slope provide the total micropore volume and the external surface area, respectively. The slope of a straight line that fits as values lower than 1 and goes through the origin of coordinates (continuous line in Fig. 3) provides the specific surface area, $a_s$, as it was proposed by Kaneko et al. [31–33]. In general, activated carbons prepared from co-solution of lignin and $H_3PO_4$ showed higher contribution of microporosity at these $H_3PO_4$/lignin mass ratios. Linearity of the high-pressure parts of the plots ($\alpha_s > 1$), associated to the multilayer region, indicates the low presence of mesopores in all the samples, independently of the procedure used. Furthermore, these $\alpha_s$ curves also present one upward swing below $\alpha_s=1$, approximately between 0.6 and 1, associated to condensation swings on supermicropores (pore sizes ≥ 1 nm). The condensation swing is more pronounced in the

UNIVERSIDAD DE MÁLAGA

activated carbons obtained by co-solution of lignin and $H_3PO_4$, suggesting the generation of larger micropores at these experimental conditions.

Table 4.1 summarizes the textural properties of the activated carbons prepared by conventional impregnation of lignin with phosphoric acid and co-solution of lignin and $H_3PO_4$ at 400 ºC and different $H_3PO_4$/lignin mass ratios. As can be seen, it is possible to prepare lignin-derived activated carbons with apparent surface area values ($A_{BET}$) higher or equal to 2000 $m^2/g$, at 400 ºC, in a range of $H_3PO_4$/lignin mass ratios between 1 to 3, obtaining a maximum $A_{BET}$ for a value of 2. This value, $A_{BET}$=2550 $m^2/g$, is one of the most highest reported for lignin-derived activated carbons prepared by chemical activation with phosphoric acid [14,34–37], and even with other activation methods [38,39]. In addition, the activation of co-solutions of lignin and $H_3PO_4$ produces an increase of $A_{BET}$, $V_s$ and $V_{mes}$ compared to the activated carbon prepared by its direct impregnation at the different $H_3PO_4$/lignin mass ratios evaluated. Specifically, the relative increase in the apparent surface area and the micropore volume follows the same tendency, that of a Gaussian curve, with a maximum at a $H_3PO_4$/lignin mass ratio of 2, and these values are almost twice as high as those obtained from conventional impregnation of lignin. However, the highest relative increase of mesopore volume is obtained for a $H_3PO_4$/lignin mass ratio value of 3.

**Table 4.1**. Textural properties of the different activated carbons prepared at 400 ºC and different $H_3PO_4$ to lignin mass ratios.

| | **$N_2$ isotherm** | | | | | **$CO_2$ isotherm** | |
|---|---|---|---|---|---|---|---|
| | **$A_{BET}$ ($m^2/g$)** | **$a_s$ ($m^2/g$)** | **$V_S$ ($cm^3/g$)** | **$A_S$ ($m^2/g$)** | **$V_{mes}$ ($cm^3/g$)** | **$A_{DR}$ ($m^2/g$)** | **$V_{DR}$ ($cm^3/g$)** |
| **L06P400** | 878 | 1026 | 0.36 | 18 | 0.03 | 546 | 0.22 |
| **L2P400** | 921 | 961 | 0.43 | 33 | 0.05 | 397 | 0.16 |
| **L4P400** | 1236 | 1316 | 0.57 | 119 | 0.27 | 545 | 0.22 |
| **LE0S400** | <1 | <1 | - | - | - | 301 | 0.12 |
| **LE06PS400** | 951 | 1118 | 0.39 | 11 | 0.02 | 598 | 0.24 |
| **LE1PS400** | 2200 | 2146 | 0.98 | 41 | 0.06 | 637 | 0.26 |
| **LE2PS400** | 2551 | 2313 | 1.22 | 67 | 0.09 | 714 | 0.29 |
| **LE3PS400** | 2040 | 1948 | 1.09 | 169 | 0.22 | 591 | 0.24 |
| **LE4PS400** | 1272 | 1277 | 0.63 | 73 | 0.24 | 478 | 0.19 |

UNIVERSIDAD DE MÁLAGA

Figure 4.4 shows the micropore size distribution for the different activated carbons prepared by conventional impregnation of lignin with $H_3PO_4$ and by co-solution of lignin and $H_3PO_4$ at 400 ºC and different $H_3PO_4$/lignin mass ratios. The samples obtained from conventional impregnation of lignin presented a bimodal micropore size distribution, with a maximum around 6.7 Å at the lowest impregnation ratio, which is shifted to 11.1 Å at impregnation ratios of 3. Higher and narrower micropores size distribution were obtained for the activated carbons prepared from co-solution of lignin and phosphoric acid, with a $H_3PO_4$/lignin mass ratio up to 2. A maximum around 12.2 Å was observed at a mass ratio of 1, which is shifted to 16.6 Å at 2, as suggested the highest upward swing below $\alpha_s$=1. In general, the increase of the $H_3PO_4$/lignin mass ratio results in a broader micropore size distribution for both preparation methods.

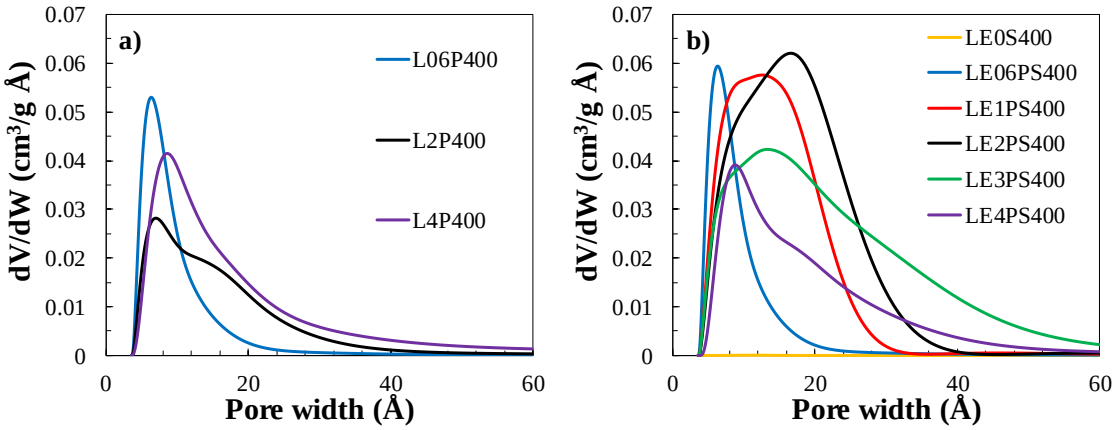


**Figure 4.4.** Micropores size distribution of the different activated carbons prepared at different $H_3PO_4$ to lignin mass ratios and at 400 ºC.

4.3.1.2 Effect of the activation temperature

The influence of the activation temperature on the textural properties of these activated carbons at a $H_3PO_4$/lignin mass ratio of 2 was analyzed. Figure 4.5 a represents the $N_2$ adsorption-desorption isotherms obtained at – 196 ºC of the activated carbons prepared at different activation temperatures between 300 and 900 ºC and at $H_3PO_4$/lignin mass ratio of 2. The increase of the activation temperature up to 400 ºC generates a significant development of the porosity, obtaining the highest volume of adsorbed $N_2$ in the entire range of relative pressures at this ratio. A further increase of the activation temperature up to 900 ºC produces a considerable reduction of this volume. In this line, it was also observed an optimum activation temperature around 400

UNIVERSIDAD DE MÁLAGA

ºC with Kraft lignin [34] and even with other lignocellulosic materials [40]. The pore size distribution for these activated carbons also showed a bimodal distribution.

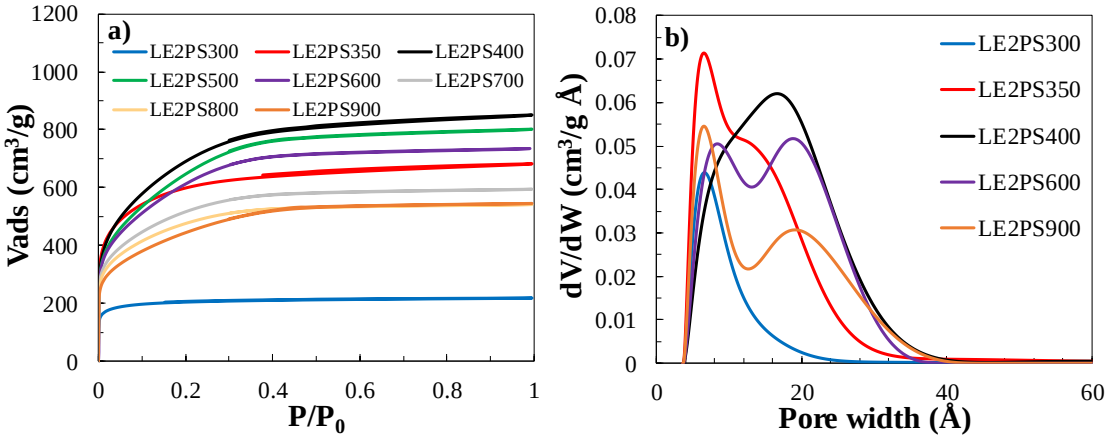


**Figure 4.5.** $N_2$ adsorption-desorption isotherms obtained at – 196 ºC (a) and pore size distribution (b) of different activated carbons prepared by co-solution of lignin and $H_3PO_4$ at different activation temperatures and with a $H_3PO_4$ to lignin mass ratio value of 2.

Table 4.2 summarizes the textural properties of the different activated carbons at different activation temperatures and a $H_3PO_4$/lignin mass ratio of 2. The apparent surface areas obtained by the BET and αs methods are also very similar for all the activated carbons. As can be seen, it is possible to obtain activated carbons from lignin with $A_{BET}$ higher than 2100 $m^2/g$ in a wide range of activation temperatures between 350 ºC and 600 ºC, and at a $H_3PO_4$/lignin mass ratio of 2, with a maximum of $A_{BET}$ and micropore volume observed at 400 ºC (2550 $m^2/g$ and 1.3 $cm^3/g$, respectively).

UNIVERSIDAD DE MÁLAGA

**Table 4.2**. Textural properties of the different activated carbons prepared by co-solution of lignin and $H_3PO_4$ at different activation temperatures and a $H_3PO_4$/lignin mass ratio of 2.

| | $N_2$ isotherm | | | | | $CO_2$ isotherm | |
|---|---|---|---|---|---|---|---|
| | $A_{BET}$ ($m^2/g$) | $a_s$ ($m^2/g$) | $V_S$ ($cm^3/g$) | $A_S$ ($m^2/g$) | $V_{mes}$ ($cm^3/g$) | $A_{DR}$ ($m^2/g$) | $V_{DR}$ ($cm^3/g$) |
| **LE2PS300** | 786 | 871 | 0.32 | 12 | 0.02 | 544 | 0.22 |
| **LE2PS350** | 2202 | 2292 | 0.98 | 57 | 0.08 | 913 | 0.37 |
| **LE2PS400** | 2551 | 2313 | 1.22 | 67 | 0.09 | 714 | 0.29 |
| **LE2PS500** | 2384 | 2239 | 1.18 | 41 | 0.06 | 688 | 0.28 |
| **LE2PS600** | 2245 | 2146 | 1.10 | 22 | 0.03 | 779 | 0.31 |
| **LE2PS700** | 1879 | 1905 | 0.89 | 19 | 0.02 | 721 | 0.29 |
| **LE2PS800** | 1727 | 1733 | 0.82 | 11 | 0.02 | 799 | 0.32 |
| **LE2PS900** | 1611 | 1583 | 0.82 | 18 | 0.02 | 611 | 0.25 |

### 4.3.2 Antipyrine adsorption

Three different adsorbents with different pore size distribution prepared by co-solution of lignin and phosphoric acid at different $H_3PO_4$/lignin mass ratios and activation temperatures were selected for the adsorption of antipyrine. The surface chemistry of these activated carbons was also analyzed.

#### 4.3.2.1 Surface chemistry

In order to study the influence of the $H_3PO_4$/lignin mass ratio and the activation temperature on the surface chemistry of these activated carbons, the activated carbons obtained at two different $H_3PO_4$/lignin mass ratios and activated at 400 ºC, and at two different activation temperatures at a $H_3PO_4$/lignin mass ratio of 2, were analyzed by TPD and XPS. Figure 6 collects CO and $CO_2$ evolution during TPD experiments of the three activated carbons used in adsorption experiments. As can be seen, the amount of $CO_2$-evolving groups is rather lower than that of CO, indicating the low presence of carboxylic acid, lactones and anhydrides groups. The higher CO evolution of these activated carbons can be related to the presence of phosphorus functional groups and to the decomposition of phenol, carbonyl and ether groups. The amount of CO evolved is quite similar for the activated carbons prepared at the different activation temperatures, however, a displacement of the main CO peak to higher temperatures is detected

UNIVERSIDAD DE MÁLAGA

with the increase of the activation temperature, which can be related to a change in the thermal stability of the oxygen surface groups. For LE2PS400, CO evolution is mainly associated to the presence of phenol, ether, anhydride groups and phosphorus functional groups of lower thermal stability. In contrast, at higher activation temperatures, the CO evolution is mainly associated to the formation of C-O-$PO_3$ surface groups, which decompose around 860 ºC [41,42].

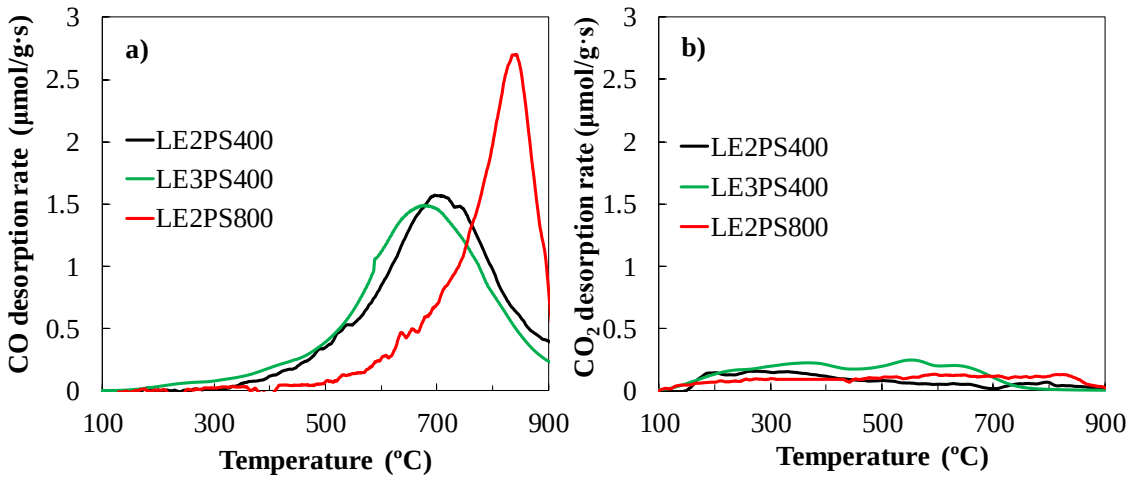


**Figure 4.6**. CO and $CO_2$ profiles of the activated carbons obtained during TPD experiments.

The amount of oxygen surface groups can also influence the adsorption of antipyrine. Table 3 collects the CO and $CO_2$ evolved amounts and the surface composition of the different activated carbons determined by XPS. As can be seen, the amount of oxygen surface groups determined from both TPD and XPS and P content (from XPS) is quite similar for the three activated carbons.

**Table 4.3.** Chemical characterization of the activated carbons prepared at different $H_3PO_4$/lignin mass ratios and activation temperatures.

| Activated carbon | DTP (mmol/g) | | Surface composition by XPS (%wt) | | |
|---|---|---|---|---|---|
| | **CO** | **$CO_2$** | C | O | P |
| **LE2PS400** | 2.47 | 0.36 | 81.8 | 16.0 | 2.2 |
| **LE3PS400** | 2.90 | 0.66 | 82.3 | 16.2 | 1.5 |
| **LE2PS800** | 2.40 | 0.46 | 85.1 | 12.8 | 2.1 |

UNIVERSIDAD DE MÁLAGA

4.3.2.2 Antipyrine adsorption results

The equilibrium adsorption isotherms of antipyrine solutions at 20 ºC are shown in Figure 4.7 for the three selected activated carbons. The isotherms are of type L according to Giles classification, commonly reported in liquid-phase adsorption. The adsorption uptakes of antipyrine for the activated carbon LE2PS800 was almost twice the amount for the others activated carbons. As can be seen, there is not a direct relationship between the adsorption capacity and the apparent surface area of the adsorbents, at least at these low concentrations.

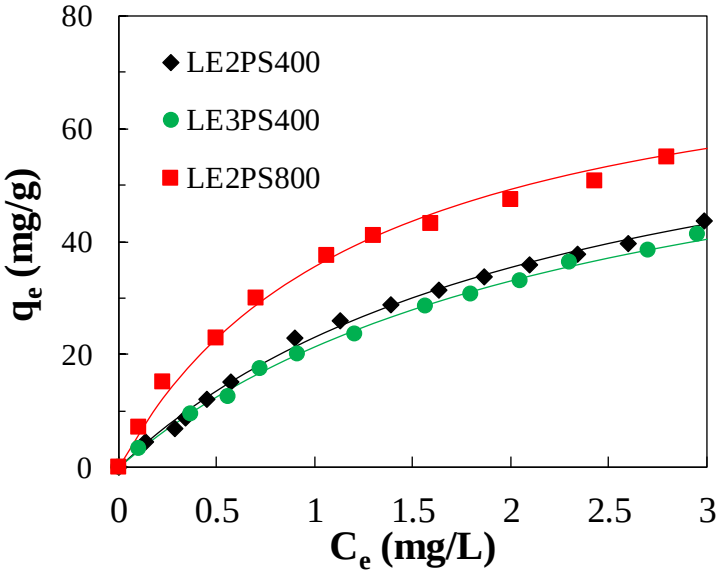


**Figure 4.7.** Adsorption isotherms of antipyrine on different activated carbons at 20 °C (symbols: experimental values; continuous lines: fitting to the Langmuir equation).

Nevertheless, the micropore size distribution of these three samples (shown in Figure 4.8) reveals that the activated carbon with the highest contribution of narrower pores (size lower than 12.5 Å) is that with the highest adsorption capacity of antipyrine. In fact, if the cumulated pore volume is calculated from the micropore size distribution, it can be observed that at pore sizes lower than 9 Å, the activated carbon LE2PS800 shows higher cumulated pore volumes than those obtained from LE3PS400 and LE2PS400, which own values very similar. Attending to the molecular dimensions of antipyrine (5.6 Å x 7.8 Å x 11.7 Å) [43], it seems that at the low pollutant concentrations used in this work, the micropores of size lower than 9 Å are the main responsible of the adsorption capacity of antipyrine.

UNIVERSIDAD DE MÁLAGA

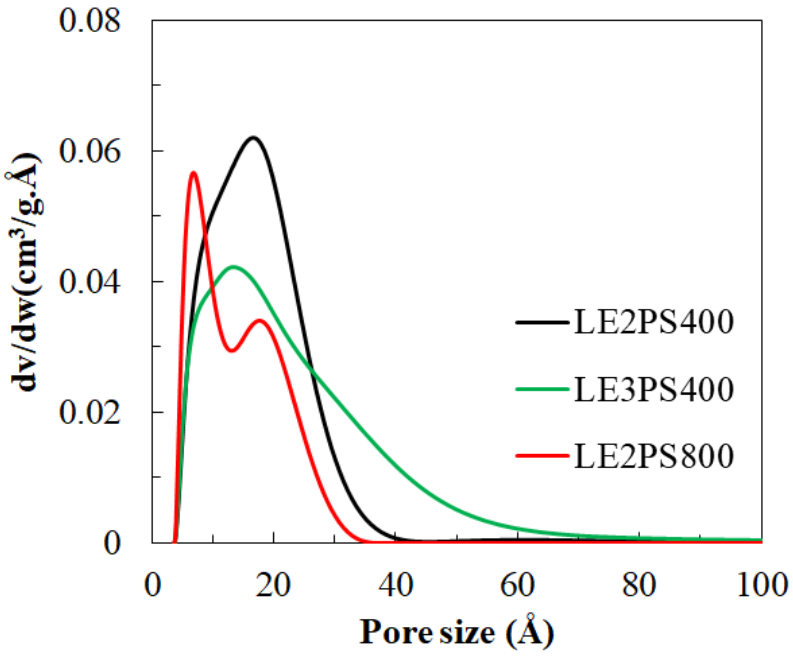


**Figure 4.8.** Micropores size distribution of the different activated carbons.

In addition, as previously mentioned, LE2PS400 and LE3PS400 have a high contribution of CO-evolving groups of less acidic character, like phenols, meanwhile CO desorption of LE2PS800 is mainly associated to the presence of phosphorus surface groups of high thermal stability with weak-moderate acidic character [44], which could have more affinity with antipyrine.

The experimental uptakes here reported for very low equilibrium concentrations of antipyrine (as those typical for emerging pollutants) are considerably high and larger than others observed for mesoporous silicas even at higher initial antipyrine concentrations [45]. Some authors also evaluated the antipyrine adsorption over activated carbons, but they used much higher equilibrium concentrations than those used in this work [5], hampering a direct comparison with our results.

The equilibrium adsorption results were adjusted to different adsorption isotherm models. The Langmuir and Freundlich adsorption parameters were calculated using a non-linear regression and their corresponding values are collected in Table 4.4:

$$qe = \frac{q_L \,.\, K_L \,.\, \mathrm{Ce}}{1 + K_L . \mathrm{Ce}} \qquad (1)$$

$$qe = K_f . (Ce)^{1/n} \qquad (2)$$

UNIVERSIDAD DE MÁLAGA

where $K_L$ is the equilibrium constant (L/mg), usually related to the adsorption enthalpy, $q_L$ is the adsorption capacity (mg/g), $K_f$ is the Freundlich constant associated to the adsorption capacity ((mg/g)(L/mg)$^{1/n}$), Ce is the equilibrium concentration of adsorbate (mg/L) and n is the empirical parameter related to the energetic heterogeneity of the adsorption sites. As can be seen, both models reproduce fairly well the experimental data, although lower errors were obtained with the Langmuir model. The heterogeneity index (1/n) of Freundlich equation provides an indication of how is the adsorption process, in this case, values higher than 1 suggest favorable adsorption for the three adsorbents.

**Table 4.4.** Langmuir and Freundlich adsorption parameters obtained from equilibrium isotherms of antipyrine for the activated carbons.

| | **Langmuir isotherm** | | | **Freundlich isotherm** | | |
|---|---|---|---|---|---|---|
| **ACs** | **$q_L$** | **$K_L$** | **$R^2$** | **$K_f$** | **n** | **$R^2$** |
| | **(mg/g)** | **(l/mg)** | | **(mg/g)(L/mg)$^{1/n}$** | | |
| **LE2PS400** | 76 | 0.43 | 0.997 | 21 | 1.52 | 0.988 |
| **LE3PS400** | 73 | 0.41 | 0.997 | 20 | 1.49 | 0.994 |
| **LE2PS800** | 80 | 0.79 | 0.997 | 34 | 2.13 | 0.995 |

The kinetics of antipyrine adsorption on the three activated carbons was analyzed in Figure 4.9. The experimental data were fitted to the second order adsorption kinetics (Eq. 3) and to a hyperbolic equation (Eq. 4) [13, 17] by using the concentration of the adsorbate on the solid ($q_t$) as a function of the contact time (t):

$$\frac{1}{(q_e - q_t)} = \frac{1}{q_e} + kt \qquad (3)$$

$$qt = \frac{a.qm.t}{1 + a.t} \qquad (4)$$

Where k (g/mg·min) is the kinetic constant for the second order adsorption kinetic; and a (min$^{-1}$) and $q_m$ (mg/g) are empirical parameters related to the kinetic curve shape; $q_m$ represents the asymptotic $q_t$ value for these experimental conditions. Therefore, $q_t$ tends to $q_m$ at the maximum contact time in the kinetic test. As can be seen, there is an important decrease in the adsorption rate at the beginning of the contact time. After that, a second stage can be observed with intermediate decreasing rate values, which finally leads to the third part of the curve, showing negligible adsorption rates. Both equations are able to reproduce fairly well the experimental data for the three activated carbons. Table 5 compiles their corresponding fitting parameters. The

UNIVERSIDAD DE MÁLAGA

kinetic constant values derived from the second order kinetic equation for the antipyrine adsorption on the different activated carbons are clearly related to the values of the apparent surface area, which follows the same tendency LE2PS400>LE3PS400>LE2PS800.

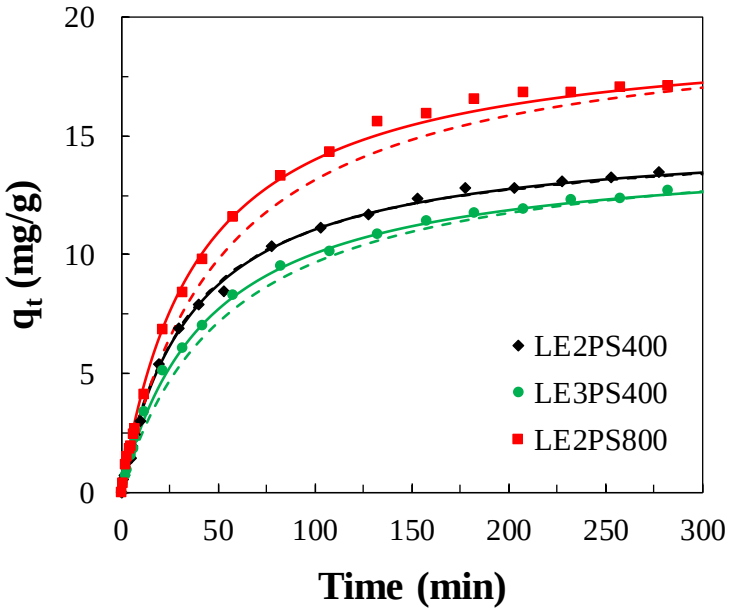


**Figure 4.9.** Adsorption kinetics of antipyrine on different activated carbons at 20 °C, $C_0$ = 1 mg/L; adsorbent concentration = 50 mg/L (Experimental data: dots; hyperbolic equation fittings: full line, second order adsorption kinetic equation: dashed line).

**Table 4.5.** Parameters obtained from kinetics curves for the antipyrine ($C_0$ = 1 mg/L; adsorbent concentration = 50 mg/L).

| | Hyperbolic | | | | 2nd order | |
|---|---|---|---|---|---|---|
| **ACs** | $q_m$ (mg/g) | a ($min^{-1}$) | $q_{texp}$ (mg/g) | $R^2$ | $k \cdot 10^4$ (g/mg.min) | $R^2$ |
| **LE2PS400** | 15.10 | 0.027 | 14.85 | 0.99 | 18.90 | 0.99 |
| **LE3PS400** | 14.50 | 0.022 | 14.36 | 0.99 | 12.40 | 0.99 |
| **LE2PS800** | 19.47 | 0.025 | 18.42 | 0.99 | 9.50 | 0.99 |

In order to evaluate the possible mass transfer limitations, the effective diffusion coefficients are obtained according to the procedure proposed by Reichenberg [48] for spherical particles, Eq. (5), where:

$$\frac{q_t}{q_e} = 1 - \frac{6}{\pi^2}\sum_{n=1}^{\infty}\frac{1}{n^2}exp\left(-\frac{n^2\pi^2}{R_p^2}D_e \cdot t\right) \qquad (5)$$

UNIVERSIDAD DE MÁLAGA

This equation supposes constant concentration of solute around the solid surface and negligible external film limitations. The solution proposed by Vermeulen is used to calculate the diffusion coefficient values with the surface coverage of adsorbate for the entire range of adsorption time by using the experimental adsorbed amount of antipyrine [49]:

$$D_e = \frac{-R_p^2}{\pi^2 t} ln\left[1 - \left(\frac{q_t}{q_e}\right)^2\right] \qquad (6)$$

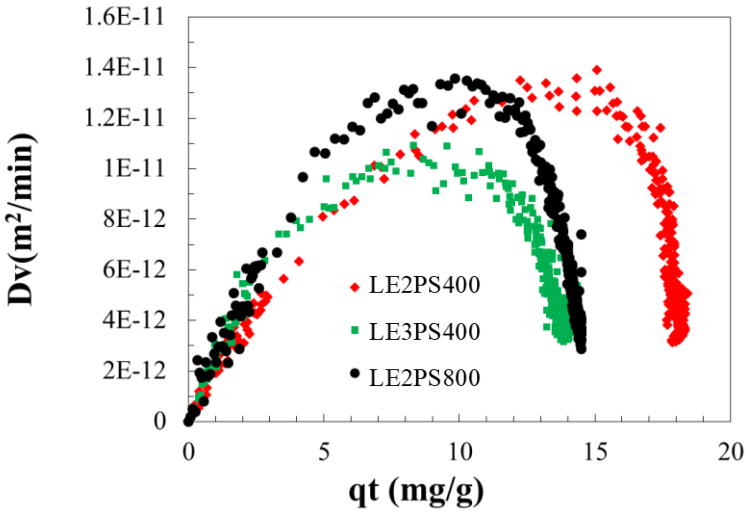


**Figure 4.10**. Effective diffusion coefficients as a function of the adsorbed amount for the activated carbons.

Figure 4.10 shows the effective diffusivity values for the activated carbons as a function of the increasing surface coverage. Initially, De values increases with the surface coverage. This stage corresponds to a fast coverage of the surface in the widest pores and the most adsorption sites, the tendency of the values can be related to the apparent surface areas of the adsorbents. However, the maximum of the curves does not present any clear relationship with the micropore and/or mesopore volumes. In addition, De values decrease with the surface coverage (or time) for the three adsorbents, but LE2PS800, the adsorbent with the narrowest porosity, keeps quite high diffusion coefficient values for longer times, even at surface coverages where the coefficients for the other two adsorbents are substantially decreased. Generally, the most used intraparticle diffusion models are the pore diffusion and the surface diffusion model. Taking into account both models, the results here presented suggest that the surface diffusion must be very important, in the case of the adsorbent with the narrowest porosity, in order to explain how the effective diffusion coefficient of LE2PS800 show higher values in a wide range of surface coverage. These results are also in concordance with the highest values of the adsorption constant

UNIVERSIDAD DE MÁLAGA

for the adsorbents with the widest pores, LE2PS400 and LE3PS400 (see Table 4.5), where the pore diffusion is faster and could be more important.

Figure 4.11 shows the breakthrough curves of antipyrine adsorption in the different activated carbon fixed-beds at 20°C and 1 mg/L. The adsorption capacities $q_t$ were calculated by the area over the breakthrough curves and their values are presented in Table 6. The shape of the curves are type S, typically observed for column operation with favorable adsorption isotherms [50]. The breakthrough time for the activated carbon LE2PS800 is twice those observed for the carbons LE2PS400 and LE3PS400 (Table 4.6). This large difference can be related to the higher volume of LE2PS800 of pores lower than 9 Å, where surface diffusion becomes more important. The results exhibit that the adsorption capacities have the same tendencies as the kinetic and equilibrium studies. Thomas model was applied to the breakthrough results to evaluate the dynamic behavior of the column. This model assumes the Langmuir isotherm for equilibrium and a second order reaction for kinetics; neglecting any mass transfer limitation. With this regard, we have previously shown that both models are able to reproduce, with very low errors, equilibrium and kinetic results from batch experiments, respectively. The linearized form of the Thomas model is expressed in equation (7) as follows:

$$ln\left(\frac{C_o}{C_t}-1\right)=\frac{k_{TH}\cdot q_{TH}\cdot m}{Q}-k_{TH}C_o t \qquad (7)$$

where $k_{TH}$ is the Thomas kinetic coefficient (mL/min mg), t is the time (min), and Q is the volumetric flow rate (mL/min). Adsorption capacity and mass of the adsorbent are denoted as $q_{TH}$ (mg/g) and m (g), respectively. As can be seen, the Thomas model is able to predict fairly well the adsorption capacities determined from the equilibrium study and the breakthrough times for the three adsorbents. In addition, the theoretical breakthrough curves derived from this model reproduces successfully the experimental data for LE2PS800, LE2PS400 and LE3PS400 adsorbents.

UNIVERSIDAD DE MÁLAGA

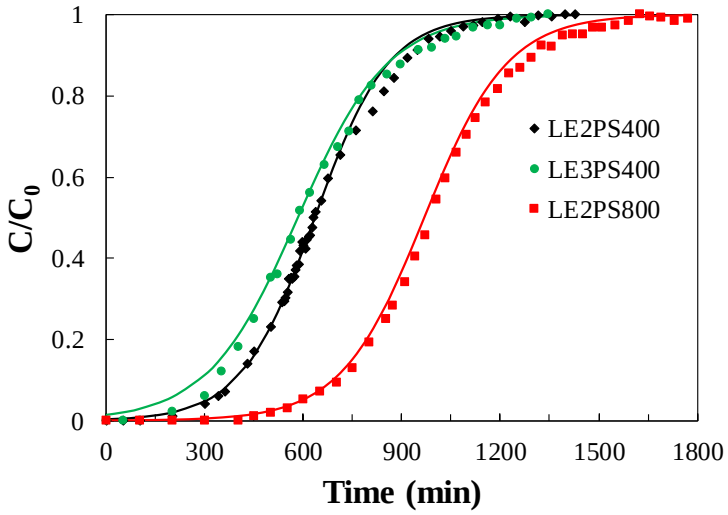


**Figure 4.11.** Breakthrough curves of antipyrine adsorption at 20°C; $C_0$ = 1 mg/L; adsorbent mass = 200 mg; flow rate = 7 mL/min. (Experimental data: dots; Thomas model: continuous line).

**Table 4.6.** Parameters obtained from experimental data of breakthrough curves of the column adsorption process of antipyrine.

| | **Bed length (cm)** | **$H_{MTZ}$ (cm)** | **Breakthough time (min)** | **$q_t$ (mg/g)** | **$K_{th}.10^3$ (L/mg.min)** | **$q_{thomas}$ (mg/g)** | **$R^2$** |
|---|---|---|---|---|---|---|---|
| **LE2PS400** | 5.80 | 2.97 | 320 | 26 | 26 | 26 | 0.95 |
| **LE3PS400** | 5.20 | 2.84 | 280 | 26 | 26 | 26 | 0.86 |
| **LE2PS800** | 3.60 | 1.44 | 600 | 37 | 37 | 37 | 0.98 |

## 4.4 Conclusions

This chapter analyzes the influence of the activating agent ($H_3PO_4$) to carbon precursor (lignin) mass ratio (values from 0.6 to 4) and the activation temperature (from 300 to 900 ºC) on the textural properties of the activated carbons prepared by co-solution of lignin and $H_3PO_4$ followed by a oxidative (air) treatment at low temperature (200 ºC) before the activation step. For the sake of comparison, activated carbons prepared by traditional impregnation of (non-solved) lignin with $H_3PO_4$ followed by the activation step at similar operation conditions of $H_3PO_4$/lignin mass ratio and activation temperature were also studied. At low activation temperature (400 ºC), the maximum development of the porous texture was reached for a value of $H_3PO_4$ to lignin mass ratio of 2, obtaining under these conditions the highest values of apparent surface area and of micropore volume (2550 $m^2/g$ and ~1.3 $cm^3/g$, respectively). At high

UNIVERSIDAD DE MÁLAGA

activation temperature (900 ºC), a gradual development of the porous texture was observed with the $H_3PO_4$/lignin mass ratio up to a value of 4, from which a slight reduction in it was initiated. In general, the resulting activated carbons showed apparent surface areas higher than 2100 $m^2/g$ for a wide range of activating temperatures, between 350 ºC and 600 ºC, and at $H_3PO_4$/lignin mass ratio of 2.

Activated carbons with different pore size distributions were tested as adsorbent for antipyrine adsorption in aqueous solution, at low concentrations and at room temperature. The activated carbon with the narrowest pore size distribution showed the highest adsorption capacity of antipyrine (37 mg/g) for an equilibrium concentration as low as 1 mg/L. The antipyrine adsorption equilibrium and kinetic results were properly fitted by the Langmuir model and hyperbolic equation, respectively. The breakthrough times in column adsorption studies were successfully predicted by the Thomas model.

## References

[1] L. Nielsen, M.J. Biggs, W. Skinner, T.J. Bandosz, The effects of activated carbon surface features on the reactive adsorption of carbamazepine and sulfamethoxazole, Carbon. 80 (2014) 419–432. https://doi.org/10.1016/j.carbon.2014.08.081.

[2] C.G. Daughton, A. Ternes, Thomas, Pharmaceuticals and Personal Care Products in the Environment: Agents of Subtle Change?, Environ. Toxicol. 28 (2009) 2663–2670. https://doi.org/10.1021/bk-2001-0791.

[3] T. Deblonde, C. Cossu-Leguille, Emerging pollutants in wastewater: A review of the literature, Int. J. Hyg. Environ. Health. 214 (2011) 442–448. https://doi.org/10.1016/J.IJHEH.2011.08.002.

[4] O. Sacco, V. Vaiano, eds., Visible Light Active Structured Photocatalysts for the Removal of Emerging Contaminants: Science and Engineering, Elsevier, 2020. https://doi.org/https://doi.org/10.1016/C2018-0-03693-2.

[5] J. Bedia, C. Belver, S. Ponce, J. Rodriguez, J.J. Rodriguez, Adsorption of antipyrine by activated carbons from $FeCl_3$-activation of Tara gum, Chem. Eng. J. 333 (2018) 58–65. https://doi.org/10.1016/j.cej.2017.09.161.

[6] M. Papageorgiou, C. Kosma, D. Lambropoulou, Seasonal occurrence, removal, mass loading and environmental risk assessment of 55 pharmaceuticals and personal care products in a municipal wastewater treatment plant in Central Greece, Sci. Total Environ. 543 (2016) 547–569. https://doi.org/10.1016/j.scitotenv.2015.11.047.

[7] R. Subha, O.A. Sridevi, D. Anitha, D. Sudha, Treatment methods for the removal of phenol from water-A Review, in: Sci. Control. Commun. Eng. Technol., 2015: pp. 199–203. http://edlib.net/2015/icssccet/ICSSCCET2015044.pdf (accessed March 10, 2018).

[8] A. Bhatnagar, I. Anastopoulos, Adsorptive removal of bisphenol A (BPA) from aqueous solution: A review, Chemosphere. 168 (2017) 885–902. https://doi.org/10.1016/J.CHEMOSPHERE.2016.10.121.

UNIVERSIDAD DE MÁLAGA

[9] M. Jagtoyen, F. Derbyshire, Activated carbons from yellow poplar and white oak by $H_3PO_4$ activation, Carbon. 36 (1998) 1085–1097. https://doi.org/10.1016/S0008-6223(98)00082-7.

[10] L.J. Kennedy, J.J. Vijaya, G. Sekaran, Effect of Two-Stage Process on the Preparation and Characterization of Porous Carbon Composite from Rice Husk by Phosphoric Acid Activation, Ind. Eng. Chem. Res. 43 (2004) 1832–1838. https://doi.org/10.1021/ie034093f.

[11] D. Montané, V. Torné-Fernández, V. Fierro, Activated carbons from lignin: Kinetic modeling of the pyrolysis of Kraft lignin activated with phosphoric acid, Chem. Eng. J. 106 (2005) 1–12. https://doi.org/10.1016/j.cej.2004.11.001.

[12] N. V. Sych, S.I. Trofymenko, O.I. Poddubnaya, M.M. Tsyba, V.I. Sapsay, D.O. Klymchuk, A.M. Puziy, Porous structure and surface chemistry of phosphoric acid activated carbon from corncob, Appl. Surf. Sci. 261 (2012) 75–82. https://doi.org/10.1016/j.apsusc.2012.07.084.

[13] Suhas, P.J.M. Carrott, M.M.L. Ribeiro Carrott, Lignin-from natural adsorbent to activated carbon: a review., Bioresour. Technol. 98 (2007) 2301–2312. https://doi.org/10.1016/j.biortech.2006.08.008.

[14] J. Hayashi, A. Kazehaya, K. Muroyama, A.P. Watkinson, Preparation of activated carbon from lignin by chemical activation, Carbon. 38 (2000) 1873–1878. https://doi.org/10.1016/S0008-6223(00)00027-0.

[15] V. Fierro, V. Torné-Fernández, A. Celzard, Kraft lignin as a precursor for microporous activated carbons prepared by impregnation with ortho-phosphoric acid: Synthesis and textural characterisation, Microporous Mesoporous Mater. 92 (2006) 243–250. https://doi.org/10.1016/j.micromeso.2006.01.013.

[16] Y. Sun, G. Yang, J. Zhang, Y. Wang, M. Yao, Activated carbon preparation from lignin by $H_3PO_4$ activation and its application to gas separation, Chem. Eng. Technol. 35 (2012) 309–316. https://doi.org/10.1002/ceat.201100309.

[17] J. Bedia, J.M. Rosas, J. Márquez, J. Rodríguez-Mirasol, T. Cordero, Preparation and characterization of carbon based acid catalysts for the dehydration of 2-propanol, Carbon. 47 (2009) 286–294. https://doi.org/10.1016/j.carbon.2008.10.008.

[18] I. Moulefera, F. J. García-Mateos, A. Benyoucef, J. M. Rosas, .J. Rodríguez-Mirasol, T. Cordero, Effect of co-solution of carbon precursor and activating agent on the textural properties of highly porous activated carbon obtained by chemical activation of lignin with $H_3PO_4$, Front. Mater. submitted (2020) 1–23.

[19] S. Brunauer, P.H. Emmett, E. Teller, Adsorption of Gases in Multimolecular Layers, J. Am. Chem. Soc. 60 (1938) 309–319.

[20] K. Kaneko, C. Ishii, Superhigh surface area determination of microporous solids, Colloids and Surfaces. 67 (1992) 203–212. https://doi.org/10.1016/0166-6622(92)80299-H.

[21] K. Kaneko, C. Ishii, M. Ruike, H. kuwabara, Origin of superhigh surface area and microcrystalline graphitic structures of activated carbons, Carbon. 30 (1992) 1075–1088. https://doi.org/10.1016/0008-6223(92)90139-N.

[22] K. Kaneko, Determination of Pore Size and Pore Size Distribution: 1. Adsorbents and Catalysts, J. Membr. Sci. 96 (1994) 59–89. https://doi.org/10.1016/0376-7388(94)00126-X.

UNIVERSIDAD DE MÁLAGA

[23] F. Rodríguez-Reinoso, M. Molina-Sabio, M.T. González, The use of steam and $CO_2$ as activating agents in the preparation of activated carbons, Carbon. 33 (1995) 15–23. https://doi.org/10.1016/0008-6223(94)00100-E.

[24] M. M. Dubinin, E. D. Zaverina, L. V. Radushkevich, Sorption and structure of active carbons. I. Adsorption of organic vapors, Zhurnal Fiz. Khimii. 21 (1947) 1352–1362.

[25] J. Jagiello, J.P. Olivier, 2D-NLDFT adsorption models for carbon slit-shaped pores with surface energetical heterogeneity and geometrical corrugation, Carbon. 55 (2013) 70–80. https://doi.org/10.1016/j.carbon.2012.12.011.

[26] A.M. Puziy, O.I. Poddubnaya, A. Martínez-Alonso, F. Suárez-García, J.M.D. Tascón, Surface chemistry of phosphorus-containing carbons of lignocellulosic origin, Carbon. 43 (2005) 2857–2868. https://doi.org/10.1016/j.carbon.2005.06.014.

[27] T. Vernersson, P.R. Bonelli, E.G. Cerrella, A.L. Cukierman, Arundo donax cane as a precursor for activated carbons preparation by phosphoric acid activation, Bioresour. Technol. 83 (2002) 95–104. https://doi.org/10.1016/S0960-8524(01)00205-X.

[28] A.K. Mohanty, M. Misra, G. Hinrichsen, Biofibres, biodegradable polymers and biocomposites: An overview, Macromol. Mater. Eng. 276/277 (2000) 1–24. https://doi.org/10.1002/(SICI)1439-2054(20000301)276:1<1::AID-MAME1>3.0.CO;2-W.

[29] M. Al Bahri, L. Calvo, M.A. Gilarranz, J.J. Rodriguez, Activated carbon from grape seeds upon chemical activation with phosphoric acid: Application to the adsorption of diuron from water, Chem. Eng. J. 203 (2012) 348–356. https://doi.org/10.1016/j.cej.2012.07.053.

[30] P.J.M. Carrott, R.A. Roberts, K.S.W. Sing, Adsorption of nitrogen by porous and non-porous carbons, Carbon. 25 (1987) 59–68. https://doi.org/10.1016/0008-6223(87)90040-6.

[31] M. Molina-Sabio, F. RodRíguez-Reinoso, F. Caturla, M.J. Sellés, Porosity in granular carbons activated with phosphoric acid, Carbon N. Y. 33 (1995) 1105–1113. https://doi.org/10.1016/0008-6223(95)00059-M.

[32] M. Jagtoyen, F. Derbyshire, Some considerations of the origins of porosity in carbons from chemically activated wood, Carbon. 31 (1993) 1185–1192. https://doi.org/10.1016/0008-6223(93)90071-H.

[33] F. Suárez-García, A. Martínez-Alonso, J.M.D. Tascón, Pyrolysis of apple pulp: Chemical activation with phosphoric acid, J. Anal. Appl. Pyrolysis. 63 (2002) 283–301. https://doi.org/10.1016/S0165-2370(01)00160-7.

[34] E. Gonzalez-Serrano, T. Cordero, J. Rodriguez-Mirasol, L. Cotoruelo, J.J. Rodriguez, Removal of water pollutants with activated carbons prepared from $H_3PO_4$ activation of lignin from kraft black liquors, Water Res. 38 (2004) 3043–3050. https://doi.org/10.1016/j.watres.2004.04.048.

[35] J.M. Rosas, R. Ruiz-Rosas, J. Rodríguez-Mirasol, T. Cordero, Kinetic study of the oxidation resistance of phosphorus-containing activated carbons, Carbon. 50 (2012) 1523–1537. https://doi.org/10.1016/j.carbon.2011.11.030.

[36] Y. Guo, D.A. Rockstraw, Physical and chemical properties of carbons synthesized from xylan, cellulose, and Kraft lignin by $H_3PO_4$ activation, Carbon. 44 (2006) 1464–1475. https://doi.org/10.1016/j.carbon.2005.12.002.

UNIVERSIDAD DE MÁLAGA

[37] V. Fierro, V. Torné-Fernández, A. Celzard, D. Montané, Influence of the demineralisation on the chemical activation of Kraft lignin with orthophosphoric acid, J. Hazard. Mater. 149 (2007) 126–133. https://doi.org/10.1016/j.jhazmat.2007.03.056.

[38] E. Gonzalez-Serrano, T. Cordero, J. Rodríguez-Mirasol, J.J. Rodríguez, Development of Porosity upon Chemical Activation of Kraft Lignin with $ZnCl_2$, Ind. Eng. Chem. Res. 36 (1997) 4832–4838. https://doi.org/10.1021/ie970261q.

[39] K. Babeł, K. Jurewicz, KOH activated lignin based nanostructured carbon exhibiting high hydrogen electrosorption, Carbon. 46 (2008) 1948–1956. https://doi.org/10.1016/j.carbon.2008.08.005.

[40] J.M. Rosas, J. Bedia, J. Rodríguez-Mirasol, T. Cordero, Preparation of hemp-derived activated carbon monoliths. Adsorption of water vapor, Ind. Eng. Chem. Res. 47 (2008) 1288–1296. https://doi.org/10.1021/ie070924w.

[41] J.M. Rosas, J. Bedia, J. Rodríguez-Mirasol, T. Cordero, Hemp-derived activated carbon fibers by chemical activation with phosphoric acid, Fuel. 88 (2009) 19–26. https://doi.org/10.1016/j.fuel.2008.08.004.

[42] M.J. Valero-Romero, F.J. García-Mateos, J. Rodríguez-Mirasol, T. Cordero, Role of surface phosphorus complexes on the oxidation of porous carbons, Fuel Process. Technol. 157 (2017) 116–126. https://doi.org/10.1016/j.fuproc.2016.11.014.

[43] S. Ge, L. Feng, L. Zhang, Q. Xu, Y. Yang, Z. Wang, K.H. Kim, Rejection rate and mechanisms of drugs in drinking water by nanofiltration technology, Environ. Eng. Res. 22 (2017) 329–338. https://doi.org/10.4491/eer.2016.157.

[44] M.J. Valero-Romero, E.M. Calvo-Muñoz, R. Ruiz-Rosas, J. Rodríguez-Mirasol, T. Cordero, Phosphorus-Containing Mesoporous Carbon Acid Catalyst for Methanol Dehydration to Dimethyl Ether, Ind. Eng. Chem. Res. 58 (2019) 4042–4053. https://doi.org/10.1021/acs.iecr.8b05897.

[45] J. Goscianska, A. Olejnik, I. Nowak, APTES-functionalized mesoporous silica as a vehicle for antipyrine – adsorption and release studies, Colloids Surfaces A Physicochem. Eng. Asp. 533 (2017) 187–196. https://doi.org/10.1016/j.colsurfa.2017.07.043.

[46] L.M. Cotoruelo, M.D. Marqués, J. Rodríguez-Mirasol, J.J. Rodríguez, T. Cordero, Lignin-based activated carbons for adsorption of sodium dodecylbenzene sulfonate: Equilibrium and kinetic studies, J. Colloid Interface Sci. 332 (2009) 39–45. https://doi.org/10.1016/J.JCIS.2008.12.031.

[47] F.J. García-Mateos, R. Ruiz-Rosas, M.D. Marqués, L.M. Cotoruelo, J. Rodríguez-Mirasol, T. Cordero, Removal of paracetamol on biomass-derived activated carbon: Modeling the fixed bed breakthrough curves using batch adsorption experiments, Chem. Eng. J. 279 (2015) 18–30. https://doi.org/10.1016/j.cej.2015.04.144.

[48] D. Reichenberg, Properties of Ion-Exchange Resins in Relation to their Structure. III. Kinetics of Exchange, J. Am. Chem. Soc. 75 (1953) 589–597. https://doi.org/10.1021/ja01099a022.

[49] T. Vermeulen, Theory for Irreversible and Constant-Pattern Solid Diffusion, Ind. Eng. Chem. 45 (1953) 1664–1670. https://doi.org/10.1021/ie50524a025.

[50] C.H. Giles, D. Smith, A. Huitson, A general treatment and classification of the solute adsorption isotherm. I. Theoretical, J. Colloid Interface Sci. 47 (1974) 755–765. https://doi.org/10.1016/0021-9797(74)90252-5.

UNIVERSIDAD DE MÁLAGA

# Chapter V

UNIVERSIDAD DE MÁLAGA

# 5 Chapter V: Alcohol Dehydrogenation on Kraft Lignin-Derived Chars with Surface Basicity


## Abstract

The properties of lignin and its potential as a renewable source make it an ideal precursor for carbon products. Specifically, the high content of Na observed in Kraft lignin makes this industrial by-product an interesting precursor for the preparation of catalysts for different applications. In this work, basic activated carbons with different textural properties and surface chemistry were obtained from Kraft lignin by direct carbonization at various temperatures. The influence of a further washing treatment and partial gasification with $CO_2$ was also evaluated. The carbon catalysts were tested as catalysts for the alcohol decomposition reaction. In this sense, 2-propanol, a molecule widely used for testing the acidic-basic character of heterogeneous catalysts, was selectively transformed into acetone, meanwhile, ethanol and methanol yielded mainly acetaldehyde and formaldehyde, respectively.


UNIVERSIDAD DE MÁLAGA

## 5.1 Introduction

Lignin is the second most abundant polymer in the world, after cellulose, and it is the most abundant renewable source of aromatic products [1,2]. Most of the lignin produced in the world is a by-product in the pulp–paper industry, with the most lignin obtained from the Kraft process [3]. In this process, lignin fraction is separated from cellulose of the lignocellulosic biomass during wood pulping, with an aqueous solution of NaOH + $Na_2S$, obtaining the corresponding black liquors enriched in lignin. Most lignin is consumed as fuel after evaporation of black liquors in this pulp–paper industry to recover energy and chemical reactants.

In a biorefinery context, an increase in cellulose production must involve a search of new alternatives to make use of lignin, different from combustion [2]. Among the different options, depolymerization is an interesting route to obtain different chemical products by biochemical, catalytic, and thermochemical processes. The production by these routes of renewable chemical products, biofuels, and high added-value materials becomes essential for the integral development of the biorefinery concept. In this way, our research group has studied alternative uses for lignin, such as the preparation of carbon materials from different types of lignin[4,5] , highlighting the creation of activated carbons from physical[6,7]and chemical activation[8,9]; all of the carbon materials have interesting applications as adsorbents[9,10] and catalyst supports[11,12]. Furthermore, the following have also been obtained: carbon materials with a high degree of graphitization[13]; nanomaterials with hierarchical porosity by the zeolite template method[14], for use in electrochemical applications [15]; and carbon fibers and tubes [16,17] also with remarkable results as electrodes[18] and electrocatalysts[19].

In the field of acid catalysis, activated carbons obtained by chemical activation with $H_3PO_4$ have proven to be very good acid catalysts [20], showing outstanding results compared to zeolites in alcohol dehydration, with high chemical and thermal stability, even in the presence of water [21,22]. Furthermore, these catalysts are very selective to olefins, producing ethylene from ethanol [23], propylene from 2-propanol [21], and 1- and 2-buthene from butanol [22]. In the case of methanol, these catalysts mainly produced the intermolecular dehydration to dimethyl-ether.

Alcohols can be molecules of great interest from the point of view of the biorefinery, given that they are raw chemical and energetic sources and, also, are easy to store and transport. In this sense, they can be obtained from biomass, in some cases directly by thermochemical or

UNIVERSIDAD DE MÁLAGA

biochemical reactions, such as pyrolysis (methanol, 2-propanol) or fermentation (ethanol, buthanol), or indirectly, as in the case of methanol, obtained from syngas derived from lignocellulosic biomass gasification.

Following our research about the preparation of carbon materials from lignocellulosic sources and their application in heterogeneous catalysis related to the biorefinery process, this work deals with the preparation of basic catalysts from Kraft lignin, with different textural properties and surface chemistries for alcohol (2-propanol, ethanol and methanol) dehydrogenation.

## 5.2 Materials and Methods

### 5.2.1 Catalyst Preparation

Sodium-lignosulphonate powder with high purity derived from wood (L), as lignocellulosic raw material, was supplied by Sappi Biotech GmbH, Stockstadt, Germany. This type of Kraft lignin has the typical proximate analyses (carbon fixed: 30.8%; volatile content: 52.3%; ash content: 16.9%). The precursor was submitted to a carbonization treatment at different temperatures between 500 and 900 ºC under a continuous $N_2$ flow (150 $cm^3$ $min^{-1}$). The carbon material obtained at 900 ºC was then washed with distillated water at 60 ºC, until a constant pH was reached, to remove part of the inorganic matter. The nomenclature used for the carbon-based catalysts was L followed by a number referring to the carbonization temperature (500, 700, and 900 ºC, respectively), and W in the case of the sample washed. The carbon materials obtained at 900 ºC , L900, and L900W, were also partially gasified under a continuous $CO_2$ atmosphere (150 $cm^3$ $min^{-1}$) at 750 ºC for 30 min, which gave rise to the corresponding samples, named as L900G and L900WG, respectively.

### 5.2.2 Catalyst Characterization

The porous texture of the catalysts was characterized by $N_2$ adsorption-desorption at −196 °C and $CO_2$ adsorption at 0 °C, using a Micromeritics ASAP2020 apparatus (Micromeritics Instrument Corp., Norcross, GA, USA). Samples were previously outgassed for 8 hours at 150 ºC under vacuum. The apparent surface area ($A_{BET}$) was calculated using the BET equation from the $N_2$ adsorption-desorption isotherm, besides, micropore volume ($V_t$) and external surface area ($A_t$) were determined by using the t-method. Mesopore volume ($V_{mes}$) was calculated as the difference between total pore volume ($V_{tot}$) at $P/P_0$ = 0.95 and micropore

UNIVERSIDAD DE MÁLAGA

volume. The Dubinin-Radushkevich equation was used for the calculation of micropore volume and specific surface area from the $CO_2$ isotherm ($V_{DR}$ and $A_{DR}$ respectively).

The surface chemistry was analyzed by X-ray photoelectron spectroscopy (XPS) analysis (Physical Electronics Inc., Chanhassen, MN, USA) and by temperature-programmed desorption (TPD) experiments. XPS analyses were carried out in a Phi 5700 model Physical Electronics apparatus with AlKα radiation (1486.6 eV). The C1s peak position was set at 284.5 eV and used as a reference to locate the other peaks. TPD experiments were carried out in a customized quartz fixed-bed reactor placed inside an electrical furnace. CO and $CO_2$, as output gases, were measured by a non-dispersive infrared (NDIR) gas analyzer, Siemens ULTRAMAT22 (Siemens AG, Munich, Germany). Eighty mg of dry carbon sample was heated from room temperature to 930 °C at a heating rate of 10 ºC $min^{-1}$ under $N_2$ flow (200 $cm^3$ $min^{-1}$).

Catalyst particle morphology was studied by Scanning Electron Microscopy (SEM) (JEOL USA, Inc., Pleasanton, CA, USA), using a JSM 6490LV JEOL microscope working at 25 kV. The atomic distribution of the particle surfaces was analyzed in a FEI Quanta 250 FEG Scanning Electron Microscope equipped with energy-dispersive X-ray analyses (SEM-EDX) (Thermo Fisher Scientific, Hillsboro, OR, USA).

### 5.2.3 Alcohol Dehydration

The activities of the catalysts were measured by the decomposition of alcohols performed at atmospheric pressures, in a quartz fixed bed microreactor (4 mm i.d.) (Alba Nueva Científica S.A., Alhaurín de la Torre, Málaga, Spain) placed inside a vertical furnace with temperature control, using 100 mg of catalyst (200–400 μm particle size). Alcohols were fed into the system in a controlled way by using a syringe pump (Cole-Parmer® 74900-00-05 model (Cole-Parmer Instrument Company, LLC., Vernon Hills, IL, USA)) and the helium flow adjusted to obtain, in each case, a total inlet stream of 100 $cm^3$ STP $min^{-1}$. To avoid condensation of alcohol or any reaction product, all lines were heated up to 130 °C. The space time used was W/Fo Alcohol = 0.073 g s·$\mu mol^{-1}$. Reactant and product concentrations were measured by gas chromatography (490 micro-GC equipped with PPQ, 5A molsieve, and Wax columns, Agilent Technologies, Santa Clara, CA, USA).

The alcohol conversion was defined as the ratio of the amount of alcohol converted to the amount of alcohol supplied to the reactor. The selectivity (in mol %) was defined as the molar ratio

UNIVERSIDAD DE MÁLAGA

of a specific hydrocarbon product to all the hydrocarbon products formed. The carbon balance was reached with an error lower than 3%.

## 5.3 Results and Discussion

### 5.3.1 Characterization of the Catalysts

Table 5.1summarizes the ash content on a dry basis (d.b.), the ultimate analyses on a dry ash free basis (d.a.f.), and the preparation yields of the different carbon catalysts obtained in this work. For the sake of comparison, the ash content and the ultimate analyses of the starting material has been also included. In this sense, the black liquors in Kraft pulp production plants, from which carbons are obtained, are alkaline 3. The evaporation of these black liquors yields solid lignin with a high content of sodium compounds. The ash content of the bio-chars is around 30%, which is approximately twice the value of the lignin raw material, L (16.9%). This increase is due to the loss of volatile matter during the carbonization, and it is in agreement with the yield of the process (around 50%), suggesting that the inorganic matter is not significantly volatilized in this stage. After the carbonization process of L at the different temperatures, the carbon and the sulfur contents significantly increased, meanwhile, the amount of oxygen and hydrogen considerably decreased, due to the devolatilization and aromatic condensation occurring during the carbonization process.

**Table 6.1.** Ash content, preparation yields, and ultimate analyses of the different samples.

| Catalysts | Preparation yields (%) | Ash (%) | Ultimate Analysis (d.a.f) | | | | |
|---|---|---|---|---|---|---|---|
| | | | C (%) | H (%) | N (%) | S (%) | O*(%) |
| **L** | - | 16.9 | 40.6 | 5.1 | 0.1 | 3.5 | 50.7 |
| **L500** | 60.5 | 28 | 62.6 | 1.7 | 0.3 | 6.5 | 28.9 |
| **L700** | 53.2 | 30 | 62.6 | 0.7 | 0.3 | 5.9 | 30.5 |
| **L900** | 38.0 | 31 | 61.6 | 0.4 | 0.3 | 7.2 | 30.5 |
| **L900W** | 18.0 | 4 | 78.6 | 1.0 | 0.3 | 3.2 | 16.9 |
| **L900G** | 21.3 (B.O.44%) | 44 | 31.8 | 1.2 | 0.2 | 0.0 | 66.8 |
| **L900WG** | 7.8 (B.O. 57%) | 8 | 76.6 | 0.4 | 0.2 | 0.4 | 22.3 |

d.a.f. = dry ash free basis; O*: by difference; B.O.: burn off

The washing of the L900 char removed most of its inorganic matter, obtaining a final ash content of 4%. However, this process was not totally effective, probably due to the narrower,

UNIVERSIDAD DE MÁLAGA

porous structure of this char. This treatment also reduced the oxygen and the sulfur amounts, and consequently increased the carbon content in the obtained carbon, L900W.

Gasification of L900 and L900W chars to obtain L900G and L900WG activated carbons, respectively, produced an increase of the ash content (L900G: 44%; L900WG: 8%), as a consequence of the carbonaceous matter loss (burn-off (B.O.) = 44% and 60%, respectively). This loss was also accompanied by an increase of the oxygen content due to formation of new carbon-oxygen surface groups which were created by chemical reactions between the activation agent ($CO_2$) and the carbon surface.

#### 5.3.1.1 Textural Properties

Figure 5.1 shows the $N_2$ adsorption-desorption isotherms at −196 °C of the different carbon catalysts prepared. The catalyst obtained by the direct carbonization at 500 ºC presents low $N_2$ adsorption in the entire relative pressure range of the isotherm, typical of a nonporous solid. The increase of the carbonization temperature produced a slight development of a porous structure, as is shown by the increased amount of adsorbed $N_2$ (Figure 5.1a), due to the activation produced by sodium oxide when the carbonization temperature was increased. The isotherms of the non-washed catalysts obtained at 900 ºC before and after the gasification step (Figure 5.1b) are very similar, due to the presence of inorganic matter that hinders the development of porosity during the gasification step, probably by hampering the complete devolatilization[23]. In contrast, the washing treatment releases to a great extent the porosity of the sample L900W due to the removal of the inorganic matter, mainly composed of Na and S. The gasification of this sample produces high porosity in L900WG, showing a type IV isotherm with an increase of the adsorbed volume in the whole relative pressure range, which corresponds to a large amount of porosity with micropores and mesopores. The presence in this sample of H4 type hysteresis loops is associated to slit-shaped pores.

UNIVERSIDAD DE MÁLAGA

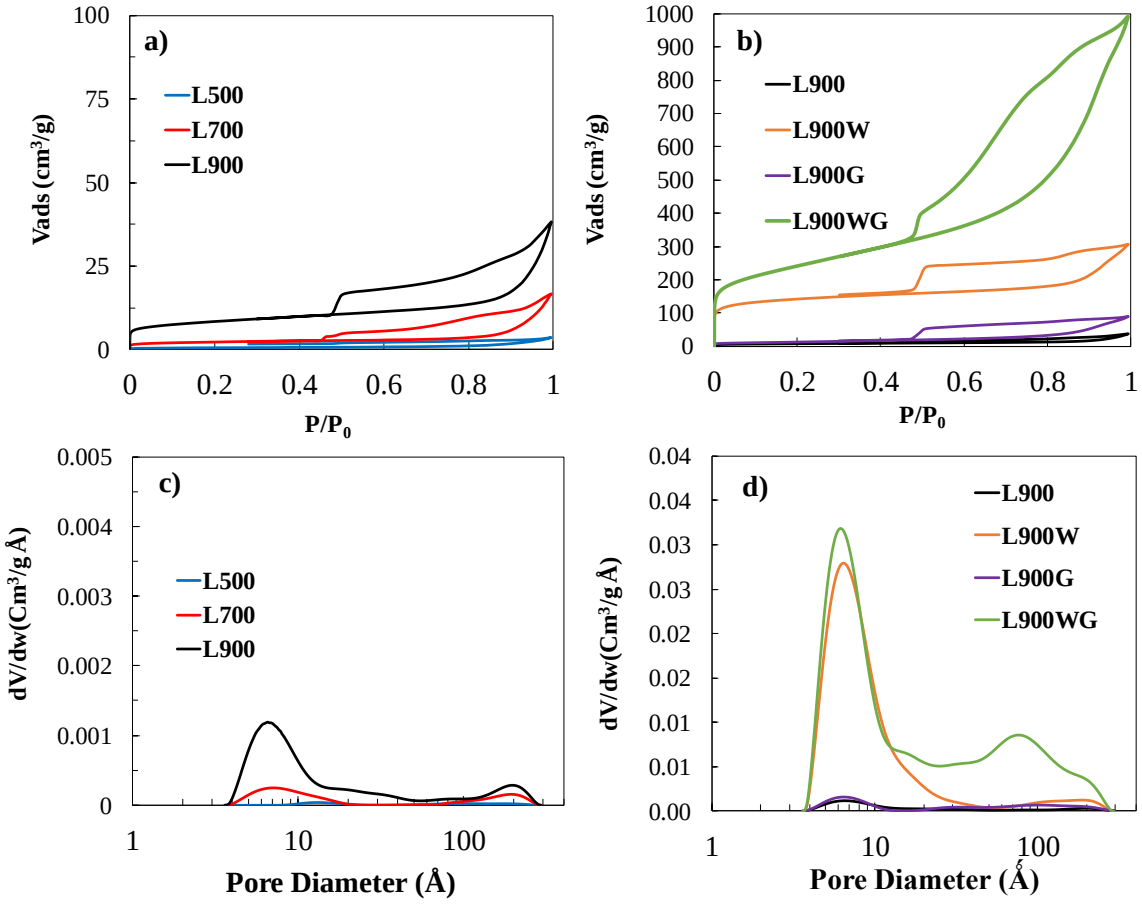


**Figure 5.1.** $N_2$ adsorption-desorption isotherms at −196 ºC of (a) the carbon catalysts obtained at different carbonization temperatures and (b) the series of carbons prepared at 900 ºC. Micropore size distributions of (c) the carbon catalysts obtained at different carbonization temperatures and (d) the series of carbons prepared at 900 ºC.

Figure 5.1c, d also shows the micropore size distribution of the different carbon catalysts. Most of the carbon materials have micropores within an effective pore width in the range of 4–15 Å. The increase of the carbonization temperature (Figure 5.1c) produces a slight increase of the micropore size as a consequence of a higher devolatilization. In this sense, the samples treated at 900 ºC present a multimodal pore size distribution. After the washing of the L900 carbon, an important widening of micropore size is revealed, showing a maximum around 6 Å. The following gasification of this sample (L900WG) produces a further broadening of the porosity, presenting another important maximum around 80 Å.

Table 5.2 summarizes the values of the textural properties that characterize the porous texture calculated from $N_2$ adsorption-desorption and $CO_2$ adsorption isotherms of the different carbon catalysts. The catalysts obtained directly by carbonization at the different temperatures show significantly higher values of specific surface area from the $CO_2$ isotherm ($A_{DR}$) than that

UNIVERSIDAD DE MÁLAGA

of apparent surface area ($A_{BET}$), indicative of a very narrow porous structure, with mean pore size values under 7Å [24]. After the washing treatment, the sample L900W has high values of micropore volume obtained from the $N_2$ isotherm ($V_t$), mesopore volume ($V_{mes}$), and micropore volume derived from the $CO_2$ isotherm ($V_{DR}$) than those of L900, revealing that the removal of the inorganic matter (from 31 to 4%) removes to a great extent the porosity. The similarities between $A_{BET}$ and $A_{DR}$ values, obtained for L900W carbon, are typical of microporous solids.

**Table 5.2.** Textural parameters obtained from $N_2$ and $CO_2$ isotherms at −196 ◦C and 0 °C, respectively, of all the carbon catalysts. $A_{BET}$ = apparent surface area; At = external surface area; Vt = micropore volume obtained from the $N_2$ isotherm; $V_{tot}$ = total pore volume; $V_{mes}$ = mesopore volume; $A_{DR}$ = specific surface area from the $CO_2$ isotherm; $V_{DR}$ = micropore volume derived from the $CO_2$ isotherm.

| Catalysts | $N_2$ Isotherm | | | | | $CO_2$ Isotherm | |
|---|---|---|---|---|---|---|---|
| | $A_{BET}$ ($m^2\ g^{-1}$) | $A_t$ ($m^2\ g^{-1}$) | $V_t$ ($cm^3\ g^{-1}$) | $V_{tot}$ ($cm^3\ g^{-1}$) | $V_{mes}$ ($cm^3\ g^{-1}$) | $A_{DR}$ ($m^2\ g^{-1}$) | $V_{DR}$ ($cm^3\ g^{-1}$) |
| **L500** | 2 | 2 | - | 0.01 | 0.01 | 214 | 0.09 |
| **L700** | 8 | 3 | - | 0.02 | 0.02 | 173 | 0.07 |
| **L900** | 30 | 12 | 0.01 | 0.06 | 0.05 | 48 | - |
| **L900W** | 528 | 83 | 0.19 | 0.47 | 0.28 | 471 | 0.19 |
| **L900G** | 48 | 46 | 0.01 | 0.14 | 0.13 | 18 | - |
| **L900WG** | 847 | 586 | 0.12 | 1.53 | 1.41 | 271 | 0.11 |

Gasification of L900 does not produce any apparent development of the porosity. This fact probably can be associated to the high ash content (44%) of the sample L900G, which may block access to the pores. In contrast, gasification of L900W generated a notable development of the porosity, obtaining an $A_{BET}$ as high as 850 $m^2\ g^{-1}$. In this case, an $A_{BET}$ higher than the value of $A_{DR}$ indicates the presence of a wide porous structure. Furthermore, $V_{mes}$ is higher than $V_t$, indicating a high contribution to mesoporosity.

#### 5.3.1.2 Surface Morphology

Figure 5.2 collects the SEM micrographs of the different carbon catalysts. The morphology of the carbon catalysts obtained at the different carbonization temperatures is very similar. The samples carbonized at 900 °C and washed (L900W) show a slight reduction of the particle size, probably due to the high reduction of the ash content. With regard to the gasification, the sample L900G suffers an important reduction of the particle size, however, as aforementioned, the

UNIVERSIDAD DE MÁLAGA

treatment does not produce any development of the porosity. These results suggest that gasification takes place, with diffusional control, on the external surface of the particle and, consequently, a shrinking unreacted core model mechanism could explain the evolution of the gasification process. In contrast, the sample L900WG presents the same particles size, indicating that gasification proceeds in the entire available particle surface, without diffusional problems, and with an important porosity development [25].

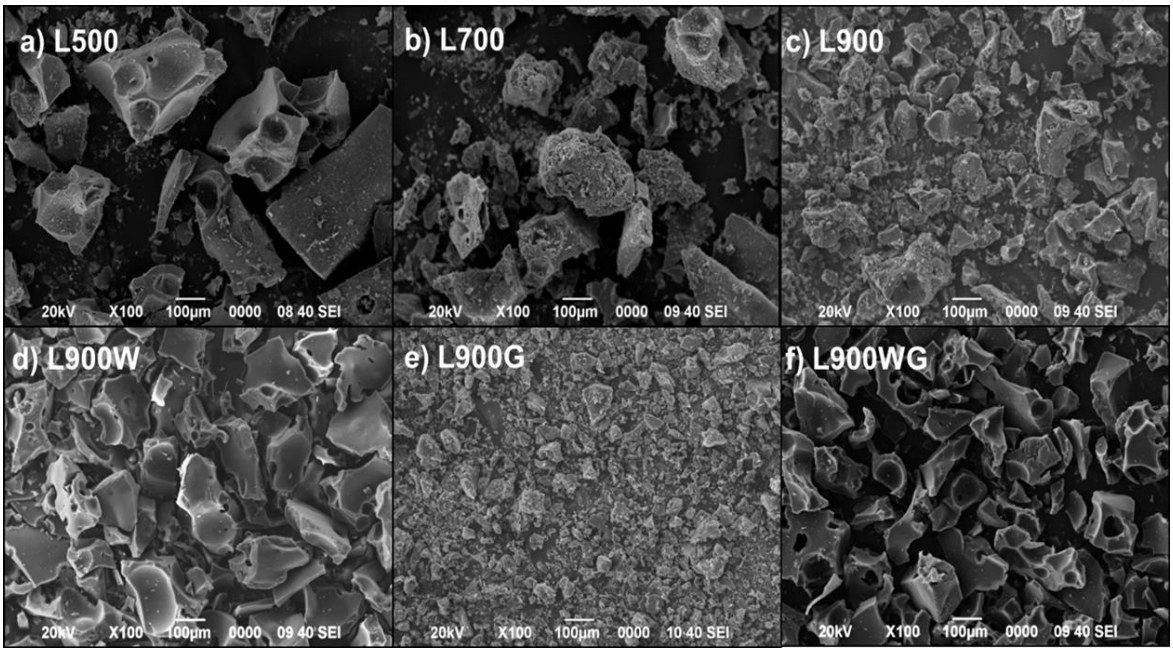


**Figure 5.2.** SEM micrographs of the different carbon catalysts. (a) L500; (b) L700; (c) L900; (d) L900W; (e) L900G; (f) L900WG.

5.3.1.3 Surface Chemistry

X-ray photoelectron spectroscopy (XPS) analyses were carried out in order to evaluate the surface element distribution and the surface chemical composition of the carbon catalysts. The main components of the carbon catalysts are carbon, oxygen, sulfur, and sodium. It is important to highlight the low carbon content of these carbon catalysts (L500, L700, and L900), these values are considerably lower than those obtained by other lignocellulosic chars [23], indicating that the main part of the inorganic matter is present in the outer surface. The weight ratio O/C determined by XPS in these three carbon catalysts is approximately 3, and the ash content is around 30%. If it is assumed that most of the inorganic matter is composed of sodium, a weight ratio $Na/C_{XPS}$ of approximately 2 can be observed. These values suggest that sodium is mainly present in the form of sodium salt (carbonates, sulfates, and sulfides). After the washing treatment, more of the ashes

UNIVERSIDAD DE MÁLAGA

are removed and, consequently, the carbon content significantly increases in detriment of the oxygen, sulfur, and sodium contents.

On the other hand, it was expected that the carbon content of L900G would decrease with respect to that of L900 as a consequence of the carbon loss by the gasification. However, the gasification process increased the carbon amount and decreased the sulfur and sodium percentages. This could be due, in part, to the carbonation of the sodium ions present on the surface during the gasification process. In this sense, some volatilization of the sulfur compounds can take place during gasification with $CO_2$, as suggested by the decrease of the sulfur content close to the formation of sodium clusters that reduce the relative concentration of this atom in the external surface, so increasing the carbon content. Gasification of the carbon L900W produces, as expected, an increase of the sulfur and sodium contents and a reduction of the carbon amount caused by the carbon gasification.

Figure 5.3 shows the C1s, O1s S2p, and Na1s spectra of the different carbon catalysts. C1s spectrum of the samples carbonized at different temperatures shows two broad peaks associated to the presence of different chemical states. In this sense, it shows the presence of C-C (284.5 eV), C-OH (285.5 eV), C-O-C (286.3 eV); C=O (288 eV), and $CO_3^{2-}$ bonds (290 eV). The contribution of carbonates is very important in these samples, being even higher than those of the other species. The C1s spectrum of the washed carbons (Figure 6.2e) shows an important reduction of the carbonates peak at the same time as an increase of the peak associated to carbon in the C-C bond. O1s spectrum shows a wide and similar band around 531.5 eV in all the carbon catalysts, this band can be deconvoluted into several peaks in the range of 530.4-530.8, 532.4-533.1, and 534.8-535.6 eV which have been ascribed to C=O groups C-OH and /or C-O-C groups, and chemisorbed oxygen and/or water respectively Furthermore, an important band around 531.1 eV can be also obtained due to oxygen atoms in the carbonate ions of sodium carbonate [26].these samples also present a broad peak found around 535.5 eV, which corresponds to sodium Auger peak (NaKLL). This last peak and the one found at 531.1 eV are considerably decreased in the washed samples.

UNIVERSIDAD DE MÁLAGA

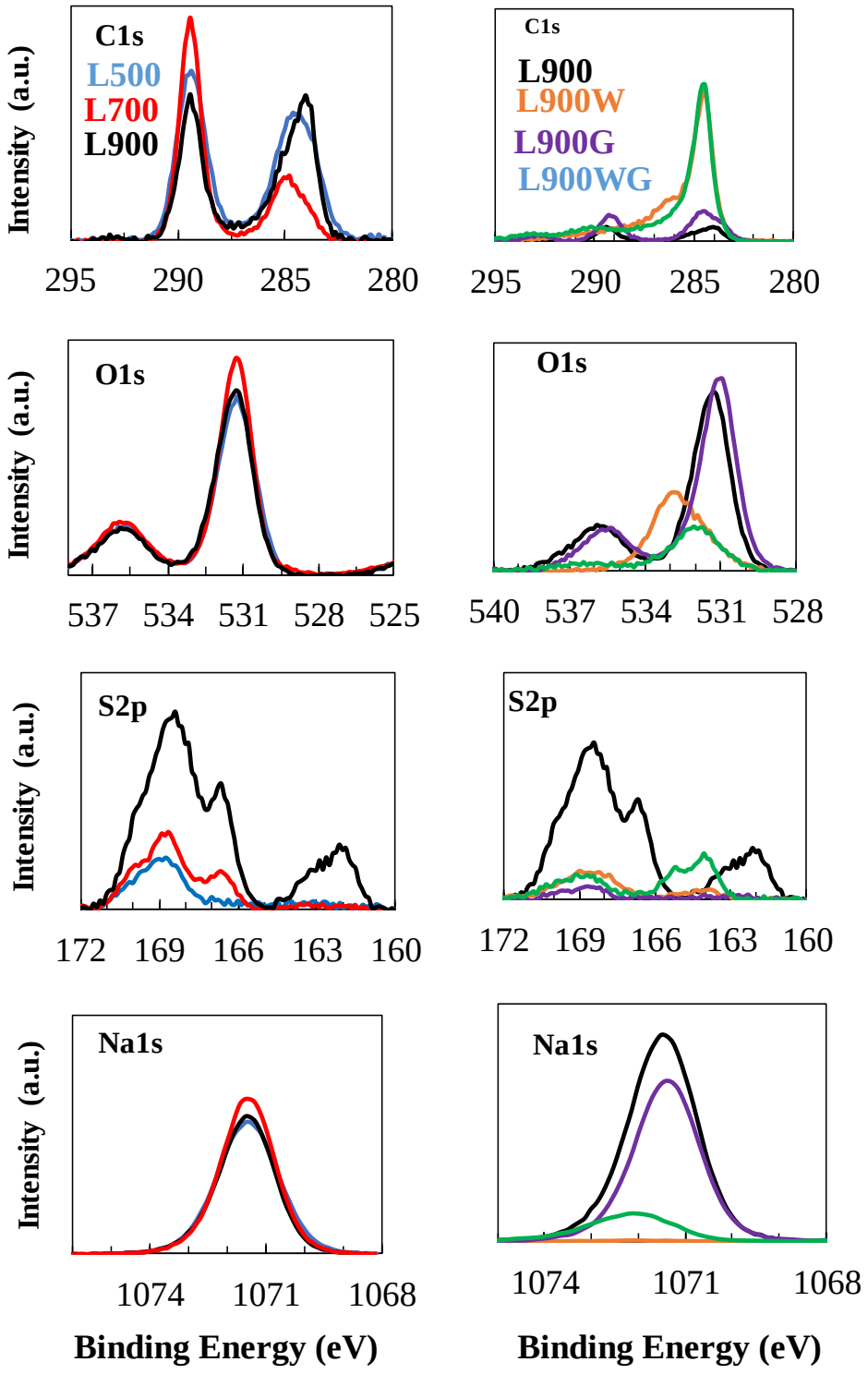


**Figure 5.3.** (a) and (e) C1s, (b) and (f) O1s, (c) and (g) S2p, and (d) and (h) Na1s spectra of the different carbon catalysts at different temperatures and carbon catalysts prepared at 900 ˚C, respectively.

The sulfur spectrum presents a doublet corresponding to $S2p_{3/2}$ and $S2p_{1/2}$. The S2p spectrums of the samples L500 and L700 show two contributions at 167.6 and 169.4 eV that could be associated to sulfite and sulfate groups, respectively. The carbonization at the highest

UNIVERSIDAD DE MÁLAGA

temperature produces the appearance of another peak at 162.1 eV, related to the formation of sulfide (thiolate) groups. The washing treatment reduces considerably the presence of sulfur, only leaving some sulfur in the form of sulfate groups. Only the sample L900WG has a peak at 163.4 eV, associated to disulfide or sulfide and unbound thiol. The Na1s spectrum for the carbon catalysts obtained at different carbonization temperatures can be assigned to sodium carbonate, sodium sulfate, and sodium sulfide, with the more significant contribution associated to sodium carbonate. These species almost disappear with the washing treatment.

Figure 5.4 displays the sodium dispersion derived from SEM equipped with energy-dispersive X-ray analyses (SEM-EDX) analyses of the different carbon catalysts obtained at 900 °C. As can be seen, sodium is well distributed in the sample carbonized at 900 °C. After the washing treatment, its distribution is very homogeneous, in spite of the important reduction of its content. The formation of sodium clusters can be noticed in the sample L900G, in agreement with the decrease of Na content detected by X-ray photoelectron spectroscopy (XPS) analyses, however, those clusters are not observed in the carbon L900WG. This difference can be associated to the lower Na content of this sample. Furthermore, Na is a well-known catalyst of the gasification reactions, and its high amount in the sample L900G can produce local increases of the temperature, favoring the sintering of clusters in that case.

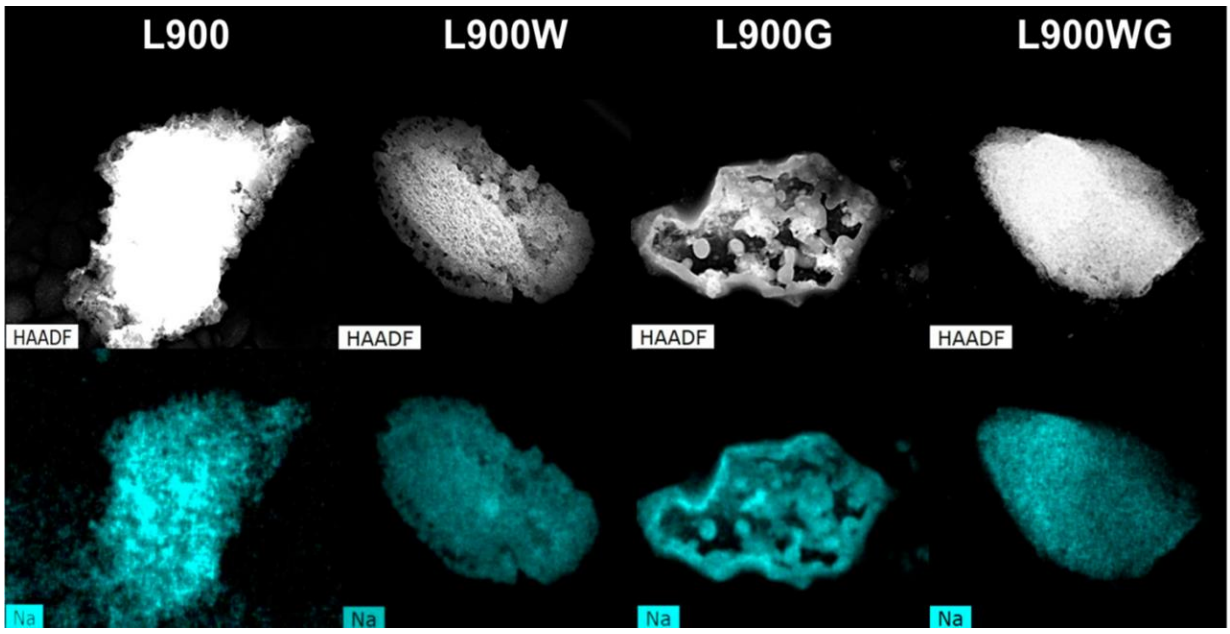


**Figure 5.4.** Sodium dispersion mapping from SEM equipped with energy-dispersive X-ray analyses (SEM-EDX) of the different carbon catalysts.

The surface chemistry of the carbon catalysts was also analyzed by the temperature-programmed desorption (TPD) technique, which is used to characterize the carbon-oxygen



UNIVERSIDAD DE MÁLAGA

groups of the samples. Carbon materials release different oxygen surface groups whose nature and quantity depend on the starting material and the activation treatment [27]. The ether, quinone) and phenol groups produce CO. Anhydride evolves as both CO and $CO_2$ [28]. Figure 5.5a–d shows, respectively, the $CO_2$ and CO evolved during the TPD experiments performed on the different carbon catalysts. Decomposition of surface oxygen complexes such as CO and $CO_2$ are quite high in all the carbon catalysts. In general, the evolution of CO is higher than that of $CO_2$. The chars obtained at the different temperatures (Figure 5.5a, c) show high amounts of very stable carbon-oxygen groups, which decompose at temperatures higher than 600 ˚C, where decomposition of both inorganic compounds and carbonyl and quinone groups takes place. The increase of the carbonization temperature produces an increase of the CO and $CO_2$ evolution. In the case of CO, the last peak associated to more stable carbon-oxygen complexes remains very similar after carbonization at the different temperatures, however, the peak around 700 ˚C decreases in the carbon catalyst prepared at 900 ˚C, probably as a consequence of the higher temperature of the treatment. On the other hand, $CO_2$ profiles increase with the carbonization temperature. The evolution at low temperatures is almost negligible, and most of the evolution is centered on 700 ˚C, which probably can be associated to the decomposition of sodium carbonates [29]. However, the different chars have very similar ash and Na content (determined by XPS analyses), so their differences must be associated to the increase of the sulfur content and its possible reduction from sulfate to sulfide groups. This reduction would produce the oxidation of the carbon to carbonate surface in the form of groups, which decompose as $CO_2$. Nevertheless, another feasible explanation could be the formation of sodium atom clusters in the external surface, decreasing the relative amount of sodium, as revealed by XPS[30] .

UNIVERSIDAD DE MÁLAGA

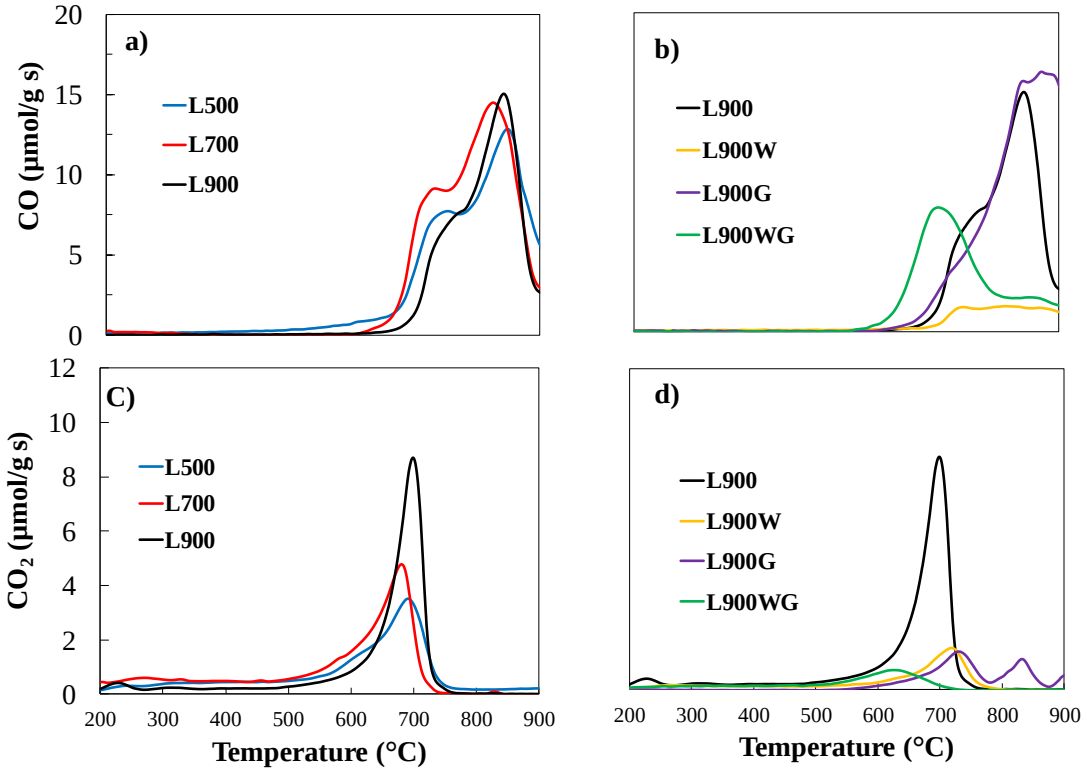


**Figure 5.5.** TPD profiles of the different carbon catalysts. (**a**, **b**) CO evolution; (**c**, **d**) $CO_2$ evolution of different carbon catalysts.

Figure 5.5 b, d collects the CO and $CO_2$ evolutions of the carbon catalysts obtained at 900 ˚C. When L900 is washed, an important reduction of the CO and $CO_2$ evolution is noticed, related to the considerable removal of the inorganic matter. With regard to the gasified samples, gasification of carbon samples with high ash content produces the increase of the amount of oxygen groups that evolved as $CO_2$ during the TPD, as occurs in the L900WG catalyst. However, the L900G sample shows a similar CO profile, and a $CO_2$ evolution substantially decreased. Specifically, the peak around 700 ˚C is significantly reduced. This decrease may be due to decomposition of alkaline metal carbonates, which can take place at temperatures below the melting point (820 ˚C) when heating carbonate-carbon mixtures. In this case, the temperature of the gasification treatment was 750 ˚C, so decomposition of the groups of L900 was probably produced during its gasification [31]. Table 5.3 also summarizes the amounts of CO and $CO_2$ evolved with temperature during the TPD experiment for the different carbon catalysts. As can be seen, the catalyst L900 presents the highest $CO_2$ evolution; meanwhile the sample L900G evolves the highest amount of CO.

UNIVERSIDAD DE MÁLAGA

**Table 5.3.** Mass surface concentration determined by X-ray photoelectron spectroscopy (XPS) analyses and amounts of CO and $CO_2$ evolved with temperature during the temperature-programmed desorption (TPD) experiment for the different carbon catalysts.

| | XPS Composition (wt %) | | | | TPD | |
|---|---|---|---|---|---|---|
| **Catalysts** | **C** | **O** | **S** | **Na** | **CO(mmol·g$^{-1}$)** | **$CO_2$(mmol·g$^{-1}$)** |
| **L500** | 15.7 | 41.6 | 1.7 | 41.0 | 12.8 | 2.5 |
| **L700** | 10.6 | 44.4 | 2.4 | 41.6 | 13.8 | 3.1 |
| **L900** | 12.5 | 40.8 | 7.6 | 39.1 | 10.8 | 3.7 |
| **L900W** | 81.3 | 17.0 | 1.2 | 0.5 | 2.4 | 1.1 |
| **L900G** | 30.2 | 39.6 | 0.7 | 29.5 | 15.4 | 1.2 |
| **L900WG** | 79.9 | 12.0 | 2.1 | 6.0 | 6.9 | 0.2 |

#### 5.3.1.4 Catalytic Activity

Alcohol molecules, mainly 2-propanol, are widely used for testing the acidic-basic character of heterogeneous catalysts [20, 21] In this sense, alcohol dehydrogenation products (aldehydes and ketones) are preferentially formed on basic catalysts, while dehydration products (olefins and ethers) are favored when acidic sites are present. Figure 5.6 shows the evolution of the steady-state conversions of 2-propanol and the selectivity to acetone and propylene with the temperature for all the carbon catalysts (Partial alcohol pressure: $Po_{ALC}$ = 0.0185 atm; space time $W/Fo_{ALC}$ = 0.073 g s μmol$^{-1}$). As expected, 2-propanol conversion increases with the reaction temperature. The increase of the carbonization temperature produces an enhancement of the steady-state conversions, showing the catalyst carbonized at 900 ˚C as the highest steady-state conversions of the three chars. On the other hand, the series of the carbon catalysts prepared at 900 ˚C (Figure 5.6b) follows the sequence L900WG > L900 > L900W > L900G. The most active catalysts correspond to the carbon with the highest development of porosity and a high dispersion of Na, meanwhile the catalyst L900G presents quite a low apparent surface area and a poor dispersion of sodium, as evidenced the SEM-EDX analyses.

UNIVERSIDAD DE MÁLAGA

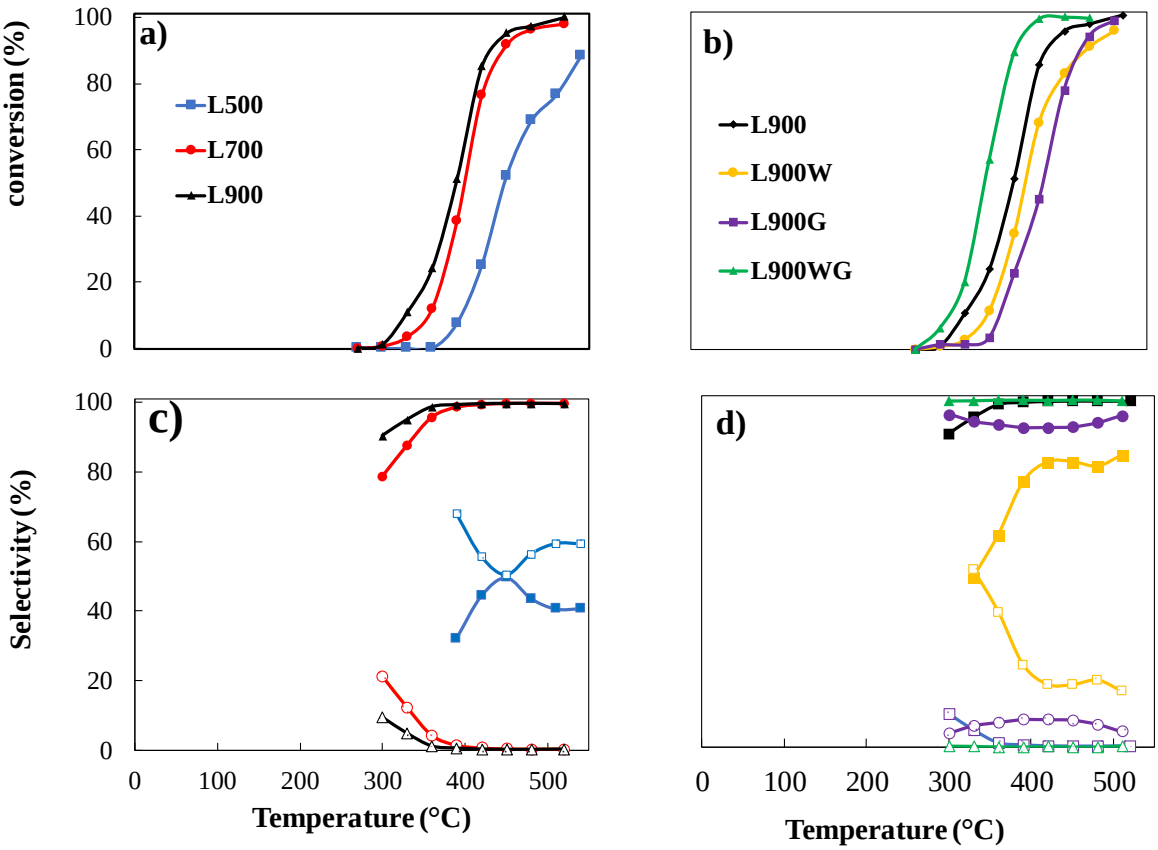


**Figure 5.6.** Evolution of the steady-state conversions of 2-propanol (**a**,**b**) and selectivity to acetone (filled marks) and propylene (hollow marks) with the temperature (**c**,**d**) for all the carbon catalysts in a helium flow ($P_{oALC}$ = 0.0185 atm; $W/F_{oALC}$ = 0.073 g s µmol$^{-1}$).

The main product is acetone in most of the carbon catalysts, obtained as 2-propanol dehydrogenation product. However, the catalyst L500 and to a lesser extent L900W also yield an important amount of propylene, indicating the presence of both acid and basic surface sites. Furthermore, most of samples carbonized at 900 ˚C, showing selectivity to acetone higher than 95% at reaction temperatures higher than 350 ˚C.

In this sense, the hydrogen atom on the hydroxyl group of alcohols is acidic in the presence of basic catalysts and/or basic sites. So, the interaction between a basic site (for example, quinone groups present in these catalysts, especially in L900WG) and an alcohol molecule causes the abstraction of the proton from the -OH group, forming a surface alkoxide intermediate. The following abstraction of a $H_\alpha$ or $H_\beta$ from the corresponding alkoxide intermediate leads to ketone or alkene formation, respectively; the latter is less favored.

UNIVERSIDAD DE MÁLAGA

Decomposition of ethanol and methanol was also evaluated for the carbon catalyst more active in the 2-propanol decomposition of L900WG. Figure 5.7 shows the evolution of the steady-state conversions of ethanol (a) and methanol (b). Furthermore, the selectivity to aldehydes (filled marks) and to ethylene and dimethyl ether (hollow marks) was also included as a function of the reaction temperature in a helium flow ($Po_{ALC}$ = 0.0185 atm; $W/Fo_{ALC}$ = 0.073 g s µmol$^{-1}$). Although the conversions observed for these catalysts were not as high as some reported in the literature [32-34], selectivity of ethanol to acetaldehyde was higher than 80% in the whole range of conversions studied, values considerably larger than those obtained by those authors. In addition, our catalyst was obtained from a renewable source by a cheap and easy synthesis method. The stability of this catalyst for the ethanol conversion was also evaluated at two different temperatures: 420 and 450 ˚C (Figure 5.7c). The catalyst showed the same activity along the experiment, with the same selectivity toward acetaldehyde.

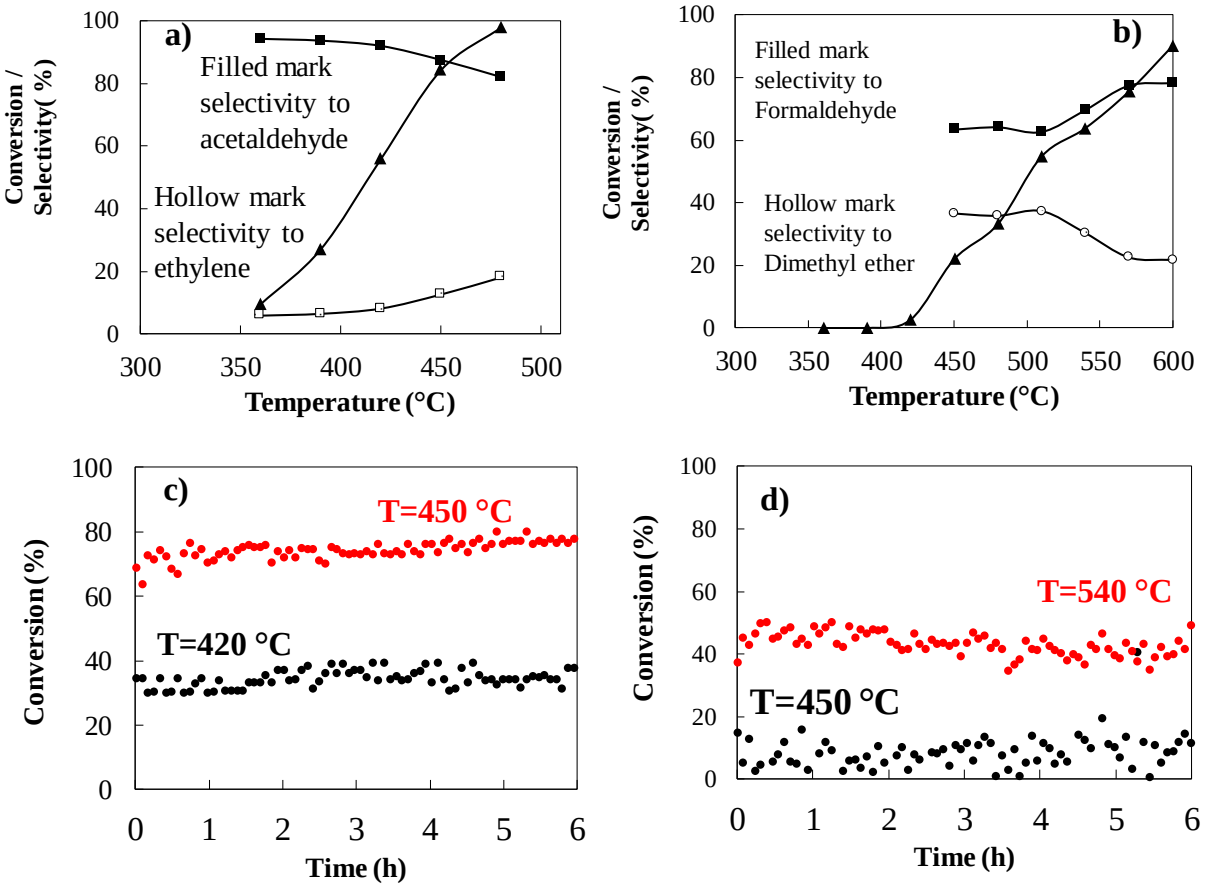


**Figure 5.7.** Evolution of the steady-state conversions of ethanol (**a**) and methanol (**b**) and selectivity to aldehydes and ketones (filled marks) and olefins and ethers (hollow marks) with the temperature for all the carbon catalysts in a helium flow ($Po_{ALC}$ = 0.0185 atm; $W/Fo_{ALC}$ =0.073 g s µmol$^{-1}$); ethanol(**c**) and methanol (**d**) conversions as a function of time on stream at different temperatures with $Po_{ALC}$ = 0.0185 atm and $W/Fo_{ALC}$ = 0.073 g s µmol$^{-1}$.

UNIVERSIDAD DE MÁLAGA

With regard to methanol, conversions were comparable to those reported in the literature [35,36]. The selectivity to formaldehyde increased gradually with temperature and reached a maximum (approximately 80%) at the highest temperature studied, which is near the commercial operation temperature. At the lowest temperatures (<475 ˚C), methanol was mainly dehydrated to dimethyl ether, making the yield of olefins (propylene or butenes) very low. The possible deactivation of the catalyst was also analyzed for 6 hours at 450 and 540 ˚C. The conversion remained the same during this reaction time.

In general, the selectivity of ethanol and methanol to acetaldehyde and formaldehyde, respectively, were lower than those observed for 2-propanol to acetone. Specifically, the formation of alkene was higher when ethanol was used versus 2-propanol, due to the chemical similarities of $H_\alpha$ and $H_\beta$ to ethanol. In the case of methanol, there is a competition between the nucleophilic substitution to yield dimethyl ether (DME) and the abstraction of $H_\alpha$, which is slower as it is less favored than in higher alcohols.

## 5.4 Conclusions

The properties of lignin and its potential as a renewable source make it an ideal precursor for carbon products. Most of the lignin in the world is produced as a by-product in the pulp and paper industry, with the most obtained from the Kraft process. The black liquors in Kraft pulp production plants, from which carbons are obtained, are alkaline solutions. The evaporation of these black liquors yields solid lignin with a high content of sodium compounds, such as sodium hydroxide, sulfate, and lignosulfonate.

The carbonization of this lignin produces chars with a high content of oxygen surface groups, as a consequence of the oxidation of carbon and the reduction of the sulfur salts to sulfide. The oxygenated groups are mainly quinone, carbonyl, and carbonate (sodium carbonate). The washing of these chars partially removes the sodium sulfide and, to a lesser extent, the sodium carbonate. Meanwhile, the gasification with $CO_2$ developed the porosity in the washed sample. The surface of the carbon shows a basic character with carbonyl and quinone groups and carbon basal planes (with high electron density), which can act as electron donor sites.

The carbon materials obtained were evaluated as catalysts for the alcohol decomposition. The catalytic test of 2-propanol decomposition supported the strong basic character of these catalysts, as alcohol was selectively transformed into acetone. Once the basic character was established, the catalyst with the highest activity, L900WG, was evaluated for the ethanol and methanol

UNIVERSIDAD DE MÁLAGA

decomposition. The results of conversions were not as high as expected. However, the selectivity of the catalyst was higher than 80%, yielding acetaldehyde and formaldehyde. Finally, the stability of the catalyst was also analyzed for 6 hours. The conversion and selectivity for both alcohols remained the same during this reaction time.

## References


[1] H.Z Chen .Biotechnology of Lignocellulose: Theory and Practice; Chemical Industry Press: Beijing, China; Springer: Dordrecht, The Netherlands, 2014; ISBN 978-9-4-0076897-0.

[2] Zhen, F.; Richard, L.S .Production of Biofuels and Chemicals from Lignin;., Jr. (Eds.) Springer: Berlin, Germany, 2016; ISBN 978-981-10-1964-7.

[3] K.T.Vijay, K.T.Manju, R.K. Michael. Handbook of Composites from Renewable Materials, Structure and Chemistry; (Eds.); Wiley: Hoboken, NJ, USA, 2017.

[4] J.M. Rosas, R. Berenguer, M.J. Valero-Romero, J. RodrÃ-guez-Mirasol, T. Cordero, Preparation of Different Carbon Materials by Thermochemical Conversion of Lignin, Front. Mater. 1 (2014) 1–17. https://doi.org/10.3389/fmats.2014.00029.

[5] J.J. Rodríguez, J.Rodríguez-Mirasol, T.Cordero.Carbon Materials From Lignin and Their Applications. In Production of Biofuels and Chemicals from Lignin, 2016. https://doi.org/10.1007/978-981-10-1965-4.

[6] J. Rodríguez-Mirasol, T. Cordero, J.J. Rodríguez, Preparation and characterization of activated carbons from eucalyptus kraft lignin, Carbon. 31 (1993).87-95. https://doi.org/10.1016/0008-6223(93)90160-C.

[7] J. Rodríguez-Mirasol, T. Cordero, J.J. Rodríguez, Activated Carbons from $CO_2$ Partial Gasification of Eucalyptus Kraft Lignin, Energy and Fuels. 7 (1993) 133–138. https://doi.org/10.1021/ef00037a021.

[8] E. Gonzalez-Serrano, T. Cordero, J. Rodríguez-Mirasol, J.J. Rodríguez, Development of Porosity upon Chemical Activation of Kraft Lignin with $ZnCl_2$ , Ind. Eng. Chem. Res. 36 (2002) 4832–4838. https://doi.org/10.1021/ie970261q.

[9] E. Gonzalez-Serrano, T. Cordero, J. Rodriguez-Mirasol, L. Cotoruelo, J.J. Rodriguez, Removal of water pollutants with activated carbons prepared from H 3PO4 activation of lignin from kraft black liquors, Water Res. 38 (2004) 3043–3050. https://doi.org/10.1016/j.watres.2004.04.048.

[10] L.M. Cotoruelo, M.D. Marqués, F.J. Díaz, J. Rodríguez-Mirasol, J.J. Rodríguez, T. Cordero, Adsorbent ability of lignin-based activated carbons for the removal of p-nitrophenol from aqueous solutions, Chem. Eng. J. 184 (2012) 176–183. https://doi.org/10.1016/J.CEJ.2012.01.026.

[11] J. Bedia, J.M. Rosas, J. Rodríguez-Mirasol, T. Cordero, Pd supported on mesoporous activated carbons with high oxidation resistance as catalysts for toluene oxidation, Appl. Catal. B Environ. 94 (2010). 8-18. https://doi.org/10.1016/j.apcatb.2009.10.015.

[12] E. Guillén, R. Rico, J.M. López-Romero, J. Bedia, J.M. Rosas, J. Rodríguez-Mirasol, T. Cordero, Pd-activated carbon catalysts for hydrogenation and Suzuki reactions, Appl. Catal. A Gen. 3368 (2009) 113-120. https://doi.org/10.1016/j.apcata.2009.08.016.


UNIVERSIDAD DE MÁLAGA

[13] J. Rodríguez-Mirasol, T. Cordero, J.J. Rodríguez, High-temperature carbons from kraft lignin, Carbon. 34 (1996). 43-52. https://doi.org/10.1016/0008-6223(95)00133-6.

[14] M.J. Valero-Romero, E.M. Márquez-Franco, J. Bedia, J. Rodríguez-Mirasol, T. Cordero, Hierarchical porous carbons by liquid phase impregnation of zeolite templates with lignin solution, Microporous Mesoporous Mater. 196 (2014) 68-78. https://doi.org/10.1016/j.micromeso.2014.04.055.

[15] R. Ruiz-Rosas, M.J. Valero-Romero, D. Salinas-Torres, J. Rodríguez-Mirasol, T. Cordero, E. Morallón, D. Cazorla-Amorós, Electrochemical performance of hierarchical porous carbon materials obtained from the infiltration of lignin into zeolite templates, ChemSusChem. 7 (2014) 1458–1467. https://doi.org/10.1002/cssc.201301408.

[16] M. Lallave, J. Bedia, R. Ruiz-Rosas, J. Rodríguez-Mirasol, T. Cordero, J.C. Otero, M. Marquez, A. Barrero, I.G. Loscertales, Filled and hollow carbon nanofibers by coaxial electrospinning of Alcell lignin without binder polymers, Adv. Mater. 19 (2007) 4292–4296. https://doi.org/10.1002/adma.200700963.

[17] R. Ruiz-Rosas, J. Bedia, M. Lallave, I.G. Loscertales, A. Barrero, J. Rodríguez-Mirasol, T. Cordero, The production of submicron diameter carbon fibers by the electrospinning of lignin, Carbon. 48 (2010) 696-705. https://doi.org/10.1016/j.carbon.2009.10.014.

[18] R. Berenguer, F.J. García-Mateos, R. Ruiz-Rosas, D. Cazorla-Amorós, E. Morallón, J. Rodríguez-Mirasol, T. Cordero, Biomass-derived binderless fibrous carbon electrodes for ultrafast energy storage, Green Chem. 18 (2016) 1506–1515. https://doi.org/10.1039/c5gc02409a.

[19] F.J. García-Mateos, T. Cordero-Lanzac, R. Berenguer, E. Morallón, D. Cazorla-Amorós, J. Rodríguez-Mirasol, T. Cordero, Lignin-derived Pt supported carbon (submicron)fiber electrocatalysts for alcohol electro-oxidation, Appl. Catal. B Environ. 211 (2017) 1506-1515. https://doi.org/10.1016/j.apcatb.2017.04.008.

[20] J. Bedia, J.M. Rosas, J. Márquez, J. Rodríguez-Mirasol, T. Cordero, Preparation and characterization of carbon based acid catalysts for the dehydration of 2-propanol, Carbon 47. (2009) 286-294. https://doi.org/10.1016/j.carbon.2008.10.008.

[21] J. Bedia, R. Ruiz-Rosas, J. Rodríguez-Mirasol, T. Cordero, A kinetic study of 2-propanol dehydration on carbon acid catalysts, J. Catal. 271 (2010) 33-42. https://doi.org/10.1016/j.jcat.2010.01.023.

[22] Z. Qiao, Z. Wang, C. Zhang, S. Yuan, Y. Zhu, J. Wang, PVAm–PIP/PS composite membrane with high performance for $CO_2/N_2$ separation, AIChE J. 59 (2012) 215–228. https://doi.org/10.1002/aic.

[23] J.M. Rosas, J. Bedia, J. Rodríguez-Mirasol, T. Cordero, On the preparation and characterization of chars and activated carbons from orange skin, Fuel Process. Technol. 91 (2010)1345-1354. https://doi.org/10.1016/j.fuproc.2010.05.006.

[24] F. Rodríguez-Reinoso, J. Garrido, J.M. Martín-Martínez, M. Molina-Sabio, R. Torregrosa, The combined use of different approaches in the characterization of microporous carbons, Carbon 27. (1989) 23-32 . https://doi.org/10.1016/0008-6223(89)90153-X.

[25] J.M. Rosas, R. Ruiz-Rosas, J. Rodríguez-Mirasol, T. Cordero, Kinetic study of the oxidation resistance of phosphorus-containing activated carbons, Carbon. 50 (2012) 1523–1537. https://doi.org/10.1016/j.carbon.2011.11.030.

UNIVERSIDAD DE MÁLAGA

[26] A. V. Zhubrikov, E.A. Legurova, V. Gutkin, V. Uvarov, N. V. Khitrov, O. Lev, T.A. Tripol'skaya, P. V. Prikhodchenko, XPS characterization of sodium percarbonate granulated with sodium silicate, Russ. J. Inorg. Chem. 54 (2009) 1455–1458. https://doi.org/10.1134/s0036023609090198.

[27] Bansal, R.C.; Donnet, J.B.; Stoeckli, H.F. Active Carbon; Marcel Dekker: New York, NY, USA, 1988

[28] J.L. Figueiredo, M.F.R. Pereira, M.M.A. Freitas, J.J.M. Orafo, Modification of the surface chemistry of activated carbons, Carbon. 37 (1999) 1397-1389. https://doi.org/10.1016/S0008-6223(98)00333-9.

[29] D.M. Nevskaia, A. Santianes, V. Muñoz, A. Guerrero-Ruíz, Interaction of aqueous solutions of phenol with commercial activated carbons: An adsorption and kinetic study, Carbon. 37 (1999) 1065-1074. https://doi.org/10.1016/S0008-6223(98)00301-7.

[30] J.A. Asenjo, B.A. Andrews, Mini-review Challenges and trends in bioseparations, Chem. Eng. 120 (2008) 117–120. https://doi.org/10.1002/jctb.

[31] M.. Lillo-Ródenas, D. Cazorla-Amorós, A. Linares-Solano, Understanding chemical reactions between carbons and NaOH and KOH, Carbon. 41 (2002) 267-275. https://doi.org/10.1016/s0008-6223(02)00279-8.

[32] J. Bedia, R. Barrionuevo, J. Rodríguez-Mirasol, T. Cordero, Ethanol dehydration to ethylene on acid carbon catalysts, Appl. Catal. B Environ. 103 (2011) 302-310. https://doi.org/10.1016/j.apcatb.2011.01.032.

[33] A.G. Sato, D.P. Volanti, D.M. Meira, S. Damyanova, E. Longo, J.M.C. Bueno, Effect of the $ZrO_2$ phase on the structure and behavior of supported Cu catalysts for ethanol conversion, J. Catal. 307 (2013) 1-17. https://doi.org/10.1016/j.jcat.2013.06.022.

[34] I.C. Freitas, S. Damyanova, D.C. Oliveira, C.M.P. Marques, J.M.C. Bueno, Effect of Cu content on the surface and catalytic properties of Cu/ZrO 2 catalyst for ethanol dehydrogenation, J. Mol. Catal. A Chem. 381 (2014).26-37. https://doi.org/10.1016/j.molcata.2013.09.038.

[35] M. Qian, M.A. Liauw, G. Emig, Formaldehyde synthesis from methanol over silver catalysts, Appl. Catal. A Gen. 238 (2003) 211-222. https://doi.org/10.1016/S0926-860X(02)00340-X.

[36] R. Ruiz-Rosas, J. Bedia, J.M. Rosas, M. Lallave, I.G. Loscertales, J. Rodríguez-Mirasol, T. Cordero, Methanol decomposition on electrospun zirconia nanofibers, Catal. Today. 187 (2012)77-87. https://doi.org/10.1016/j.cattod.2011.10.031.

UNIVERSIDAD DE MÁLAGA

# Chapter VI

UNIVERSIDAD
DE MÁLAGA

# 6 Chapter VI: General Conclusions and Future Perspectives

The properties of lignin and its potential as a renewable source make it an ideal precursor for carbon materials. The study of valorization of different types of lignin, Organosolv (Alcell) and Kraft, by the preparation of highly porous activated carbons with different textural and surface chemistry properties that allow a large adsorption capacity of emerging pollutants in aqueous phase and a high catalytic activity for alcohols decomposition reactions in gas phase has been analyzed in this thesis.

On one hand, porous acid activated carbons from Alcell lignin were prepared by chemical activation with phosphoric acid ($H_3PO_4$). The preparation method here proposed consisted of dissolving Alcell lignin with ethanol to simulate the composition of dissolved lignin in the Organosolv liquors. Then, co-solution of lignin with the activating agent was performed, followed by a two steps activation treatment (stabilization/activation), based on a first treatment in air at 200ºC, followed by activation in $N_2$. The influence of the activating agent ($H_3PO_4$) to carbon precursor (lignin) mass ratio (values from 0.6 to 5) and the activation temperature (from 300 to 900 ºC) on the textural properties of the activated carbons prepared by co-solution of lignin and $H_3PO_4$ followed by a oxidative (air) treatment at low temperature (200 ºC) before the activation step has been studied. In this sense, some minor chemical modifications were produced only mixing lignin/ethanol with phosphoric acid. However, the combination of the co-solution of lignin with phosphoric acid and the oxidative treatment in air generated carbon materials with a very high-development of the microporosity, after the activation process. The highest porosity was obtained with a $H_3PO_4$ to lignin mass ratio of 2 and activated at 400 ºC, specifically, Alcell lignin derived activated carbons with very high apparent surface area ($A_{BET}$=2550$m^2$/g) and pore volume (1.30 $cm^3$/g) were prepared. These values are considerably higher than those obtained by the conventional procedure (mixing the activating agent directly with the raw material, powder lignin), $A_{BET}$=903 $m^2$/g and pore volume (0.47 $cm^3$/g) , at the same conditions ($H_3PO_4$ to lignin mass ratio and activation temperature). Up to now, this is one of the highest values of apparent surface area reported not only for activated carbons prepared from lignin, but even for porous carbons prepared by chemical activation of other lignocellulosic materials with phosphoric acid.

UNIVERSIDAD DE MÁLAGA

These significant differences can be initially associated to a more homogeneous interaction between lignin and the phosphoric acid after their solubilization with ethanol, which may increase the formation of phosphate esters that promote crosslinking between phosphoric acid and the carbonaceous matrix. The treatment at 200ºC of the oxidative treatment is high enough to promote the formation of these phosphate esters.

Some activated carbons with different pore size distributions were tested as adsorbent for antipyrine adsorption in aqueous solution, at very low concentrations of antipyrine and at room temperature. The activated carbon with the narrowest pore size distribution showed the highest adsorption capacity of antipyrine (37 mg/g) for an equilibrium concentration as low as 1 mg/L. The antipyrine adsorption equilibrium and kinetic results were properly represented by the Langmuir model and hyperbolic equation, respectively. The breakthrough times in column adsorption studies were successfully predicted by the Thomas model.

On the other hand, the preparation of basic activated carbons from Kraft lignin was studied by physical activation with $CO_2$. The direct carbonization of the raw material produced chars with a developed pore structure and a high content of oxygen surface groups. The chars obtained mainly contained quinone, carbonyl and sodium carbonate surface groups. The washing of these chars partially removes the sodium sulfide and, to a lesser extent, the sodium carbonate. Meanwhile, the gasification with $CO_2$ developed the porosity in the washed sample. The catalytic test of 2-propanol decomposition was carried out on these carbon catalysts to evaluate their acidic/basic character. The alcohol was selectively transformed into acetone, which supported the strong basic character of these catalysts. Once the basic character was established, the catalyst with the highest activity was assessed for the ethanol and methanol decomposition. The results of conversions were not as high as expected. However, the selectivity of the catalyst was higher than 80%, yielding acetaldehyde and formaldehyde respectively. Finally, the stability of the catalyst was also analyzed for 6 h of time on stream. The conversion and selectivity for both alcohols remained the same during this reaction time.

This thesis can be a starting point for the preparation of activated carbons from the liquors derived from the different pulping processes, which could boost the techno-economical feasibility of lignocellulosic biorefinery by the production of value-added products. In addition, due to the high porosity of the activated carbons prepared, and the possibility of modifying their surface chemistry, the study of alternative applications for the activated carbons here obtained would be very useful.

UNIVERSIDAD DE MÁLAGA

# Abstract

UNIVERSIDAD
DE MÁLAGA

# Abstract

The extended concern over fossil fuel scarcity, green house effects, climate warming issues and environmental pollution have promoted the use of renewable materials and processes. The use of biomass as renewable raw materials can be an interesting approach. Among the different biomass components, lignin is present in the cell walls of wood or agricultural crops and plants, in order to provide structural strength.

Lignin is the second largest renewable carbon source after cellulose and the most important source of aromatic compounds on Earth. It is a polyphenolic polymer with a three-dimensional network, although the final structure of the isolated lignin may present great differences due to the variety of separation methods and conditions used in the diverse delignification process. In fact, the development of methods for lignin isolation was devoted to wood materials in the paper industry, although these methods have also been applied to grass plants, but with limited success. Some other processes for lignin isolation by industrial pulping such as soda, alkali-hydrogen peroxide and organosolv have also been studied. Currently, the main use of lignin is as fuel and power generation, and only a small percentage of the produced lignin is being market. However, lignin has also a high potential for its conversion into value-added products (advanced chemicals and carbon materials) that could considerably enhance the economics of a biorefinery. Due to its high carbon content (varying between 51and 65%), lignin can be deemed as an ideal precursor for carbon materials such as carbon black, glassy carbon, amorphous carbon, fullerenes, carbon nanotubes, intercalation compounds, pyrolytic carbon, polymer-derived carbon, carbon fibers, and also activated carbons.

Activated carbons are carbon materials, which typically have a well-developed porous texture with a high internal surface area ranging from 500 to 2000 $m^2/g$, high thermal and chemical stability and, furthermore, with a surface chemistry that can be easily modified. These properties become those very interesting materials for different industrial applications. Several raw materials are commonly used to manufacture activated carbons, like sawdust, peat, lignite, coal, wood, residues, coconut shells, coke, among others. In addition to the nature of the precursor material, the preparation conditions have a bearing on the properties of the resulting activated carbons.

The aim of this PhD thesis is the study of valorization of different types of lignin, Organosolv (Alcell) and Kraft, by the preparation of porous carbons with different textural and

UNIVERSIDAD DE MÁLAGA

surface chemistry properties that allow a large adsorption capacity of emerging pollutants in aqueous phase and a high catalytic activity for alcohols decomposition reactions in gas phase.

Specifically, the effect of co-solution of carbon precursor and activating agent on the textural and surface chemistry properties of activated carbons prepared by chemical activation of Alcell lignin with phosphoric acid was analyzed, highlighting the possibility of using directly the liquors produced in organosolv process (Alcell) to prepare activated carbons by chemical activation with phosphoric acid. The influence of different parameters, such as $H_3PO_4$ to lignin mass ratio, activation temperature, gas atmosphere (oxidant or inert) and a further low temperature oxidative treatment on the porosity and surface chemistry of the resulting activated carbons was studied. The properties of these activated carbons were compared to those of activated carbons prepared by the conventional method of Alcell lignin impregnation with the activation agent ($H_3PO_4$) at similar preparation conditions. The activated carbons thus prepared were tested for the adsorption of an emerging contaminant (antipyrine) from water at low concentrations and at room temperature.

On the other hand, the preparation of basic activated carbons by carbonization of kraft lignin (sodium-lignosulphonate powder) at various temperatures followed by partial gasification with $CO_2$ was analyzed. The influence of the inorganic matter of the kraft lignin on the textural, surface chemistry and catalytic properties of the final activated carbons was also investigated. In this sense, the catalytic activity of the activated carbons obtained for the 2-propanol, ethanol and methanol decomposition reaction was also studied.

This thesis is divided into five chapters. The first one is a bibliographic review that provides information about (i) the different types of lignin and their valorization possibilities; (ii) the definition of activated carbons and their preparation methods; and (iii) the main applications of activated carbons, with special attention to adsorption (emerging pollutant from water) and heterogeneous catalysis (alcohol decomposition reactions) processes. Then, it is followed by a second chapter that describes the general methodology and experimental set-ups used in this thesis. Specifically, this chapter analyses the preparation of the different carbon materials, their characterization and the equipment and installations used for the adsorption and catalytic experiments.

The effect of co-solution of carbons precursor and activation agent on the on the porosity and surface chemistry properties of the activated carbons obtained by chemical activation of

UNIVERSIDAD DE MÁLAGA

lignin with phosphoric acid was analysed in chapter III. The aim of this study was to assess the possibility of directly using the liquors produced in the Organosolv process to avoid the precipitation and lignin separation stages. Alcell lignin was used as raw material for the activated carbons preparation by different procedures. Concretely, Alcell lignin was dissolved in ethanol to simulate the composition of dissolved lignin in the Organosolv liquors. The amounts of lignin and $H_3PO_4$ used were those to obtain a final $H_3PO_4$ to lignin mass ratio of 2. The samples were subsequently submitted to a low temperature oxidative treatment at 200 ºC, in air atmosphere for 1.5 h, followed by an activation treatment under inert atmosphere at 400°C. Once the activation temperature was reached the samples were cooled inside the furnace and then washed with distilled water at 60°C. For the sake of comparison, solid Alcell lignin was also directly impregnated with aqueous $H_3PO_4$, and also activated at the same previously mentioned conditions. $H_3PO_4$ impregnated lignin and the solid derived from the lignin/ethanol/$H_3PO_4$ solution, once dried, were denoted as L2P and LE2P, respectively. The two samples submitted to the oxidative treatment in air were denoted by adding the letter S to the corresponding names (L2PS and LE2PS, respectively). The final activated carbons were denoted by adding 400 (the activation temperature) to the respective notations.

Firstly, the influence of dissolving lignin in ethanol was analyzed. The normalized CPMAS $^{13}C$ NMR spectra of Alcell lignin and that dissolved in ethanol showed some variations, indicating that ethanol was not only dissolving lignin, but that certain lignin structure modification was detected. The key difference between the two spectra was in the 15-27 ppm range, which could be correlated with terminal $CH_3$ groups. The increase of this signal indicated that saturated alkyl structures accumulate after dissolution with ethanol. The FTIR spectra of both samples were also analyzed. The lignin spectrum is complicated, and the majority of the bonds observed are created by the contribution of different types of vibrations of different functional groups. Alcell lignin showed a broad band at 3410–3460 $cm^{-1}$, attributed to the hydroxyl groups in phenolic and aliphatic structures, which remained the same after dissolving with ethanol, In the sample dissolving with ethanol also appeared a band around 2965 $cm^{-1}$ related to stretching vibration of aliphatic C-H, this appearance was also suggested by CPMAS $^{13}C$ NMR spectra.

The solid derived from the lignin/ethanol/$H_3PO_4$ solution was studied by FTIR. The spectra of samples L2P and LE2P are very similar, showing a substantial reduction in bands strength at 1600, 1515 and 1425 $cm^{-1}$ associated with aromatic skeleton vibrations, as well as a band about 1460 $cm^{-1}$ associated to the C–H deformation combined with aromatic ring vibration. The band

UNIVERSIDAD DE MÁLAGA

at 635 $cm^{-1}$ in samples submitted to an oxidative treatment at 200 ºC L2PS and LE2PS suggested the development of more oxidized species of phosphorus during air treatment or the decomposition of non-stable species.

Thermal decomposition of the different impregnated samples was studied by TG analysis. In general, three different ranges can be observed in all the samples. First, there was a small weight loss at temperatures lower than 200 ºC that can be initially attributed to release of water. Water can come from the phosphoric acid solution and produced by the reaction between phosphoric acid and lignin. At temperatures lower than 150 ºC, the acid catalyzes the hydrolysis of ether linkages, leading to the formation of ketones. These and other bond cleavage reactions that proceed through ionic mechanism promotes the release of $H_2O$, CO, $CO_2$ and $CH_4$ at these low temperatures, and can contribute to the corresponding weight loss observed. Between 200 and 500 ºC, a further decrease of mass was observed associated to the release of light compounds from lignin degradation. In this temperature range, crosslinking reactions dominate over bond cleavage and de-polimerization reactions. At 250 ºC the structures are considered to be small polyaromatic units connected mainly by phosphate and polyphosphate bridges, including polyethylene linkages. As the temperature increases, cyclization and condensation reactions lead to increases in aromaticity and size of the poliaromatic units, enabled by the scission of P-O-C bonds. At temperatures higher than 500 ºC a change in the slope of the weight-loss curve can be also observed, probably associated to volatilization of carbon–oxygen complexes generated by the activation process, and to a lesser extent, to decomposition of phosphorous-compounds (as $P_2O_5$), produced by the reaction of phosphoric acid with the carbon matrix.

The results obtained from XPS analyses confirmed the presence of phosphorus groups on the surface of L2P, LE2P, L2PS and LE2PS samples. It seems that co-solution of lignin with phosphoric acid generated a higher contribution of oxidized P surface groups to the total P surface groups than the traditional impregnation process (LE2P vs L2P). On the other hand, the lower P content value observed for LE2P, when compared to that for L2P, suggests that this sample presents more P in the inner part of the lignin matrix, due probably to a better dispersion and to a more homogeneous distribution of P through the entire lignin matrix obtained by co-solution of the activating agent, phosphoric acid, and the carbon precursor, lignin. However, the amount of surface O was significantly higher for the sample prepared by co-solution of lignin and $H_3PO_4$, LE2PS, which suggests that this preparation procedure enhances the lignin oxidation process at low temperature.

UNIVERSIDAD DE MÁLAGA

## Abstract

With regard to the activated carbons, the isotherm of the activated carbon L2P400 is a type I isotherm, characteristic of a typical microporous solid. No significant changes in the $N_2$ isotherm were observed when lignin was co-dissolved with the activating agent. However, the treatment with air at 200 ºC produced solids with a remarkable increased $N_2$ adsorbed volume up to 0.4 of relative pressure. This increase in $N_2$ adsorption volume was significantly more pronounced when co-solution of lignin and phosphoric acid was carried out previously to the oxidative stabilization step (air at 200 ºC). The apparent surface area ($A_{BET}$) values considerably increased from 912 $m^2/g$, for L2P400, to 1937 $m^2/g$, for L2PS400, and to 2551 $m^2/g$, for LE2PS400. This last value is much higher than others reported in the literature for lignin-derived activated carbons using other activation methods. Only a few works reported the preparation of activated carbons from lignin with higher apparent surface areas (~3000 $m^2/g$) by using KOH activation, but at much higher activation temperatures than those used in this work. In the method here proposed, the use of lower activation temperatures would substantially decrease the cost of the obtained activated carbons, without compromising the high development of porosity. In addition, the preparation yield is around 63%, which is considerably higher than others reported in the literature for lignin and even for other lignocellulosic materials.

TPD analyses were carried out for the different activated carbons. Activated carbons prepared by chemical activation with phosphoric acid presented most of CO evolution at temperatures higher than 700 ºC, due to the presence of oxygen-containing P surface groups, which may include metaphosphates, C-O-$PO_3$ groups and C-$PO_3$ groups. In other hand, activated carbons prepared from dissolved and not-dissolved lignin are very similar, showing most of their CO release between 700 and 900 ºC. However, the treatment with air at 200 ºC and the combined use of this treatment with co-solution of lignin and the activating agent provided a higher release of CO, even at temperatures lower than 700 ºC. The sample LE2PS400 presented the highest CO evolution between 700 and 800 ºC, which suggests a higher presence of metaphosphates (C-O-$PO_3$ and/or C-$PO_3$ type) surface groups on this sample. The larger evolution of CO observed in the TPD for LE2PS400 can be associated to a higher generation of phosphate esters during the preparation process, as it was evidenced by FTIR and XPS results.

In order to analyze the influence of the oxidative treatment on the resulting activated carbons, an oxidative treatment, at different temperatures between 100 and 300 ºC, was carried to the samples prepared by co-solution of lignin with the activating agent. The results indicate that the treatment at 100 ºC is not high enough to generate large porosity development compared to the sample without any oxidative treatment. The textural properties of the sample treated at


UNIVERSIDAD DE MÁLAGA

100 ºC are very similar to those reported for the sample without any treatment. A maximum of pore volume (1.31 $cm^3/g$) and apparent surface area (2551 $m^2/g$) is obtained when the oxidative treatment is carried out at 200 ºC. An increase of this temperature to 300 ºC slightly reduced the $N_2$ adsorbed volumes. Therefore, it seems that in our experimental conditions, the presence of oxygen at intermediate temperatures, where cross-linking reactions dominate, promote the porosity development due to the creation of more phosphate esters, but at higher temperatures, where the aromatization process takes place preferentially, an excess of oxygen was counter-productive, generating an over-oxidation that would inhibit the increase of the porosity.

Chapter IV analyzes the influence of the activating agent ($H_3PO_4$) to carbon precursor (lignin) mass ratio (values from 0.6 to 5) and the activation temperature (from 300 to 900 ºC) on the textural properties of the activated carbons, prepared by co-solution of lignin and $H_3PO_4$, followed by an oxidative (air) treatment at low temperature (200 ºC) before the activation step. For the sake of comparison, activated carbons prepared by traditional impregnation of (non-solved) lignin with $H_3PO_4$, followed by the activation step at similar operation conditions of $H_3PO_4$/lignin mass ratio and activation temperature were also studied. Activated carbons with different pore size distributions were tested as adsorbents for adsorption of antipyrine in liquid phase, in batch and column experiments. The adsorption equilibrium and kinetics of antipyrine were evaluated on the different adsorbents.

Total yields values (mass of activated carbon to mass of initial lignin) from about 52%, for a low phosphoric acid to lignin mass ratio (0.6), to about 68%, for a high ratio value (4), were obtained for activated carbons prepared by co-solution of lignin/$H_3PO_4$. These values were slightly lower than those determined for activated carbons obtained by conventional impregnation of lignin (from about 62 to 71%) due to a more homogeneous and a better interaction of lignin oxygen groups and phosphoric acid in the case of co-solution of lignin with $H_3PO_4$, increasing the formation of phosphate and polyphosphate bridges, which are responsible for connecting and crosslinking the lignin fragments and for an enhancement of the oxidation process al low temperature, promoting a larger degree of activation (during the last step), with the consequent increase in the final loss of mass. The porosity of the activated carbons prepared by chemical activation of lignin or lignin co-solutions, at $H_3PO_4$ to lignin mass ratios between 0.6 and 4 and activated at 400 ºC was analyzed. For the case of conventional activation procedure, an increase in the relative amount of activation agent to lignin resulted in an increase of $N_2$ adsorption, indicating a higher development of porosity with the $H_3PO_4$ to lignin ratio. The isotherms for these activated carbons are mainly type I and exhibit an almost horizontal plateau

UNIVERSIDAD DE MÁLAGA

starting at very low relative pressure, indicating that the porosity consists predominantly of narrow micropores. With the increase of the impregnation ratio up to 4, the amount of adsorbed $N_2$ increased in the whole relative pressure range and the presence of a hysteresis loop at high relative pressures revealed a widening of the porosity, in general, with a higher contribution of mesoporosity.

The activated carbons prepared by the co-solution of lignin and phosphoric acid showed isotherms type I at low $H_3PO_4$/lignin mass ratio (0.6), very similar to that observed for the activated carbon prepared by conventional impregnation at this low ratio. As this ratio increased up to a value of 2, the amount of adsorbed $N_2$ significantly increased in the whole range of relative pressure, well above the values observed for the isotherms of the activated carbons prepared by the conventional impregnation method at equal ratios, particularly at low relative pressures, which suggests a remarkable development of the wider microporosity. A further increase of the $H_3PO_4$/lignin mass ratio up to a value of 4 gradually reduced the amount of adsorbed $N_2$, changing the isotherm profile to type IV (due to a porosity widening), in which a hysteresis loop at medium values of relative pressure was clearly observed, indicating the presence of narrow mesopores.

An increase of the relative amount of phosphoric acid compared to that of lignin would increase the formation of phosphate and polyphosphate bridges and so the connections and crosslinking of lignin fragments, with the consequent enhancement of the oxidation process at low temperature and the larger degree of activation, responsible for the significant increase of porosity development up to a $H_3PO_4$ to lignin ratio of 2 for the activated carbons prepared by co-solution of $H_3PO_4$ and lignin. In this sense, a value of $H_3PO_4$ to lignin ratio between 1 and 2 would promote the highest formation of C-O-P type groups between lignin and phosphoric acid, particularly in the case of co-solution of lignin with $H_3PO_4$, which would enhance the low temperature oxidation process. However, an excess of phosphoric acid on the surface of the carbonaceous matrix may act as a barrier for oxygen reaching the carbonaceous surface during the low temperature oxidative treatment. This could be the case for high values of $H_3PO_4$ to lignin ratio for activated carbons prepared by co-solution of lignin and $H_3PO_4$. For a $H_3PO_4$ to lignin ratio value of 4, the reactive groups of phosphoric acid would far exceed the oxygen groups of lignin, making in this case much less significant (almost negligible) the positive effect of the co-solution of lignin and $H_3PO_4$. The negative barrier impact of excess $H_3PO_4$ for the oxidation of the carbonaceous surface during the low temperature oxidative treatment explains the very similar porosity of LE4PS400 compared to that of L4P400, this last prepared by the conventional

UNIVERSIDAD DE MÁLAGA

impregnation method. The low amount of phosphoric acid involved in the case of very low value of $H_3PO_4$ to lignin ratio (0.6) did not seem to play an important role to make a significant difference in the porous texture of the final activated carbons when they were prepared by any of the two procedures.

In other hand, the $\alpha_s$ curves for the different activated carbons prepared from powder and dissolved lignin, at different $H_3PO_4$ to lignin mass ratios between 1 and 3 and at 400 ºC was also analyzed. In general, activated carbons prepared from co-solution of lignin show higher contribution of microporosity at these $H_3PO_4$ to lignin mass ratios. Linearity of the high pressure parts of the plots ($\alpha_s > 1$), associated to the multilayer region, indicates the low presence of mesopores in all the samples, independently of the procedure used. Furthermore, these $\alpha_s$ curves also present one upward swing below $\alpha_s=1$, approximately between 0.6 and 1, associated to condensation swings on supermicropores (pore sizes ≥ 1 nm). The condensation swing is more pronounced in the activated carbons obtained by co-solution of lignin and $H_3PO_4$, suggesting the generation of larger micropores at these experimental conditions.

As can be seen, it is possible to prepare lignin-derived activated carbons with apparent surface area values ($A_{BET}$) higher or equal to 2000 $m^2/g$, at 400 ºC, in a range of $H_3PO_4$/lignin mass ratios between 1 to 3, obtaining a maximum $A_{BET}$ for a value of 2. This value, $A_{BET}$=2550 $m^2/g$, is one of the most highest reported for lignin-derived activated carbons prepared by chemical activation with phosphoric acid, and even with other activation methods. In addition, the activation of co-solutions of lignin and $H_3PO_4$ produces an increase of $A_{BET}$, $V_s$ and $V_{mes}$ compared to the activated carbon prepared by its direct impregnation at the different $H_3PO_4$/lignin mass ratios evaluated. Specifically, the relative increase in the apparent surface area and the micropores volume follows the same tendency, that of a Gaussian curve, with a maximum at a $H_3PO_4$/lignin mass ratio of 2, and these values are almost twice as high as those obtained from conventional impregnation of lignin. However, the highest relative increase of mesopores volume is obtained for a $H_3PO_4$/lignin mass ratio value of 3.The micropores size distribution for the different activated carbons prepared at different $H_3PO_4$ to lignin mass ratios and at 400 ºC showed a bimodal micropore size distribution for the activated carbons prepared from powder lignin, obtaining a maximum around 6.7 Å at the lowest $H_3PO_4$ to lignin mass ratio, which is shifted to 11.1 Å at $H_3PO_4$ to lignin mass ratio of 3. Higher and narrower micropores size distribution were obtained for the activated carbons prepared from co-solution of lignin and phosphoric acid, with a $H_3PO_4$/lignin mass ratio up to 2. A maximum around 12.2 Å at $H_3PO_4$ to lignin mass ratio of 1, and at 16.6 Å at 2, as suggested the highest upward swing below $\alpha_s=1$.

UNIVERSIDAD DE MÁLAGA

In general, the increase of the $H_3PO_4$ to lignin mass ratio results in a broader micropore size distribution for both preparation methods.

The influence of the activation temperature on the textural properties of these activated carbons at a $H_3PO_4$ to lignin mass of 2 was analyzed. The increase of the activation temperature up to 400 ºC generates a significant development of the porosity, obtaining the highest volume of adsorbed $N_2$ in the entire range of relative pressures at this ratio. A further increase of the activation temperature up to 900 ºC produces a considerable reduction of this volume.

Three different adsorbents with different pore size distribution prepared by co-solution of lignin and phosphoric acid at different $H_3PO_4$/lignin mass ratios and activation temperatures were selected for the adsorption of antipyrine. Specifically, the extraction of pharmaceuticals and their metabolites from water has become a major challenge for society in recent times. Among them, antipyrine (phenazone) is an analgesic and antipyretic detected in average loads below 10 mg/day/1000 inhabitants in streams leaving wastewater treatment plants, (WWTPs), where a relatively low removal efficiency has been reported (average 35%). Adsorption on powdered activated carbons is a well-known method for water purification.

In order to study the influence of the $H_3PO_4$ to lignin mass ratio and the activation temperature on the surface chemistry of these activated carbons, TPD and XPS analyses were carried out. The results indicated the low presence of carboxylic acid, lactones and anhydrides groups. The high CO evolution of these activated carbons can be related to the presence of phosphorus functional groups and to the decomposition of phenol, carbonyl and ether groups. The amount of CO evolved is quite similar for the activated carbons prepared at the different activation temperatures, however, a displacement of the main CO peak to higher temperatures is detected with the increase of the activation temperature, which can be related to a change in the thermal stability of the oxygen surface groups. The activated carbon obtained at a $H_3PO_4$ to lignin mass ratio of 2 and activated at 800 ºC showed the highest CO evolution around 860 ºC, associated to decomposition of C-O-$PO_3$ groups.

The isotherms for the adsorption of antipyrine at 20 ºC of the selected activated carbons are of type L according to Giles classification, commonly reported in liquid-phase adsorption. The amount of antipyrine adsorbed, using an equilibrium concentration of 1 mg/l, for the activated carbon obtained at a $H_3PO_4$ to lignin mass ratio of 2 and activated at 800 ºC was higher than that of the other two activated carbons in spite of having the lowest apparent surface area value, which suggested that there was not a direct relationship between the adsorption capacity and the apparent surface area of the adsorbents, at least at these low concentrations. Nevertheless,

UNIVERSIDAD DE MÁLAGA

the micropore size distribution of these three samples reveals that the activated carbon with the highest contribution of narrower pores is that with the highest adsorption capacity of antipyrine. Attending to the molecular dimensions of antipyrine, it seems that at the low pollutant concentrations used, the micropores of size lower than 9 Å are the main responsible for the adsorption capacity. In addition, as previously mentioned, the activated carbons prepared at different $H_3PO_4$ to lignin mass ratio and activated at 400 ºC have less acidic character, like phenols, meanwhile the activated carbon obtained at a $H_3PO_4$ to lignin mass ratio of 2 and activated at 800 ºC was mainly composed of phosphorus surface groups of high thermal stability with weak-moderate acidic character, which could have more affinity with antipyrine. The equilibrium isotherm data were fitted to both Langmuir and Freundlich equations. Both models reproduce fairly well the experimental data, although lower errors were obtained with the Langmuir model. The heterogeneity index (1/n) of Freundlich equation provides an indication of how is the adsorption process, in this case, values higher than 1 suggest favorable adsorption for the three adsorbents.

The kinetics of antipyrine adsorption on the three activated carbons was also analyzed. The results obtained showed that there is an important decrease in the adsorption rate at the beginning of the contact time. After that, a second stage can be observed with intermediate decreasing rate values, which finally leads to the third part of the curve, showing negligible adsorption rates. The experimental data were fitted to the second order adsorption kinetics and to a hyperbolic equation by using the concentration of the adsorbate on the solid ($q_t$) as a function of the contact time (t). Both equations are able to reproduce fairly well the experimental data for the three activated carbons. The kinetic constant values derived from the second order kinetic equation for the antipyrine adsorption on the different activated carbons are clearly related to the values of the apparent surface areas of the activated carbons.

The antipyrine adsorption was also evaluated in column studies. The breakthrough curves for the different activated carbon fixed-beds were obtained at 20°C and 1 mg/L of antipyrine. The total adsorption capacities were calculated by the area over the breakthrough curve. The shape of the curves is of type S, typically observed for column operation with favorable adsorption isotherms. The breakthrough time for the activated carbon obtained at a $H_3PO_4$ to lignin mass ratio of 2 an activated at 800 ºC is twice those observed for the activated carbons prepared at different $H_3PO_4$ to lignin mass ratios and activated at 400 ºC. This large difference can be related to the higher volume of pores lower than 9Å for the activated carbon obtained at a $H_3PO_4$ to lignin mass ratio of 2 an activated at 800 ºC, where surface diffusion can become more important. The results exhibit that the adsorption capacities have the same tendencies as

UNIVERSIDAD DE MÁLAGA

the kinetic and equilibrium studies. Thomas model was applied to the breakthrough results to evaluate the dynamic behavior of the column. Thomas model is able to predict fairly well the adsorption capacities determined from the equilibrium study and the breakthrough times for the three adsorbents. In addition, the theoretical breakthrough curves derived from this model reproduces successfully the experimental data for these three adsorbents.

Most of the lignin in the world is produced as a by-product in the pulp and paper industry, with the most obtained from the Kraft process. The black liquors in Kraft pulp production plants are alkaline solutions. The evaporation of these black liquors yields solid lignin with a high content of sodium compounds, such as sodium hydroxide, sulfate, and lignosulfonate. This high content of Na observed in Kraft lignin makes this industrial by-product an interesting precursor for the preparation of catalysts for different applications. In this sense, the chapter V studied the preparation of activated carbons with different textural properties and surface chemistry from Kraft lignin by direct carbonization at various temperatures (500, 700, 900 ºC). The influence of a further washing treatment and partial gasification with $CO_2$ was also evaluated. The resulting activated carbons were tested as catalysts for the alcohol decomposition reaction.

The activity of the catalysts was measured by the decomposition of alcohols performed at atmospheric pressures, in a quartz fixed bed microreactor placed inside a vertical furnace with temperature control, by using an alcohol partial pressure of $Po_{AlC}$ =0.0185 atm and a space time pf $W/Fo_{Alc}$= 0.073 g s·µmol$^{-1}$.

The textural properties of the different carbon catalysts prepared at temperatures between 500-900 ºC were analyzed. The catalyst obtained by the direct carbonization at 500 ºC presents low $N_2$ adsorption volume, typical of a nonporous solid. The increase of the carbonization temperature produced a slight development of the porous structure due to the activation produced by sodium oxide when the carbonization temperature was increased. The isotherms of the catalysts obtained at 900 ºC before and after the gasification step are very similar, due to the presence of inorganic matter that hinders the development of porosity during the gasification step. In contrast, if an washing treatment is carried out, a great extent of the porosity is released due to the partial removal of the inorganic matter. The gasification of this sample (L900WG) produces a high porosity development with an apparent surface area of ~850 m$^2$/g, showing a type IV isotherm, with large presence of micropores and mesopores.

The carbonization step produces chars with a high content of oxygen surface groups, as a consequence of the oxidation of carbon and the reduction of the sulfur salts to sulfide. The

UNIVERSIDAD DE MÁLAGA

oxygenated groups are mainly quinone, carbonyl, and carbonate (sodium carbonate). The washing of these chars partially removes the sodium sulfide and, to a lesser extent, the sodium carbonate. The surface of the carbon shows a basic character with carbonyl and quinone groups and carbon basal planes (with high electron density), which can act as electron donor sites.
Alcohol molecules, mainly 2-propanol, are widely used for testing the acidic-basic character of heterogeneous catalysts. In this sense, alcohol dehydrogenation products (aldehydes and ketones) are preferentially formed on basic catalysts, while dehydration products (olefins and ethers) are favoured when acidic sites are present. The carbon materials obtained were evaluated as catalysts for the alcohol decomposition. As expected, 2-propanol conversion increases with the reaction temperature. The increase of the carbonization temperature produces an enhancement of the steady-state conversions. The catalyst carbonized at 900 showed the highest steady-state conversions of the three chars. On the other hand, the series of the carbon catalysts prepared at 900 ºC follows the sequence L900WG > L900 > L900W > L900G. The most active catalyst corresponds to the carbon with the highest development of porosity and a high dispersion of Na, meanwhile the catalyst L900G presents quite a low apparent surface area and a poor dispersion of sodium, as evidenced the SEM-EDX analyses. The catalytic test of 2-propanol decomposition supported the strong basic character of these catalysts, as alcohol was selectively transformed into acetone. All samples carbonized at 900 ºC present conversion higher than 95% at 350 ºC and selectivity to acetone greater than 95%.

Once the basic character was established, the catalyst with the highest activity for 2-propanol dehydrogenation, L900WG, was also evaluated for the ethanol and methanol decomposition. The results of conversions were not as high as expected. However, the selectivity of the catalyst was higher than 80%, yielding acetaldehyde and formaldehyde. Finally, the stability of the catalyst was also analyzed for 6 h. The conversion and selectivity for both alcohols remained the same during this reaction time.

To sum up, this study can be a starting point for the preparation of activated carbons from the liquors derived from the different pulping processes, which could boost the techno-economical feasibility of lignocellulosic biorefinery by the production of value-added products. In addition, due to the high porosity of the activated carbons prepared, and the possibility of modifying their surface chemistry, the study of alternative applications for the activated carbons here obtained would be very useful.

UNIVERSIDAD DE MÁLAGA

# Resumen

UNIVERSIDAD
DE MÁLAGA

# Resumen

La preocupación generalizada por la escasez de combustibles fósiles, el efecto invernadero, los problemas de calentamiento global y la contaminación ambiental han promovido el uso de materiales y procesos renovables. El uso de biomasa como materia prima renovable puede ser un enfoque interesante. Entre los diferentes componentes de la biomasa, la lignina está presente en las paredes celulares de la madera o de los cultivos y plantas agrícolas, a fin de proporcionar resistencia estructural.

La lignina es la segunda fuente de carbono renovable más importante después de la celulosa y la fuente más importante de compuestos aromáticos en la Tierra. Es un polímero polifenólico con una red tridimensional, pero la estructura final de la lignina aislada puede tener grandes diferencias debido a los diferentes métodos y condiciones de separación utilizados en los procesos de delignificación De hecho, el desarrollo de métodos para el aislamiento de lignina se inició para la madera en la industria papelera, aunque estos métodos también se han aplicado a diferentes hierbas, pero con un éxito limitado. La obtención de pulpa de papel también se ha llevado a cabo mediante otros procesos que usan sosa, peróxido de hidrógeno en presencia de alcalis y disolventes orgánicos (organosolv). Actualmente, el principal uso de la lignina es como combustible y generación de energía, y sólo un pequeño porcentaje de la lignina producida se comercializa en el mercado. Sin embargo, la lignina tiene también un alto potencial para su conversión en productos de alto valor añadido (productos químicos avanzados y materiales de carbono) que podrían mejorar considerablemente la economía de una biorrefinería. Debido a su alto contenido de carbono (que varía entre el 51 y el 65%), la lignina puede considerarse un precursor ideal para materiales de carbono como el negro de humo, el carbono vítreo, carbón amorfo, fulerenos, nanotubos de carbono, compuestos de intercalación, carbono pirolítico, fibras de carbono y también carbones activados.

Los carbones activos son materiales de carbono, que suelen tener una textura porosa bien desarrollada con una elevada superficie interna que oscila entre 500 y 2000 $m^2/g$, una gran estabilidad térmica y química y, además, con una química superficial fácilmente modificable. Estas propiedades los convierten en materiales muy interesantes para diferentes aplicaciones industriales. Para la fabricación de carbones activados se utilizan comúnmente varias materias primas, como serrín, turba, lignito, carbón mineral, madera, residuos, cáscaras de coco, coque, entre otros. Además de la naturaleza del material precursor, las condiciones de preparación influyen en las propiedades de los carbones activados resultantes.

UNIVERSIDAD DE MÁLAGA

El objetivo de esta tesis doctoral es el estudio de la valorización de diferentes tipos de ligninas, Organosolv (Alcell) y Kraft, mediante la preparación de carbones activos porosos con diferentes propiedades texturales y de su química superficial. Estos carbones activados se probaron como adsorbente de contaminantes emergentes en fase líquida y, directamente, como catalizadores en las reacciones de descomposición de alcoholes.

Concretamente, se analizó el efecto de la co-solución del precursor de carbono y el agente activante en las propiedades químicas y texturales de los carbones activos preparados por activación química de lignina Alcell con ácido fosfórico. El principal objetivo fue estudiar la viabilidad de utilizar directamente los licores producidos en el proceso organosolv (Alcell) para preparar carbones activos por activación química con ácido fosfórico. Se estudió la influencia de diferentes parámetros, como la relación másica $H_3PO_4$/lignina, la temperatura de activación, la atmósfera de gas (oxidante o inerte) y la realización de un tratamiento oxidante a baja temperatura sobre la porosidad y la química superficial de los carbones activos resultantes. Las propiedades de estos carbones activos se compararon con las de los carbones activados preparados por el método convencional de impregnación de lignina Alcell con el agente activante ($H_3PO_4$) en condiciones de preparación similares. Los carbones activos así preparados se probaron para la adsorción de un contaminante emergente (antipirina) en fase acuosa a bajas concentraciones y a temperatura ambiente.

Por otra parte, se analizó la preparación de carbones activos básicos mediante la carbonización de lignina kraft (polvo de lignosulfonato de sodio) a diversas temperaturas seguida de una gasificación parcial con $CO_2$. También se investigó la influencia de la materia inorgánica de la lignina kraft en la textura, la química superficial y las propiedades catalíticas de los carbones activos finales. En este sentido, también se estudió la actividad catalítica de los carbones activos obtenidos para la reacción de descomposición del 2-propanol, etanol y metanol.

Esta tesis se divide en cinco capítulos. El primero es una revisión bibliográfica que proporciona información sobre: i) los diferentes tipos de lignina y sus posibilidades de valorización; ii) la definición de los carbones activados y sus métodos de preparación; y iii) las principales aplicaciones de los carbones activados, con especial atención a los procesos de adsorción (contaminante emergente del agua) y de catálisis heterogénea (reacciones de descomposición del alcohol). A continuación, sigue un segundo capítulo que describe la metodología general y los montajes experimentales utilizados en esta tesis. Concretamente, en

UNIVERSIDAD DE MÁLAGA

este capítulo se analiza la preparación de los diferentes materiales de carbono, su caracterización y el equipo y las instalaciones utilizadas para los experimentos de adsorción y catálisis.

El efecto de la co-disolución del precursor de carbono (lignina Alcell) y el agente activante (ácido fosfórico) sobre la porosidad y la química superficial de los carbones activos obtenidos por activación química se analiza en el capítulo III, prestando especial atención a la porosidad y la química de la superficie de los carbones activos resultantes. El objetivo de este capítulo fue evaluar la posibilidad de utilizar directamente los licores producidos en el proceso Organosolv para evitar las etapas de precipitación y separación de la lignina. La lignina Alcell se utilizó como materia prima para la preparación de carbones activos por diferentes procedimientos. Concretamente, la lignina Alcell se disolvió en etanol para simular la composición de la lignina disuelta en los licores Organosolv. Las cantidades de lignina y $H_3PO_4$ utilizadas fueron de 2 (masa $H_3PO_4$/masa de lignina). Posteriormente, las muestras se sometieron a un tratamiento oxidativo a baja temperatura a 200 ºC en atmósfera de aire durante 1,5 h, seguido de un tratamiento de activación bajo atmósfera inerte a 400ºC. Una vez alcanzada la temperatura de activación, las muestras se enfriaron en el interior del horno y luego se lavaron con agua destilada a 60°C. A modo de comparación, el polvo de lignina Alcell se impregnó directamente con $H_3PO_4$, y posteriormente, se activó en las mismas condiciones anteriormente mencionadas. La lignina impregnada con $H_3PO_4$ y el sólido derivado de la solución de lignina/etanol/$H_3PO_4$ una vez seco se denominaron L2P y LE2P, respectivamente. Las dos muestras sometidas al tratamiento oxidativo en el aire se denotaron añadiendo la letra S a la nomenclatura correspondiente (L2PS y LE2PS, respectivamente). Los carbones activos finales se nombraron añadiendo 400 (la temperatura de activación) a los acrónimos correspondientes.

En primer lugar, se analizó la influencia de la disolución de la lignina en el etanol. Los espectros normalizados de RMN-CPMAS $^{13}C$ de la lignina de Alcell y de la lignina disuelta en el etanol mostraron algunas variaciones, lo que indica que el etanol no disuelve la lignina, sino que produce cierta modificación en la estructura de la lignina. La diferencia clave entre los dos espectros se encontraba en el rango de 15-27 ppm, donde aparecen los grupos terminales -$CH_3$. El aumento de esta señal indica que las estructuras alquílicas saturadas se acumulan después de la disolución con el etanol. También se obtuvieron los espectros FTIR de ambas muestras. El espectro de lignina es complicado, y la mayoría de los enlaces observados se crean por la contribución de diferentes tipos de vibraciones de diferentes grupos funcionales. La lignina Alcell muestra una banda ancha a 3410-3460 $cm^{-1}$, atribuida a los grupos hidroxilo en las

UNIVERSIDAD DE MÁLAGA

estructuras fenólicas y alifáticas, que permanece igual después de disolverse con etanol. Además, en la muestra que se disuelve con etanol también aparece una banda alrededor de 2965 $cm^{-1}$ relacionada con la vibración de estiramiento de la C-H alifática, de acuerdo a los resultados obtenidos mediante RMN-CPMAS $^{13}C$.

El sólido resultante de la mezcla de lignina/etanol/$H_3PO_4$ también fue estudiado mediante FTIR. Los espectros de las muestras L2P y LE2P son muy similares, mostrando una reducción sustancial en la intensidad de las bandas a 1600, 1515 y 1425 $cm^{-1}$, asociada a las vibraciones del esqueleto aromático, así como una banda a unos 1460 $cm^{-1}$ asociada a la deformación C-H, combinada con la vibración del anillo aromático. La banda que aparecía a 635 $cm^{-1}$ en las muestras sometidas a un tratamiento oxidativo a 200 ºC L2PS y LE2PS sugería el desarrollo de más especies oxidadas de fósforo durante el tratamiento del aire o a la posible descomposición de especies a esta temperatura.

La descomposición térmica de las diferentes muestras impregnadas se estudió mediante análisis de termogravimetría (TG). En general, se pueden observar tres rangos diferentes en todas las muestras. En primer lugar, hay una pequeña pérdida de peso a temperaturas inferiores a 200 ºC que puede atribuirse inicialmente a la liberación de agua. El agua puede provenir de la solución de ácido fosfórico y producirse por la reacción entre el ácido fosfórico y la lignina. A temperaturas inferiores a 150 ºC, el ácido cataliza la hidrólisis de los enlaces del éter, lo que conduce a la formación de cetonas. Éstas y otras reacciones de ruptura de enlaces, que transcurren mediante un mecanismo iónico, promueven la liberación de $H_2O$, CO, $CO_2$ y $CH_4$ a estas bajas temperaturas, y pueden contribuir a la correspondiente pérdida de peso observada. Entre 200 y 500 ºC, se observa una mayor disminución de masa asociada a la liberación de compuestos ligeros procedentes de la degradación de la lignina. En este rango de temperaturas, las reacciones de entrecruzamiento dominan sobre las reacciones de ruptura de enlaces y de despolimerización. A 250 ºC se considera que las estructuras son pequeñas unidades poliaromáticas conectadas principalmente por puentes de fosfato y polifosfato. A medida que aumenta la temperatura, las reacciones de ciclación y condensación dan lugar a aumentos en la aromaticidad y el tamaño de las unidades poliaromáticas, lo que es posible gracias a la escisión de los enlaces P-O-C. A temperaturas superiores a 500 ºC también se puede observar un cambio en la pendiente de la curva de pérdida de peso, probablemente asociado a la volatilización de los complejos carbono-oxígeno generados por el proceso de activación y, en menor medida, a la descomposición de los compuestos de fósforo (como el $P_2O_5$), producida por la reacción del ácido fosfórico con la matriz de carbono.

UNIVERSIDAD DE MÁLAGA

Los resultados obtenidos de los análisis XPS confirmaron la presencia de grupos de fósforo en la superficie de las muestras L2P, LE2P, L2PS y LE2PS. Parece que la co-solución de la lignina con el ácido fosfórico genera una mayor contribución de los grupos superficiales de P oxidados con respecto a los grupos superficiales de P totales que el proceso de impregnación tradicional (LE2P vs L2P). Por otra parte, el menor valor del contenido de P observado para el LE2P, cuando se compara con el de L2P, sugiere que esta muestra presenta más fósforo en la parte interna de la matriz de lignina, debido probablemente a una mejor dispersión y a una distribución más homogénea del fósforo a través de toda la matriz de lignina, obtenida por la co-solución del agente activante, el ácido fosfórico, y el precursor de carbono, la lignina. Sin embargo, la cantidad de oxígeno superficial fue significativamente mayor para la muestra preparada por co-solución de lignina y $H_3PO_4$, LE2PS, lo que sugiere que este procedimiento de preparación mejora el proceso de oxidación de lignina a baja temperatura.

En cuanto a los carbones activos, la isoterma del carbón activo L2P400 es una isoterma de tipo I, característica de un sólido típicamente microporoso. No se observaron cambios significativos en la isoterma de $N_2$ cuando la lignina fue co-disuelta con el agente activante. Sin embargo, el tratamiento con aire a 200 ºC produjo sólidos con un notable aumento del volumen de $N_2$ adsorbido hasta 0,4 de presiones relativas. Este aumento del volumen de $N_2$ adsorbido fue significativamente más pronunciado cuando se llevó a cabo la co-solución de lignina y ácido fosfórico previamente a la etapa de estabilización oxidativa (aire a 200 ºC). En cuanto a los parámetros texturales, los valores del área superficial aparente ($A_{BET}$) aumentaron considerablemente de 912 $m^2/g$, para el L2P400, a 1937 $m^2/g$, para el L2PS400, y a 2551 $m^2/g$, para el LE2PS400. Este último valor es mucho más alto que otros que aparecen en bibliografía para carbones activos derivados de lignina que utilizan otros métodos de activación. Sólo unos pocos trabajos han publicado la preparación de carbones activos a partir de lignina con superficies aparentes más elevadas (~3000 $m^2/g$), sin embargo, se obtuvieron mediante activación con KOH, a temperaturas de activación mucho más altas que las utilizadas en este trabajo. En el método aquí propuesto, el uso de temperaturas de activación más bajas disminuiría sustancialmente el coste de los carbones activos obtenidos, sin comprometer el alto desarrollo de la porosidad. Además, el rendimiento de la preparación es de alrededor del 63%, lo que es considerablemente mayor que otros publicados en la literatura para la lignina, e incluso para otros materiales lignocelulósicos.

Para analizar la cantidad y tipo de grupos oxigenados superficiales se realizaron análisis de desorción térmica programada (DTP) sobre los diferentes carbones activos. Los carbones

UNIVERSIDAD DE MÁLAGA

activos preparados por activación química con ácido fosfórico presentaron la mayor parte de la evolución de CO a temperaturas superiores a 700 ºC, debido a la presencia de grupos superficiales de fósforo, que pueden incluir polifosfatos y metafosfatos (grupos C-O-$PO_3$ y grupos C-$PO_3$). Por otra parte, los carbones activos preparados a partir de la lignina disuelta o por el método convencional son muy similares, mostrando la mayor parte de la evolución de CO entre 700 y 900 ºC. Sin embargo, el tratamiento con aire a 200 ºC y el uso combinado de este tratamiento con la co-solución de lignina y el agente activante proporcionó una mayor descomposición de grupos en forma de CO, incluso a temperaturas inferiores a 700 ºC. Es decir,la muestra LE2PS400 presentó la mayor descomposición de grupos en forma de CO entre 700 y 800 ºC, asociada a la presencia de grupos superficiales de fósforo (tipo C-O-$PO_3$ y/o C-$PO_3$) formados durante el proceso de preparación, como sugerían los resultados de FTIR y XPS.

Para analizar la influencia del tratamiento oxidativo en los carbones activos resultantes, las muestras preparadas por co-solución de lignina con el agente activante fueron sometidas a un tratamiento oxidativo, a diferentes temperaturas entre 100 y 300 ºC. Los resultados indican que el tratamiento a 100 ºC no es lo suficientemente alto como para generar un gran desarrollo de porosidad en comparación con la muestra sin ningún tratamiento oxidante. Los parámetros texturales de la muestra tratada a 100 ºC son muy similares a los de la muestra sin ningún tratamiento. Sin embargo, cuando el tratamiento oxidante se lleva a cabo a 200 ºC se obtiene un valor máximo de volumen de poro (1,31 $cm^3/g$) y de área superficial aparente (2551 $m^2/g$). Finalmente, cuando el tratamiento oxidante se realiza a 300 ºC, se observa una disminución significativa del área superficial aparente hasta 2128 $m^2/g$. Estos resultados sugieren que, en nuestras condiciones experimentales, la presencia de oxígeno a temperaturas intermedias, en las que predominan las reacciones de entrecruzamiento, favorece el desarrollo de la porosidad debido a la creación de más ésteres de fosfato, pero a temperaturas más altas, en las que el proceso de aromatización tiene lugar de forma preferente, un exceso de oxígeno resulta contraproducente, generando una sobre oxidación que inhibiría el aumento de la porosidad.

En el capítulo IV se analiza la influencia de la relación másica $H_3PO_4$/lignina y la temperatura de activación en las propiedades texturales de los carbones activos y se comparó con el uso lignina en polvo. De entre los carbones activos obtenidos, se seleccionaron tres carbones activos con distribución de tamaños de poros diferentes para ser usados como adsorbentes de antipirina en fase líquida. Para ello, se realizaron experimentos en discontinuo y en continuo (en columna), donde se analizaron tanto el equilibrio de adsorción, como la cinética de adsorción de antipirina en los diferentes adsorbentes.

UNIVERSIDAD DE MÁLAGA

Se analizó la influencia de la relación de masa de $H_3PO_4$/masa de lignina y la temperatura de activación en las propiedades texturales de los carbones activos y se comparó con los carbones preparados a partir lignina en polvo mediante el método convencional. La cantidad de masa de $H_3PO_4$/masa de lignina se varió de 0 a 4 y las temperaturas de activación entre 300 y 900 °C. En estas condiciones, se obtuvieron carbones activados con rendimientos totales entre el 52 y el 68%, siendo estos valores menores a los obtenidos mediante la activación directa de la lignina impregnada (del 62 al 71%). Esta disminución se debe a una mejor y más homogénea interacción de los grupos oxigenados de la lignina con el ácido fosfórico, lo que provoca un aumento de los puentes fosfatos y/o polifosfatos, encargados de conectar y entrecruzar los fragmentos de lignina. Además, la presencia de estas conexiones aumenta con el proceso oxidativo a baja temperatura, lo que promueve un mayor grado de activación, y por tanto, una mayor pérdida de masa.

La porosidad de los carbones activos preparados por activación química de lignina y co-solución de lignina y el agente activante, a relaciones de masa $H_3PO_4$/masa de lignina entre 0.6 y 4 y activados a 400 ºC fue también analizada. En general, un aumento en la cantidad relativa de agente activante resulta en un mayor desarrollo de la porosidad. Las isotermas de los carbones activos obtenidos por el método convencional son principalmente del tipo I y presentan una meseta casi horizontal que comienza a una presión relativa muy baja, lo que indica la presencia predominantemente de microporos estrechos. Con el aumento de la relación de masa de $H_3PO_4$/masa de lignina hasta 4, se produce un aumento de la cantidad de $N_2$ adsorbida en todo el rango de presiones relativas y aparece un ciclo de histéresis a altas presiones relativas, lo que sugiere el ensanchamiento de la estructura porosa, con una mayor contribución de la mesoporosidad.

Los carbones activos preparados por co-solución de lignina muestran isotermas tipo I a bajas relaciones de masa de $H_3PO_4$/masa de lignina (0,6), muy similares a las obtenidas por el método convencional. Pero al aumentar la cantidad de agente activante hasta relaciones de 2, la cantidad de $N_2$ adsorbida aumenta significativamente en todo el rango de presiones relativas, si se comparan con las isotermas obtenidas por el método convencional a las mismas cantidades de agente activante. Eso ocurre sobre todo a bajas presiones relativas, lo que sugiere un considerable desarrollo de la microporosidad. Un aumento hasta relaciones másicas $H_3PO_4$/lignina hasta 4 provoca una reducción del $N_2$ adsorbido, obteniéndose, en estos casos, carbones activos con isotermas tipo IV, en las que aparece un ciclo de histéresis a presiones relativas intermedias, asociado a la presencia de mesoporos estrechos.

UNIVERSIDAD DE MÁLAGA

El aumento de la cantidad relativa de $H_3PO_4$/lignina, a valores en torno a 2, para el caso de la co-solución de la lignina y el agente activante, parece favorecer la formación de puentes fosfatos y/o polifosfatos, y por tanto, las conexiones y entrecruzamientos de los fragmentos de la lignina, que junto con la mejora asociada al tratamiento oxidativo a baja temperatura, aumenta el grado de activación, y produce un desarrollo significativo de la porosidad. En este sentido, valores de relaciones másicas $H_3PO_4$/lignina entre 1 y 2 parecen promover la formación de enlace C-O-P entre la lignina y el ácido fosfórico, particularmente en el caso de la co-solución de la lignina y el agente activante, que incluso aumentaría las mejoras proporcionadas por el proceso oxidativo a bajas temperaturas. Sin embargo, debido al efecto retardante de la oxidación del ácido fosfórico, un exceso del mismo sobre la superficie de la lignina actuaría como una barrera, evitando la oxidación de la matriz carbonosa durante este proceso oxidativo. Esto podría explicar el casi despreciable aumento de la porosidad de los carbones activos preparado por co-solución de la lignina y el agente activante, a altas relaciones másicas $H_3PO_4$/lignina (4), cuando se comparan con aquellos obtenidos a estas mismas relaciones, pero mediante el método convencional de preparación. A bajas relaciones másicas $H_3PO_4$/lignina (0,6), la cantidad de ácido fosfórico no parece suficiente como para provocar una mejora considerable en la estructura porosa de los carbones activos obtenidos mediante ambos procedimientos.

Por otro lado, también se analizaron las curvas $\alpha_s$ de los diferentes carbones activos preparados a partir de polvo de lignina y la co-disolución de la lignina y el agente activante, a diferentes proporciones de masa de $H_3PO_4$/masa de lignina entre 1 y 3 y a 400 ºC. En general, los carbones activos preparados a partir de la co-solución de lignina muestran una mayor contribución de microporosidad, a estas relaciones de masa de $H_3PO_4$/ masa de lignina, independientemente del método de preparación usado. Los resultados sugieren que el uso de la co-solución de lignina y $H_3PO_4$ produce un aumento de la microporosidad más ancha en comparación con el carbón activo preparado por su impregnación directa.

Los resultados evidencian que mediante este método de preparación se pueden obtener carbones activos con área superficial aparente mayor de 2000 $m^2/g$ a 400 ºC, en un rango de relaciones másicas $H_3PO_4$/lignina entre 1 y 3. El máximo valor obtenido, $A_{BET}$=2550 $m^2/g$, es uno de los mayores valores publicados en bibliografía para carbones activos preparados a partir de lignina. Además, se observa que el aumento relativo de la superficie aparente y del volumen de los microporos sigue la misma tendencia, obteniéndose una curva gaussiana, con un máximo en 2, donde estos valores son casi el doble de los obtenidos por el método convencional. Sin

UNIVERSIDAD DE MÁLAGA

embargo, el mayor aumento relativo del volumen de mesoporos se obtiene para la relación masa de $H_3PO_4$/ masa de lignina de 3.

La distribución del tamaño de microporos para los diferentes carbones activos preparados a diferentes relaciones de masa de $H_3PO_4$/masa de lignina y a 400 ºC mostró una distribución bimodal del tamaño de microporos para los carbones activos preparados a partir de lignina en polvo por el método convencional, obteniéndose un máximo de alrededor de 6,7 Å en la relación de impregnación más baja, que se desplaza a 11. 1 Å para la relación de impregnación de 3. La distribuciones de tamaño de microporos se vuelven más altas y más estrechas para los carbones activos preparados a partir de la co-solución de lignina y $H_3PO_4$ hasta relaciones masa de $H_3PO_4$/ masa de lignina de 2, obteniéndose un máximo alrededor de 12,2 Å para la relación masa de $H_3PO_4$/masa de lignina de 1, y de 16,6 Å a 2. En general, el aumento de la relación de masa de $H_3PO_4$/masa de lignina da lugar a una distribución de microporos más ancha mediante ambos métodos de preparación.

Por otro lado, se analizó la influencia de la temperatura de activación en las propiedades texturales de los carbones activos obtenidos a una relación masa de $H_3PO_4$/masa de lignina de 2. El aumento de la temperatura de activación hasta 400 ºC generó un desarrollo significativo de la porosidad, obteniendo un mayor volumen de $N_2$ adsorbido en todo el rango de presiones relativas. Un aumento adicional hasta 900 ºC produjo una considerable reducción de este volumen.

Tres carbones activos con diferente distribución de tamaños de poros, obtenidos a diferentes relaciones masa de $H_3PO_4$/masa de lignina y temperaturas de activación, fueron usados como adsorbentes para la eliminación de contaminantes emergentes en fase líquida. Específicamente, la extracción de productos farmacéuticos y sus metabolitos del agua se ha convertido en un gran desafío para la sociedad en los últimos tiempos. Entre ellos, la antipirina (fenazona) es un analgésico y antipirético que se detecta en cargas medias inferiores a 10 mg/día/1000 habitantes en los cursos de agua que salen de las depuradoras, donde se ha informado de una eficiencia de eliminación relativamente baja (media del 35%). La adsorción en carbones activados en polvo es un método bien conocido de purificación del agua.

Con el fin de estudiar la influencia de la relación de masa de $H_3PO_4$/ masa de lignina y la temperatura de activación en la química superficial de estos carbones activos, se realizaron análisis mediante DTP y XPS. Los resultados indicaron la baja presencia de ácidos carboxílicos, lactonas y grupos de anhídridos. La elevada evolución de CO de estos carbones activos puede relacionarse con la presencia de grupos funcionales de fósforo y con la descomposición de

UNIVERSIDAD DE MÁLAGA

grupos fenólicos, carbonilos y éteres. La cantidad de CO liberado es bastante similar para los carbones activos preparados a las diferentes temperaturas de activación, sin embargo, con el aumento de la temperatura de activación se detecta un desplazamiento del pico principal de CO a temperaturas más altas, lo que puede relacionarse con un cambio en la estabilidad térmica de los grupos superficiales de oxígeno. El carbón activo obtenido a una relación de masa de $H_3PO_4$/ masa de lignina de 2 y activado a 800 ºC mostró la mayor evolución del CO en torno a 860 ºC, asociada a la descomposición de los grupos C-O-$PO_3$.

Las isotermas de adsorción de antipirina obtenidas sobre los carbones activos seleccionados a 20 ºC son de tipo L, según la clasificación de Giles, típicamente usadas en la adsorción en fase líquida. La cantidad de antipirina adsorbida para el carbón activo preparado a una relación masa de $H_3PO_4$/masa de lignina de 2 y activado a 800 ºC, y utilizando una concentración de equilibrio de antipirina de 1 mg/l, fue mayor que la de los otros dos carbones a pesar de tener un valor de área superficial aparente más bajo, lo que sugiere que no hay una relación directa entre la capacidad de adsorción y el área superficial aparente de los adsorbentes, al menos a estas bajas concentraciones. No obstante, la distribución del tamaño de microporos de estas tres muestras revela que el carbón activo con la mayor contribución de poros más estrechos es el que tiene la mayor capacidad de adsorción de antipirina. Atendiendo a las dimensiones moleculares de la antipirina, parece que, a las bajas concentraciones de antipirina utilizadas, los microporos de tamaño inferior a 9 Å son los principales responsables de la capacidad de adsorción. Además, los carbones activos preparados a relaciones de masa de $H_3PO_4$/masa de lignina diferentes y activados a 400 ºC, tienen un carácter menos ácido, mientras que el carbón activo obtenido a una relación de masa de $H_3PO_4$/masa de lignina de 2 y activado a 800 ºC presenta principalmente grupos superficiales de fósforo de alta estabilidad térmica con carácter ácido débil-moderado, que podrían tener más afinidad por la antipirina. Los datos de la isoterma de equilibrio se ajustaron a las ecuaciones de Langmuir y Freundlich. Ambos modelos reproducen bastante bien los datos experimentales, aunque se obtuvieron menores errores con el modelo de Langmuir. El índice de heterogeneidad (1/n) de la ecuación de Freundlich proporciona una indicación de cómo es el proceso de adsorción, en este caso, los valores superiores a 1 sugieren una adsorción favorable para los tres adsorbentes.

También se analizó la cinética de la adsorción de antipirina en los tres carbones activos. Los resultados obtenidos mostraron que hay una importante disminución en la velocidad de adsorción al comienzo del tiempo de contacto. Después de eso, se puede observar una segunda etapa con valores intermedios de velocidad decreciente, que finalmente conduce a la tercera

UNIVERSIDAD DE MÁLAGA

parte de la curva, mostrando velocidades de adsorción insignificantes. Los datos experimentales se ajustaron a una cinética de adsorción de segundo orden y a una ecuación hiperbólica utilizando la concentración de adsorbato en el sólido en función del tiempo de contacto. Ambas ecuaciones son capaces de reproducir bastante bien los datos experimentales con los tres carbones activos. Los valores de la constante cinética derivados de la ecuación cinética de segundo orden para la adsorción antipirina en los diferentes carbones activos están claramente relacionados con los valores de las áreas superficiales aparentes de los carbones activos.

La adsorción de antipirina también se evaluó en experimentos en columna. Las curvas de ruptura para los diferentes carbones activos se obtuvieron en lecho fijo a 20°C y 1 mg/L de antipirina. Las capacidades totales de adsorción se calcularon mediante el área sobre la curva de ruptura. La forma de las curvas es de tipo S, típicamente observada para el funcionamiento en columna con isotermas de adsorción favorables. El tiempo de ruptura del carbón activo obtenido a una relación de masa de $H_3PO_4$/masa de lignina de 2 y activado a 800 ºC es el doble del observado para los carbones preparados con diferentes masas de $H_3PO_4$/masa de lignina y activados a 400 ºC. Esta gran diferencia puede relacionarse con el mayor volumen de poros inferior a 9Å del carbón activado, LE2PS800, donde la difusión superficial puede ser más importante. Los resultados muestran que las capacidades de adsorción tienen las mismas tendencias que los estudios cinéticos y de equilibrio.

El modelo de Thomas se aplicó para evaluar el comportamiento dinámico de la columna. Éste modelo fue capaz de predecir bastante bien las capacidades de adsorción determinadas a partir del estudio de equilibrio y los tiempos de ruptura para los tres adsorbentes. Además, las curvas de ruptura predichas por este modelo reproducen bastante bien los datos experimentales para los tres adsorbentes.

En otro bloque de la tesis, dentro del capítulo V se estudió la preparación de carbones activos con diferentes propiedades texturales y química superficiales a partir de la lignina Kraft mediante carbonización directa a diversas temperaturas (500, 700, 900 ºC). La mayor parte de la lignina en el mundo se produce como subproducto en la industria de la pulpa y el papel, siendo mayoritario el proceso Kraft. Los licores negros de las plantas de producción de pulpa de papel mediante el proceso Kraft son soluciones alcalinas. La evaporación de estos licores negros produce una lignina sólida con un alto contenido de compuestos de sodio, como hidróxido de sodio, sulfato y lignosulfonato. Este alto contenido de Na que se observa en la

UNIVERSIDAD DE MÁLAGA

lignina Kraft la convierte en un precursor interesante para la preparación de catalizadores para diferentes aplicaciones. En este sentido, se evaluó la influencia de esta materia inorgánica mediante un tratamiento de lavado y de una gasificación parcial con $CO_2$. Los carbones activados resultantes se probaron como catalizadores para la reacción de descomposición de alcoholes. La actividad de los catalizadores para la descomposición de los alcoholes se evaluó a presión atmosférica, en un microreactor de lecho fijo de cuarzo colocado dentro de un horno vertical con control de temperatura. La presión parcial del alcohol usada fue de $Po_{Alcohol}$ =0.0185 atm y el tiempo espacial utilizado de $W/Fo_{Alcohol}$ = 0.073 g s-µmol$^{-1}$.

Inicialmente se evaluaron las propiedades texturales de los diferentes carbones preparados mediante la carbonización directa a temperaturas entre 500-900 ºC. El catalizador obtenido por carbonización directa a 500 ºC presenta una baja adsorción de $N_2$, típica de un sólido no poroso. El aumento de la temperatura de carbonización produjo un ligero desarrollo de la estructura porosa debido a la activación producida por el óxido de sodio al aumentar la temperatura de carbonización. Las isotermas de los catalizadores no lavados obtenidos a 900 ºC antes y después de la etapa de gasificación son muy similares, debido a la presencia de materia inorgánica que impide el desarrollo de la porosidad durante la etapa de gasificación. En cambio, si se realiza un tratamiento de lavado, se libera una gran parte de la porosidad debido a la eliminación parcial de la materia inorgánica. La gasificación de esta muestra (L900WG) produce un alto desarrollo de la porosidad, obteniendo una superficie de ~850 m$^2$/g, y una isoterma tipo IV, con gran presencia de microporos y mesoporos.

La etapa de carbonización produce una gran cantidad de grupos superficiales de oxígeno, como consecuencia de la oxidación de la superficie y la reducción de las sales de azufre a sulfuro. Estos grupos superficiales de oxígeno son principalmente grupos quinonas, carbonilos y carbonatos (carbonato de sodio). El lavado de estos carbonizados elimina parcialmente el sulfuro de sodio y, en menor medida, el carbonato de sodio. La superficie de estos carbonizados muestra un carácter básico con grupos carbonilos y quinonas y planos basales de carbono (con alta densidad de electrones), que pueden actuar como sitios donantes de electrones.

Las moléculas de alcohol, principalmente el 2-propanol, se utilizan ampliamente para evaluar el carácter ácido-básico de catalizadores heterogéneos. En este sentido, los productos de deshidrogenación del alcohol (aldehídos y cetonas) se forman preferentemente en sitios básicos, mientras que los productos de deshidrogenación (olefinas y éteres) se ven favorecidos

UNIVERSIDAD DE MÁLAGA

cuando hay sitios ácidos. Los carbones obtenidos se evaluaron como catalizadores para la descomposición de 2-propanol. Como era de esperar, la conversión de 2-propanol aumenta con la temperatura de reacción. El aumento de la temperatura de carbonización produce un aumento de las conversiones en estado estacionario, siendo el carbonizado obtenido a 900 ºC, el catalizador con las mayores conversiones en estado estacionario de los tres carbonizados. Por otro lado, la serie de los catalizadores preparados a 900 ºC sigue la secuencia L900WG (lavado y gasificado) > L900 > L900W (lavado) > L900G (gasificado). El catalizador más activo, L900WG, corresponde al carbón con mayor desarrollo de porosidad y una alta dispersión de Na, mientras que el peor, fue el catalizador L900G (gasificado), que presenta un área superficial aparente bastante baja, junto con una pobre dispersión del sodio, como evidencian los análisis SEM-EDX. Los resultados de la descomposición del 2-propanol sugieren el fuerte carácter básico de estos catalizadores, ya que el alcohol se transformó selectivamente en acetona. Todas las muestras carbonizadas a 900 ºC presentan una conversión superior al 95% a 350 ºC y una selectividad a acetona también superior al 95%.

Una vez establecido el carácter básico, el catalizador de mayor actividad para la deshidrogenación de 2-propanol, L900WG, también se evaluó para la descomposición de etanol y metanol. Las conversiones obtenidas no fueron tan altas como se esperaba. Sin embargo, la selectividad del catalizador fue superior al 80%, produciéndose acetaldehído y formaldehído, respectivamente. Finalmente, la estabilidad del catalizador también fue analizada durante 6 h de operación. La conversión y la selectividad de ambos alcoholes se mantuvieron constantes durante todo ese tiempo de reacción.

Como conclusión final, es importante resultar que este estudio puede ser un punto de partida para la preparación de carbones activados a partir de los licores derivados de los diferentes procesos de pulpeo, lo que podría potenciar la viabilidad tecno-económica de las biorrefinería lignocelulósicas mediante la producción de productos de alto valor añadido. Además, debido a la alta porosidad de los carbones activados preparados y a la posibilidad de modificar su química superficial con alta facilidad, sería muy útil el estudio de aplicaciones alternativas para los carbones activados aquí obtenidos.

UNIVERSIDAD DE MÁLAGA

# ملخص

UNIVERSIDAD
DE MÁLAGA

## ملخص

القلق المفرط بشأن ندرة الوقود الأحفوري، قضايا الإحتباس الحراري، والتلوث البيئي، حث على استخدام مواد متجددة صديقة للبيئة. إستعمال الكتلة الحيوية كمواد خام متجددة يمكن أن يكون نهجا مثيرًا للإهتمام. من بين مكونات الكتلة الحيوية المختلفة، اللجنين المتواجد في جدران الخلايا من الخشب أو المحاصيل الزراعية والنباتات، من أجل توفير القوة الهيكلية.

اللجنين هو ثاني أكبر مصدر متجدد للكربون بعد السليلوز، وأهم مصدر للمركبات العطرية على الأرض. هو عبارة عن بولي فينول البوليمر مع شبكة ثلاثية الأبعاد. قد يكون لهيكل اللجنين اختلافات كبيرة نظرا لأساليب العزل المختلفة. في الواقع هناك عدة طرق متطورة تُكرَّس لعزل اللجنين من المواد الخشبية عن طريق عمليات اللباب الصناعية مثل صناعات لب الورق والورق (أي كرافت أو الليجنوسولفونات) أو مواد وسيطة جديدة خاصة بمخطط المصافي البيولوجية (Organosolv). حاليا، الاستخدام الرئيسي للجنين هو توليد الوقود والطاقة، وفقط نسبة قليلة يجرى تسويقها. ومع ذلك، يمكن استخدام اللجنين في مجموعة واسعة من التطبيقات، بدءا من الوقود إلى المواد الكيميائية والمواد المتقدمة. نظرًا لمحتواه العالي من الكربون (يتراوح بين51 و65%)، يمكن اعتباره مصدر مثالي للمواد الكربونية مثل الكربون الأسود، الكربون الزجاجي، الكربون غير المتبلور، الأوفيين، والأنابيب الكربونية النانوية والكربون المشتق من البوليمر، ألياف الكربون، والفحم المنشط أيضًا.
الكربونات المنشطة هي مواد كربونية، والتي عادة ما يكون لها بنية مسامية متطورة مع مساحة سطح داخلية عالية تتراوح بين 500 إلى 2000 م$^2$/ غ، وإستقرار حراري وكيميائي عالي، وعلاوة على ذلك، يمكن تعديل كيمياء أسطحها بسهولة وبذلك تصبح هذه الخصائص مثيرة جدا للإهتمام لمختلف التطبيقات الصناعية لتلك المواد. ويمكن إستخدام عدة مواد لإنتاج الكربون المنشط، من بينها، المواد الليجنوسيليلوزية التي تعتبر أحسن مصدرلإنتاج الكربونات المسامية مثل نشارة الخشب، الخث، الليجنين، الفحم، مخلفات الخشب، قشورجوزالهند، فحم الكوك، الخ. بالإضافة إلى طبيعة المواد الأولية، لظروف التحضير تأثير واضح على خصائص الفحم المنشط الناتج.

إن الهدف وراء هذه الرسالة هو تثمين أنواع مختلفة من اللجنين (Organosolv Alcell) والكرافت، من خلال إعداد الكربونات المنشطة المسامية مع خصائص أسطح وكيمياء سطحية مختلفة. تم إختبارهذه الكربونات المنشطة في عملية إمتزازالملوثات في الحالة السائلة وكذلك كمحفز لتفاعلات تحلل الكحول.

أولاً، تم تقييم إمكانية الاستخدام المباشر للمشروبات الكحولية المنتجة في عملية اورجانوسولف السال (Alcell) لإعداد الكربونات المنشطة عن طريق التنشيط الكيميائي مع حمض الفوسفوريك. في هذا السياق، تم التحقيق في تأثير المحلول المشترك لمصدر الكربون (السل لجنين) وعامل التنشيط (حمض الفوسفوريك) على الخصائص النسيجية وكيمياء السطح للكربونات المنشطة الناتجة. تمت مقارنة خصائص هذه الكربونات المنشطة بخصائص الكربونات المنشطة التي تم إعدادها عن طريق خلط لجنين السيل مباشرة مع عامل التنشيط (حمض الفوسفوريك).
من ناحية أخرى، تمت دراسة الكربونات المنشطة الأساسية التي يتم إعدادها عن طريق التنشيط الفيزيائي لكرافت لجنين (مسحوق اللجنين الصوديوم- لقنوسلفونات) حيث هذا النوع من اللجنين يحتوي على نسبة مواد غير عضوية كبيرة. كما تم

UNIVERSIDAD DE MÁLAGA

التحقيق في تأثير خطوة الغسل لإزالة هذه المادة غير العضوية والتغويز الجزئي مع ثاني أكسيد الكربون. ليتم استخدام الكربون المنشط الذي تم الحصول عليه كمحفزات لتفاعل تحلل الكحول 2-بروبانول والإيثانول والميثانول.

تنقسم هذه الرسالة إلى خمسة فصول. يعرض الأول دراسة مراجع توفر معلومات حول الأنواع المختلفة للجنين وإمكانيات تقييمها. تعريف الكربون المنشط وطرق إعداده؛ والتطبيقات الرئيسية للكربونات المنشطة، مع إيلاء إهتمام خاص للتطبيقات كالإمتزاز في الحالة السائلة وكمحفز لتفاعلات تحلل الكحول. ثم يتبعها فصل ثان يطور المنهجية العامة والإعدادات التجريبية المستخدمة. على وجه التحديد، الفصل يحلل طرق إعداد مواد الكربون المختلفة، خصائصها والمعدات المستخدمة في عمليات الإمتزاز وتجارب التحفيز.

تم تحليل تأثير المحلول المشترك لمصادر الكربونات وعامل التنشيط على خصائص الكربونات المنشطة التي تم الحصول عليها عن طريق التنشيط الكيميائي للجنين بحمض الفوسفوريك في الفصل الثالث، مع إعطاء إهتمام خاص لمسامية وكيمياء السطح للكربونات المنشطة الناتجة. وكان الهدف من هذه الدراسة تقييم إمكانية إستخدام المشروبات الكحولية المنتجة مباشرة في عملية التحليل-العضوي لتجنب مراحل فصل اللجنين المستعمل في طرق المعالجة. وقد أُستخدم آلسيل لجنين كمادة خام لإعداد الكربونات المنشطة من قبل بوسائل مختلفة. أين تم إذابة آلسيل لجنين في الإيثانول لمحاكاة تكوين اللجنين في سوائل التحليل العضوي. وكانت كميات اللجنين وحمض الفوسفوريك المستخدمة متوافقة للحصول على نسبة حمض/كتلة اللجنين تساوي 2. وضعت العينات فيما بعد تحت معالجة أكسدة ذات درجة حرارة منخفضة عند 200 درجة مئوية، بوجود الهواء لمدة ساعة واحدة، يليها علاج التنشيط بوجود الهواء الخامل عند 400 درجة مئوية. بمجرد الوصول إلى درجة حرارة التنشيط المرغوبة تم تبريد العينات داخل الفرن ثم غسلها بالماء المقطر عند 60 درجة مئوية. من أجل المقارنة، تم غمس آلسيل اللجنين مباشرة مع حمض الفوسفوريك، وأيضا تفعيلها في نفس الشروط المذكورة سابقا. اللجنين المغمس بحمض الفوسفوريك والمواد الصلبة المستمدة من محلول اللجنين / الإيثانول / $H_3PO_4$ بعد تجفيفها، تم تسميتها ب L2P وLE2P على التوالي. وقد أشير إلى العينتين المعالجتين بالأكسدة في الهواء بإضافة الحرف S إلى الإسمين الموافقين (L2PS و LE2PS، على التوالي). تم الإشارة إلى الكربونات المنشطة النهائية بإضافة 400 (درجة حرارة التنشيط) إلى ذات التسميات.

أولاً، تم تحليل تأثير حل اللجنين في الإيثانول. وأظهرت أطياف الرنين المغناطيسي النووي CPMAS $^{13}C$ NMR لآلسيل اللجنين وتلك التي ذابت في الإيثانول بعض الإختلافات، مما يشير إلى أن الإيثانول لم يقم باذابة اللجنين فحسب، بل تم إكتشاف بعض التعديلات في بنية اللجنين. وكان الفرق الرئيسي بين الأطياف في نطاق الاشارة 15-27 جزء في المليون، والتي يمكن أن تكون مرتبطة مع مجموعات $CH_3$ الطرفية. تشير زيادة هذه الاخيرة إلى أن هياكل الألكيل المشبعة تتراكم بعد الإنحلال مع الإيثانول. كما تم تحليل أطياف الاشعة تحت الحمراء FTIR لكلا العينتين. طيف اللجنين معقد، أين تم إنشاء غالبية الروابط التي تمت ملاحظتها من خلال مساهمة أنواع مختلفة من الاهتزازات من مجموعات وظيفية مختلفة. آلسيل لجنين يُظهر نطاق واسع في 3410-3460 سم$^{-1}$، يعزى إلى مجموعات الهيدروكسيل في الهياكل الفينولية والأليفاتية، الذي لا يزال هو نفسه بعد إذابته مع الإيثانول. ايضا في العينة الذائبة مع الإيثانول تظهر رابطة في النطاق حول 2965 سم$^{-1}$ المتعلقة بالاهتزازات الاليفاتية ل C-H, وتمت ملاحظة هذا المظهر أيضا من قبل طيف CPMAS $^{13}C$ NMR.

UNIVERSIDAD DE MÁLAGA

تمت دراسة المادة الصلبة المستمدة من محلول اللجنين / الإيثانول / $H_3PO_4$ بتقنية FTIR أطياف العينات L2P وLE2P متشابهة جدا، مما يدل على إنخفاض كبير في قوة الروابط عند 1600، 1515 و 1425 سم$^{-1}$ المرتبطة باهتزازات الهياكل العطرية، وكذلك رابطة عند 1460 سم$^{-1}$ المرتبطة بتشوه C-H المقترن مع إهتزاز حلقة عطرية. الرابطة عند 635 سم$^{-1}$ في العينات المعالجة بالأكسدة عند 200 درجة مئوية 2PSL وLE2PS تظهر تطور أنواع أكثر من الفوسفور المؤكسد أثناء المعالجة بالهواء أو تحلل الأصناف غير المستقرة.

وقد تمت دراسة التحلل الحراري للعينات المنشطة المختلفة من خلال تحليل TG. بشكل عام، يمكن ملاحظة ثلاث نطاقات مختلفة في جميع العينات. أولا، هناك فقدان وزن صغير عند درجات حرارة أقل من 200 درجة مئوية التي يمكن أن تعزى في البداية إلى تبخر المياه. يمكن أن يأتي الماء من محلول حمض الفوسفوريك وينتج عن التفاعل بين حمض الفوسفوريك واللجنين. في درجات حرارة أقل من 150 درجة مئوية، يحفز الحمض التحلل المائي لروابط الأثير، مما يؤدي إلى تكوين الكيتونات. هذه وغيرها من تفاعلات الإنقسام التي تحدث من خلال الآلية الأيونية تعزز الإفراج عن $H_2O$، $CO$، $CO_2$ و $CH_4$ في درجات الحرارة المنخفضة هذه ، ويمكن ايضا أن تسهم في فقدان الوزن. بين 200 و500 درجة مئوية، لوحظ إنخفاض آخر في الكتلة يرتبط بإطلاق مركبات الضوء من إنحلال اللجنين. في نطاق درجة الحرارة هذه، ردود فعل الربط المتبادل تهيمن على إنشقاق الروابط وردود فعل دي-بلمرة. وفي 250 درجة مئوية، تعتبر الهياكل وحدات صغيرة متعددة الحلقات ترتبط أساساً بجسور الفوسفات والبولي فوسفات، بما في ذلك روابط البولي إيثيلين. مع إرتفاع درجة الحرارة، تؤدي تفاعلات الربط المحوري والتكاثّف إلى زيادات في العطرية وحجم الوحدات العطرية المتعددة، الناتجة من خلال شق روابط P-O-C. في درجات حرارة أعلى من 500 درجة مئوية يمكن ملاحظة تغير في ميل منحنى فقدان الوزن أيضا، المرجح ان يكون مرتبطا بتطاير معقدات الكربون والأكسجين التي تولدها عملية التنشيط، وبدرجة أقل، إلى تحلل مركبات الفوسفور (كما $P_2O_5$)، التي ينتجها تفاعل حمض الفوسفوريك مع مصفوفة الكربون.

أكدت النتائج التي تم الحصول عليها من تحليلات نظام XPS وجود مجموعات فوسفورية على سطح عينات L2P و LE2P و L2PS و LE2PS. يبدو أن المحلول المشترك للجنين مع حمض الفوسفوريك ولد أعلى مساهمة من مجموعات P السطحية المؤكسدة ضمن المجموعات السطحية P الإجمالية من عملية التنشيط التقليدية (LE2P مقابل L2P). من ناحية أخرى، فإن قيمة المحتوى P الأقل لوحظت لـ LE2P ، بالمقارنة مع تلك الخاصة بـL2P ، تشير هذه الاخيرة إلى أن هذه العينة تقدم المزيد من P في الجزء الداخلي من مصفوفة اللجنين ، ربما بسبب تشتت أفضل وتوزيع أكثر تجانسًا لـ P من خلال مصفوفة اللجنين بأكملها التي تم الحصول عليها عن طريق المحلول المشترك للعامل المنشط ، حمض الفوسفوريك ، ومصادر الكربون ، اللجنين. ومع ذلك، كانت كمية سطح O أعلى بكثير للعينة التي أعدت عن طريق المحلول المشترك من اللجنين والحمض،LE2PS، مما يشير إلى أن هذا الإجراء يحسن عملية أكسدة اللجنين في درجة حرارة منخفضة.

فيما يتعلق بالكربونات المنشطة، isotherm الكربون المنشط L2P400 هو نوع isotherm I ، سمة المواد الصلبة النموذجية ذات المسامات المجهرية microporous. لم تلاحظ أي تغييرات كبيرة في isotherm الآزوت عندما تم حل اللجنين مع عامل تنشيط. ومع ذلك، تم ملاحظة ان المعالجة مع الهواء في 200 درجة مئوية أنتج بنية صلبة مع زيادة ملحوظة في حجم الآزوت $N_2$ الممتز تصل إلى 0.4 من الضغط النسبي. وكانت هذه الزيادة أكثر وضوحا بكثير عندما تم تمرير المحلول المشترك من اللجنين وحمض الفوسفوريك سابقا إلى خطوة التثبيت المؤكسِد (الهواء في 200 درجة مئوية). تزيد قيم المساحة السطحية الظاهرة ($A_{BET}$) بشكل كبيرمن 912 م$^2$/غ ، لـ L2P400 ، إلى 1937 م$^2$/غ، لـ L2PS400 ، وإلى 2551

UNIVERSIDAD DE MÁLAGA

م$^2$/غ، لـ LE2PS400. هذه القيمة الأخيرة أعلى بكثير من غيرها من التقارير المذكورة في أدبيات الكربونات المنشطة المشتقة من اللجنين باستخدام أساليب تنشيط أخرى. فقط عدد قليل من الأعمال ذكرت إعداد الكربونات المنشطة من اللجنين مع مناطق سطح ظاهرة أعلى (\3000 م$^2$/غ) باستخدام تفعيل KOH، ولكن في درجات حرارة تنشيط أعلى بكثير من تلك المستخدمة في هذا العمل. في الطريقة المقترحة هنا، فإن استخدام درجات حرارة التنشيط المنخفضة من شأنه أن يقلل بشكل كبير من تكلفة الكربونات المنشطة المتحصل عليها، دون المساس بالتطورالعالي للمسامية. وبالإضافة إلى ذلك، فإن عائد عملية التحضير حوالي 63٪، وهو أعلى بكثير من غيرها المذكورة في تقارير الأدبيات للجنين وحتى بالنسبة للمواد ليجنوسليلوزية الأخرى..

أجريت تحليلات TPD لمختلف مركبات الكربون المنشطة. الكربونات المنشطة المعدة بطريقة التنشيط الكيميائي مع حمض الفوسفوريك اظهرت تطورمعظم ثاني أكسيد الكربون في درجات حرارة أعلى من 700 درجة مئوية، وذلك بسبب وجود مجموعات سطح P المحتوية على الأكسجين، والتي قد تشمل ميتافوسفاتس، مجموعات C-O-$PO_3$ ومجموعات C-$PO_3$. في ناحية أخرى، فإن الكربونات المنشطة المعدة من اللجنين المذاب وغير المذاب متشابهة للغاية، مما يظهر إطلاق معظم ثاني أكسيد الكربون بين 700 و900 درجة مئوية. ومع ذلك، فإن المعالجة بالهواء عند 200 درجة مئوية والاستخدام المشترك لهذا الاخيرمع المحلول المشترك للجنين وعامل التنشيط ادى الى إصدار أعلى ل CO، حتى في درجات حرارة أقل من 700 درجة مئوية. العينة LE2PS400 ابدت أعلى تطورل CO بين 700 و800 درجة مئوية، مما يشير إلى وجود عالي لمجموعات الميتافوسفات السطحية (نوع C-O-$PO_3$ و/أو C-$PO_3$) على هذه العينة. يمكن ربط التطور الأكبر لثاني أكسيد الكربون الذي لوحظ في TPD لـ LE2PS400 بتوليد أعلى لاسترات الفوسفات أثناء عملية التحضير، كما يتضح من نتائج FTIR وXPS.

من اجل تحليل تأثير المعالجة بالأكسدة على الكربونات المنشطة الناتجة، تم القيام بتعريض العينات التي أعدت عن طريق المحلول المشترك من اللجنين مع عامل التنشيط للأكسدة، في درجات حرارة مختلفة بين 100 و300 درجة مئوية. تشير النتائج إلى أن المعالجة عند 100 درجة مئوية ليس مرتفعًا بما يكفي ليؤدي الى تطور المسامات الكبيرة مقارنة بالعينة دون أي معالجة تأكسدية. اي أن الخصائص التركيبية من العينة المعالجة في 100 درجة مئوية هي مشابهة جدا مع العينة دون أي معالجة. يتم الحصول على الحد الأقصى لحجم المسام (1.31 سم$^3$/g) ومساحة السطح الظاهرة (2551 م$^2$/غ) عند إجراء المعالجة التأكسدية عند 200 درجة مئوية. وفي الوقت نفسه، لوحظ انخفاض كبير في مساحة السطح الظاهر إلى 2128 م$^2$/غ عند إجراء الاكسدة عند 300 درجة مئوية. لذلك، يبدو أنه في ظروفنا التجريبية، كان وجود الأكسجين في درجات حرارة متوسطة، حيث تهيمن ردود الفعل عبر الربط، عزز تطور المسامية بسبب إنشاء المزيد من استرات الفوسفات، ولكن في درجات حرارة أعلى، حيث تجري العمليات العطرية بشكل تفضيلي، ادى فائض الأكسجين إلى نتائج عكسية ، حيث أدى إلى زيادة الأكسدة التي من شأنها أن تمنع زيادة المسامية.

مرة اخرى و لاثبات أن المشروبات الكحولية من عملية اورقانوسولف يمكن استخدامها بنجاح لإعداد الكربونات المنشطة. أجريت المزيد من التجارب لتحسين الظروف التجريبية من أجل زيادة مسامية الكربونات المنشطة الناتجة. مع هذا الهدف، الفصل الرابع كرس لدراسة تأثير نسبة $H_3PO_4$ على كتلة اللجنين ودرجة حرارة التنشيط على الخصائص النسيجية للكربونات المنشطة وبالمقارنة مع استخدام مسحوق واللجنين المجفف. تم اختبار مجموعة من هذه الكربونات المنشطة كممتزات للامتزاز من مضادات الانتيبيرين في الحالة السائلة في التجارب الثابتة والعمودية. كما تم دراسة توازن الامتزاز

UNIVERSIDAD DE MÁLAGA

وحركية الانتيبيرين على الممتزات المختلفة.

تم تحليل تأثير نسبة $H_3PO_4$ إلى كتلة اللجنين ودرجة حرارة التنشيط على الخصائص السطحية للكربونات المنشطة ومقارنتها مع الكربونات المعدة من المسحوق واللجنين المجفف. اين نسبة $H_3PO_4$/ كتلة لجنين متغيرة من 0 إلى 4 ومختلف درجات حرارة التنشيط بين 400 و 900 درجة مئوية..

تم الحصول على الكربونات المنشطة ذات مردودية إجمالية بين 71 إلى 78٪ باستخدام المحلول المشترك للجنين وحمض الفوسفوريك باستخدام نسب مختلفة ل $H_3PO_4$/ كتلة اللجنين وعند درجة حرارة تنشيط 400 درجة مئوية، كونها هذه القيم أعلى من تلك التي تم الحصول عليها باستخدام التنشيط المباشر للجنين المشرب (من 51 إلى 68٪). تم تحليل مسامية الكربونات المنشطة التي اعدت عن طريق التنشيط الكيميائي او المحلول المشترك للجنين، في نسب $H_3PO_4$ / كتلة اللجنين تختلف بين 0.6 و 4 وتنشيطها عند 400 درجة مئوية. بشكل عام، تؤدي الزيادة في الكمية النسبية لعامل التنشيط إلى تطور عالي للمسامية. isotherm الكربونات المنشطة التي تم الحصول عليها من مسحوق اللجنين تنتمي أساسا الى النوع الأول وتبدي هضبة أفقية تقريبا عند قيم الضغط النسبي المنخفضة جدا، مما يشير إلى وجود معتبر للمسامات الدقيقة. مع زيادة نسبة $H_3PO_4$ إلى كتلة اللجنين تصل إلى 4، نرى وجود حلقة في المنحنى عند الضغوط النسبية العالية تدل عن توسيع في الهياكل المسامية، والحصول على مساهمة أعلى من المسامات الدقيقة mesoporosity. الكربونات المنشطة المعدة من المحلول المشترك من اللجين تظهر isotherm النوع الأول في نسب منخفضة ل $H_3PO_4$ /كتلة اللجنين والنوع الرابع عند القيم العليا. كما يمكن ملاحظته، هناك حد أقصى من حجم $N_2$ الممتز بنسبة 2. من هذه النسبة، الزيادة في نسبية $H_3PO_4$ /كتلة اللجنين إلى 3 تنتج توسيع مسامية العينات. ومع ذلك، فإن ارتفاع اكتر في النسبة تصل إلى 4 ادى الى بعض النقصان في امتزاز النيتروجين التي يمكن أن ترتبط بتدهور هيكل المسامي، الناجمة عن تدمير الجدار بين المسامات المجاورة عن طريق التفاعلات بين فائض حمض الفوسفوريك..

إذا تمت مقارنة كل نسبة من المصادر المختلفة، يمكن ملاحظة أن isotherm الكربونات المنشطة التي تم الحصول عليها بنسب منخفضة (0.6) تظهر هضبة أفقية تقريبا بدءا من الضغط النسبي المنخفض جدا، الموافقة لنوع isotherm I ، بغض النظر عن اللجنين المستخدم لإعدادها. ومع ذلك، هناك اختلافات هامة في isotherm اللجنين المختلفة عند نسب $H_3PO_4$ / كتلة اللجنين أعلى من 1. نوع ال isotherm مختلف تماما بالنسبة للعينة التي أعدت في نسبة $H_3PO_4$ /كتلة اللجنين تساوي 3. عند نسب أعلى (4)، تأثير نوع الجنين انخفض مؤديا فقط الى تطور طفيف في المسامية مع المعالجات التالية.

في هذا السياق، يبدو أن استخدام اللجنين المذاب يعزز تفاعلًا أكثر تجانسًا بين اللجنين وعامل التنشيط الذي يمكن أن يزيد من تكوين استرات الفوسفات التي تدعم الربط المتبادل بين حمض الفوسفوريك والمصفوفة الكربونية. من ناحية أخرى، يمكن أن تعزز المعالجة المؤكسدة مع الهواء عند 200 درجة مئوية أيضًا تكوين جسور الفوسفات والبولي فوسفات. يتم إدراج هذه المجموعات الفوسفورية في مصفوفة الكربون، بفصل الأصناف العضوية. ينتج هذا الإدراج عملية توسعية تترك المصفوفة في حالة موسعة بعد الغسيل، مع مسامية عالية. لذلك، فإن الاختلافات الصغيرة في isotherm عند نسبة كتلة $H_3PO_4$/lignin منخفضة (0.6) تشير إلى أن جميع حمض الفوسفوريك متاح لتشكيل جسور الفوسفات والبولي فوسفات، واستخدام اللجنين المذاب والبودرة لا تحفز أي تعزيز إضافي. ومع ذلك، يمكن أن ترتبط الاختلافات عند أعلى نسب ل $H_3PO_4$ /كتلة اللجنين إلى تغطية حمض الفوسفوريك لكامل سطح اللجنين. يتفاعل حمض الفوسفوريك هذا مع جميع مجموعات الهيدروكسيل المتاحة من اللجنين لإنتاج روابط الايثر-اريل الموافقة. وبهذه الطريقة، يمكن أن تؤدي معالجة

UNIVERSIDAD DE MÁLAGA

التثبيت المؤكسدة مع الهواء عند 200 درجة مئوية إلى أكسدة روابط C-H من أجل تعزيز تشكيل مجموعات هيدروكسيل جديدة، وبالتالي، إنشاء أكثر لأسترات الفوسفات. اما في نسبة $H_3PO_4$ / كتلة اللجنين من 4 ، يمكن أن يكون فائض حمض الفوسفوريك بمثابة حاجز فيزيائي، مؤديا إلى حد ما الى عدم أكسدة الروابط C-H ؛ حيث وصول الهواء سيكون أكثر تقييدًا وسيكون له تأثير أصغر على العملية.

في ناحية أخرى، تم تحليل منحنيات $\alpha_s$ لمختلف الكربونات المنشطة المعدة من مسحوق واللجنين المذاب، عند نسب $H_3PO_4$ /كتلة اللجنين مختلفة بين 1 و 3 وعند 400 درجة مئوية. بشكل عام، تظهر الكربونات المنشطة المعدة من المحلول المشترك للجنين مساهمة أعلى من المسامية الدقيقة عند نسب $H_3PO_4$/lignin السالفة الذكر. يشير البيان الخطي لأجزاء الضغط العالي من المنحنيات ($\alpha_s > 1$) ، المرتبطة بالمنطقة المتعددة الطبقات ، إلى انخفاض وجود المسامات الدقيقة في جميع العينات ، بغض النظر عن اللجنين المستخدم. وعلاوة على ذلك، هذه المنحنيات تظهر أيضا تأرجح أعلى واحد تحت $\alpha_s = 1$، تقريبا بين 0.6 و 1، المرتبطة بتأرجح التكاثف على المسامات فوق لمجهرية (أحجام المسام $\leq$ 1 نانومتر). وأشارت النتائج إلى أن تفعيل المحاليل المشتركة للجنين و$H_3PO_4$ ينتج زيادة في مساحة السطح الظاهر وحجم المسامات المجهرية والدقيقة مقارنة بالكربون المنشط المتحصل عليه من خلال التنشيط المباشر لمختلف النسب $H_3PO_4$ /كتلة اللجنين المستعملة. وعلى وجه التحديد، يمكن ملاحظة أن الزيادة النسبية في مساحة السطح الظاهر وحجم المسامات الدقيقة تتبع نفس الاتجاه، حيث تحصل على منحنى غوسي، بحد أقصى يساوي 2، حيث تبلغ هذه القيم ضعف تلك التي تم الحصول عليها من التنشيط المباشر للجنين. وتعود أعلى زيادة نسبية في حجم المسامات الدقيقة المتحصل عليها الى المواد ذات نسبة $H_3PO_4$/ كتلة اللجنين تساوي 3.

وأظهر توزيع حجم المسامات المجهرية لمختلف الكربونات المنشطة التي أعدت عند مختلف نسب $H_3PO_4$ /كتلة اللجنين وعند 400 درجة مئوية توزيع ثنائي الشكل للكربونات المنشطة المعدة من مسحوق اللجنين، يصل لحد أقصى حوالي 6.7 Å عند أدنى نسبة ل $H_3PO_4$/ كتلة اللجنين، والتي يتم انسحابها إلى 11.1 Å عند نسبة $H_3PO_4$/ lignin تساوي 3. بالنسبة للمشروبات الكحولية المشتقة من الكربونات المنشطة، يصبح توزيع حجم المسامات المجهرية أعلى وأضيق حتى نسبة 2 ، والحصول على الحد الأقصى حوالي 12.2 Å عند نسبة $H_3PO_4$/ كتلة اللجنين من 1 ، و16.6 Å عند نسبة 2 ، كما اقترح أعلى تأرجح تصاعدي أقل من $\alpha_s$=1. بشكل عام، تؤدي زيادة نسبة $H_3PO_4$/كتلة اللجنين إلى توزيع أوسع في حجم المسامات المجهرية في كلا النوعين من اللجنين.

تم تحليل تأثير درجة حرارة التنشيط على الخصائص النسيجية لهذه الكربونات المنشطة عند $H_3PO_4$ /كتلة اللجنين تساوي 2. أدت زيادة درجة حرارة التنشيط إلى 400 درجة مئوية إلى تطوير كبير للمسامية، حيث ادت الى الحصول على أعلى حجم من امتصاص $N_2$ في كامل نطاق الضغوط النسبية. وأي زيادة أخرى أبعد تصل إلى 900 درجة مئوية تنتج انخفاضا كبيرا في هذا الحجم.

أُستُخدمت مجموعة مختارة من هذه الكربونات المنشطة لإزالة الملوثات في الحالة السائلة. على وجه التحديد، إستخراج المواد الصيدلانية ومستقلباتها من المياه أصبحت تحديا كبيرا للمجتمع في الآونة الأخيرة. من بينها، مضاد انتيبيرين (فينازون) وهو مسكن وخافض للحرارة تم اكتشافه في متوسط التراكيز أقل من 10 ملغ/يوم/1000 نسمة في مجاري WWTPs، حيث تم الإبلاغ عن كفاءة إزالة منخفضة نسبيا (متوسط 35٪). الامتزاز على الكربونات المنشطة المجففة طريقة جد معروفة

UNIVERSIDAD DE MÁLAGA

لتنقية المياه. في هذا السياق، تم اختيار ثلاثة ممتزات مختلفة للامتزاز المضادة للانتيبيرين أعدت عند نسب $H_3PO_4$/ كتلة اللجنين ودرجات حرارة تنشيط مختلفة من المحلول المشترك من اللجنين السيل وحمض الفوسفوريك.

من أجل دراسة تأثير نسبة $H_3PO_4$/ كتلة اللجنين ودرجة حرارة التنشيط على الكيمياء السطحية لهذه الكربونات المنشطة، تم إجراء تحليلات TPD و XPS. وأشارت النتائج إلى انخفاض في وجود حمض الكربوكسيليك واللاكتونات ومجموعات أنهيدريد التطور العالي لثاني أكسيد الكربون لهذه الكربونات المنشطة يمكن أن يرتبط بوجود مجموعات وظيفية فوسفورية وتحلل مجموعات الفينول والكربونيل والأثير. كمية CO التي تطورت مشابهة تماما لتلك بالنسبة للكربونات المنشطة التي أعدت في مختلف درجات حرارة التنشيط ، ومع ذلك، يتم الكشف عن انسحاب في اشارة ثاني أكسيد الكربون الرئيسية إلى درجات حرارة أعلى مع زيادة درجة حرارة التنشيط، والتي يمكن أن تكون ذات صلة بتغيير في الاستقرار الحراري لمجموعات سطح الأكسجين. أظهر الكربون المنشط الذي تم الحصول عليه عند $H_3PO_4$/ نسبة كتلة اللجنين تساوي 2 وتنشيطها عند 800 درجة مئوية أعلى تطور لثاني أكسيد الكربون حول 860 درجة مئوية، المرتبطة بتحلل مجموعات $C-O-PO_3$.

isotherms امتزاز مضادات الانتبرين في 20 درجة مئوية على الكربونات المنشطة المختارة هي من نوع L وفقا لتصنيف جيلز, المذكورة عادة في امتصاص الحالة السائلة. كمية امتصاص مضادات الانتبرين، وذلك باستخدام تركيز التوازن 1 ملغ / لتر، بالنسبة للكربون المنشط الذي تم الحصول عليه عند نسبة $H_3PO_4$ / كتلة اللجنين تساوي 2 والمنشط عند 800 درجة مئوية كانت أعلى من الكربونين الآخرين المنشطين على الرغم من اكتسابه أدنى قيمة للمساحة السطحية الظاهرة، مما يشير إلى أنه لم تكن هناك علاقة مباشرة بين قدرة الامتزاز والمساحة السطحية الظاهرة للممتزات، على الأقل عند هذه التركيزات المنخفضة. ومع ذلك، فإن توزيع حجم المسامات المجهرية لهذه العينات الثلاث يكشف عن أن الكربون المنشط مع أعلى مساهمة من المسام الفوق مجهرية هو ذات الأعلى قدرة على امتزاز مضادات الانتبرين. وبالنظر إلى الأبعاد الجزيئية للانتبرين، يبدو أنه عند التركيزات المنخفضة للملوثات، فإن المسامات الدقيقة ذات الحجم الأقل من 9 هي المسؤول الرئيسي عن القدرة على الامتزاز. وبالإضافة إلى ذلك، كما ذكر سابقا، الكربونات المنشطة التي أعدت عند نسب $H_3PO_4$ /كتلة اللجنين المختلفة وتفعيلها في 400 درجة مئوية لها درجة حموضة اقل، مثل الفينولات، وفي الوقت نفسه الكربون المنشط التي تم الحصول عليه عند نسبة $H_3PO_4$ / كتلة اللجنين تساوي 2 وتنشيط في 800 درجة مئوية كانت تتألف أساسا من مجموعات سطح الفوسفور ذات استقرار حراري عالي مع ميزة حمضية ضعيفة-معتدلة، والتي يمكن أن يكون لها أكثر تقارب مع الانتبرين. تم تمثيل بيانات التوازن لكل من معادلات لونغمير( Langmuir) و فراندليش (Freundlich). كلا النموذجين مثّلا إلى حد ما البيانات التجريبية بشكل جيد، على الرغم من وجود بعض الأخطاء الطفيفة مع نموذج لونغمير. مؤشر التغاير(n/1) من معادلة فرندليش يعطي مؤشرا على كيفية حصول عملية الامتزاز، في هذه الحالة، القيم أعلى من 1 و تشيرالى امتزاز مواتي للممتزات الثلاثة.

كما تم تحليل حركية الامتزاز للانتبيرين على الكربونات المنشطة الثلاثة. وأظهرت النتائج التي تم الحصول عليها أن هناك انخفاضا هاما في معدل الامتزاز في بداية وقت الاتصال. بعد ذلك، يمكن ملاحظة مرحلة ثانية مع قيم معدل انخفاض وسيطة، مما يؤدي في النهاية إلى الجزء الثالث من المنحنى، الذي يظهر معدلات امتزاز بتأثير لا يذكر. ناسبت البيانات التجريبية حركية امتصاص الدرجة الثانية ومعادلة قطعية باستخدام تركيز الامتصاص على المادة الصلبة ($q_t$) كدالة لوقت الاتصال (t). كلا المعادلتين قادرة إلى حد ما على إعادة تمثيل وبشكل جيد البيانات التجريبية للكربونات المنشطة الثلاثة. ترتبط القيم

UNIVERSIDAD DE MÁLAGA

الثابتة للحركية المستمدة من المعادلة الحركية من الدرجة الثانية للامتزاز الانتبيرين على مختلف الكربونات المنشطة ارتباطا واضحا بقيم المناطق السطحية الظاهرة للكربونات المنشطة.

كما تم تقييم امتزازالانتبيرين في دراسات الأعمدة. تم الحصول على المنحنيات لمختلف الكربونات المنشطة ثابت الأسرّة في 20 درجة مئوية و 1 ملغ/لتر من الانتبيرين. تم حساب إجمالي قدرات الامتزاز من المساحة أعلى المنحنى. شكل المنحنيات هو من نوع S، الملاحظ عادة في تجارب العمود مع isotherms الامتزاز مواتية. وقت الاختراق للكربون المنشط الذي تم الحصول عليه عند نسبة $H_3PO_4$/كتلة اللجنين تساوي 2 وتنشيط في 800 درجة مئوية هو ضعف تلك التي لوحظت للكربونات المنشطة التي أعدت عند مختلف نسب $H_3PO_4$/كتلة اللجنين وتفعيلها في 400 درجة مئوية. يمكن أن يرتبط هذا الاختلاف الكبير بارتفاع حجم المسام أقل من 9 Å للكربون المنشط الذي تم الحصول عليه عند نسبة $H_3PO_4$/كتلة اللجنين من 2 تنشيط عند 800 درجة مئوية، حيث يمكن أن يصبح النشر عند السطح أكثر أهمية. تظهر النتائج أن قدرات الامتزاز لها نفس الميول مثل الدراسات الحركية والتوازن. تم تطبيق نموذج توماس على نتائج الاختراق لتقييم السلوك الديناميكي للعمود. وكان هذا الاخير قادرا على التنبؤ بشكل جيد بقدرات الامتزاز المستخلصة من دراسة التوازن وأوقات الاختراق للممتزات الثلاثة. وبالإضافة إلى ذلك، فإن منحنيات الاختراق النظري المستمدة من هذا النموذج تستنسخ بنجاح البيانات التجريبية للكربون المنشط التي تم الحصول عليها عند نسبة $H_3PO_4$/كتلة اللجنين تساوي 2 و تنشيط في 800 درجة مئوية.

يتم إنتاج معظم اللجنين في العالم كمنتج ثانوي في صناعة اللب والورق، مع الحصول على معظمها من عملية الكرافت. المشروبات الكحولية السوداء في مصانع إنتاج اللب من الكرافت هي حلول قلوية. ينتج عن تبخر هذه المشروبات الكحولية السوداء اللجنين الصلب مع نسبة عالية من مركبات الصوديوم، مثل هيدروكسيد الصوديوم والكبريتات اللجنوسولفونات. هذا المحتوى العالي من الصوديوم الملاحظ في اللجنين كرافت يجعل هذا المنتج الثانوي الصناعي مادة اولية مثيرة للاهتمام لإعداد المواد الحفازة لمختلف التطبيقات. في هذا الصدد، الفصل الخامس تطرق لإعداد الكربونات المنشطة مع خصائص نسيجية وكيمياء سطحية مختلفة من اللجنين كرافت عن طريق الاحتراق المباشر في درجات حرارة مختلفة (500 ، 700 ، 900 درجة مئوية). كما تم تقييم تأثيرالمعالجة بالغسل والتغويز الجزئي بثاني أكسيد الكربون. تم اختبار الكربون المنشط الناتج كمحفزات لتفاعل تحلل الكحول.

تم قياس نشاط المحفزات من خلال تحلل الكحول التي أجريت تحت الضغط الجوي، في مفاعل كوارتزصغيرو ثابت وضع داخل فرن عمودي مع التحكم في درجة الحرارة، باستخدام الضغط الجزئي للكحول من $Po_{AlC}$ =0.0185 ووقت الاتصال PF W/ $Fo_{Alc}$ =0.073 g s·µmol$^{-1}$

تم تحليل الخصائص النسيجية لمحفزات الكربون المختلفة التي تم إعدادها في درجات حرارة تتراوح بين 500-900 درجة مئوية. المحفز الذي تم الحصول عليه من الاحتراق المباشر عند 500 درجة مئوية يقدم حجم امتصاص $N_2$ منخفض، وهو نموذجي لمادة صلبة غير مسامية. أدت زيادة درجة حرارة الاحتراق إلى تطور طفيف في الهيكل المسامي بسبب التنشيط الذي ينتجه أكسيد الصوديوم عند ارتفاع درجة حرارة الاحتراق. Isotherms المحفزات غير المغسولة التي تم الحصول عليها في 900 درجة مئوية قبل وبعد خطوة التغويز متشابهة جداً، بسبب وجود مادة غير عضوية تعيق تطور المسامية أثناء خطوة التغويز. في المقابل، يتيح المعالجة بالغسل إلى حد كبير بفتح المسامية بسبب إزالة المادة غير العضوية. ينتج تغويز هذه العينة (L900WG) تطورًا عاليًا في المسامية مع مساحة ظاهرة تبلغ حوالي 850 $m^2/g$، مما يظهر Isotherm من النوع الرابع IV، مع وجود كبير للمسامات المجهرية والمسامات الدقيقة.

UNIVERSIDAD DE MÁLAGA

تنتج خطوة الاحتراق فحم ذات محتوى عالٍ من مجموعات الأكسجين السطحية، نتيجة لأكسدة الكربون وارجاع أملاح الكبريت إلى كبريتيد. المجموعات المؤكسدة أساسا هي كونيون، كاربونيل، وكربونات (كربونات الصوديوم). غسل هذه الفحوم يزيل جزئيا كبريتيد الصوديوم، وبدرجة أقل، كربونات الصوديوم. سطح الكربون يظهر طابع أساسي مع مجموعات الكربونيل والكينون والمستويات القاعدية للكربون (مع كثافة عالية للإلكترون)، والتي يمكن أن تكون بمثابة مواقع المتبرعين للإلكترون.

جزيئات الكحول، أساسا 2 بروبانول، تستخدم على نطاق واسع لاختبار الطابع الحمضي الأساسي للمحفزات غير المتجانسة. في هذا السياق، فإن منتجات إزالة الهيدروجين الكحولية (ألدهيد والكيتونات) تتشكل بشكل أفضل على المواد المحفزة الأساسية، في حين أن منتجات التجفيف (الأوليفينات والأثيرات) مفضلة عندما تكون المواقع الحمضية موجودة. تم تقييم المواد الكربونية التي تم الحصول عليها كمحفزات لتحلل الكحول. كما هو متوقع، 2-بروبانول يزيد التحويل مع درجة حرارة التفاعل. الزيادة في درجة حرارة الاحتراق تنتج تعزيز التحويلات ثابتة الحالة، مبينة ان الحافز المحترق عند 900 درجة مئوية لها أعلى التحويلات المستقرة للفحوم الثلاثة. من ناحية أخرى، سلسلة محفزات الكربون التي أعدت في 900 درجة مئوية تتبع التسلسل L900WG > L900 > L900W > L900G. وتتوافق أكثر المحفزات نشاطاً مع الكربون ذو أعلى تطور للمسامية واوسع انتشار للصوديوم، وفي الوقت نفسه يقدم المحفز L900G مساحة سطحية ظاهرة منخفضة جداً وانتشار ضعيف للصوديوم، كما يتضح من تحليلات SEM-EDX. الاختبار المحفز لتحلل 2-بروبانول يدعم الطابع الأساسي القوي لهذه المحفزات، حيث تم تحويل الكحول بشكل انتقائي إلى أسيتون. جميع العينات الكربونية المحظّرة عند 900 درجة مئوية اظهرت نسبة تحويل أكثر من 95٪ عند 350 درجة مئوية والانتقائية إلى الأسيتون أعلى من 95٪.

حين تتأسس ميزة الأساس، المحفز مع أعلى نشاط ل 2 بروبانول، L900WG، كما تم تقييم تفكك الإيثانول والميثانول. لم تكن نتائج التحويلات مرتفعة كما كان متوقعا. ومع ذلك، كانت انتقائية المحفز أعلى من 80٪، مما أسفر عن الأسيتالديهيد والفورمالديهايد. وأخيرا، تم تحليل استقرار المحفز أيضا لمدة 6 ساعات. وظل التحويل والانتقائية لكلا الكحولين نفسهما خلال وقت التفاعل هذا.

وبالختام، يمكن أن تكون هذه الدراسة نقطة انطلاق لإعداد الكربونات المنشطة من المشروبات الكحولية المستمدة من عمليات اللباب المختلفة، والتي يمكن أن تعزز الجودة التكنولوجية والاقتصادية للمصفاة الحيوية اللجنوسبلولوزيكية من خلال إنتاج منتجات ذات قيمة مضافة. بالإضافة إلى ذلك، نظرًا للمسامية العالية للكربونات المنشطة المعدة، وإمكانية تعديل كيمياء سطحها، فإن دراسة التطبيقات البديلة للكربونات المنشطة هنا ستكون مفيدة للغاية.

UNIVERSIDAD DE MÁLAGA

# *Acknowledgments*

UNIVERSIDAD
DE MÁLAGA

# Dédicace

Aux deux êtres qui me sont très chers dans cette vie, à savoir ***mon père et ma mère***. Je leur dis merci ***papa*** du fond de mon cœur pour ton éducation, ton sacrifice, ton assistance et pour ce que tu m'as fait et qui m'a permis d'avoir cette réussite et ce bonheur. Je te dis merci et mille fois merci ***maman*** pour ta patience, ton courage et ton sacrifice pour moi. Avec toute ma fidélité et tout mon amour pour vous, mes parents, je ne pourrai jamais égaler votre mérite

Également à toute ma famille notamment mes frères et mes sœurs. À ma deuxième famille à Malaga, *Zahira* et son fils Jamal.

À mes amis : *Amina Safer, Fatima, Rachida, Amina, Faiza, Salima, Mohamed, Wahiba, Nabila Faiza et la charmante Souad*, pour leur encouragement et soutient moral avant tout.

À mon cher ami *Sami* celui qui m'a conseillé et m'a guidé mes pas vers la lumière.

Tout simplement à tous ceux qui ont été à mes côtés au plein moment de doute, de désespoir et de faiblesse. Ceux qui avec leurs support et présence, ce travail a pu être achevé avec succès.

UNIVERSIDAD DE MÁLAGA

# *Acknowledgments*

This work has been done from November 2014 to April 2020 in the laboratory of the Researcher group TERMA at Universidad de Malaga(Spain) and laboratoire des sciences et thechniques de l'eau at university of Mascara (Algeria).

My deepest gratitude and appreciations go first to *Professor* ***Jose Rodriguez Mirasol***- director of this work- for his valuable and constructive suggestions during the planning and development of this work. I really appreciate his help to clarify all my doubts and presence in time of need. This work could not be done successfully without his excellent scientific contributions.

Also, special thanks go to ***Juana Mª Rosas Martínez*** without her, I would not finish my research. I am gratified to her for suggestions and corrections while publishing the scientific articles which have been of immense help to me. Not just for our long conversations about research and work, but also about customs and traditions, literature and cultures. I have learned a lot.

I would like to express my thanks to *Professor* **Abdelghani *Benyoucef*** for all his help and guidance that he has given me all these years and also for giving me the opportunity to do an international cotutelle thesis.

I want to thank Professor ***Tomas Cordero*** for sharing me his knowledge and contributions. I am also so grateful to him for his scientific advises.

My inmost thankfulness is addressed to ***Fran*** for his patient guidance, enthusiastic encouragement and useful critiques of this research work. His fast reactions to solve the problems substantially speed up my work.

It was a real pleasure to work with my colleagues from ***TERMA*** Group at Universidad de Malaga during the whole period of my research *Jaunjo, Jose, Ramiro, Maria Jose, Javier, Miguel, Miguel Angel, Mari Carmen, Eli, Paul, Lourdes, Elizabet, Olaya, Lilia and also IMpho,*

UNIVERSIDAD DE MÁLAGA

*Rafael, Cinthia, Sandra, Jose luis, June and to all those who I met in the laboratory since 2014, simply thank you for been there.*

Special thanks are addressed to the technical services of SCAI for valuable technical contributions in materials characterizations, and chemical analysis.

Aussi un remerciement s'adresse à toute la communauté de *l'université de mascara* (Mustapha Istambouli). Mes remerciements également vont pour le ***MESRS*** (Ministère de l'Enseignement supérieur et de la Recherche scientifique Algérienne) pour m'avoir accordé la bourse Programme National Exceptionnel (PNE) 2019-2020.

Finally, I would like to thank all my family for their support and understanding during these years, specially my father who is my hero in life et ma mère, mon ange dans la vie. Vraiment un grand merci ne suffit jamais pour m'exprimer envers ce que vous m'avez fait. Grâce à vous je suis devenue la fille qui je suis aujourd'hui. Que DIEUX vous garde pour moi.

*Merci, Gracias, Thank you* شكرا

IMANE

UNIVERSIDAD DE MÁLAGA

**Departamento de Ingeniería Química**
**Facultad de Ciencias**
**Universidad de Málaga**
**and**
**Département de Génie Procédés**
**Faculté de Science et Technologie**
**Université de Mascara**

**Programa de Doctorado:**

**Química y Tecnologías Químicas, Materiales y Nanotecnología**

**Tecnología de Residuos y Medioambiente**
**Universidad de Málaga**